MODULATION OF HOST IMMUNE RESPONSES BY *BARTONELLA* EFFECTOR PROTEINS

Inauguraldissertation

zur

Erlangung der Würde eines Doktors der Philosophie

vorgelegt der

Philosophisch-Naturwissenschaftlichen Fakultät

der Universität Basel

von

Yun-Yueh Lu

aus Taiwan

Basel, 2015

Originaldokument gespeichert auf dem Dokumentenserver der Universität Basel

edoc.unibas.ch

Genehmigt von der Philosophisch-Naturwissenschaftlichen Fakultät auf Antrag von

Prof. Dr. Christoph Dehio
Prof. Dr. Dirk Bumann

Basel, den 17.02.2015

Prof. Dr. Jörg Schibler

Dekan

Statement of my thesis

This work has been performed in the group of prof. Christoph Dehio in the focal area of infection Biology at the Biozentrum of University of Basel in Switzerland.

My PhD committee consists of:

Prof. Christoph Dehio

Prof. Dirk Bumann

Prof. Antonius G. Rolink

My thesis is written in a cumulative format. It consists of a synopsis covering a variety of aspects related to my work and result sections including the scientific publication, the manuscript in preparation and additional unpublished data. Finally, I resume the major findings and discuss various facets of this work.

Index

1. GENERAL INTRODUCTION - 1 -

1.1 Host defense mechanisms - 2 -

1.1.1 Host innate immunity - 2 -

1.1.2 Host adaptive immunity - 6 -

1.1.3 Dendritic cells - 8 -

1.2 Bacterial defense against host immune responses - 9 -

1.2.1 Avoidance of phagocytosis - 10 -

1.2.2 Prevention of intracellular pathogen degradation - 11 -

1.2.3 Attenuation of pro-inflammatory responses - 12 -

- Interference with intracellular signal transduction cascades
- Suppression of innate immune secretory mechanisms

1.2.4 Exploitation of anti-inflammatory cytokines - 16 -

1.2.5 Suppression of antigen presentation - 17 -

1.2.6 Blockage of acquired immunity - 18 -

1.3 *Bartonella* species - 19 -

1.3.1 Cycle of *Bartonella* infection - 20 -

1.3.2 *Bartonella* virulence factors - 22 -

- *Bartonella* adhesin A
- VirB/D4 type IV secretion system
- Trw type IV secretion system

1.3.3 Immune evasion and immunomodulation - 26 -

1.4 References - 29 -

2. AIM OF THE THESIS - 41 -

3. RESULTS - 43 -

3.1 Research article I (published) - 44 -

Bartonella henselae trimeric autotransporter adhesin BadA expression interferes with effector translocation by the VirB/D4 type IV secretion system.

3.1.1 Summary - 45 -

3.1.2 Manuscript - 46 -

3.2 Research article II (manuscript in preparation) - 60 -

Bartonella translocated effectors, BepA and BepD, interfere with the maturation of dendritic cells

3.2.1 Summary - 61 -

3.2.2 Introduction - 62 -

3.2.3 Materials and Methods - 66 -

3.2.4 Results - 78 -

- *Bartonella* inhibits a full maturation of infected BMDCs through T4SS dependent manner
- $BepA_{Bhe}$ and $BepD_{Bhe}$ display immunomodulatory effects on DCs
- The functions of $BepA_{Bhe}$ and $BepD_{Bhe}$ are related to its BID domain and the N-terminal fragment, respectively
- CD40 expression and inflammatory cytokine secretion are negatively regulated by $BepA_{Bhe}$ homologs
- The effects of $BepA_{Bhe}$ homologs are in association with the acceleration of cellular cyclic AMP level
- $BepD_{Bhe}$ homologs possess conserved activities on inhibition of MHCII and CD86 expression, as well as pro-inflammatory cytokine secretion
- The functional EPIYA-related motifs are delineated in BepD-$BXBID_{Bhe}$ by tyrosine to phenylalanine exchanges
- Ectopic expression of BepD-$BXBID_{Bhe}$ actively suppresses JAWSII responses to *E. coli* LPS stimuli
- BepD-$BXBID_{Bhe}$ co-immunoprecipitates with SHP2 and STAT3 in a phosphorylation-dependent manner
- Phosphorylation of STAT3 strongly correlates with semi-maturation phenotype of BMDCs
- A murine model with *B. taylorii* intradermal infection is established for functional analysis of Beps *in vivo*
- Through intradermal infection, *Bta* Δ*bepAD* seems to lose the fitness of bacteremia development

3.2.5 Discussion - 89 -

- Impaired DC maturation by *Bartonella* infection
- cAMP in *Bartonella* pathogenicity
- Relevance of Beps' function *in vivo*
- Perspective in immune-attenuation by *Bartonella* infection

3.2.6 Figure Legends - 95 -

3.2.7 Figures - 104 -

3.2.8 Supplementary Tables - 137 -

3.2.9 References - 148 -

3.3 Additional data (preliminary) - 154 -

3.3.1 Upregulation of co-stimulatory molecules by *Bhe* Δ*bepA-G* infection is MyD88-independent - 155 -

3.3.2 *B. birtlesii* infection with a lower-dose inoculum induces higher bacteremia. - 160 -

3.3.3 *B. birtlesii* infection leads to lymphadenopathy in mice - 163 -

3.3.4 *Bartonella*-infected BMDCs migrate from the site of injection to draining LNs - 169 -

3.3.5 *B. taylorii* infection in the neonatal murine model leads to extremely high bacteremia but not to bacterial persistence - 174 -

3.3.6 *Bta* Δ*bepDE* loses the fitness of bacteremia development - 179 -

3.3.7 References - 182 -

4. CONCLUSIONS AND OUTLOOK - 185 -

- Functional interaction between BadA and VirB/D4 T4SS
- Immunomodulatory properties of BepA and BepD
- Immunological signaling triggered by *Bartonella* infection
- *Bartonella* transport at an early stage of infection
- A potential model of *Bartonella* stealth-infection strategy

5. ACKNOWLEDGMENTS - 191 -

6. CURRICULUM VITAE - 195 -

1. GENERAL INTRODUCTION

This chapter highlights the dynamic relationship between mammalian hosts and bacterial pathogens. Under mutual influence, hosts and pathogens modify their activities and functions during evolution. The consequence of an infection on the host organism relies mainly on the effectiveness of host defense systems. Successful pathogens have evolved a variety of unique strategies to circumvent this and breakdown or evade the host immunity at different stages. The virulence factors of pathogens are tailored to facilitate their entry, replication, and persistence by modulating host cellular processes.

1.1 Host defense mechanisms

Host defense lines against bacterial infection include natural barriers as well as nonspecific and specific immune responses. Natural barriers such as the skin, mucous membranes, and the respiratory tract develop the physical obstruction to bar the invading microorganisms. Once these barriers are overcome, a complex combination of the innate and adaptive immune systems provides a potent protection of the host against infectious pathogens. Generally, bacterial invasion triggers a couple of immune responses comprised of innate and adaptive components. When the immune surveillance detects foreign agents in the host, the inflammatory and phagocytic responses are immediately activated. Subsequently, specific immune responses are soon encountered responsible for elimination of pathogens and generation of host immunological memory.

1.1.1 Host innate immunity

The innate immune response constitutes the first line of defense to combat microbial infections or tissue damage. The innate leukocytes comprise natural killer (NK) cells, mast cells, eosinophils, and basophils; the phagocytic cells include macrophages, neutrophils, and dendritic cells (DCs). Upon pathogen invasion, the rapid inflammatory response can direct various immune cells to the infection sites. Guided by chemotaxis, phagocytes are drawn to pathogens and engulf them to limit the microbial spread. In phagocytes, phagocytic lysosomal contents are released to destroy pathogens [2]. To initiate the action of innate immunity, early recognition of the pathogen-associated molecular patterns (PAMPs) and damage-associated

molecular patterns (DAMPs) plays an essential role through a limited number of germline-encoded pattern recognition receptors (PRRs). PAMPs contain various components of bacterial cell wall (e.g., lipopolysaccharide (LPS), peptidoglycan (PG), and lipopeptides), flagellin, bacterial DNA and viral double-stranded RNA. DAMPs include intracellular proteins (e.g., heat shock proteins) and proteins derived from the extracellular matrix (e.g., hyaluronan fragments). Furthermore, four families of PRRs have been classified including transmembrane proteins, e.g., the Toll-like receptors (TLRs) and C-type lectin receptors (CLRs), and cytoplasmic proteins, e.g., the Retinoic acid-inducible gene (RIG)-I-like receptors (RLRs) and NOD-like receptors (NLRs) [1]. PRR-induced signal transduction pathways result in synthesis of various molecules including cytokines, chemokines, cell adhesion molecules, and immunoreceptors. These PRRs are not only present on DCs and macrophages, but also on several non-immune cell types (e.g., epithelial cells, endothelial cells, and fibroblasts), which regulate receptor-mediated inflammation [2].

Among PRRs, the family of TLRs is the most extensively studied. Based on homology to the *Drosophila* Toll protein, TLRs are evolutionarily conserved with an extracellular domain containing leucine-rich-repeat (LRR) motifs and a cytoplasmic domain homologous to the interleukin (IL)-1 receptor, termed the Toll/IL-1R homology (TIR) domain [3, 4]. TLRs play a pivotal role in cell activation in response to PAMPs. Based on related PAMPs, TLRs can be further divided into several subfamilies: the subfamilies of TLR1, TLR2, and TLR6 on the cell surface recognize lipopeptides, whereas TLR3, TLR7, TLR8, and TLR9, which are found exclusively in intracellular compartments, recognize nucleic acids. Furthermore, TLR4 and TLR5 recognize bacterial LPS and flagellin from flagellated bacteria, respectively. Upon engagement with ligands, TLRs first recruit the adaptor proteins via the cytoplasmic TIR domain. They bind myeloid differentiation primary-response protein 88 (MyD88), MYD88-adaptor-like protein (Mal; also known as TIRAP), TIR domain-containing adaptor inducing IFN-β (TRIF; also known as TICAM-1), and TRIF-related adaptor molecule (TRAM) [5]. Based on the usage of the different adaptor proteins, each TLR induces unique signaling cascades. A detailed overview of TLR signal transduction is shown in Figure 1 [6].

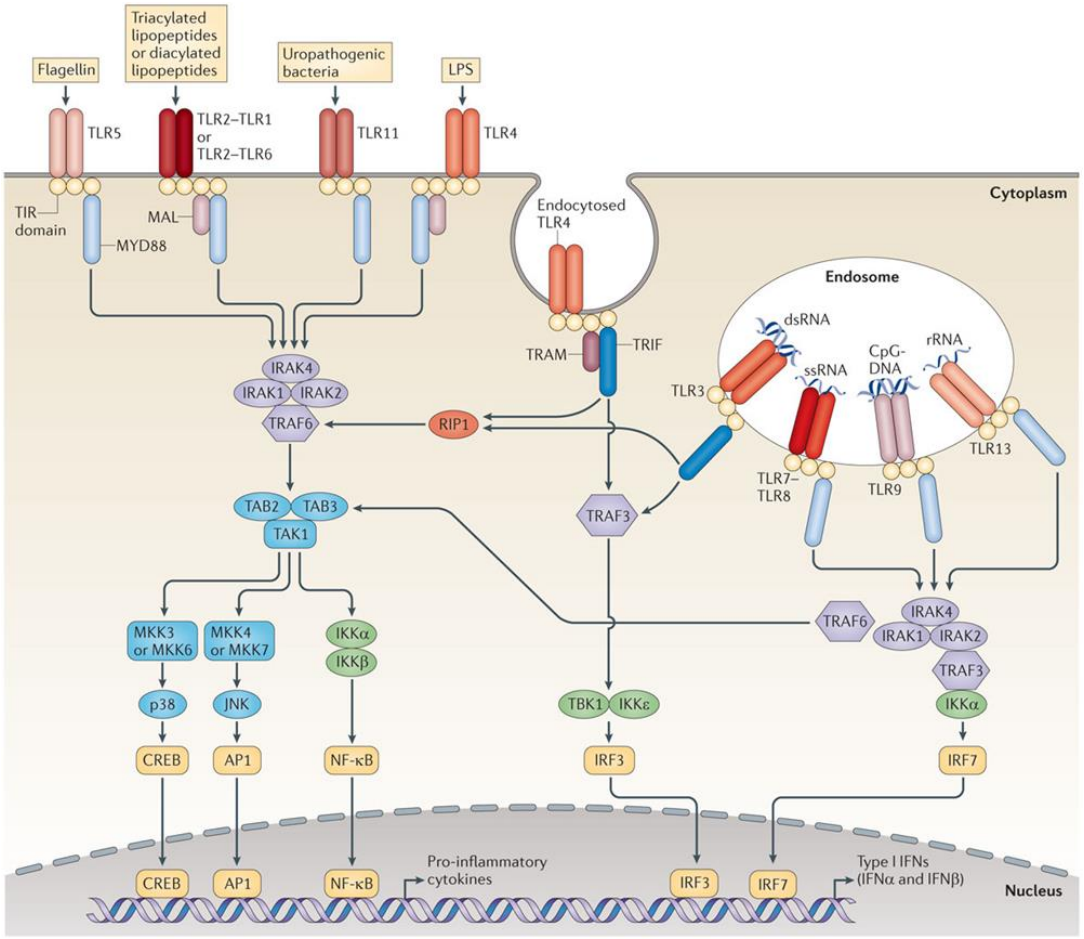

Figure 1. Mammalian TLR signaling pathways. TLR5, TLR11, TLR4, and the heterodimers of TLR2-TLR1 or TLR2-TLR6 bind to their respective ligands at the cell surface, whereas TLR3, TLR7-TLR8, TLR9, and TLR13 localize to endosomes, where they sense microbial and host-derived nucleic acids. TLR4 localizes at both the plasma membrane and the endosomes. TLR signaling is initiated by ligand induced dimerization of receptors. Following this, the TIR domains of TLRs engage TIR domain-containing adaptor proteins (either MYD88 and MAL, or TRIF and TRAM). Engagement of the adaptors stimulates downstream signaling pathways that involve interactions between IRAKs and the TRAFs. Followed by the activation of MAPKs, JNK and p38, this leads to the activation of transcription factors, such as NF-κB, IRFs, CREB and AP1 [6].

The MyD88-dependent pathway is commonly shared by all TLR signaling pathways, with the exception of TLR3-mediated responses. For instance, TLR2 and TLR4 signaling require the adaptor Mal as the bridge linking to MyD88. Subsequently, MyD88 interacts with IL-1R-associated kinase (IRAK)-4 to activate other IRAK family members, IRAK-1 and IRAK-2. Upon activation, the IRAKs dissociate from MyD88 and interact with TNFR-associated factor 6 (TRAF6). Together with an E2 ubiquitin-conjugating enzyme, the complex catalyzes the synthesis of a lysine 63 (K63)-linked polyubiquitin chain on TRAF6. TRAF6-medicated K63-linked polyubiquitination promotes TGF-β-activated kinase 1 (TAK1) activation. In turn,

TAK1 activates in the nuclear factor κB (NF-κB) pathway the IKK complex composed of IKK-α, IKK-β, and NF-κB essential modulator (NEMO). Subsequently, the IKK complex phosphorylates the NF-κB inhibitory protein IκBα, which is then degraded and leads to the release of NF-κB into the nucleus. Other than for the activation of the NF-κB pathway, TAK1 phosphorylates MKK6 in the mitogen activated protein kinase (MAPK) signaling. The activation of the MAP kinase cascade results in the formation of the transcription factor complex AP-1. Ultimately, both NF-κB and AP-1 complexes transcriptionally upregulate pro-inflammatory cytokines such as IL-1, IL-12, and tumor necrosis factor alpha (TNF-α) [7]. In addition to NF-κB-regulated cytokine expression, TLR7 and TLR9 are responsible for the production of type I Interferons (IFNs). TLR7 and TLR9 recognize viral single-stranded RNA and unmethylated cytosine-phosphate-guanine (CpG)-DNA, respectively. In a MyD88-dependent manner, the formation of a complex with IRAKs, TRAF6, TRAF3, IKK-α, and interferon regulatory factor 7 (IRF-7) is triggered. In the following, phosphorylated IRF7 translocates to the nucleus and subsequently activates the expression of type I IFNs for a potent antiviral defense in DCs [8, 9].

While TLR4 is internalized at cytoplasmic membrane and is trafficked to endosomes, its downstream signaling is switched from the MyD88-dependent to the TRIF-dependent pathway and requires TRAM as adaptor. Similarly, TLR3 triggers interferon-mediated antiviral defense through the adaptor TRIF instead of MyD88. TRIF in turn interacts with RIP1 and RIP3 (receptor interacting protein 1 and 3) through its C-terminal RIP homotypic interaction motif (RHIM). The N-terminal TRIF contains TRAF-binding motifs, which associate with TRAF3 and TRAF6. It was shown that TRAF3 promotes the activation of two IKK-related kinases, TANK-binding kinase 1 (TBK1) and IKK-*i* (also known as IKK-ε). Upon activation, TBK1 and IKK-*i* phosphorylate the transcription factor IRF3, which can induce IFN-β expression [10]. Furthermore, the TNFR1-associated death domain protein (TRADD) is critical in TRIF-dependent signaling. TRADD can form a complex with FAS-associated death domain-containing protein (FADD) and RIP1. On one hand, TRADD mediates the attachment of K63-polyubiquitin chains on RIP1, which is sufficient to activate the NF-κB pathway directly [11]. On the other hand, NF-κB-dependent inflammatory responses are indirectly also triggered by the activation of caspase-8 and caspase-10 through FADD [12].

1.1.2 Host adaptive immunity

During the presentation of bacterial antigens to the immune system, the adaptive immunity is developed. It is composed of antibody-mediated immunity (AMI) and cell-mediated immunity (CMI) which are carried out by B cells and T cells, respectively (Fig. 2) [13]. In AMI, activation of B cells results in expanding two types of daughter cells, plasma cells and memory B cells. The plasma cells produce a variety of specific antibodies (Abs), known as immunoglobulins (Ig), which are secreted to circulate in the blood stream and the lymphatic system. The classical functions of Abs include the neutralization of toxins and viral particles by directly blocking their access to host receptors. Moreover, Abs facilitate microbial clearance. They bind as so-called "opsonins" to foreign components and label them for clearance. Such antibody-ligand complexes are recognized and neutralized by immune cells, which bind the antibodies through the interaction with specific Fcγ receptors (FcγRs) and complement receptors (CRs). The most potent opsonins is IgG, which is bound to FcγRI (CD64) on the surface of macrophages and neutrophils, thereby promoting phagocytosis. The alternative complement system utilizes immune complexes formed by IgG or IgM with antigens to clear complement-coated pathogens via osmotic lysis [14]. Furthermore, antibody-dependent cellular cytotoxicity (ADCC) occurs when immunoglobulin G (IgG) simultaneously engages the antigens on the target cells and FcγRIII (CD16) on natural killer (NK) cells. During this process, activated NK cells synthesize cytokines such as IFN-γ and mediate the killing of target cells [15]. In addition, it has been shown that eosinophils also use ADCC to kill IgE-coated parasitic worms known as helminths [16].

CMI is the major defensive response against intracellular bacteria. First, foreign antigens are detected by antigen-presenting cells (APCs), such as DCs and macrophages. Upon the activation of APCs, fragments of the antigen are displayed with the major histocompatibility complex (MHC) at the surface of APCs to initiate the T cell-mediated responses. Two types of T cells play pivotal roles in CMI: $CD4^+$ helper T cells (Th) and $CD8^+$ cytotoxic T cells (CTL). In a classical model, the $CD4^+$ helper T cell responses are subdivided into type 1 Th (Th1) and type 2 Th (Th2) immunities. Generally, Th1 cells regulated by the transcription factor Tbet produce distinct cytokines, particularly IFN-γ. Th1-dominant responses predominantly support

phagocytic cells to attack the intracellular pathogens and develop the delayed-type hypersensitivity (DTH) skin in response to viral or bacterial antigens. By contrast, Th2 cells regulated by the transcription factor GATA3 are heavily reliant on IL-4 to trigger the humoral immunity and eosinophil activation to eliminate extracellular organisms. Th1 and Th2 responses are considered mutually exclusive due to specific cytokines secreted in the microenvironment [17]. However, both are inhibited by a heterogeneous family of T cells, known as adaptive T regulatory (Treg) cells. Treg cells are devoted to suppressing immune responses by producing anti-inflammatory cytokines such as transforming growth factor-β (TGF-β) and IL-10 [18, 19]. Recently, beyond the Th1 and Th2 cells, a distinct subset of CD4+ T cells has been discovered and named as Th17 cells. Initially, the function of Th17 cells appears to be the clearance against bacteria and fungi. Other than that, increasing evidence suggests that Th17 cells are potent inducers of tissue inflammation in association with autoimmune diseases, such as multiple sclerosis, rheumatoid arthritis, and Crohn's disease [20].

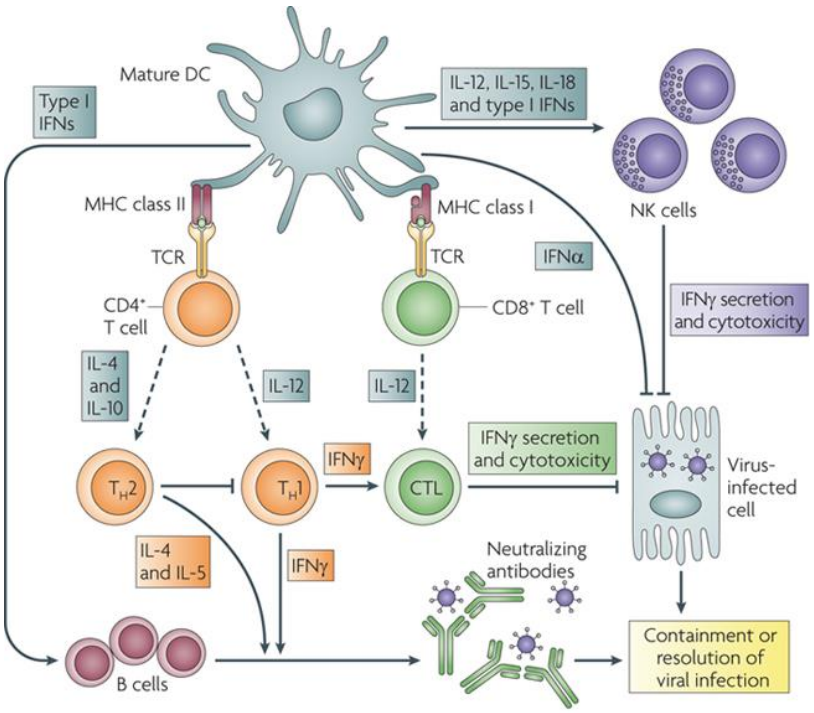

Figure 2. Function of dendritic cells in the immune response. Following the uptake of foreign antigens, dendritic cells migrate to lymphoid tissue to prime naïve $CD4^+$ T cells and $CD8^+$ T cells. In addition, activated DCs produce a range of cytokines, such as IFNα, IL-12, and IL-15, which in turn activate NK cells. Depending on the cytokine signal, $CD4^+$ T cells differentiate into Th1 or Th2 cells (dashed arrows). Th1 cell-mediated IFNγ secretion stimulates the activation of CTLs and the production of antibodies by B cells. Th2 cell-mediated cytokine production simulates antibody production by B cells but inhibits activation of Th1 cells [13].

In addition to the $CD4^+$ effector cell response, $CD8^+$ CTLs eliminate the intracellular microbes by recognizing foreign peptides presented by MHC class I complex on the surface of infected target cells which have to be eliminated. The pro-apoptosic function of CTLs is based on the cytotoxic proteins: perforin and granzymes. The main function of perforin is to facilitate delivery of the granzymes into target cells by forming pores in the target cell membrane. Upon release into the cytoplasm, the granzymes cleave various substrates, including caspases, to initiate apoptosis. However, CTLs can kill target cells also in a granule-independent mechanism through a unique membrane receptor-ligation complex. The Fas ligand of $CD8^+$ and of some $CD4^+$ T cells is able to induce apoptosis when it binds to Fas of the target cells. Besides the direct cell killing, IFN-γ secreted by CTLs synergistically contributes to the inhibition of viral replication and activation of macrophages for host defense [21].

1.1.3 Dendritic cells

The immune response to bacterial infection is based on a combination of both innate and adaptive immunity. As known, DCs are the most effective APCs specialized in the cross talk between innate and adaptive immune responses. Although DCs are a heterogeneous group of cells, they share several common features. All DCs originate from CD34 bone marrow stem cells. Through the blood stream, precursor DCs are strategically seeded to peripheral sites such as the lung, skin, or gut for antigen acquisition. Upon sensing of foreign antigens, phagocytic DCs mature and are transformed into efficient APCs which are able to activate T cell responses and initiate the adaptive immunity. Contrary to macrophages and neutrophils mediating the direct clearance of pathogens, the endocytic proteolysis of pathogens in DCs is aimed to produce antigenic peptides loaded onto MHC I and MHC II molecules and are presented on the DC surface to enhance the immune reaction. Moreover, DCs activated by pathogen encounter upregulate and display a variety of co-stimulatory molecules (e.g., CD40, CD80, and CD86) which bind to the complementary molecules on T cells (e.g., CD40L, CTLA-4, and CD28). In their maturation process, DCs have undergone cytoskeletal arrangements upregulate the expression of chemokine receptors (e.g., CCR7 and CXCR4) and adhesion molecules, which makes them ready for migration through the lymph to secondary lymphoid organs [22]. In the T cell zone of secondary lymphoid organs, antigen-presenting DCs deliver the

activating signals to naïve T cells through the engagement of pathogen-derived peptides and co-stimulatory molecules. Simultaneously, cytokines (e.g., IL-12) secreted by maturated DCs also condition the Th1 immunity and/or CTL development. All signals appear to be required for full effector T cell generation (Fig. 3) [23-25]. Despite the function of DCs majorly as mediator between a pathogen assault and the cellular immune response, DCs are more than a simple "on/off" switch of the immune response. The developmental stages of DCs are critical for influencing the character of T cell differentiation. In the steady state, the secondary lymphoid organs contain mainly immature DCs that maintain T cell anergy. Furthermore, Naïve T cells can also be driven into a regulatory cell fate characteristic for tolerance. Under this condition, DCs reach a stage of semi-maturation where they express high levels of MHC II and co-stimulatory molecules, but the pro-inflammatory cytokine production is low or absent [26, 27].

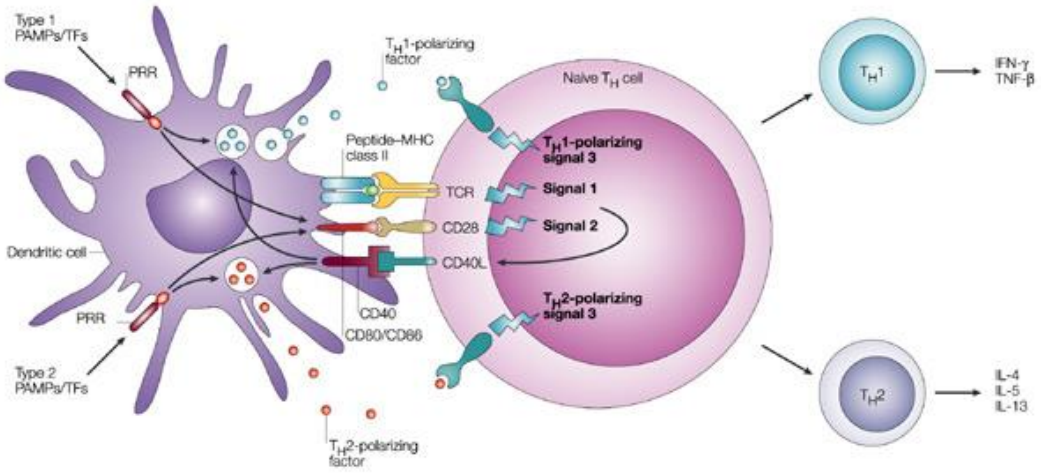

Figure 3. Three dendritic cell-derived signals required for T cell stimulation. Signal 1 is the antigen-specific signal mediated through T cell receptor (TCR) triggering by MHC II-associated peptides. Signal 2 is the co-stimulatory signal, mainly mediated by ligation of CD28 with CD80 and CD86. Signal 3 is the polarizing signal that is regulated by various soluble or membrane-bound factors, such as IL-12 and CCL2, which promote the development of Th1 or Th2 cells, respectively [24].

1.2 Bacterial defense against host immune responses

Central components of innate and adaptive immune responses to counter infectious agents are the phagocytes. Phagocytic cells are able to internalize pathogens for clearance and recruit additional immune cells to amplify host immune responses.

However, bacteria evolve rapidly in relation to their host. Consequently, pathogenic bacteria have developed a range of strategies to overcome host immunological defenses, which contribute to the virulence of the microbe and the pathology of the disease. In the following paragraphs, various molecular mechanisms used by bacteria to subvert the functions of phagocytes in order to hide from the host immune system will be discussed.

1.2.1 Avoidance of phagocytosis

Phagocytosis constituting the first line of host defense provides an efficient way for the removal and destruction of microbial pathogens. Unlike intracellular bacteria that develop sophisticated strategies to survive within phagocytic cells, other bacteria have evolved mechanisms to prevent phagocytosis, thereby impairing the development of cellular immunity and enhancing the extracellular survival. The first step of phagocytosis is the receptor-mediated recognition, classified into opsonin-dependent (e.g., FcγRs and CRs) or opsonin-independent (e.g., mannose receptors, type A scavenger receptors, and integrins) mechanisms [28]. To counter their recognition, surface antigenic variation is one of the most common strategies of bacteria. For example, *Neisseria spp.* alters the antigenicity of several surface molecules, including pilus components, to avoid FcγR-mediated phagocytosis. Other bacteria (e.g., *Streptococcus pneumoniae*, *Escherichia coli* (*E. coli*) K1, *Klebsiella pneumoniae*, *Neisseria meningitidis* and *Staphylococcus aureus*) create capsules of surface polysaccharides to physically prevent the complement deposition in the opsonization process [29-33]. In the case of *Streptococcus pyogenes*, its M proteins are not only major virulence and antigenic determinants, but play themselves a major and so far controversial role in resistance to phagocytosis [34]. Similarly, YadA adhesin of *Yersinia enterocolitica* binds plasma proteins (e.g., factor H) to interfere with complement-mediated opsonization [35].

Other than surface molecule variation, pathogenic bacteria harbor antiphagocytic properties in their effector proteins that they deliver through secretion systems at the site of bacterial direct contact. The protein tyrosine phosphatase (PTP) YopH of *Y. enterocolitica* was first effector described with an antiphagocytic function. It dephosphorylates host signaling proteins which are activated by the engagement of

surficial receptors [36]. Another *Yersinia* effector YopE mimicking a eukaryotic GTPase activating protein prevents actin polymerization and phagocytosis by inactivating small GTPases [37]. Similarly as YopE, two toxins of *Pseudomonas aeruginosa*, ExoS and ExoT, disrupt the internalization by targeting the GTPase family [39, 40]. YopT, a cysteine protease, exerts an influence on actin filaments, which results in excessive depolymerization and suggests for YopT a role in antiphagocytosis [38]. A mechanism neither targeting small GTPases nor actin directly, is used by the extracellular pathogen *enteropathogenic E. coli* (EPEC), which shows neutralization of phagocytic activity via inhibition of the PI3K-dependent phagocytic signals through its T3SS-dependent effectors [41].

1.2.2 Prevention of intracellular pathogen degradation

Various bacteria reside in an assortment of organelles: early endosomes (*Mycobacterium tuberculosis*), late endosomes (*Salmonella* typhimurium), lysosomes (*Coxiella burnetii*), and rough endoplasmic reticulum (*Legionella pneumophila*) [42, 43]. For intracellular bacteria to survive within phagocytes, they have to divert themselves from fatal delivery to the lysosome. To escape from the phagosome, *Shigella* is released into the cytosol via Ipa-mediated lysis of the endocytic structure surrounding it. *Listeria monocytogenes* and some *Rickettsia* species secrete lysins to effectively perforate the vacuolar membrane. The common strategy of intracellular bacteria to escape their degradation in a lysosomal compartment is the blockage of phagosome-lysosome fusion, although it is not well understand how these pathogens alter the involved vesicle transport to their benefit. *M. tuberculosis* persists in macrophages and arrests the phagosomal maturation. To achieve this, a bacteria-containing phagosome recruits early phagosomal proteins such as coronin-1 but excludes the vesicular proton ATPase from the phagosomal membrane, which results in a failure of organelle acidification and helps maintain an intraphagosomal environment permissive for pathogen survival [44, 45]. Similarly, VacA of *Helicobacter pylori* disrupts the process of phagosome maturation by the recruitment and retention of coronin-1. Besides that, VacA supports the formation of large vesicular compartments called megasomes for *H. pylori* persistence in macrophages [46]. Likewise, many other bacterial factors are described to support the exploitation and modification of endocytic compartments to the benefit of the pathogen. For

example, the RalF protein of *L. pneumophila* is delivered through the Dot/ICM type IV secretion system to the host cytoplasm where it functions as a GTPase exchange factor to recruit ARF1 to bacteria-containing phagosomes for creation of a replicative organelle [47]. Whereas in *L. pneumophila* the T4SS plays a central role, it is the T3SS in *S.* typhimurium. The Salmonella pathogenicity island 2 (SPI-2) T3SS is used to secrete two effector proteins SseJ and SifA, which were identified to be responsible for the vacuolar membrane stability, which is crucial for bacterial replication within the host cell [48].

Another antimicrobial mechanism of phagocytic cells to keep intracellular pathogens in check is through reactive nitrogen intermediates (RNIs). To protect themselves from such toxic intermediates, *S.* typhimurium interferes with the recruitment of nitric oxide synthase (iNOS) to the *Salmonella*-containing phagosome by the action of SPI2 [49]. Similarly, *Salmonella* SPI2 is also required to prevent phagocyte NADPH oxidase-mediated killing [50]. Bacterial pathogens have also evolved ways to detoxify iNOS and thereby avoid killing. *H. pylori* produces arginase to degrade the iNOS substrate L-arginine, thereby avoiding NO-dependent killing [51]. For *Citrobacter rodentium*, an infection causes a remarkable iNOS activity but the iNOS level surrounding the bacteria is very low, suggesting that bacteria locally limit their exposure to host-derived NO [52].

1.2.3 Attenuation of pro-inflammatory responses

Interference with intracellular signal transduction cascades

Upon antigen recognition, a diverse set of cellular PRRs triggers intracellular signal transduction cascades for the secretion of immunomodulatory chemokines and cytokines as antimicrobial defense mechanisms. An increasing number of examples shows that bacterial pathogens utilize their secreted proteins to dampen host innate immune responses by interfering with two main inflammatory pathways: the MAPK signaling and the NF-κB pathway (Fig. 4) [53]. One of the earliest studies discovered anthrax lethal toxin (LF) of *Bacillus anthracis* as a metalloproteinase, which cleaves the amino terminus of MAPKK1 and MAPKK2 for the direct inhibition of MAPKs [54]. In addition, the acetyltransferase YopJ of *Y. pestis* targets multiple members of the MAPK kinase superfamily (e.g., all mitogen-activated protein kinase kinases

(MKKs) and IKKβ, excluding IKKα) to prevent them from target phosphorylation. The functional consequence of YopJ is the suppression not only of MAPK, but also of NF-κB pathways, which results in downregulation of various cytokines, chemokines, and adhesion molecules (e.g., TNF-α, IL-8, and intercellular adhesion molecule-1 (ICAM-1)) [55]. Both AvrA of *Salmonella* and VopA/P of *Vibrio parahaemolyticus* which are homologous to YopJ show similar acetyltransferase activity. AvrA specifically targets MAPK4 and MAPK7 of the c-Jun NH2-terminal kinase (JNK) signaling pathway [56]. VopA/P inhibits the MAPK signaling pathways by acetylating MKKs [57, 58]. A different strategy to interfere with MAPK signaling is followed by *Shigella flexneri*. Its type III effector protein OspF (a homolog to the *Salmonella* SpvC and *Pseudomonas syringae* HopAI1) was discovered as a phosphothreonine lyase to catalyze a β-elimination reaction of phosphothreonine to a β-methyldehydroalanine, thus permanently dephosphorylating host MAPK enzymes. The OspF family takes advantage of a conserved MAPK docking motif (D motif) in mammals to specifically target the host substrates and inhibit the inflammatory activation [59].

Beside the MAPK kinase signaling, the NF-κB pathway is another essential route involving TLR recognition. In the classical NF-κB pathway, NF-κB/p65 proteins are bound and inhibited by IκB proteins. Upon stimulation, kinase activity of the NEMO/IKKα/IKKβ complex is activated to free NF-κB/p65 complexes, which translocate to the nucleus and induce target gene expression. Several bacterial pathogens take advantage of the inhibition of NF-κB signaling pathways, thus greatly suppressing the induction of inflammation. *Shigella*, for instance, has evolved several unique mechanisms to interfere with NF-κB signaling transduction. OspI of *S. flexneri* deamidates the E2 ubiquitin ligase UBC13, thus prohibiting TRAF6 autopolyubiquitination [60]. *Shigella* IpaH9.8, an E3 ubiquitin ligase, targets the NEMO complex for proteasomal degradation [61]. Besides, *Shigella* OspG is designed to inhibit the NF-κB-mediated inflammation by reducing E3-mediated ubiquitination of IκB and thereby preventing the dissociation of IκB/NF-κB/p65 complexes [62]. The modulation of NF-κB-dependent responses is also critical to the success of attaching/effacing (A/E) human pathogenic *E. coli* (EPEC and EHEC). One of the type III effector proteins discovered in A/E pathogens is the translocated intimin receptor (Tir), which contributes dual functions to bacterial pathogenicity,

including the strong bacterial attachment to host cells and the suppression of host innate immune responses. To down-regulate the inflammatory cytokines, the tyrosine-based inhibitory motif (ITIM)-like motifs of the Tir effector promote recruitment of SHP-1 and SHP-2 to subsequently inhibit the ubiquitination of TRAF6, thereby dampening both MAPK and NF-κB pathways as introduction in chapter 1.1.1 [63, 64]. Beyond Tir, some Nle proteins of A/E pathogens are identified to specifically inhibit NF-κB activation. In response to TNF-α stimulation, NleB targets glyceraldehyde-3-phosphate dehydrogenase (GAPDH) as an interaction partner to suppress TNF-α-dependent TRAF2-mediated polyubiquitination [65]. Furthermore, NleC and NleD catalyze the cleavage of p65 and thereby block NF-κB and AP-1 activation [66]. NleE, a homolog of *Shigella* OspZ, possesses S-adenosyl-L-methionine-dependent methyltransferase activity to disrupt the binding of TAB2 and TAB3 to ubiquitin chains, which disables the activation of TAK1 and IKKs. Ultimately, NleE prevents thus the NF-kB components from being released for translocation to the nucleus [67].

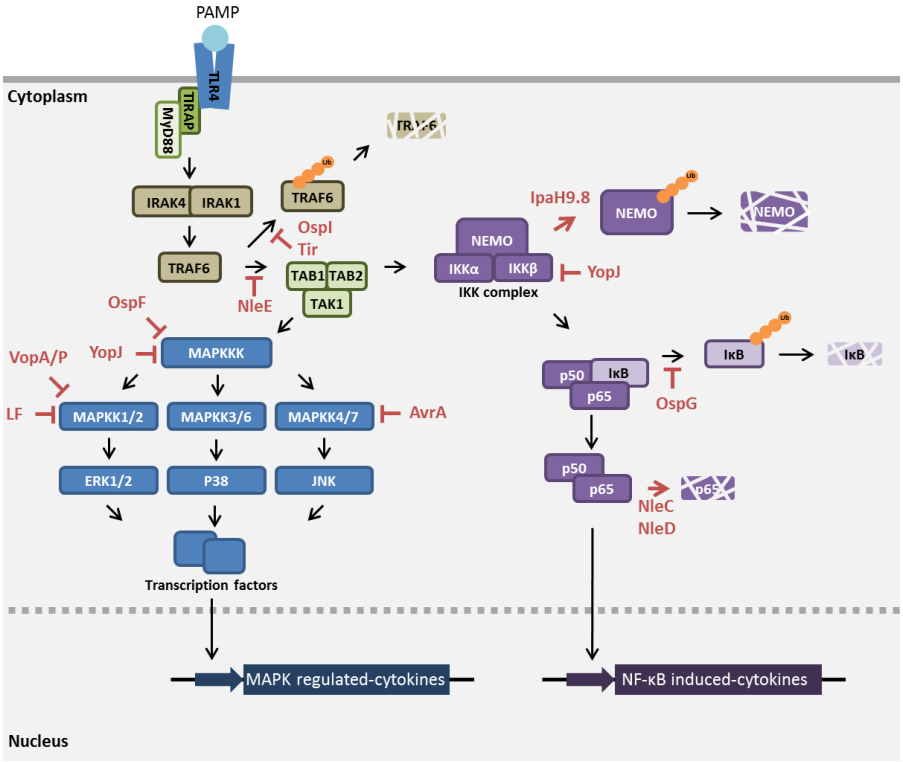

Figure 4. Bacterial effectors that manipulate inflammatory pathways. In a MyD88-dependent manner, TLRs trigger intracellular signal transduction cascades (MAPK and NF-κB) for the secretion of immunomodulatory cytokines. Bacterial effector proteins inhibit this process in many different ways [52].

Some cases of bacterial infections show a dampening effect on the host inflammatory cytokines, but the molecular mechanisms behind such phenotypes are not well elucidated. With unknown targets, *Yersinia* YopH contributes to the downregulation of TNF-α, IL1β, and the monocyte chemoattractant protein-1 (MCP-1) by suppressing the PI3K/Akt pathway. Furthermore, YopM possibly interferes with the expression of IL-15 receptor α (IL-15Rα) and IL-15, thereby resulting in global depletion of NK cells in hosts [68]. A recent study reveals that YopM directly binds caspase-1 and blocks formation of the mature inflammasome to prevent cell death and inflammation [69]. Unlike *Yersinia* which establishes acute infection, *M. tuberculosis* promotes long-term persistence. In the latent phase of infection, *M. tuberculosis* suppresses IL-12 expression. Furthermore, *M. tuberculosis* and LPS of *H. pylori* bind to the C-type lectin DC-SIGN, which blocks Th1 development and blocks DC maturation. [70, 71]. Additionally contributing to the inability of bacterial eradication during *M. tuberculosis* infection is the inhibition of macrophage responses to IFN-γ without inhibiting the production of NO [72]. In another bacterial pathogen, *Brucella abortus*, the TIR-contaning protein Btp1 (a homolog of *Salmonella* TlpA) inhibits the process of DC maturation including the repression of cytokines and the limitation of antigen presentation [73]. Although *Francisella tularensis* induces the phenotypic maturation of infected DCs, it represses the secretion of pro-inflammatory cytokines (e.g., TNF-α) and replicates efficiently within DCs [74].

Suppression of innate immune secretory mechanisms

Bacterial pathogens harbor a variety of elegant strategies to dampen the host inflammatory response by interfering with cellular signal pathways. Recent evidence reveals that bacteria have evolved alternative mechanisms to inhibit innate immunity by blocking protein trafficking. The host general secretory pathway (GSP) delivers molecular cargo (e.g., cell-surface receptors and cytokines) from the endoplasmic reticulum (ER) to the Golgi apparatus and eventually releases proteins from the cell by vesicular fusion of the cytokine- and receptor-containing carriers with the plasma membrane. In general, secretory proteins cotranslationally enter the ER and are subsequently transported through different membrane bound compartments by means of vesicular transport. The latter requires coat proteins, which help collect cargo and

support vesicle formation. Key small GTPases in this process are ARF1 and SAR1, which regulate coat protein complexes I and II (COPI and COPII), which have their function in the vesicular anterograde and retrograde ER-Golgi and intra-Golgi transport. The type III effector proteins NleA (EspI), NleF, and EspG of A/E pathogens function as GSP inhibitors by targeting the early steps of GSP. Although the mechanism is not fully understood, it is clear that NleA directly interacts with the Sec24 subunit of COPII to inhibit the production of cargo-containing COPII vesicles at the ER-membrane destined for anterograde transport [75]. In contrast, NleF binds to the transmembrane protein Tmp21 to block COPI-type vesicles in the retrograde transport [76]. Furthermore, EspG servers as a bacterial catalytic scaffold and induces bi-directional traffic arrest by preventing the cycling of ARF1-GTP and by simultaneously inactivating Rab1 signaling [77]. *S. flexneri*, which is not an A/E pathogen, shows a similar strategy for GSP inhibition. Its VirA protein, a homolog of EspG, mediates the suppression of Rab1-mediated ER-to-Golgi trafficking [78]. Another *Shigella* effector IpaJ specifically cleaves the myristoylated glycine of ARF1 and numerous lipid-modified substrates, thereby resulting in profound Golgi fragmentation [79]. The rapid turnover of GTPase signaling networks is essential for surficial receptor localization and cytokine secretion. Thus targeting the host GTPases and their downstream pathways by bacterial effectors constitutes a powerful mechanism for host immune evasion.

1.2.4 Exploitation of anti-inflammatory cytokines

Inflammation is a sophisticated and protective response to infection by the host immune system. Secreted cytokines provide signals for the communication between various immune cells to coordinate their actions. Although the acute inflammatory response provides a beneficial front-line defense against the bacterial infection, a dysregulation of inflammatory processes may lead to a harmful and chronic state, which can lead to destruction of tissues and result in autoimmune disorders. To balance host inflammatory responses, immunosuppressive cytokines (e.g., IL-10) function as negative feedback mechanisms to deactivate macrophages and abate the development of Th1 immunity. IL-10 is produced by macrophages, DCs, B cells, and various subsets of $CD4^+$ and $CD8^+$ T cells. Effects of IL-10 on monocytes and macrophages include the inhibition of MHC class II and co-stimulatory molecule

expression as well as the downregulation of pro-inflammatory cytokine and chemokine secretion. Besides, IL-10 can act directly on $CD4^+$ T cells to inhibit cell proliferation and production of IL-2, IFN-γ, IL-4, IL-5, and TNF-α [80].

Many bacterial pathogens with a stealth strategy (e.g., *Bordetella bronchiseptica*, *M. tuberculosis*, *H. pylori*, and *L. monocytogenes*) markedly exploit these immunosuppressive properties of IL-10 to shut off the host inflammatory responses [81]. This can be exemplified by the type III effector BopN of *B. bronchiseptica*. BopN, involved in the downregulation of MAP kinases, is translocated into the nucleus and enhances the nuclear translocation of NF-κB associated with increased IL-10 production [82]. Upon *M. tuberculosis* infection, macrophages and monocytes secrete not only pro-inflammatory, but also anti-inflammatory, cytokines, notably IL-10. A recent publication reveals that TLR3 is important for the sensing of mycobacterial RNA to induce IL-10 production through PI3K/AKT signaling [83]. *H. pylori* infection causes the formation of tolerogenic DCs, which secrete IL-18 and efficiently induce $Foxp3^+$ regulatory Treg cells. This promotes host immune tolerance and consequently enhances bacterial persistence [84]. Besides Treg cells, IL-10 producing B cells are expanded at a relative early stage of *H. pylori* infection [85]. Similarly, B cells in the splenic marginal zone are dominant IL-10 producing cells in response to *L. monocytogenes* infection [86]. Interestingly, the impact of IL-10 is clearly determined by the timing and the site of its production where elevated IL-10 correlates with poor pathogen control by the host. Thus, IL-10 represents a regulatory cytokine which is exploited by the bacterial pathogens to establish a state of chronic infection.

1.2.5 Suppression of antigen presentation

As described in the above paragraphs, inhibition of phagocyte activation by bacterial effectors always results in the downregulation of secreted cytokines and along with it in the inability of antigen-presentation. Evidence exists bacteria also developed unique strategies to specifically disrupt the antigen-presenting complex. For example, one function of the 19 kDa lipoprotein of *M. tuberculosis* is to inhibit MHC class II processing and presentation. This inhibition is attributed to intracellular sequestration of MHC II molecules and to decreased expression of the class II transactivator (CIITA)

[87, 88]. Besides the MHC class II complex, CD1 expression on DCs, which is responsible for presenting lipid antigens to T cell recognition, is also interfered with by *Mycobacteria* infection. Via CR-3-mediated phagocytosis, *Mycobacteria* infection activates ATF-2, which binds to the CD1A promoter and thereby inhibits CD1 transcription [89]. Another example taken from *Salmonella* infection is the SPI2-T3SS-dependent suppression of intracellular loading of peptides on the MHC class II complex in DCs. The type III effectors (PipB2, SifA, SlrP, SopD2, and SspH2) of *Salmonella* are equally important for the interference with antigen presentation [90]. Furthermore, *Salmonella* infection induces T3SS-dependent polyubiquitination of HLA-DR which leads to removal of mature, peptide loaded MHC class II complexes from the cell surface [91]. This precise targeting of MHC class II molecules to reduce the presentation of antigens to T cells is crucial for bacterial evasion from the host adaptive immune response.

1.2.6 Blockage of acquired immunity

Most bacterial pathogens evade from the adaptive immune response by avoiding its activation as described above. However, few examples have shown that bacteria can directly counteract host acquired immunity. *Yersinia* YopH is responsible for inhibiting both T cell specific cytokine production and expression of the co-stimulatory receptor CD86 on B cells based on its phosphatase activity [92]. Also two cytotoxins of *H. pylori*, CagA through the type IV secretion system and VacA via a type V auto-transport secretion system, display immunomodulatory properties. It was shown that ectopical expression of CagA inhibits B cell proliferation by suppressing JAK/STAT signaling [93]. VacA in turn inhibits the stimulation-induced proliferation of $CD4^+$ T cells, $CD8^+$ T cells, and B cells [94]. In $CD8^+$ T cells but not in $CD4^+$ T cells, the cytoplasmic presence of VacA inhibits NFAT nuclear translocation and subsequently downregulates IL-2 secretion by blocking the calcium influx [95]. VacA also causes an aberrant Rac activation what results in actin polymerization disorders and ultimately in defects in T cell activation [96]. Also *Neisseria gonorrhoeae* infection arrests the activation and proliferation of $CD4^+$ T cells. The *Neisseria* Opa proteins bind to CEACAM1 containing an ITIM motif (cf. chapter 1.2.3), thereby suppressing T cell responses [97]. Another strategy developed by several mucosal pathogens (e.g., *Neisseria spp.* and various *Streptococci*) is to

secrete bacterial IgA proteases by an auto-transporter mechanism. The IgA proteases specifically cleave the secretory antibody IgA1 in the hinge region, thereby annihilating IgA1-mediated agglutination and bacterial elimination [98].

1.3 *Bartonella* species

The genus *Bartonella* constitutes a group of facultative intracellular pathogens with 24 different species evolutionarily subdivided into four lineages (Fig. 5) [99, 100]. *Bartonella* species (spp.) are highly adapted to mammalian reservoir hosts, and an infection thus results in a long-lasting intraerythrocytic bacteremia through distinct stealth-attack strategies [101, 102]. Depending on the level of adaptation to the host, the disease develops a broad spectrum of symptoms from subclinical to clinical manifestations with limited morbidity to even fatal disease. Although *Bartonella* infections are ubiquitous among mammals as principal reservoir hosts, the majority of human diseases are caused by three species: the human-specific species *B. bacilliformis* and *B. quintana*, and the zoonotic feline-specific species *B. henselae* [103]. *B. bacilliformis* elicits life-threatening Carrión's disease with two clinical phases: a primary acute stage of hemolytic anemia called "Oroya fever", and a secondary chronic stage "verruga peruana" characterized by skin nodules and mulaire lesions (erythematous round lesions) along with bleeding, which lead to fibrosis [104, 105]. Trench fever caused by *B. quintana* is usually mild and rarely fatal with characteristic five-day cycle of relapsing fever [106]. People are usually infected with *B. henselae* through cat scratches or cat fleas and immunocompetent patients typically suffer from cat scratch disease (CSD), characterized by local lymph node swelling and fever [107]. In contrast, immunocompromised patients (e.g., acquired immune deficiency syndrome (AIDS) patients) with *B. henselae* or *B. quintana* infections can develop vasoproliferative lesions (bacillary angiomatosis). Bacillary angiomatosis is often associated with peliosis hepatis, which is characterised by multiple blood-filled cavities throughout the liver. [108]. These tumor-like lesions arise from bacterial infection of vascular endothelial cells leading to their enhanced migration and proliferation [109].

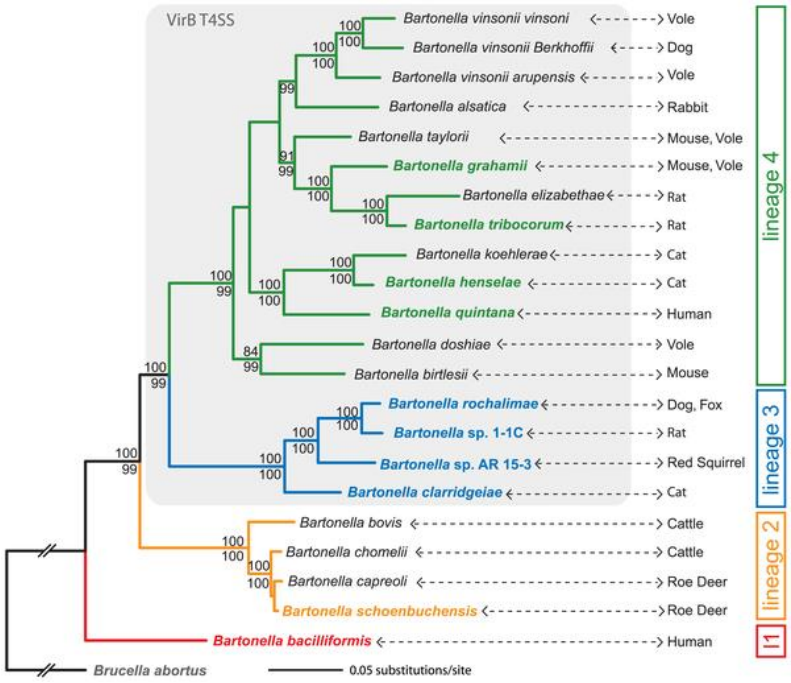

Figure 5. Phylogeny tree of *Bartonella spp*. The phylogenetic analysis is based on 478 core genome genes of ten sequenced *Bartonella spp.* (indicated by bold and color font) and *Brucella abortus*. Bartonellae are subdivided into the ancestral Lineage 1 and the modern Lineages 2-4. Lineages harboring the VirB T4SS are shaded in gray. The primary mammalian hosts are indicated for each species [100].

1.3.1 Cycle of *Bartonella* infection

The infection cycle of *Bartonella* is initiated with the inoculation of a mammalian reservoir host, following transmission via bloodsucking arthropods (Fig. 6) [110, 111]. Sand fly (*Lutzomyia verrucarum*) is the most important vector for *B. bacilliformis* as the agent of human bartonellosis [112]. Moreover, previous studies have shown that *B. quintana*, *B. henselae*, and *B. schoenbuchensis* can infect and replicate in the digestive systems of their vectors: human body lice (*Pediculus humanus corporis*), cat fleas (*Ctenocephalides felis*), and deer ked (*Lipoptena cervi*), respectively [113-115]. Generally, other hematophagous arthropods are also to be considered as transmission vectors in which *Bartonella* can survive and gain access to new hosts. For example, ticks and biting flies are potential vectors of *Bartonella* spp. in nature.

Little evidence is available to understand precisely *Bartonella* infection stages between the inoculation into the skin (e.g., from the feces of arthropod vectors) and the bacteremic stage. As exemplified by *B. tribocorum* infection in the rat model, a preceding period of residence in a primary niche is essential before intravenous

inoculation. *B. tribocorum* seems unable to directly enter erythrocytes and thus rapidly clear out from circulating blood. During the primary phase of residence in a niche, bacteria remain below detectable levels for about four days and subsequently re-appear in the bloodstream, implying that *Bartonella* persists and becomes competent for erythrocyte interaction during colonization of the primary niche prior to blood-stage infection [116]. The synchronous release of bacteria into the bloodstream may recur at intervals of approximately five days and sustain the bacteremia for about ten weeks. Upon invasion of erythrocytes, bacterial replication and intraerythrocytic persistence enable continuous vector transmission [117].

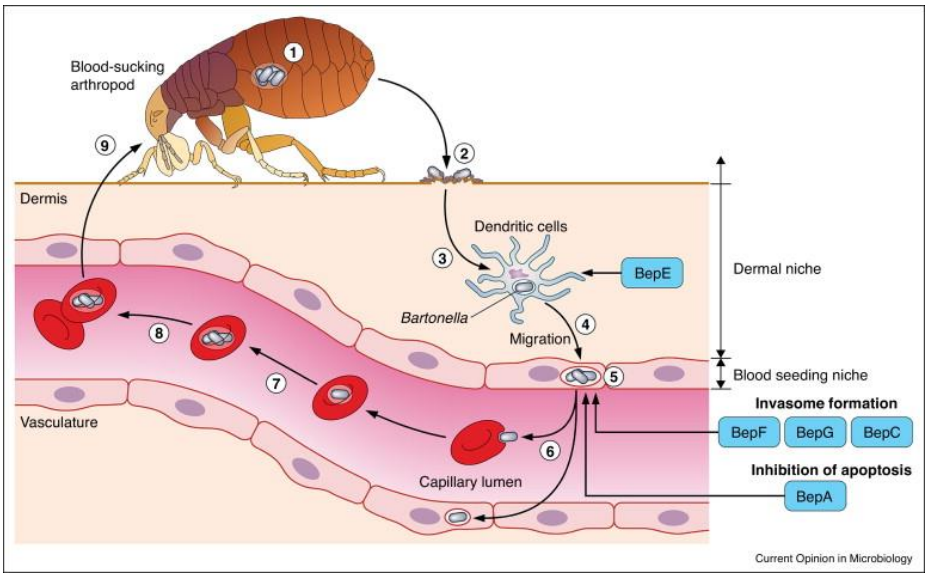

Figure 6. *Bartonella* infection strategy Following transmission by an arthropod vector (1), bartonellae colonize the dermis (2) and enter into migratory cells, likely DCs (3). DCs may disseminate bartonellae towards the primary niche (4). The vascular endothelium is considered as the primary niche and is referred to as the blood seeding niche (5). Bacteria are released into the bloodstream (6), where they invade erythrocytes and likely reinfect the primary niche. After limited replication (7), bacteria persist intraerythrocytically (8) competent for transmission by a bloodsucking arthropod (9) [111].

In vitro data show the marked affinity of *Bartonella* for endothelial cells. Their proximity to the bloodstream leads to the suggestion that endothelial cells may be one of the constituents of the primary niche. [118]. However, it remains elusive how it reaches its primary niche in the host. Although it is not yet supported by experimental data, it is tempting to speculate that *Bartonella* initially enters migratory cells, such as DCs, which assist the passage of bacteria from the typical intradermal inoculation environment to the primary site of infection. Moreover, the lymph node swelling caused by *Bartonella* infections may indicate that *Bartonella* is transported via the

lymphatic system. Consistently, a murine model of *B. henselae* infection showed that bacteria DNA are detectable in liver and lymph nodes already within six hours post intraperitoneal injection, proposing that lymphocytes or mononuclear phagocytes could be the vehicles of *Bartonella* transport [119]. Further, the most recent publication has revealed that *Bartonella* is capable of translocating bacterial effectors into DCs, thereby affecting cell migration [120]. Overall, current evidences strongly suggest that DCs may contribute the dissemination of *Bartonella* from the dermis to the lymphatic system eventually culminating in their release to the bloodstream. Further studies supporting this hypothesis including how *Bartonella* interacts with DCs by *in vitro* and *in vivo* models will be addressed in the next chapters.

1.3.2 *Bartonella* virulence factors

Bartonella adhesin A

The trimeric autotransporter adhesins (TAAs) are important virulence factors in numerous gram-negative bacteria, e.g., *Y. enterocolitica*, *N. meningitides*, *Haemophilus influenzae*, and *Moraxella catarrhalis*. TAAs are modularly constructed consisting of typical head, stalk and anchor domains and they perform type Vc secretion [121]. Most research on the TAAs of *Bartonella* has been performed on *Bartonella* adhesin A (BadA) which is the largest identified TAA with the size of 328 kDa per monomer and a length of about 240 nm [122]. The key functions of BadA in the molecular pathogenesis of *B. henselae* have been thoroughly studied with the Marseille strain (i.e., in the absence of a functional VirB/D4 T4SS: see chapter 1.3.3. for VirB/D4 T4SS). BadA contributes to the adhesion of *B. henselae* to extracellular matrix proteins (e.g., fibronectin (Fn), laminin, and collagens) and possesses antiphagocytic properties [123]. Furthermore, BadA plays an important role in the induction of host cell proangiogenic responses. In a VirB/Bep-independent manner, BadA promotes the activation of hypoxia-inducible factor 1 (HIF-1), a key transcription factor of angiogenesis [124], and the subsequent secretion of vasoproliferative cytokines, such as vascular endothelial growth factor (VEGF) [125]. With the exception of Fn binding, these functional properties are mediated by both the head and stalk domain of BadA whereas the stalk domain is exclusively responsible for Fn binding [126, 127].

VirB/D4 type IV secretion system

Type IV secretion systems (T4SSs) are ancestrally related to bacterial conjugation systems. A variety of bacteria intimately interacting with eukaryotic hosts utilize T4SSs to translocate bacterial effectors into recipient cells [128]. For the adaption to a wide range of mammalian hosts, *Bartonella* evolved two T4SSs, VirB/D4 and Trw. According to the prototype of *Agrobacterium tumefaciens*, the VirB/D4 T4SS consists of ten essential components, VirB2-11, and the coupling protein VirD4 serving as a substrate recognition module. Two signature-tagged mutagenesis (STM) screens in *B. birtlesii* and *B. tribocorum* showed that VirB/D4 T4SS is indispensible for the development of a successful bacteremia [129, 130]. Besides, the *B. tribocorum* infection model in rats strongly indicates that the VirB/D4 system is required at an early stage of infection before the onset of intraerythrocytic bacteremia [131]. To date, the VirB/D4 T4SS of *B. henselae* and its translocated effector proteins (Beps) are well studied in the Houston-1 strain (i.e., in the absence of a functional BadA). Although both VirB/D4 T4SS and BadA play crucial roles in *B. henselae* pathogenicity, most research studying *B. henselae* infections of human cells has been performed using *B. henselae* strains that either express a VirB/D4 T4SS but lack a full-length BadA or vice versa. The direct investigation of the potential functional interaction between BadA and the VirB/D4 T4SS is addressed in the Research article I (chapter 3.1). We show that VirB/D4-dependent effector secretion is negatively affected by BadA, but the functions of BadA itself remain intact when both factors are coexpressed in *B. henselae* [132]. However, in an earlier publication of our lab, a certain regulatory antagonism between VirB/D4 and BadA was found. Transcriptional analysis revealed that the expression of the VirB/D4 T4SS is upregulated whereas the one of BadA is downregulated under certain conditions in the *in vitro* model [133]. Therefore, VirB/D4 and BadA might not only have a functional interaction, but also their expression may be linked to balance the incorporation of both pathogenicity factors. Further experiments elucidating the regulatory patterns of these two systems are needed to understand the underlying mechanisms of gene regulation.

Seven distinct Beps (BepA-G) of *B. henselae* have been identified as conjugative substrates delivered through the VirB/D4 T4SS (Fig. 7) [109]. The Beps display a highly modular architecture by sharing at least one copy of the Bep-intracellular delivery (BID) domain and positively charged residues at the C terminus together

acting as secretion signal for their transport through the VriB/D4 T4SS. In a subset of the Beps (BepE-G), additional BID domains are present and likely developed functions adapted to interfere with the host cell. BepG is exclusively composed of four BID domains. Moreover, BepA-C are homologs carrying a N-terminal filamentation induced by cAMP (FIC) domain. FIC domains of *B. schoenbuchensis* VbhT and *B. rochalimae* Bep2 were shown to mediate AMPylation, i.e., the covalent transfer of an AMP moiety onto hydroxyl side chains of target proteins, thereby contributing to the posttranslational regulation of protein function [134-136]. This peculiar enzymatic activity is also detected for BepA of *B. henselae* [137]. The N-terminal regions of BepD-F contain tandem-repeated tyrosine-containing sequences as EPLYA (Glu-Pro-Ile-Tyr-Ala)-related motifs [138]. Upon translocation into endothelial cells, tyrosine residues of BepD and BepE undergo phosphorylation [139]. Further validation revealed that BepE binds Csk and SHP-2 in a phosphorylation-dependent manner [140]. However, none of the FIC domains or EPIYA-related motifs of *B. henselae* effectors has been demonstrated to contribute to *Bartonella* virulence. In the Research article II (chapter 3.2), we demonstrate for the first time that the subversion of cellular functions relates to the EPIYA-related motifs of BepD by using *in vitro* and *in vivo* models.

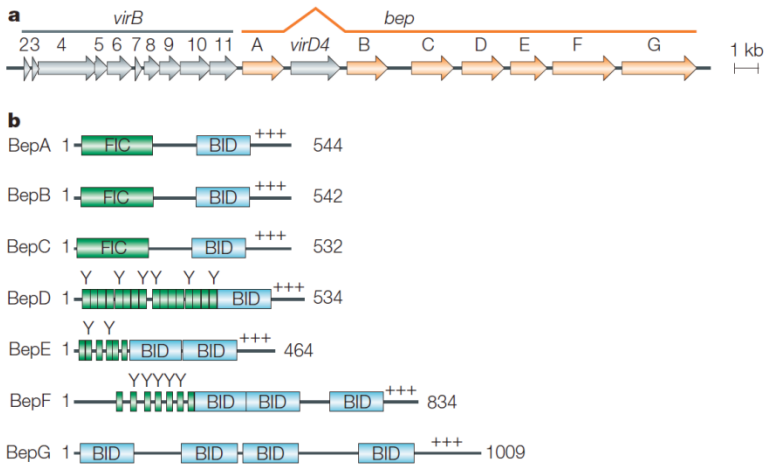

Figure 7. *Bartonella* VirB/VirD4 and Beps (a) The genetic structure of the *virB/virD4/bep* pathogenicity island, which encodes 18 type IV secretion-related proteins. (b) The domain structure of BepA-G. BID, Bep intracellular delivery; Fic, filamentation induced by cAMP; Y, tyrosine residue within a putative phosphorylation motif [109].

So far, several T4SS-dependent cellular phenotypes caused by *B. henselae* infection are described in association with a single effector or a subset of Beps. One example is the entry of *B. henselae* into host cells via invasomes. In a sequential process, *B.*

henselae is first taken up by the host cell in *Bartonella*-containing vacuoles (BCVs) within few hours after pathogen exposure [142]. A combination of BepC and BepF or BepG alone subsequently stall BCV-formation and lead to bacterial uptake in huge clusters, so called invasomes [143, 144]. This process goes along with massive rearrangements of the actin cytoskeleton and takes 16 to 24 hours [141, 142]. Invasome formation is elicited due to the inhibition of endocytosis-like uptake of individual bacteria in BCVs [143, 144]. It has been shown that the assembly of the F-actin invasome structure by *B. henselae* infection results from β1-integrin outside-in signaling mediated by FAK, Src kinase, paxillin, and vinculin in combination with talin1-mediated inside-out signaling [145]. A further example for the impact of Beps on host cell behavior relates to angiogenic properties of *B. henselae*. An in vitro three-dimensional spheroid sprouting assay disclosed that BepA profoundly induces capillary-like sprouting while the same process is inhibited by BepG; thus, both proteins seem to play a opposing role in controlling the angiogenic response triggered by *B. henselae* infection [143]. While promoting sprout formation, the VirB/Bep system antagonizes exogenous angiogenic stimulation of VEGFR2 signaling by VEGF, which is *Bartonella* induced [146]. These two independent lines of evidences suggest that the VirB/Bep system as an important factor balances the angiogenic potential of *B. henselae* with both pro- and anti-angiogenic characteristics. Furthermore, BepA efficiently prevents infected endothelial cells from apoptosis via elevating the cytosolic concentration of the second messenger cAMP [147, 148]. This BepA-mediated elevation of cAMP level depends on the stimulus of Gαs released from a G protein-coupled receptor [149]. Both *in vitro* phenotypes of BepA are closely related to its BID domain, likely through the same molecular activity. Additionally to the above, a recent publication of our lab shows that a deleterious cell fragmentation phenotype caused by BepC is restored by BID domains of BepE via the RhoA signaling pathway. Moreover, BepE is required for systemic dissemination from the dermal inoculation site to the bloodstream in the *in vivo* infection model [120].

Trw type IV secretion system

Unlike VirB/D4, the Trw T4SS apparently neither harbors a coupling protein nor does it translocates any known effectors. It carries multiple tandem gene duplications of *trwL* and *trwJIH* forming a multiprotein complex that spans the inner and outer

bacterial membranes and possesses a hypothetical pilus structure [150]. Moreover, only TrwJ1 and TrwJ2 are localized at the cell surface and bind to the band3 protein, one of the major outer-membrane glycoproteins of erythrocytes, thereby promoting the recognition of erythrocytes [151]. Strikingly, host specificity is defined by the capacity of *Bartonella* species to adhere exclusively to erythrocytes of their reservoir host in a Trw T4SS-dependent manner [129, 130].

1.3.3 Immune evasion and immunomodulation

Some bacterial pathogens cause an acute infection characteristically inducing disease symptoms that overwhelm the host innate defenses. In contrast, *Bartonella* using stealth-attack strategies characteristically avoid elicitation of a host immune response via both passive immune evasion and active immunomodulation. At a late stage of *Bartonella* infection, the colonization of the intraerythrocytic niche protects bartonellae from both innate and adaptive immunity [152]. As described above (see chapter 1.1.1), the LPS of gram-negative bacteria are endotoxins recognized by TLR4 and trigger a strong inflammatory response, which prohibits bacterial persistence. Critically, LPS of *Bartonella* shows unusual structural features connected to a significantly lower endotoxic activity [153]. The immunomodulatory property of *Bartonella* LPS is extensively studied in *B. quintana*. Interestingly, *B. quintana* LPS acts as a TLR4 antagonist leading to transcriptional downregulation of the pro-inflammatory cytokines (e.g., TNF-α, IL-1β, and IL-6) whose production is triggered by *E. coli* LPS. However, a LPS-associated component of *B. quintana* selectively stimulates the secretion of IL-8 likely via TLR2 and induces leukocytosis [154-156]. Furthermore, many studies have reported that *Bartonella* infection (e.g., *B. bacilliformis*, *B. quintana*, and *B. henselae*) elevates IL-10 levels in human patients and various experimental models [157-160]. IL-10, as a multifunctional immunoregulatory molecule, is critically involved in persistence of bacteria by disarming innate and adaptive responses. [161]. Strikingly, *B. birtlesii* loses the ability to establish bacteremia in the IL-10 deficient mice, implicating that IL-10 plays a pivotal role for *Bartonella* pathogenicity [162].

From the severity point of view of the disease symptoms, *B. birtlesii* infection establishes longer and higher bacteremia in CD4 deficient mice (i.e., lacking T helper

cells) compared to wild-type mice. In contrast, the bacteremia development is indistinguishable between CD8 deficient and wild-type mice [162]. In accordance with the central role of phagocytic cells and humoral immunity in *Bartonella* clearance, the course of *B. grahamii* bacteremia is transient in immunocompetent mice. However, bacteremia persists in $Igh^{-/-}$ mice (i.e., lacking Ig-producing B cells) and $Rag^{-/-}$ mice (i.e., devoid of both an intact B and T cell compartment). To further demonstrate that antibodies are necessary to abrogate *B. grahamii* infection, adoptive transferring of immune serum against *B. grahamii* into infected immunocompromised recipients results in a transient bacteremia congruent with the situation in an immunocompetent host [163]. In the case of feral cats with a natural infection of the feline-specific *B. henselae*, Th2 responses are induced culminating in the secretion of specific antibodies. Although the production of specific antibodies plays an important role in removing *Bartonella* from the bloodstream, it cannot eliminate relapses of bacteremia [164, 165]. Consistently, another report showed that passive antibodies to *B. henselae* protect cats from clinical disease symptoms but fail to prevent the establishment of bacteremia [166]. The induction of Th2, which is known to suppress Th1 immune responses, may contribute to the establishment of *B. henselae* persistence in naturally infected cats [167]. In accordance with this, experimental infection with *B. henselae* in cats revealed that rapid bacteremia clearance is associated with Th1 immune responses including IFN-γ and TNF-α production [156]. Consistently, various studies of the heterologous murine model have reported that *B. henselae* infection elicits Th1 responses and fails to cause bacteremia [119, 158, 168]. In addition, although *B. henselae* is able to enter and survive within the mouse macrophags cell line J774, IFN-γ mediated activation of macrophages significantly decreases the number of recoverable bacteria [169]. These results strongly suggest that the Th1 responses associated with IFN-γ secretion play a crucial role in recruiting phagocytes and activating T helper-mediated immunity for the elimination of bartonellae. Even so, it remains unclear how natural infection of *Bartonella* in the reservoir host leads to Th2-dominated responses instead of the Th1 immunity which is triggered in the experimental setup. In light of the complex interplay between pathogen and immune system, it has to be emphasized that the inflammatory profile observed after *Bartonella* infection in different hosts is inconsistent. This may partially explain the distinct outcome of *Bartonella* infection in reservoir and

incidental hosts.

Among CSD patients, the characteristic lymphadenopathy originates from the formation of B cell rich granulomas with continuous recruitment of infected macrophages. These macrophages undergo apoptosis and likely lead to self-limitation of CSD [170]. *In vitro* analysis revealed that *B. henselae*-driven DC activation goes along with classical phenotypic changes as the increase of surface expression of co-stimulatory molecules and MHC class II complex as well as the release of cytokines (e.g., TNFα, IL-6, IL-10, CXCL8, and CXCL13). These cytokines are known to activate and recruit B cells. Remarkably, CXCL13-producing DCs are observed in CSD granulomas and likely contribute to the B cell and neutrophil recruitment [160]. To investigate the mechanisms causing lymphadenopathy *in vivo*, a comparative analysis of *B. henselae* (feline-specific species) and *B. grahamii* (rodent-specific species) was performed by subcutaneous infection in mice. Interestingly, only *B. henselae* infection causes a massive and long-lasting regional lymph node (LN) swelling in wild-type mice as incidental hosts. *In vitro* analysis showed that the production of IFN-α/β by bone marrow-derived dendritic cells (BMDCs) is significantly lower in response to *B. henselae* compared to *B. grahamii*. As opposed to that, both *B. henselae* and *B. grahamii* are able to induce lymphadenopathy in IFN-α/β receptor-deficient (IFNARI$^{-/-}$) mice. Taken together, these findings indicate that homologous infection with *Bartonella* may induce the IFN-α/β secretion, which in turn exerts an inhibitory effect on the development of lymphadenopathy in its reservoir hosts [171]. In summary, both cellular and humoral immunity are essential for complete eradication of bartonellae from the hosts. Apparently, *Bartonella* actively counteracts the establishment of host immune responses to create a moderated inflammatory profile which is beneficial for bacterial persistence. However, *Bartonella* immunosuppression is restricted by host specificity. A mild *Bartonella* infection course is mostly observed in reservoir hosts, while the morbid course of infection in incidental hosts results from the failure in immunomodulation. Despite the phenotypic description of immunological attenuation during *Bartonella* infection, it is still elusive how *Bartonella* obstructs functions of the host immune system and which *Bartonella* virulence factors may contribute to it. These aspects will be addressed in the next chapters of the thesis.

1.4 References

1. Tang, D., et al., PAMPs and DAMPs: signal 0s that spur autophagy and immunity. Immunol Rev, 2012. 249(1): p. 158-75.
2. Medzhitov, R. and C. Janeway, Jr., Innate immunity. N Engl J Med, 2000. 343(5): p. 338-44.
3. Medzhitov, R., P. Preston-Hurlburt, and C.A. Janeway, Jr., A human homologue of the Drosophila Toll protein signals activation of adaptive immunity. Nature, 1997. 388(6640): p. 394-7.
4. Bowie, A. and L.A. O'Neill, The interleukin-1 receptor/Toll-like receptor superfamily: signal generators for pro-inflammatory interleukins and microbial products. J Leukoc Biol, 2000. 67(4): p. 508-14.
5. Akira, S., S. Uematsu, and O. Takeuchi, Pathogen recognition and innate immunity. Cell, 2006. 124(4): p. 783-801.
6. O'Neill, L.A., D. Golenbock, and A.G. Bowie, The history of Toll-like receptors - redefining innate immunity. Nat Rev Immunol, 2013. 13(6): p. 453-60.
7. Takeda, K. and S. Akira, TLR signaling pathways. Semin Immunol, 2004. 16(1): p. 3-9.
8. Negishi, H., et al., Evidence for licensing of IFN-gamma-induced IFN regulatory factor 1 transcription factor by MyD88 in Toll-like receptor-dependent gene induction program. Proc Natl Acad Sci U S A, 2006. 103(41): p. 15136-41.
9. Schmitz, F., et al., Interferon-regulatory-factor 1 controls Toll-like receptor 9-mediated IFN-beta production in myeloid dendritic cells. Eur J Immunol, 2007. 37(2): p. 315-27.
10. Tenoever, B.R., et al., Multiple functions of the IKK-related kinase IKKepsilon in interferon-mediated antiviral immunity. Science, 2007. 315(5816): p. 1274-8.
11. Ermolaeva, M.A., et al., Function of TRADD in tumor necrosis factor receptor 1 signaling and in TRIF-dependent inflammatory responses. Nat Immunol, 2008. 9(9): p. 1037-46.
12. Takahashi, K., et al., Roles of caspase-8 and caspase-10 in innate immune responses to double-stranded RNA. J Immunol, 2006. 176(8): p. 4520-4.
13. Lambotin, M., et al., A look behind closed doors: interaction of persistent viruses with dendritic cells. Nat Rev Microbiol, 2010. 8(5): p. 350-60.
14. Quie, P.G., Humoral factors in host defense against microbial invaders. Scand J Infect Dis Suppl, 1982. 31: p. 34-40.
15. Wang, S.Y., et al., NK-cell activation and antibody-dependent cellular cytotoxicity induced by rituximab-coated target cells is inhibited by the C3b component of complement. Blood, 2008. 111(3): p. 1456-63.

16. Giembycz, M.A. and M.A. Lindsay, Pharmacology of the eosinophil. Pharmacol Rev, 1999. 51(2): p. 213-340.
17. Mosmann, T.R., et al., Two types of murine helper T cell clone. I. Definition according to profiles of lymphokine activities and secreted proteins. J Immunol, 1986. 136(7): p. 2348-57.
18. Kidd, P., Th1/Th2 balance: the hypothesis, its limitations, and implications for health and disease. Altern Med Rev, 2003. 8(3): p. 223-46.
19. Romagnani, S., Regulation of the T cell response. Clin Exp Allergy, 2006. 36(11): p. 1357-66.
20. Bedoya, S.K., et al., Th17 cells in immunity and autoimmunity. Clin Dev Immunol, 2013. 2013: p. 986789.
21. Janeway CA Jr, T.P., Walport M, et al. , Immunobiology: The Immune System in Health and Disease., 2001.
22. MartIn-Fontecha, A., et al., Regulation of dendritic cell migration to the draining lymph node: impact on T lymphocyte traffic and priming. J Exp Med, 2003. 198(4): p. 615-21.
23. Guermonprez, P., et al., Antigen presentation and T cell stimulation by dendritic cells. Annu Rev Immunol, 2002. 20: p. 621-67.
24. Kapsenberg, M.L., Dendritic-cell control of pathogen-driven T-cell polarization. Nat Rev Immunol, 2003. 3(12): p. 984-93.
25. Reis e Sousa, C., Dendritic cells in a mature age. Nat Rev Immunol, 2006. 6(6): p. 476-83.
26. Mahnke, K., et al., Tolerogenic dendritic cells and regulatory T cells: a two-way relationship. J Dermatol Sci, 2007. 46(3): p. 159-67.
27. Lutz, M.B. and G. Schuler, Immature, semi-mature and fully mature dendritic cells: which signals induce tolerance or immunity? Trends Immunol, 2002. 23(9): p. 445-9.
28. Celli, J. and B.B. Finlay, Bacterial avoidance of phagocytosis. Trends Microbiol, 2002. 10(5): p. 232-7.
29. Claverys, J.P., et al., Adaptation to the environment: Streptococcus pneumoniae, a paradigm for recombination-mediated genetic plasticity? Mol Microbiol, 2000. 35(2): p. 251-9.
30. Silver, R.P., W. Aaronson, and W.F. Vann, The K1 capsular polysaccharide of Escherichia coli. Rev Infect Dis, 1988. 10 Suppl 2: p. S282-6.
31. Alvarez, D., et al., Capsular polysaccharide is a major complement resistance factor in lipopolysaccharide O side chain-deficient Klebsiella pneumoniae clinical isolates. Infect Immun, 2000. 68(2): p. 953-5.
32. Vogel, U., et al., Complement factor C3 deposition and serum resistance in

isogenic capsule and lipooligosaccharide sialic acid mutants of serogroup B Neisseria meningitidis. Infect Immun, 1997. 65(10): p. 4022-9.

33. Thakker, M., et al., Staphylococcus aureus serotype 5 capsular polysaccharide is antiphagocytic and enhances bacterial virulence in a murine bacteremia model. Infect Immun, 1998. 66(11): p. 5183-9.
34. Fischetti, V.A., Streptococcal M protein: molecular design and biological behavior. Clin Microbiol Rev, 1989. 2(3): p. 285-314.
35. China, B., et al., Role of the YadA protein in prevention of opsonization of Yersinia enterocolitica by C3b molecules. Infect Immun, 1993. 61(8): p. 3129-36.
36. Rosqvist, R., I. Bolin, and H. Wolf-Watz, Inhibition of phagocytosis in Yersinia pseudotuberculosis: a virulence plasmid-encoded ability involving the Yop2b protein. Infect Immun, 1988. 56(8): p. 2139-43.
37. Rosqvist, R., A. Forsberg, and H. Wolf-Watz, Intracellular targeting of the Yersinia YopE cytotoxin in mammalian cells induces actin microfilament disruption. Infect Immun, 1991. 59(12): p. 4562-9.
38. Zumbihl, R., et al., The cytotoxin YopT of Yersinia enterocolitica induces modification and cellular redistribution of the small GTP-binding protein RhoA. J Biol Chem, 1999. 274(41): p. 29289-93.
39. Garrity-Ryan, L., et al., The arginine finger domain of ExoT contributes to actin cytoskeleton disruption and inhibition of internalization of Pseudomonas aeruginosa by epithelial cells and macrophages. Infect Immun, 2000. 68(12): p. 7100-13.
40. Goehring, U.M., et al., The N-terminal domain of Pseudomonas aeruginosa exoenzyme S is a GTPase-activating protein for Rho GTPases. J Biol Chem, 1999. 274(51): p. 36369-72.
41. Celli, J., M. Olivier, and B.B. Finlay, Enteropathogenic Escherichia coli mediates antiphagocytosis through the inhibition of PI 3-kinase-dependent pathways. EMBO J, 2001. 20(6): p. 1245-58.
42. Swanson, M.S. and E. Fernandez-Moreira, A microbial strategy to multiply in macrophages: the pregnant pause. Traffic, 2002. 3(3): p. 170-7.
43. Rosenberger, C.M. and B.B. Finlay, Phagocyte sabotage: disruption of macrophage signalling by bacterial pathogens. Nat Rev Mol Cell Biol, 2003. 4(5): p. 385-96.
44. Sturgill-Koszycki, S., et al., Lack of acidification in Mycobacterium phagosomes produced by exclusion of the vesicular proton-ATPase. Science, 1994. 263(5147): p. 678-81.
45. Ferrari, G., et al., A coat protein on phagosomes involved in the intracellular

survival of mycobacteria. Cell, 1999. 97(4): p. 435-47.
46. Zheng, P.Y. and N.L. Jones, Helicobacter pylori strains expressing the vacuolating cytotoxin interrupt phagosome maturation in macrophages by recruiting and retaining TACO (coronin 1) protein. Cell Microbiol, 2003. 5(1): p. 25-40.
47. Nagai, H., et al., A bacterial guanine nucleotide exchange factor activates ARF on Legionella phagosomes. Science, 2002. 295(5555): p. 679-82.
48. Ruiz-Albert, J., et al., Complementary activities of SseJ and SifA regulate dynamics of the Salmonella typhimurium vacuolar membrane. Mol Microbiol, 2002. 44(3): p. 645-61.
49. Chakravortty, D., I. Hansen-Wester, and M. Hensel, Salmonella pathogenicity island 2 mediates protection of intracellular Salmonella from reactive nitrogen intermediates. J Exp Med, 2002. 195(9): p. 1155-66.
50. Vazquez-Torres, A., et al., Salmonella pathogenicity island 2-dependent evasion of the phagocyte NADPH oxidase. Science, 2000. 287(5458): p. 1655-8.
51. Gobert, A.P., et al., Helicobacter pylori arginase inhibits nitric oxide production by eukaryotic cells: a strategy for bacterial survival. Proc Natl Acad Sci U S A, 2001. 98(24): p. 13844-9.
52. Vallance, B.A., et al., Modulation of inducible nitric oxide synthase expression by the attaching and effacing bacterial pathogen citrobacter rodentium in infected mice. Infect Immun, 2002. 70(11): p. 6424-35.
53. Reddick, L.E. and N.M. Alto, Bacteria fighting back: how pathogens target and subvert the host innate immune system. Molecular cell, 2014. 54(2): p. 321-8.
54. Duesbery, N.S., et al., Proteolytic inactivation of MAP-kinase-kinase by anthrax lethal factor. Science, 1998. 280(5364): p. 734-7.
55. Mukherjee, S., et al., Yersinia YopJ acetylates and inhibits kinase activation by blocking phosphorylation. Science, 2006. 312(5777): p. 1211-4.
56. Wu, H., R.M. Jones, and A.S. Neish, The Salmonella effector AvrA mediates bacterial intracellular survival during infection in vivo. Cell Microbiol, 2012. 14(1): p. 28-39.
57. Trosky, J.E., et al., Inhibition of MAPK signaling pathways by VopA from Vibrio parahaemolyticus. J Biol Chem, 2004. 279(50): p. 51953-7.
58. Trosky, J.E., et al., VopA inhibits ATP binding by acetylating the catalytic loop of MAPK kinases. J Biol Chem, 2007. 282(47): p. 34299-305.
59. Wei, P., et al., Bacterial virulence proteins as tools to rewire kinase pathways in yeast and immune cells. Nature, 2012. 488(7411): p. 384-8.
60. Sanada, T., et al., The Shigella flexneri effector OspI deamidates UBC13 to dampen the inflammatory response. Nature, 2012. 483(7391): p. 623-6.

61. Ashida, H., et al., A bacterial E3 ubiquitin ligase IpaH9.8 targets NEMO/IKKgamma to dampen the host NF-kappaB-mediated inflammatory response. Nat Cell Biol, 2010. 12(1): p. 66-73; sup pp 1-9.
62. Zhou, Y., et al., The Shigella type three secretion system effector OspG directly and specifically binds to host ubiquitin for activation. PLoS One, 2013. 8(2): p. e57558.
63. Yan, D., et al., Inhibition of TLR signaling by a bacterial protein containing immunoreceptor tyrosine-based inhibitory motifs. Nat Immunol, 2012. 13(11): p. 1063-1071.
64. Yan, D., et al., Enteropathogenic Escherichia coli Tir recruits cellular SHP-2 through ITIM motifs to suppress host immune response. Cell Signal, 2013. 25(9): p. 1887-94.
65. Gao, X., et al., NleB, a bacterial effector with glycosyltransferase activity, targets GAPDH function to inhibit NF-kappaB activation. Cell Host Microbe, 2013. 13(1): p. 87-99.
66. Yen, H., et al., NleC, a type III secretion protease, compromises NF-kappaB activation by targeting p65/RelA. PLoS Pathog, 2010. 6(12): p. e1001231.
67. Zhang, L., et al., Cysteine methylation disrupts ubiquitin-chain sensing in NF-kappaB activation. Nature, 2012. 481(7380): p. 204-8.
68. Navarro, L., N.M. Alto, and J.E. Dixon, Functions of the Yersinia effector proteins in inhibiting host immune responses. Curr Opin Microbiol, 2005. 8(1): p. 21-7.
69. LaRock, C.N. and B.T. Cookson, The Yersinia virulence effector YopM binds caspase-1 to arrest inflammasome assembly and processing. Cell Host Microbe, 2012. 12(6): p. 799-805.
70. Geijtenbeek, T.B., et al., Mycobacteria target DC-SIGN to suppress dendritic cell function. J Exp Med, 2003. 197(1): p. 7-17.
71. Bergman, M.P., et al., Helicobacter pylori modulates the T helper cell 1/T helper cell 2 balance through phase-variable interaction between lipopolysaccharide and DC-SIGN. J Exp Med, 2004. 200(8): p. 979-90.
72. Fortune, S.M., et al., Mycobacterium tuberculosis inhibits macrophage responses to IFN-gamma through myeloid differentiation factor 88-dependent and -independent mechanisms. J Immunol, 2004. 172(10): p. 6272-80.
73. Salcedo, S.P., et al., Brucella control of dendritic cell maturation is dependent on the TIR-containing protein Btp1. PLoS Pathog, 2008. 4(2): p. e21.
74. Bosio, C.M. and S.W. Dow, Francisella tularensis induces aberrant activation of pulmonary dendritic cells. J Immunol, 2005. 175(10): p. 6792-801.
75. Thanabalasuriar, A., et al., Sec24 interaction is essential for localization and

virulence-associated function of the bacterial effector protein NleA. Cell Microbiol, 2012. 14(8): p. 1206-18.
76. Olsen, R.L., et al., The enterohemorrhagic Escherichia coli effector protein NleF binds mammalian Tmp21. Vet Microbiol, 2013. 164(1-2): p. 164-70.
77. Selyunin, A.S., et al., Selective protection of an ARF1-GTP signaling axis by a bacterial scaffold induces bidirectional trafficking arrest. Cell Rep, 2014. 6(5): p. 878-91.
78. Dong, N., et al., Structurally distinct bacterial TBC-like GAPs link Arf GTPase to Rab1 inactivation to counteract host defenses. Cell, 2012. 150(5): p. 1029-41.
79. Burnaevskiy, N., et al., Proteolytic elimination of N-myristoyl modifications by the Shigella virulence factor IpaJ. Nature, 2013. 496(7443): p. 106-9.
80. Moore, K.W., et al., Interleukin-10 and the interleukin-10 receptor. Annu Rev Immunol, 2001. 19: p. 683-765.
81. Couper, K.N., D.G. Blount, and E.M. Riley, IL-10: the master regulator of immunity to infection. J Immunol, 2008. 180(9): p. 5771-7.
82. David, R., Immune evasion: Bordetella escapes by inducing IL-10. Nat Rev Immunol, 2010. 10(2): p. 84-85.
83. Bai, W., et al., TLR3 regulates mycobacterial RNA-induced IL-10 production through the PI3K/AKT signaling pathway. Cell Signal, 2014. 26(5): p. 942-50.
84. Oertli, M. and A. Muller, Helicobacter pylori targets dendritic cells to induce immune tolerance, promote persistence and confer protection against allergic asthma. Gut Microbes, 2012. 3(6): p. 566-71.
85. Wei, L., J. Wang, and Y. Liu, Prior to Foxp3 regulatory T-cell induction, interleukin-10-producing B cells expand after Helicobacter pylori infection. Pathog Dis, 2014.
86. Lee, C.C. and J.T. Kung, Marginal zone B cell is a major source of Il-10 in Listeria monocytogenes susceptibility. J Immunol, 2012. 189(7): p. 3319-27.
87. Wojciechowski, W., et al., Attenuation of MHC class II expression in macrophages infected with Mycobacterium bovis bacillus Calmette-Guerin involves class II transactivator and depends on the Nramp1 gene. J Immunol, 1999. 163(5): p. 2688-96.
88. Noss, E.H., et al., Toll-like receptor 2-dependent inhibition of macrophage class II MHC expression and antigen processing by 19-kDa lipoprotein of Mycobacterium tuberculosis. J Immunol, 2001. 167(2): p. 910-8.
89. Gagliardi, M.C., et al., Mycobacteria exploit p38 signaling to affect CD1 expression and lipid antigen presentation by human dendritic cells. Infect Immun, 2009. 77(11): p. 4947-52.
90. Halici, S., et al., Functional analysis of the Salmonella pathogenicity island

2-mediated inhibition of antigen presentation in dendritic cells. Infect Immun, 2008. 76(11): p. 4924-33.

91. Lapaque, N., et al., Salmonella regulates polyubiquitination and surface expression of MHC class II antigens. Proc Natl Acad Sci U S A, 2009. 106(33): p. 14052-7.
92. Yao, T., et al., Suppression of T and B lymphocyte activation by a Yersinia pseudotuberculosis virulence factor, yopH. J Exp Med, 1999. 190(9): p. 1343-50.
93. Umehara, S., et al., Effects of Helicobacter pylori CagA protein on the growth and survival of B lymphocytes, the origin of MALT lymphoma. Oncogene, 2003. 22(51): p. 8337-42.
94. Torres, V.J., et al., Helicobacter pylori vacuolating cytotoxin inhibits activation-induced proliferation of human T and B lymphocyte subsets. J Immunol, 2007. 179(8): p. 5433-40.
95. Gebert, B., et al., Helicobacter pylori vacuolating cytotoxin inhibits T lymphocyte activation. Science, 2003. 301(5636): p. 1099-102.
96. Boncristiano, M., et al., The Helicobacter pylori vacuolating toxin inhibits T cell activation by two independent mechanisms. J Exp Med, 2003. 198(12): p. 1887-97.
97. Boulton, I.C. and S.D. Gray-Owen, Neisserial binding to CEACAM1 arrests the activation and proliferation of CD4+ T lymphocytes. Nat Immunol, 2002. 3(3): p. 229-36.
98. Kilian, M., et al., Biological significance of IgA1 proteases in bacterial colonization and pathogenesis: critical evaluation of experimental evidence. APMIS, 1996. 104(5): p. 321-38.
99. Breitschwerdt, E.B., et al., Bartonellosis: an emerging infectious disease of zoonotic importance to animals and human beings. J Vet Emerg Crit Care (San Antonio), 2010. 20(1): p. 8-30.
100. Engel, P., et al., Parallel evolution of a type IV secretion system in radiating lineages of the host-restricted bacterial pathogen Bartonella. PLoS Genet, 2011. 7(2): p. e1001296.
101. Chomel, B.B., et al., Ecological fitness and strategies of adaptation of Bartonella species to their hosts and vectors. Vet Res, 2009. 40(2): p. 29.
102. Chomel, B.B., et al., Bartonella spp. in pets and effect on human health. Emerg Infect Dis, 2006. 12(3): p. 389-94.
103. Maguina, C. and E. Gotuzzo, Bartonellosis. New and old. Infect Dis Clin North Am, 2000. 14(1): p. 1-22, vii.
104. Ihler, G.M., Bartonella bacilliformis: dangerous pathogen slowly emerging from deep background. FEMS Microbiol Lett, 1996. 144(1): p. 1-11.

105. Maguina, C., et al., Bartonellosis (Carrion's disease) in the modern era. Clin Infect Dis, 2001. 33(6): p. 772-9.
106. Bass, J.W., J.M. Vincent, and D.A. Person, The expanding spectrum of Bartonella infections: I. Bartonellosis and trench fever. Pediatr Infect Dis J, 1997. 16(1): p. 2-10.
107. Florin, T.A., T.E. Zaoutis, and L.B. Zaoutis, Beyond cat scratch disease: widening spectrum of Bartonella henselae infection. Pediatrics, 2008. 121(5): p. e1413-25.
108. Koehler, J.E., et al., Molecular epidemiology of bartonella infections in patients with bacillary angiomatosis-peliosis. N Engl J Med, 1997. 337(26): p. 1876-83.
109. Dehio, C., Bartonella-host-cell interactions and vascular tumour formation. Nat Rev Microbiol, 2005. 3(8): p. 621-31.
110. Harms, A. and C. Dehio, Intruders below the radar: molecular pathogenesis of Bartonella spp. Clin Microbiol Rev, 2012. 25(1): p. 42-78.
111. Siamer, S. and C. Dehio, New insights into the role of Bartonella effector proteins in pathogenesis. Curr Opin Microbiol, 2014. 23C: p. 80-85.
112. Caceres, A.G., et al., Possible role of Lutzomyia maranonensis and Lutzomyia robusta (Diptera: Psychodidae) as vectors of human bartonellosis in three provinces of region nor Oriental del Maranon, Peru. Rev Inst Med Trop Sao Paulo, 1997. 39(1): p. 51-2.
113. Fournier, P.E., et al., Experimental model of human body louse infection using green fluorescent protein-expressing Bartonella quintana. Infect Immun, 2001. 69(3): p. 1876-9.
114. Higgins, J.A., et al., Acquisition of the cat scratch disease agent Bartonella henselae by cat fleas (Siphonaptera:Pulicidae). J Med Entomol, 1996. 33(3): p. 490-5.
115. Dehio, C., U. Sauder, and R. Hiestand, Isolation of Bartonella schoenbuchensis from Lipoptena cervi, a blood-sucking arthropod causing deer ked dermatitis. J Clin Microbiol, 2004. 42(11): p. 5320-3.
116. Schulein, R., et al., Invasion and persistent intracellular colonization of erythrocytes. A unique parasitic strategy of the emerging pathogen Bartonella. J Exp Med, 2001. 193(9): p. 1077-86.
117. Seubert, A., R. Schulein, and C. Dehio, Bacterial persistence within erythrocytes: a unique pathogenic strategy of Bartonella spp. Int J Med Microbiol, 2002. 291(6-7): p. 555-60.
118. Dehio, C., Bartonella interactions with endothelial cells and erythrocytes. Trends Microbiol, 2001. 9(6): p. 279-85.
119. Karem, K.L., et al., Characterization of Bartonella henselae-specific immunity in

BALB/c mice. Immunology, 1999. 97(2): p. 352-8.
120. Okujava, R., et al., A translocated effector required for bartonella dissemination from derma to blood safeguards migratory host cells from damage by co-translocated effectors. PLoS Pathog, 2014. 10(6): p. e1004187.
121. Linke, D., et al., Trimeric autotransporter adhesins: variable structure, common function. Trends Microbiol, 2006. 14(6): p. 264-70.
122. Riess, T., et al., Bartonella adhesin a mediates a proangiogenic host cell response. J Exp Med, 2004. 200(10): p. 1267-78.
123. O'Rourke, F., et al., Adhesins of Bartonella spp. Adv Exp Med Biol, 2011. 715: p. 51-70.
124. Kempf, V.A., et al., Activation of hypoxia-inducible factor-1 in bacillary angiomatosis: evidence for a role of hypoxia-inducible factor-1 in bacterial infections. Circulation, 2005. 111(8): p. 1054-62.
125. Kempf, V.A., et al., Evidence of a leading role for VEGF in Bartonella henselae-induced endothelial cell proliferations. Cell Microbiol, 2001. 3(9): p. 623-32.
126. Kaiser, P.O., et al., The head of Bartonella adhesin A is crucial for host cell interaction of Bartonella henselae. Cell Microbiol, 2008. 10(11): p. 2223-34.
127. Kaiser, P.O., et al., Analysis of the BadA stalk from Bartonella henselae reveals domain-specific and domain-overlapping functions in the host cell infection process. Cell Microbiol, 2012. 14(2): p. 198-209.
128. Christie, P.J., et al., Biogenesis, architecture, and function of bacterial type IV secretion systems. Annu Rev Microbiol, 2005. 59: p. 451-85.
129. Saenz, H.L., et al., Genomic analysis of Bartonella identifies type IV secretion systems as host adaptability factors. Nat Genet, 2007. 39(12): p. 1469-76.
130. Vayssier-Taussat, M., et al., The Trw type IV secretion system of Bartonella mediates host-specific adhesion to erythrocytes. PLoS Pathog, 2010. 6(6): p. e1000946.
131. Schulein, R. and C. Dehio, The VirB/VirD4 type IV secretion system of Bartonella is essential for establishing intraerythrocytic infection. Mol Microbiol, 2002. 46(4): p. 1053-67.
132. Lu, Y.Y., et al., Bartonella henselae trimeric autotransporter adhesin BadA expression interferes with effector translocation by the VirB/D4 type IV secretion system. Cell Microbiol, 2013. 15(5): p. 759-78.
133. Quebatte, M., et al., The BatR/BatS two-component regulatory system controls the adaptive response of Bartonella henselae during human endothelial cell infection. J Bacteriol, 2010. 192(13): p. 3352-67.
134. Engel, P., et al., Adenylylation control by intra- or intermolecular active-site

obstruction in Fic proteins. Nature, 2012. 482(7383): p. 107-10.
135. Roy, C.R. and S. Mukherjee, Bacterial FIC Proteins AMP Up Infection. Sci Signal, 2009. 2(62): p. pe14.
136. Pieles, K., et al., An experimental strategy for the identification of AMPylation targets from complex protein samples. Proteomics, 2014. 14(9): p. 1048-52.
137. Palanivelu, D.V., et al., Fic domain-catalyzed adenylylation: insight provided by the structural analysis of the type IV secretion system effector BepA. Protein Sci, 2011. 20(3): p. 492-9.
138. Hayashi, T., H. Morohashi, and M. Hatakeyama, Bacterial EPIYA effectors--where do they come from? What are they? Where are they going? Cell Microbiol, 2013. 15(3): p. 377-85.
139. Schulein, R., et al., A bipartite signal mediates the transfer of type IV secretion substrates of Bartonella henselae into human cells. Proc Natl Acad Sci U S A, 2005. 102(3): p. 856-61.
140. Selbach, M., et al., Host cell interactome of tyrosine-phosphorylated bacterial proteins. Cell Host Microbe, 2009. 5(4): p. 397-403.
141. Dehio, C., et al., Interaction of Bartonella henselae with endothelial cells results in bacterial aggregation on the cell surface and the subsequent engulfment and internalisation of the bacterial aggregate by a unique structure, the invasome. J Cell Sci, 1997. 110 (Pt 18): p. 2141-54.
142. Kyme, P.A., et al., Unusual trafficking pattern of Bartonella henselae -containing vacuoles in macrophages and endothelial cells. Cell Microbiol, 2005. 7(7): p. 1019-34.
143. Scheidegger, F., et al., Distinct activities of Bartonella henselae type IV secretion effector proteins modulate capillary-like sprout formation. Cell Microbiol, 2009. 11(7): p. 1088-101.
144. Truttmann, M.C., T.A. Rhomberg, and C. Dehio, Combined action of the type IV secretion effector proteins BepC and BepF promotes invasome formation of Bartonella henselae on endothelial and epithelial cells. Cell Microbiol, 2011. 13(2): p. 284-99.
145. Truttmann, M.C., et al., Bartonella henselae engages inside-out and outside-in signaling by integrin beta1 and talin1 during invasome-mediated bacterial uptake. J Cell Sci, 2011. 124(Pt 21): p. 3591-602.
146. Scheidegger, F., et al., The Bartonella henselae VirB/Bep system interferes with vascular endothelial growth factor (VEGF) signalling in human vascular endothelial cells. Cell Microbiol, 2011. 13(3): p. 419-31.
147. Schmid, M.C., et al., A translocated bacterial protein protects vascular endothelial cells from apoptosis. PLoS Pathog, 2006. 2(11): p. e115.

148. Schmid, M.C., et al., The VirB type IV secretion system of Bartonella henselae mediates invasion, proinflammatory activation and antiapoptotic protection of endothelial cells. Mol Microbiol, 2004. 52(1): p. 81-92.
149. Pulliainen, A.T., et al., Bacterial effector binds host cell adenylyl cyclase to potentiate Galphas-dependent cAMP production. Proc Natl Acad Sci U S A, 2012. 109(24): p. 9581-6.
150. Seubert, A., et al., A bacterial conjugation machinery recruited for pathogenesis. Mol Microbiol, 2003. 49(5): p. 1253-66.
151. Deng, H.K., et al., Identification of Bartonella Trw host-specific receptor on erythrocytes. PLoS One, 2012. 7(7): p. e41447.
152. Merrell, D.S. and S. Falkow, Frontal and stealth attack strategies in microbial pathogenesis. Nature, 2004. 430(6996): p. 250-6.
153. Zahringer, U., et al., Structure and biological activity of the short-chain lipopolysaccharide from Bartonella henselae ATCC 49882T. J Biol Chem, 2004. 279(20): p. 21046-54.
154. Popa, C., et al., Bartonella quintana lipopolysaccharide is a natural antagonist of Toll-like receptor 4. Infect Immun, 2007. 75(10): p. 4831-7.
155. Matera, G., et al., The Janus face of Bartonella quintana recognition by Toll-like receptors (TLRs): a review. Eur Cytokine Netw, 2008. 19(3): p. 113-8.
156. Kabeya, H., et al., Experimental infection of cats with Bartonella henselae resulted in rapid clearance associated with T helper 1 immune responses. Microbes Infect, 2009. 11(6-7): p. 716-20.
157. Capo, C., et al., Bartonella quintana bacteremia and overproduction of interleukin-10: model of bacterial persistence in homeless people. J Infect Dis, 2003. 187(5): p. 837-44.
158. Kabeya, H., et al., Characterization of Th1 activation by Bartonella henselae stimulation in BALB/c mice: Inhibitory activities of interleukin-10 for the production of interferon-gamma in spleen cells. Vet Microbiol, 2007. 119(2-4): p. 290-6.
159. Papadopoulos, N.G., et al., Circulating cytokines in patients with cat scratch disease. Clin Infect Dis, 2001. 33(6): p. e54-6.
160. Vermi, W., et al., Role of dendritic cell-derived CXCL13 in the pathogenesis of Bartonella henselae B-rich granuloma. Blood, 2006. 107(2): p. 454-62.
161. Mege, J.L., et al., The two faces of interleukin 10 in human infectious diseases. Lancet Infect Dis, 2006. 6(9): p. 557-69.
162. Marignac, G., et al., Murine model for Bartonella birtlesii infection: New aspects. Comp Immunol Microbiol Infect Dis, 2010. 33(2): p. 95-107.
163. Koesling, J., et al., Cutting edge: antibody-mediated cessation of hemotropic

infection by the intraerythrocytic mouse pathogen Bartonella grahamii. J Immunol, 2001. 167(1): p. 11-4.

164. Kordick, D.L. and E.B. Breitschwerdt, Relapsing bacteremia after blood transmission of Bartonella henselae to cats. Am J Vet Res, 1997. 58(5): p. 492-7.
165. Kabeya, H., et al., Predominant T helper 2 immune responses against Bartonella henselae in naturally infected cats. Microbiol Immunol, 2006. 50(3): p. 171-8.
166. O'Reilly, K.L., et al., Passive antibody to Bartonella henselae protects against clinical disease following homologous challenge but does not prevent bacteremia in cats. Infect Immun, 2001. 69(3): p. 1880-2.
167. Fiorentino, D.F., M.W. Bond, and T.R. Mosmann, Two types of mouse T helper cell. IV. Th2 clones secrete a factor that inhibits cytokine production by Th1 clones. J Exp Med, 1989. 170(6): p. 2081-95.
168. Arvand, M., et al., Bartonella henselae-specific cell-mediated immune responses display a predominantly Th1 phenotype in experimentally infected C57BL/6 mice. Infect Immun, 2001. 69(10): p. 6427-33.
169. Musso, T., et al., Interaction of Bartonella henselae with the murine macrophage cell line J774: infection and proinflammatory response. Infect Immun, 2001. 69(10): p. 5974-80.
170. Schweyer, S. and A. Fayyazi, Activation and apoptosis of macrophages in cat scratch disease. J Pathol, 2002. 198(4): p. 534-40.
171. Kunz, S., et al., Lymphadenopathy in a novel mouse model of Bartonella-induced cat scratch disease results from lymphocyte immigration and proliferation and is regulated by interferon-alpha/beta. Am J Pathol, 2008. 172(4): p. 1005-18.

2. AIM OF THE THESIS

Started in May 2011, my first project was collaborated with the group of Prof. Kempf in the Institute of Medical Microbiology and Infection Control at the University Hospital of the Johann Wolfgang Goethe-University in Frankfurt. Two pathogenicity factors of *Bartonella henselae* have been greater characterized in individual activities: the trimeric autotransporter *Bartonella* adhesin A (BadA) and the type IV secretion system VirB/D4 (VirB/D4 T4SS). In this study, we deeply investigated how these major virulence factors affect each other in their specific activities.

In the second project, I focused on the natural host interface with *Bartonella*, particularly on the bacterial defense mechanisms against host immunity. To achieve this, my work was divided into two directions. One was to identify which *Bartonella* effector proteins as immunomodulatory molecules involved in intracellular communications to subvert the immunological signaling cascade. The other was to find the primary niche of *Bartonella* entry and replication in the natural reservoir host. By understanding the *Bartonella* infection cycle, I aimed to explore how *Bartonella* manipulate host immunity towards its pathogenicity *in vivo*. Taken *in vitro* and *in vivo* results together, I sought to complete this project with a comprehensive insight into which Bep displays immunosuppressive properties, how it works and what are the consequences of its function on host immunity.

3. RESULTS

3.1 Research article I

Bartonella henselae trimeric autotransporter adhesin BadA expression interferes with effector translocation by the VirB/D4 type IV secretion system.

Yun-Yueh Lu[#], Bettina Franz[#], Matthias C. Truttmann[#], Tanja Riess, Marco Faustmann, Volkhard A.J. Kempf[*] and Christoph Dehio[*]

[#] These authors contributed equally

[*] Corresponding authors

Cellular Microbiology, May 2013, Volume 15, Issue 5, pages 759–778

Statement of my contribution

The project is collaborated with the group of Prof. V. Kempf in the Institute of Medical Microbiology and Infection Control at the University Hospital of the Johann Wolfgang Goethe-University in Frankfurt. In this study, the interaction of BadA and the VirB/D4 T4SS in *B. henselae* was analyzed. Our group focused on the functional analysis of the VirB/D4 T4SS and the BadA specific phenotypes were studied by the group of Prof. Kempf. My contributions include the characterization of clinical *Bartonella henselae* (*Bhe*) isolates and constructed *Bhe* mutants by analyzing BadA and VirB coexpression through the western blot and immunofluorescent labeling (Fig. 1, 4A, and S2A). The phenotypic T4SS-dependent effects were studied in a variety of clinical *Bhe* isolates and constructed *Bhe* mutants by invasome formation and CRAfT assay (Fig. 3, 5, and 7). Moreover, to visualize the BadA structures and to further investigate the negative effect of BadA on the function of the VirB/D4 T4SS, *Bhe* infected cell samples were prepared for transmission electron microscopy (Fig. 6). The stability of the Cre-BID fusion constructs was showed by the western blot and CRAfT assay (Fig. S1A and S2B). Besides the protein level, gene regulation of *bepD*, *virB4* and *virB7* of *Bhe* mutants was analyzed by quantitative PCR (Fig. S2C). Finally, the manuscript was written by me, Dr. B. Franz, Dr. M. Truttmann, Prof. V. Kempf, and Prof. C. Dehio.

3.1.1 Summary

The trimeric autotransporter *Bartonella* adhesin A (BadA) and the type IV secretion system VirB/D4 (VirB/D4 T4SS) of *Bartonella spp.* represent two of the most important pathogenicity factors of this genus - each displaying multiple functions in host cell interaction. The key functions of BadA in the molecular pathogenesis of *B. henselae* have been thoroughly studied with the Marseille strain (i.e., in the absence of a functional VirB/D4 T4SS). BadA mediates the binding to fibronectin (Fn), adherence to endothelial cells (ECs) and secretion of vascular endothelial growth factor (VEGF). The VirB/D4 T4SS of *B. henselae* are well studied in Houston-1 strain (i.e., in the absence of a functional BadA). It translocates several *Bartonella* effector proteins (Beps) into the cytoplasm of infected ECs, resulting in uptake of bacterial aggregates via the invasome structure, inhibition of apoptosis and activation of a proangiogenic phenotype. Despite this knowledge of the individual activities of BadA or VirB/D4, it is unknown whether these major virulence factors affect each other in their specific activities. In this study, expression and function of BadA and VirB/D4 were analyzed in a variety of clinical *B. henselae* isolates. Data revealed that most isolates have lost expression of either BadA or VirB/D4 during *in vitro* passages. However, the phenotypic effects of coexpression of both virulence factors were studied in one clinical isolate stably coexpressing BadA and VirB/D4, as well as by ectopic expression of BadA in a strain only expressing VirB/D4. Our results showed that BadA forming a dense layer on the bacterial surface negatively affected VirB/D4-dependent Bep translocation and invasome formation by likely preventing close contact between the bacterial cell envelope and the host cell membrane. In contrast, BadA-dependent phenotypes, e.g., Fn binding, adhesion to ECs, and VEGF secretion, were not affected by a functional VirB/D4 T4SS. However, a certain regulatory antagonism is shown from previous transcriptional data that expression of the VirB/D4 T4SS was upregulated and that of BadA downregulated under certain conditions in the *in vitro* model, implying these essential virulence factors BadA and VirB/D4 are likely differentially expressed during different stages of the infection cycle of *Bartonella*. Further experiments elucidating the regulatory patterns of these two systems are needed to understand the underlying mechanisms of gene regulation in detail.

3.1.2 Manuscript

Cellular Microbiology (2013) **15**(5), 759–778
doi:10.1111/cmi.12070
First published online 6 December 2012

Bartonella henselae trimeric autotransporter adhesin BadA expression interferes with effector translocation by the VirB/D4 type IV secretion system

Yun-Yueh Lu,[1†] Bettina Franz,[2†] Matthias C. Truttmann,[1†] Tanja Riess,[2] Jérémie Gay-Fraret,[1] Marco Faustmann,[1‡] Volkhard A. J. Kempf[2] and Christoph Dehio[1*]**

[1]*Focal Area Infection Biology, Biozentrum of the University of Basel, Klingelbergstrasse 70, CH-4056 Basel, Switzerland.*

[2]*Institute of Medical Microbiology and Infection Control, University Hospital Johann Wolfgang Goethe University Frankfurt am Main, Paul-Ehrlich-Strasse 40, D-60596 Frankfurt/Main, Germany.*

Summary

The Gram-negative, zoonotic pathogen *Bartonella henselae* is the aetiological agent of cat scratch disease, bacillary angiomatosis and peliosis hepatis in humans. Two pathogenicity factors of *B. henselae* – each displaying multiple functions in host cell interaction – have been characterized in greater detail: the trimeric autotransporter *Bartonella* adhesin A (BadA) and the type IV secretion system VirB/D4 (VirB/D4 T4SS). BadA mediates, e.g. binding to fibronectin (Fn), adherence to endothelial cells (ECs) and secretion of vascular endothelial growth factor (VEGF). VirB/D4 translocates several *Bartonella* effector proteins (Beps) into the cytoplasm of infected ECs, resulting, e.g. in uptake of bacterial aggregates via the invasome structure, inhibition of apoptosis and activation of a proangiogenic phenotype. Despite this knowledge of the individual activities of BadA or VirB/D4 it is unknown whether these major virulence factors affect each other in their specific activities. In this study, expression and function of BadA and VirB/D4 were analysed in a variety of clinical *B. henselae* isolates. Data revealed that most isolates have lost expression of either BadA or VirB/D4 during *in vitro* passages. However, the phenotypic effects of coexpression of both virulence factors was studied in one clinical isolate that was found to stably coexpress BadA and VirB/D4, as well as by ectopic expression of BadA in a strain expressing VirB/D4 but not BadA. BadA, which forms a dense layer on the bacterial surface, negatively affected VirB/D4-dependent Bep translocation and invasome formation by likely preventing close contact between the bacterial cell envelope and the host cell membrane. In contrast, BadA-dependent Fn binding, adhesion to ECs and VEGF secretion were not affected by a functional VirB/D4 T4SS. The obtained data imply that the essential virulence factors BadA and VirB/D4 are likely differentially expressed during different stages of the infection cycle of *Bartonella*.

Received 5 June, 2012; revised 7 November, 2012; accepted 9 November, 2012. For correspondence. *E-mail christoph.dehio@unibas.ch; Tel. (+41) 61 267 2140; Fax (+41) 61 267 2118; **E-mail volkhard.kempf@kgu.de; Tel. (+49) 69 6301 5019; Fax (+49) 69 6301 83431.
†These authors contributed equally. ‡Deceased on 20 February 2010.

© 2012 Blackwell Publishing Ltd

Introduction

Bartonella henselae is a Gram-negative, arthropod-borne and facultative intracellular bacterial pathogen with worldwide distribution and is considered to be the most relevant human pathogenic *Bartonella* species (Anderson and Neuman, 1997; Franz and Kempf, 2011; Harms and Dehio, 2012). Cats have been identified as the primary reservoirs of *B. henselae*. Zoonotic transmission from infected cats to humans occurs via cat scratches or cat fleas (Rolain *et al.*, 2001; Dehio, 2004). Human infections with *B. henselae* can manifest in a broad spectrum of clinical symptoms. Immunocompetent patients typically suffer from cat scratch disease (CSD), characterized by local lymph node swelling and fever (Florin *et al.*, 2008). In contrast, immunocompromised patients (e.g. AIDS patients) can develop vasoproliferative lesions in the skin (bacillary angiomatosis) or the liver (peliosis hepatis) respectively (Relman *et al.*, 1990; 1991). These tumour-like lesions arise from bacterial infection of vascular ECs leading to enhanced ECs migration and proliferation (Dehio, 2005).

Two major pathogenicity factors of *B. henselae* have been identified: VirB/D4, a type IV secretion system (T4SS) translocating Bartonella effector proteins (Beps)

into mammalian host cells (Schülein *et al.*, 2005; Dehio, 2008) and the *Bartonella* adhesin A (BadA) belonging to the family of the trimeric autotransporter adhesins (TAAs) (Riess *et al.*, 2004; Linke *et al.*, 2006).

T4SS are ancestrally related to bacterial conjugation systems. A variety of bacteria intimately interacting with eukaryotic hosts utilize T4SSs to translocate bacterial effectors into recipient cells (Christie *et al.*, 2005). To date, the VirB/D4 T4SS of *B. henselae* and its translocated substrates (Beps) are well characterized for the subversion of various endothelial cell functions, including: (i) massive rearrangements of the actin cytoskeleton leading to the formation and internalization of large bacterial aggregates into structures known as the invasomes (Dehio *et al.*, 1997), (ii) activation of the nuclear factor κB-dependent pro-inflammatory response resulting in the enhanced expression of cell adhesion molecules (ICAM-1 and E-selectin) and the secretion of IL-8 (Fuhrmann *et al.*, 2001; Schmid *et al.*, 2004), (iii) inhibition of endothelial cell apoptosis (Schmid *et al.*, 2004) and (iv) capillary-like sprout formation of ECs embedded in a collagen 3D matrix (Scheidegger *et al.*, 2009). Seven distinct Beps (BepA to BepG) of *B. henselae* have been identified to promote the described T4SS-dependent cellular phenotypes resulting from *B. henselae* infections of host cells (Schülein *et al.*, 2005). BepA was shown to efficiently inhibit EC apoptosis (Schmid *et al.*, 2006). Additionally, BepA induces capillary-like sprouting in an endothelial spheroid infection model while the same process is inhibited by BepG; therefore, both proteins seem to play a role in controlling the angiogenic response triggered by a *B. henselae* infection (Scheidegger *et al.*, 2009). Furthermore, the combination of BepC and BepF, but also BepG by itself, promote invasome-mediated internalization of large *B. henselae* aggregates coupled to the inhibition of endocytosis-like uptake of individual bacteria (Rhomberg *et al.*, 2009; Truttmann *et al.*, 2011c).

Alike bacterial T4SS, TAAs are important virulence factors in numerous Gram-negative bacteria, e.g. *Yersinia enterocolitica, Haemophilus influenzae, Neisseria meningitidis* or *Moraxella catarrhalis*. TAAs perform type Vc secretion and are modularly constructed consisting of typical head, stalk and anchor domains (Linke *et al.*, 2006). BadA is the largest so far identified TAA with the size of 328 kDa per monomer and a length of about 240 nm (Riess *et al.*, 2004). It contributes to the adhesion of *B. henselae* to host cells and to extracellular matrix proteins such as fibronectin (Fn), laminin or collagens (O'Rourke *et al.*, 2011). Furthermore, BadA plays an important role in the induction of proangiogenic host cell responses, including (i) the activation of hypoxia-inducible factor 1 (HIF-1), a key transcription factor of angiogenesis (Kempf *et al.*, 2005) and (ii) the subsequent secretion of vasoproliferative cytokines, e.g. VEGF (Kempf *et al.*, 2001; Riess *et al.*, 2004). With the exception of Fn binding, these functional properties are mediated by both the head and stalk domain of BadA whereas the stalk domain is exclusively responsible for Fn binding (Kaiser *et al.*, 2008; 2012).

Both VirB/D4 and BadA play crucial roles in *B. henselae* pathogenicity. However, most of the work to study *B. henselae* infections of human cells has been performed using *B. henselae* strains that either express a functional VirB/D4 T4SS but lack a functional full-length BadA or vice versa. The role of VirB/D4 has been analysed using a spontaneous streptomycin-resistant variant of *B. henselae* ATCC49882^T (Regnery *et al.*, 1992) (further referred to as ATCC49882 var-1). Unlike ATCC49882^T var-2 (Riess *et al.*, 2007) that expresses BadA, ATCC49882^T var-1 encodes for frameshifted BadA and does not express BadA on the surface (Riess *et al.*, 2004). Studies on the function of BadA have utilized an early passage *B. henselae* patient isolate named 'Marseille' (Drancourt *et al.*, 1996). As described in Kaiser *et al.* (2011) and Scheidegger *et al.* (2011) based on preliminary data, *B. henselae* Marseille might be unable to build up a functional VirB/D4 T4SS. However, it is worth mentioning that due to differences in isolation and passaging histories, different variants of defined *Bartonella* strains may display distinct characteristics and infection phenotypes. As a result of our individual and independent analysis of sole key virulence factors, it remains unclear whether there is any functional interaction between BadA and VirB/D4 T4SS.

In this study, we analysed the interaction of BadA and VirB/D4 in *B. henselae*. Out of a panel of clinical isolates tested we found only two expressing both virulence systems and these strains were found to display normal BadA functionality, but reduced VirB/D4 functionality. Further, we demonstrate that overexpression of full-length and truncated BadA in *B. henselae* ATCC49882 var-1 affected T4SS-dependent Bep translocation and invasome formation depending on the length of BadA. In contrast, BadA-dependent cell adhesion, Fn binding and VEGF secretion was not affected in the presence of a functional VirB/D4 T4SS. We provide evidence that VirB/D4-dependent effector secretion is negatively affected by BadA but the functions of BadA itself remain intact when both factors are coexpressed in *B. henselae*.

Results

Most human B. henselae *isolates express either BadA or VirB/D4 T4SS*

To explore the co-occurrence of BadA and VirB/D4 in various *B. henselae* strains, we first analysed the expres-

sion of BadA and the VirB/D4 components VirB5 and VirB7 and the VirB/D4 effector BepD in 10 different clinical isolates from human patients [ATCC49793 (Oklahoma) (Welch *et al.*, 1992), ATCC49882^T (Houston-1), ATCC49882 var-1, ATCC49882 var-2, Berlin-1 (Arvand *et al.*, 1998), G-5436 (Zbinden *et al*, 1995), Marseille, San Antonio 1, San Antonio 2 and San Antonio 3]. Supplementary Table S1 describes the different *B. henselae* isolates and their respective origins. First, *B. henselae* strains were tested in an immunofluorescence-based assay, in which all bacteria were stained for the presence of BadA using primary antibodies raised against the BadA head of strain Marseille. A comprehensive table listing all antibodies used in this study is provided as Supplementary Table S2. Our results demonstrate that only five of the 10 clinical isolates tested express BadA (Fig. 1A). While BadA expression appeared to be homogeneous for strains ATCC49882 var-2, Marseille, G-5436 and San Antonio 2, in strain San Antonio 3 a subset of bacteria did not express BadA. We plated serial dilutions of this San Antonio 3 strain on CBA to obtain single colonies and identified two different morphotypes, one appearing smooth-wet (further referred to as San Antonio 3 var-1) and the other rough-dryish (further referred to as San Antonio 3 var-2). Analysis of BadA presence in these strains showed that only San Antonio 3 var-2 expresses BadA (Fig. 1A). To confirm these results and to investigate simultaneous expression of T4SS components, we analysed total lysates of these strains by immunoblot analysis for BadA, BepD, VirB5 and VirB7 (Fig. 1B). Strains expressing BadA showed at most faint signals for BepD, VirB5 and VirB7 while all strains that did not express BadA revealed strong positive signals for BepD, VirB5 and VirB7. The only exceptions turned out to be ATCC49882^T and San Antonio 3 var-2. While ATCC49882^T showed as faint signals for BepD, VirB5 and VirB7 as the BadA expressing strains, isolate San Antonio 3 var-2 expressed all four proteins (BadA, BepD, VirB5 and VirB7) at significant levels. In summary, the majority of clinical isolates expressed either BadA or the VirB/D4 T4SS, while San Antonio 3 var-2 coexpresses both virulence factors at high levels.

Functional analysis of BadA and VirB/D4 in human clinical isolates

Next, we determined whether (i) BadA-expressing strains showed typical BadA-dependent functions and (ii) VirB/D4-expressing strains built a functional T4SS and secreted effector proteins into host cells. When HUVEC were infected with *B. henselae*, all BadA-expressing strains showed strong adherence to ECs, while BadA-negative strains were diminished significantly in their adhesive phenotype (Fig. 2A). Infection of HeLa-229 cells with the BadA-expressing *B. henselae* strains ATCC49882 var-2, G-5436, Marseille and San Antonio 3 var-2 triggered significant VEGF secretion (Fig. 2B). Compared with uninfected HeLa-229 cells, the BadA-positive strains San Antonio 2 and San Antonio 3 displayed slight but not significant induction of VEGF secretion. However, induction of VEGF secretion was significantly ($P < 0.05$) higher in both strains than that caused by the BadA-negative strain San Antonio 1. Finally, Fn binding by *B. henselae* was limited to BadA-expressing strains (Fig. 2C).

Invasome formation and effector translocation assays were performed to analyse VirB/D4-dependent phenotypes. All *B. henselae* clinical isolates expressing BepD, VirB5 and VirB7, i.e. ATCC49793, ATCC49882^T, ATCC49882 var-1, Berlin-1, San Antonio 1, San Antonio 3, San Antonio 3 var-1 and San Antonio 3 var-2 triggered invasome formation on infected endothelial hybridoma cells (Ea.hy926/pRS56-c#B1) (Fig. 3A). The percentage of invasome-positive cells promoted by San Antonio 3 var-1 was three times as high as by San Antonio 3 var-2, suggesting a negative effect of BadA on VirB/D4-dependent Bep secretion. However, the possibility of altered expression of other proteins of San Antonio 3 var-1 and San Antonio 3 var-2 cannot be fully excluded.

In order to perform effector translocation assays with the different *B. henselae* strains using the Cre-recombinase reporter assay for translocation (CRAfT), plasmid pRS51 or pML007 was introduced into the different clinical isolates by conjugation. These two plasmids encode an identical NLS–Cre–BID fusion protein but vary in their resistance cassette. The NLS–Cre–BID fusion protein serves as an artificial substrate for the VirB/D4 T4SS and, upon translocation into Ea.hy926/pRS56-c#B1 cells and transport into the nucleus triggers a recombination event which results in GFP–expression (Schülein *et al.*, 2005). Control experiments comparing ATCC49882 var-1/pRS51 and ATCC49882 var-1/pML007 showed that the difference in the antibiotic resistance cassette did not affect the outcome of the NLS–Cre–BID reporter assay (Fig. S1A). As depicted in Fig. 3B, infection with ATCC49882 var-1/pRS51 and Berlin-1/pRS51 resulted in 20–30% GFP-positive cells while infection with ATCC49793/pRS51, San Antonio 1/pRS51, San Antonio 3/pRS51 and San Antonio 3 var-1/pML007 resulted in 5–10% GFP-positive cells. These findings correlate with expression of VirB/D4 as shown in Fig. 1B. Strains ATCC49882^T and San Antonio 3 var-2 again turned out to be exceptions. Here, ATCC49882^T failed to take up a plasmid by conjugation and therefore effector translocation could not be analysed for this strain for technical reasons. Despite VirB-positive signals in immunoblotting, the BadA-expressing strain San Antonio 3 var-2 was tested negative in the T4SS-indicating CRAfT assay.

© 2012 Blackwell Publishing Ltd,

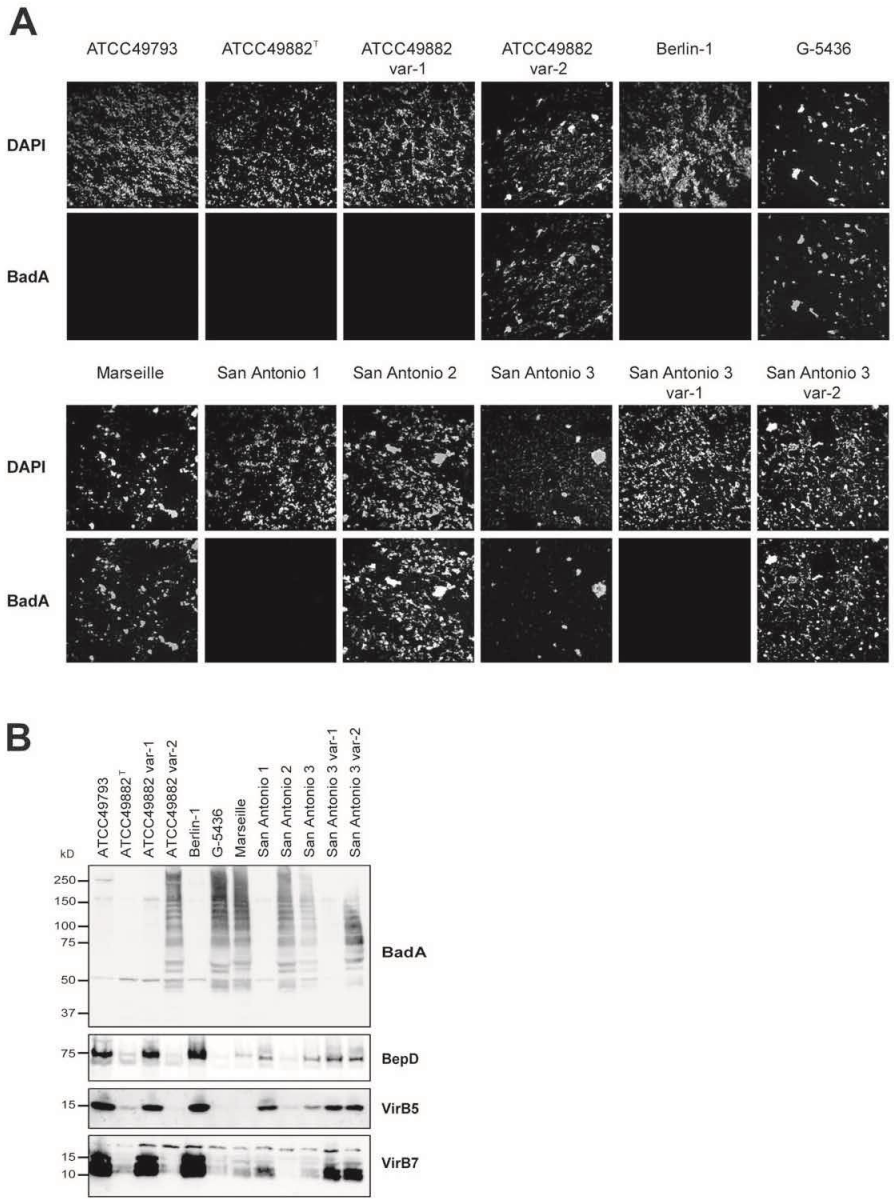

Fig. 1. Analysis of BadA, BepD, VirB5 and VirB7 expression in primary clinical *B. henselae* isolates.
A. Bacteria of the indicated *B. henselae* strains were stained with DAPI and anti-BadA antibodies and examined by fluorescence microcopy. Notably, strain San Antonio 3 displayed a heterogeneous BadA expression. ATCC49882 var-2, G-5436, Marseille, San Antonio 2 and San Antonio 3 var-2 isolated from San Antonio 3 showed homogeneous BadA expression whereas in ATCC49793, ATCC49882, ATCC49882 var-1, Berlin-1, San Antonio 1 and San Antonio 3 var-1 isolated from San Antonio 3 BadA expression was not detectable.
B. Immunoblot analysis of total bacterial lysates of the indicated *B. henselae* isolates with antibodies directed against BadA, BepD, VirB5 and VirB7. ATCC49882 var-2, G-5436, Marseille, San Antonio 2, San Antonio 3 and San Antonio 3 var-2 were BadA positive (congruent to Fig. 1A). Among the BadA-positive strains, strain San Antonio 3 var-2 was positive for BepD, VirB5 and VirB7 expression. BadA-negative strains, including ATCC49793, ATCC49882, ATCC49882 var-1, Berlin-1, San Antonio 1 and San Antonio 3 var-1 were positive for BepD, VirB5 and VirB7 expression.

© 2012 Blackwell Publishing Ltd, *Cellular Microbiology*, **15**, 759–778

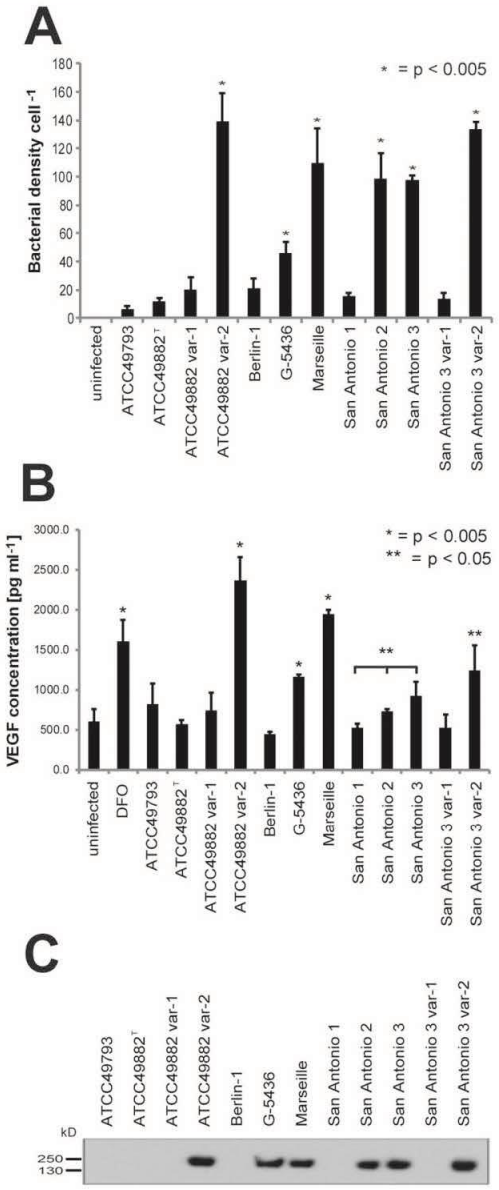

Fig. 2. BadA-dependent cell adhesion, VEGF secretion and Fn binding of *B. henselae* isolates.
A. HUVEC infected with the indicated clinical *B. henselae* isolates at moi of 100 for 30 min were fixed, stained with TRITC-labelled phalloidin and DAPI, followed by quantification of bacterial binding to cells by fluorescent microscopy. Compared with strain ATCC49882^T, all strains expressing BadA showed significantly ($P < 0.005$) enhanced binding (marked by asterisks).
B. VEGF concentrations were determined in supernatants of HeLa-229 cells infected with the indicated clinical *B. henselae* isolates at moi 500 for 48 h. Compared with uninfected HeLa-229 cells, strains that induced a significant increase in VEGF concentration were labelled with one asterisk ($P < 0.005$). The BadA-positive strains San Antonio 2 and San Antonio 3 displayed slight induction of VEGF secretion which was significantly higher than that caused by the BadA-negative strain San Antonio 1 labelled with two asterisks ($P < 0.05$).
C. Bacteria of the indicated *B. henselae* isolates grown on Fn-containing agar plates for 4 days were harvested, lysed, and total lysates were separated by SDS-PAGE, blotted to nitrocellulose and probed with anti-Fn antibodies. All strains expressing BadA showed Fn binding.

Taken together, all BadA-expressing strains showed a significant increase in VEGF secretion, adherence to ECs and Fn binding compared with BadA-negative strains. Furthermore, all strains tested positive for BepD, VirB5 and VirB7 were able to build up a functional VirB/D4 T4SS and promote effector translocation as well as invasome formation with the sole exception of San Antonio 3 var-2. Since the San Antonio 3 variants differ in BadA expression, the results indicate that BadA negatively influences the function of the VirB/D4 T4SS of *B. henselae*.

Construction and initial characterization of artificial BadA expressing ATCC49882 var-1 strains

To further investigate details of the functional interference between BadA and VirB/D4, we first introduced plasmids pPK7 (Kaiser *et al.*, 2012) and pBF1, respectively, into the BadA-negative but VirB/D4-positive strain ATCC49882 var-1, resulting in strains ATCC49882 var-1/pPK7 and ATCC49882 var-1/pBF1. Plasmid pPK7 encodes an engineered BadA from strain Marseille that lacks 18 of 22 neck-stalk repeats while plasmid pBF1 encodes full-length BadA of strain Marseille. Next, plasmid pML007 encoding for the NLS–Cre–BID translocation reporter protein was introduced into ATCC49882 var-1, ATCC49882 var-1/pPK7 and ATCC49882 var-1/pBF1 resulting in strains ATCC49882 var-1/pML007, ATCC49882 var-1/pPK7+pML007 and ATCC49882 var-1/pBF1+pML007. Both plasmids pPK7 and pBF1 encode a *rep* origin of replication that is compatible with *ori* ColE1 of plasmid pML007 (Kovach *et al.*, 1995). In addition, plasmids pML007 and pRS51 were introduced in *B. henselae* Marseille and *B. henselae* Marseille BadA$^-$, resulting in strains Marseille/pML007 and Marseille BadA$^-$/pRS51. In strain Marseille BadA$^-$ the *badA* gene is interrupted by a transposon (Riess *et al.*, 2004). All of the constructed *B. henselae* strains were tested by immunofluorescent labelling (Fig. 4A) revealing a homogeneous BadA surface expression on ATCC49882

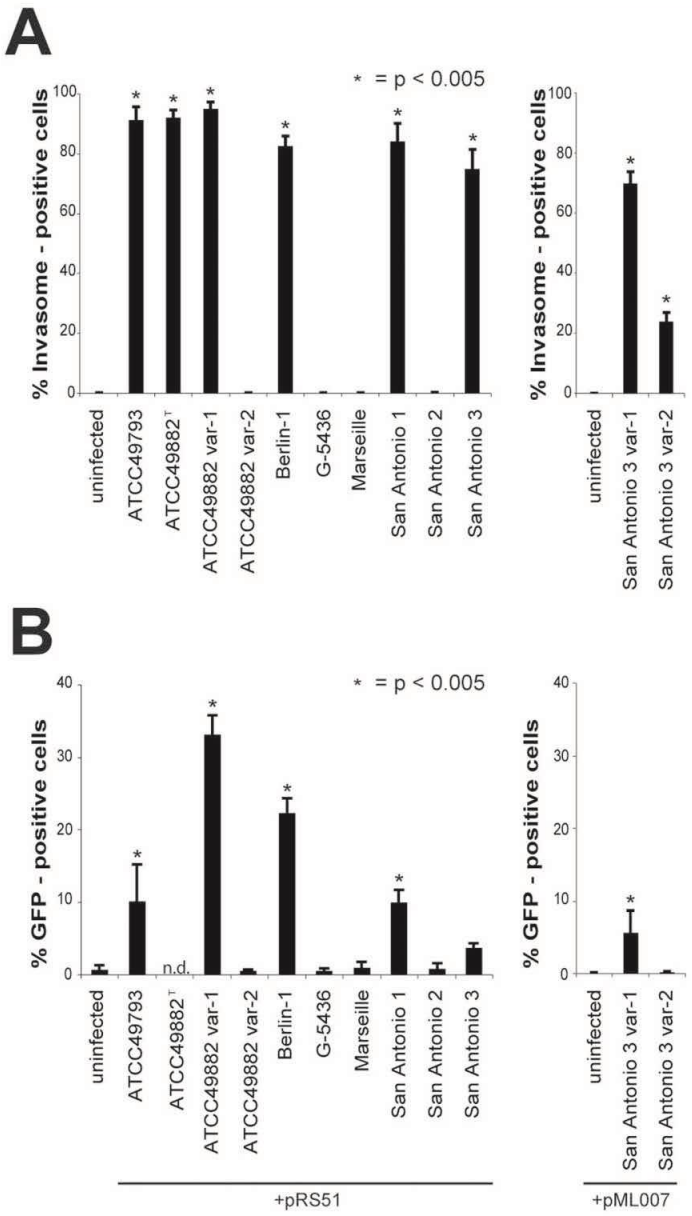

Fig. 3. T4SS-dependent phenotypes of primary clinical isolates of *B. henselae* include invasome formation and effector translocation assays.
A. In invasome formation assay, Ea.hy926/pRS56-c#B1 cells were infected with *B. henselae* clinical isolates at moi = 100 for 48 h. Following fixation, staining with TRITC-phalloidin and DAPI and image acquisition by automated epifluorescence microscopy, invasomes were quantified ($n > 500$ cells). ATCC49793, ATCC49882, ATCC49882 var-1, Berlin-1, San Antonio 1, San Antonio 3 and San Antonio 3 var-1 induced invasomes in a high percentage (70–90%) of infected cells. Infection with San Antonio 3 var-2 resulted in around 20% invasome-positive cells. ATCC49882 var-2, G-5436, Marseille and San Antonio 2 infections prevented invasome formation. Data marked by an asterisk differ statistically significantly ($P < 0.005$) from uninfected control.
B. In CRAfT assays, Ea.hy926/pRS56-c#B1 cells were infected with *B. henselae* clinical isolates containing pRS51 or pML007 at moi = 400 for 96 h. Following fixation, staining with DAPI and image acquisition by automated epifluorescence microscopy, GFP-positive cells were quantified ($n > 500$ cells). Infection with ATCC49882 var-1/pRS51 and Berlin-1/pRS51 resulted in ~ 20–30% GFP-positive cells while infections with ATCC49793/pRS51, San Antonio 1/pRS51, San Antonio 3/pRS51 and San Antonio 3 var-1/pML007 resulted in ~ 5–10% GFP-positive cells. ATCC49882 var-2/pRS51, G-5436/pRS51, Marseille/pRS51, San Antonio 2/pRS51 and San Antonio 3 var-2/pML007 did not show any GFP signal above background levels. Data marked by an asterisk differ statistically significantly ($P < 0.005$) from uninfected control.

var-1/pPK7+pML007 and ATCC49882 var-1/pBF1+pML007, but not on the parental control ATCC49882 var-1/pML007 nor on Marseille BadA$^-$/pRS51. To confirm these findings, *B. henselae* total lysates were analysed by immunoblotting using antibodies targeting the BadA head, VirB7, VirB5 or BepD (Fig. S2A). Furthermore, expression of the NLS–Cre–BID fusion protein was verified by immunoblot analysis in all mutants (Fig. S2B).

Our results demonstrate that we successfully constructed a set of *B. henselae* mutants with a BadA-negative/VirB/D4-positive (ATCC49882 var-1/pML007), truncated BadA-positive/VirB/D4-positive (ATCC49882

© 2012 Blackwell Publishing Ltd, *Cellular Microbiology*, **15**, 759–778

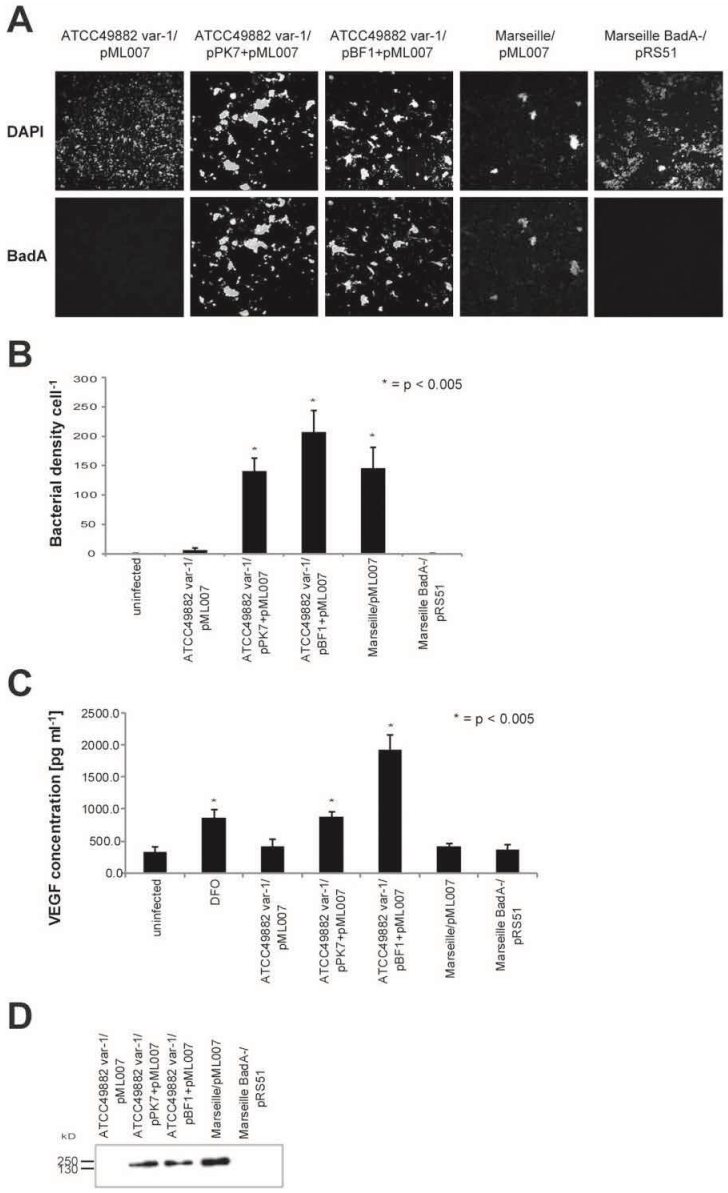

Fig. 4. Functional analysis of BadA in *B. henselae* mutants.
A. By immunofluorescent labelling using anti-BadA-staining, ATCC49882 var-1/pPK7+pML007, ATCC49882 var-1/pBF1+pML007 and Marseille/pML007 showed homogeneous BadA surface expression, whereas ATCC49882 var-1/pML007 and Marseille BadA$^-$/pRS51 were BadA negative.
B. The BadA expressing recombinant strains ATCC49882 var-1/pPK+pML007, ATCC49882 var-1/pBF1+pML007 and Marseille/pML007 showed significantly ($P < 0.005$) enhanced binding to HUVEC compared with isogenic BadA-negative strains (ATCC49882 var-1/pML007 and Marseille BadA$^-$/pRS51).
C. Mutants ATCC49882 var-1/pPK+pML007 and ATCC49882/pBF1+pML007 induced a significant ($P < 0.005$) induction of VEGF secretion of HeLa-229 cells compared with uninfected control cells.
D. Strains ATCC49882/pPK7+pML007, ATCC49882/pBF1+pML007 and Marseille/pML007 exhibited Fn binding in an immunoblot-based analysis.

© 2012 Blackwell Publishing Ltd, *Cellular Microbiology*, **15**, 759–778

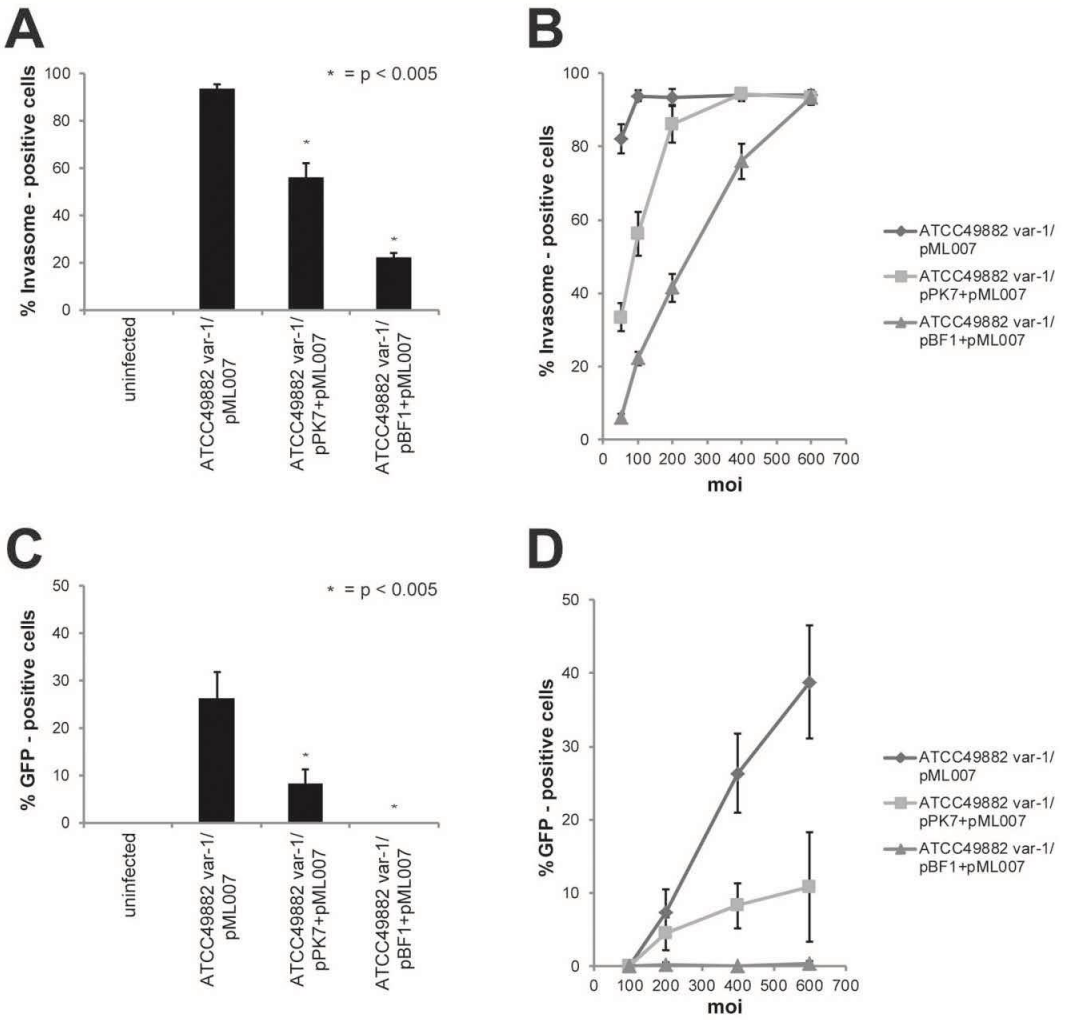

Fig. 5. Functional analysis of VirB/D4 T4SS in the presence of BadA.
A. For analysis of invasome formation, Ea.hy926/pRS56-c#B1 cells were infected with ATCC49882 var-1/pML007, ATCC49882 var-1/pPK7+pML007 or ATCC49882 var-1/pBF1+pML007. Invasomes were quantified ($n > 500$ cells) by automated epifluorescence microscopy. Infection with ATCC49882 var-1/pML007 resulted in 90% invasome-positive cells while ATCC49882 var-1/pPK7+pML007 caused 50% and ATCC49882 var-1/pBF1+pML007 20% invasome-positive cells. Data marked by an asterisk differ statistically significantly ($P < 0.005$) from ATCC49882 var-1/pML007 infection.
B. The percentage of invasome-positive cells increased with ascending moi (from 50 to 600) for all tested strains.
C. For CRAfT assays, Ea.hy926/pRS56-c#B1 cells were infected with ATCC49882 var-1/pML007, ATCC49882 var-1/pPK7+pML007 or ATCC49882 var-1/pBF1+pML007. GFP-positive cells were quantified ($n > 500$ cells) by automated epifluorescence microscopy. Infection with ATCC49882 var-1/pML007 resulted in ~ 30% GFP-positive cells; with ATCC49882 var-1/pPK7+pML007 in ~ 10% GFP-positive cells whereas infection with ATCC49882 var-1/pBF1+pML007 did not result in GFP-positive cells. Data marked by an asterisk differ statistically significantly ($P < 0.005$) from the ATCC49882 var-1/pML007 infection.
D. In CRAfT assays, the percentage of GFP-positive cells upon infection with ATCC49882 var-1/pML007 or ATCC49882 var-1/pPK7+pML007 increased with the increasing moi (from 100 to 600). Infection with ATCC49882 var-1/pBF1+pML007 did not result in GFP-expressing cells.

© 2012 Blackwell Publishing Ltd, *Cellular Microbiology*, **15**, 759–778

effect. However, we cannot fully exclude that expression of BadA might affect transcriptional regulation of genes other than *bepD, virB5* and *virB7* and/or synthesis of proteins affecting the function of the VirB/D4 T4SS.

Disruption of BadA in strain Marseille restores VirB/D4 T4SS-dependent phenotypes

Clinical isolate Marseille was on the basis of immunoblot analysis categorized into the group of BadA-positive/VirB/D4-negative strains (Fig. 1B). Further, this strain was negative in invasome formation as well as CRAfT assay for effector translocation (Fig. 3A and B). Interestingly, the Marseille-derived BadA-negative strain Marseille BadA$^-$/pRS51 was able to trigger invasome formation and efficiently translocate the NLS–Cre–BID translocation reporter fusion protein into Ea.hy926/pRS56-c#B1 cells in a moi-dependent manner in contrast to the BadA-positive strain Marseille/pML007 (Fig. 7A–D). Analysis of the transcription levels of *bepD*, *virB4* and *virB7* in strains Marseille/pML007 and Marseille BadA$^-$/pRS51 by qPCR showed similar to the situation in ATCC49882 var-1/pML007 an approximately twofold upregulation of *virB4* and *virB7* in the absence of BadA (Fig. S2C). Importantly, the *virB* operon was similarly induced in both tested strains when cultivated in M199/10% FCS medium in comparison with CBA (Fig. S2C). These results confirm that VirB/D4 T4SS-dependent effector secretion was enabled by the disruption of BadA in strain Marseille rather than by a transcriptional gene regulatory effect.

To gain further information about the VirB/D4 T4SS in strain Marseille, we sequenced the respective genomic region including the *virB* operon, *virD4* and the *bep* genes. To date, sequence information of strain Marseille was limited only to a few genes including *badA*. Furthermore, sequence information for the *vir* operon was only available of strain Houston-1 (Accession No. NC_005956.1). Therefore, sequencing of strain Marseille's *vir* operon allowed us to correlate the nucleotide and deduced protein sequence data with further functional analysis of the VirB/D4 T4SS in strain Marseille. For sequencing purposes, primers for creating overlapping PCR fragments were deduced from the published *B. henselae* str. Houston-1 genome and fragments were subsequently sequenced. The assembled nucleotide sequence displayed only minor differences within the nucleotide positions when it was compared with the Houston-1 genomic region containing the *virB* operon, *virD4* and *bep* genes. However, the Marseille sequence revealed four bigger deletions of 192, 30, 108 and 252 bp respectively (corresponding to base-pairs 1525708–1525900, 1530926–1530956, 1534886–1534994 and 1535050–1535302 in genomic sequence of strain Houston-1 respectively). Annotation of the strain Marseille genomic fragment revealed open reading frames encoding for proteins that show high similarities to VirB2-11, BepA-G and VirD4 of *B. henselae* str. Houston-1 while the genes were arranged in the same order like in strain Houston-1. Furthermore, like in strain Houston-1, a small protein of unknown function is encoded between *virB11* and *bepA*. Deleted regions in strain Marseille span part of the intergenic region between *virD4* and *bepB*, part of *bepD* and two parts of *bepF*.

Sequence alignments using CLUSTALW2 revealed that Houston-1 and Marseille VirB proteins and VirD4 are nearly identical with very few amino acid changes within the sequences while VirB2 and the central part of VirB5 differed to a certain degree from each other (Fig. S3). Furthermore, most Beps of Houston-1 and Marseille showed a high degree of identity, however, with major differences in BepD and BepF (Fig. S3). Within BepD the deduced amino acids corresponding to positions 55–65 of Houston-1 BepD were missing. Marseille BepF missed deduced amino acids that match positions 145–170 and 202–285 of Houston-1 BepF and therefore tyrosine phosphorylation sites Y_{149}, Y_{213}, Y_{241} and Y_{269} (Truttmann *et al.*, 2011a) are missing while *Bartonella* intracellular delivery (BID) domains F1, F2 and F3 are identical to Houston-1 BepF domains.

Discussion

In our study, we investigated the interaction between the two pathogenicity factors BadA and VirB/D4 T4SS of *B. henselae*. Interactions between adhesins and type III (T3SS) or T4SS play significant roles in infection processes in numerous Gram-negative pathogens. In *Helicobacter pylori* for example, the Cag-T4SS mediates the injection of the bacterial toxin CagA into host cells (Backert and Selbach, 2008) and its adhesins BabA, SabA and others promote an initial and sustained host cell contact (Backert *et al.*, 2011). Furthermore, binding between BabA and its host cell receptor potentiates T4SS-mediated secretion of CagA resulting in inflammation, intestinal metaplasia and disruption of tight junctions between epithelial cells within the intestinal mucosa and enables interaction of the T4SS with integrins on the basolateral side of the epithelial cells (Ishijima *et al.*, 2011). In enteropathogenic *Escherichia coli* (EPEC), the translocated intimin receptor (Tir) is delivered into host cells via a T3SS and subsequent binding of the adhesin intimin to Tir promotes translocation of factors necessary to disrupt tight junctions between epithelial cells (Miyake *et al.*, 2005). In *Pseudomonas aeruginosa*, bacterial adherence by type IV pili or alternative adhesins is a prerequisite for effective T3SS-dependent delivery of exoenzymes (Sundin *et al.*, 2002) and also in *Salmonella enterica a* close cooperation of the adhesin SiiE and the

T3SS encoded in *Salmonella* pathogenicity island 1 (SPI1) is required to infect polarized epithelial cells from their apical side (Gerlach *et al.*, 2008).

In analogy to these described synergistic mechanisms, one could assume that expression of BadA may be essential to ensure efficient function of the VirB/D4 T4SS in *B. henselae* (Kaiser *et al.*, 2011). However, our results showed that BadA rather suppresses than enhances effector protein secretion by the VirB/D4 T4SS: expression of full-length BadA completely abolished Cre-fusion protein translocation by the VirB/D4 T4SS positive strain ATCC49882 var-1. Accordingly, inactivation of *badA* by a transposon recovered VirB/D4 T4SS-dependent effector translocation in strain Marseille. Furthermore, in contrast to clinical isolate San Antonio 3 var-1 (BadA-negative), San Antonio 3 var-2 (BadA-positive) was unable to translocate Cre-fusion proteins although both strains showed similar expression of VirB5, VirB7 and BepD.

Like effector protein translocation, invasome formation was also affected by the presence of full-length and truncated BadA, but in contrast to Cre-fusion protein translocation, invasome formation was reduced but not completely abolished by the overexpression of BadA. Strains ATCC49882 var-1/pPK7+pML007 (expressing truncated BadA) and ATCC49882 var-1/pBF1+pML007 (expressing full-length BadA) were still able to trigger a comparable number of invasomes per cells as the wild-type strain ATCC49882 var-1/pML007 (BadA negative), however at much higher moi. These results could be explained by different assay sensitivities between the invasome formation assay and the CRAfT effector translocation assay.

The negative effect of the VirB/D4 T4SS functions depended on the length of BadA since ATCC49882 var-1/pPK7+pML007 which expresses truncated BadA was still able to translocate effector proteins, however in a strongly reduced number. TEM observations of ECs infected with *B. henselae* strains ATCC49882 var-1/pPK7+pML007 (length of BadA: ~ 40 nm) and ATCC49882 var-1/pBF1+pML007 (length of BadA: ~ 240 nm) revealed a remarkable spacing between bacteria and host cell membranes. To date, the structure of the VirB/D4 T4SS can only be modelled, mainly based on results from structural analysis of subcomplexes (Mainardi *et al.*, 1996). In the putative model, a T4SS apparatus consists of three subparts, including a cytoplasmic membrane complex, a double membrane spanning channel and an external pilus. However, unlike for T3SS, the existence of a needle-like pilus structure for VirB/D4 T4SS remains elusive. Although the existence of such a pilus is still under debate, the enormous distance between *B. henselae* and the host cell membrane due to BadA expression severely affected VirB/D4 T4SS-dependent effector secretion. Interestingly, a similar regulatory mechanism is described for the trimeric autotransporter adhesin YadA and the T3SS of *Y. enterocolitica*. Studies comparing YadA and T3SS of *Y. enterocolitica* showed that increasing the distance between the injectisome and the host cell by shortening the needle tip of T3SS or by lengthening YadA resulted in the reduction of protein translocation and indicated that contact between the T3SS and the host cell membrane is necessary to trigger effector protein translocation (Mota *et al.*, 2005). Furthermore, a defect in glycosylation that elongates the O-antigen (OAg) of the lipopolysaccharides of *Shigella flexneri* subsequently leads to decreased effector translocation via the T3SS (West *et al.*, 2005). Also, *S. enterica* strains defective in synthesis of long OAg species showed increased translocation of a SPI1-T3SS effector protein and increased invasion (Holzer *et al.*, 2009), further suggesting that an optimal distance between bacterial surface and host cell membrane is a prerequisite for T3SS-dependent effector translocation. In contrast to YadA or glycosylated OAgs that provide a distance that allows effective protein translocation via T3SS, BadA strongly interferes with effector translocation by the VirB/D4 T4SS. This might indicate on the one hand that BadA and VirB/D4 interact under conditions present in the human host that were not taken into account in our *in vitro* assays comparable to the interaction between the above mentioned SiiE and SPI1-T3SS of *S. enterica* that only occurred during infection of polarized epithelial cells but was not observed during infection of non-polarized epithelial cells (Gerlach *et al.*, 2008). Under certain conditions, BadA might bend during binding to the host cell which decreases the distance between the bacterial surface and the host cell membrane, therefore allowing effector protein translocation via the VirB/D4 T4SS. On the other hand our results might indicate that both pathogenicity factors have different functions during the infection process.

The current model for the development of vasoproliferative disorders in humans proposes an initial colonization of ECs subsequently leading to a direct mitogenic stimulation and inhibition of apoptosis (Franz and Kempf, 2011; Harms and Dehio, 2012). A pro-inflammatory activation in the infected ECs recruits macrophages to the site of infection. Finally, *B. henselae* colonizes macrophages or other host cells and induces secretion of VEGF that leads to a mitogenic stimulation of ECs in a paracrine loop manner (Kempf *et al.*, 2001; Resto-Ruiz *et al.*, 2002). Based on *in vitro* experiments, both BadA and the VirB/D4 T4SS contribute to various steps in this model and complement one another. BadA mediates adherence to extracellular matrix proteins and ECs under static and dynamic conditions (Riess *et al.*, 2004; Müller *et al.*, 2011) and *B. henselae* subsequently colonizes ECs via endocytic uptake (Kyme *et al.*, 2005). In absence of BadA,

© 2012 Blackwell Publishing Ltd,

isolates. In contrast to other adhesins in Gram-negative bacteria, BadA did not support the functions of a protein secretion system (here: VirB/D4 T4SS). Rather, BadA negatively affected the functions of the T4SS by inhibiting direct contact between the T4SS by acting as a spacer between the bacterial cell envelope and the host cell membrane. In contrast, BadA-dependent Fn binding, VEGF secretion and adhesion to ECs were not affected by a functional VirB/D4 T4SS suggesting a strict regulation of BadA expression under physiological conditions to enable the functions of the VirB/D4 T4SS during infections. The identification of strains expressing both pathogenicity factors in conjunction with appropriate culture and animal models will enable further experiments to understand the role of BadA and the VirB/D4 T4SS in the development of vasoproliferative disorders in humans in response to *B. henselae* infections.

Experimental procedures

Bacterial strains, growth conditions and conjugations

Bartonella henselae strains were grown on Columbia base agar plates supplemented with 5% sheep blood (Bioreba, Reinach, Switzerland or Becton Dickinson, Heidelberg, Germany) (CBA) or cultured in medium M199 (Caisson Labs, North Logan, UT, USA)/ 10% fetal calf serum (FCS) (Life technologies, Carlsbad, CA, USA) with appropriate antibiotics at 37°C and 5% CO_2 for 2–4 days. Bacterial stock suspensions were produced as described in Kaiser *et al.* (2012). Dilution streaking of bacteria was performed based on the three sector T streak pattern. *E. coli* strains were cultivated in Luria–Bertani liquid broth (LB) or solid agar plates supplemented with appropriate antibiotics at 37°C overnight. Antibiotics were purchased at Sigma-Aldrich (Deisenhofen, Germany) and used in the following concentrations: kanamycin 30 μg ml^{-1}, gentamicin 10 μg ml^{-1}, chloramphenicol 1 μg ml^{-1}. Constructed plasmids were transferred into *B. henselae* by triparental matings or electroporation. Triparental matings between *B. henselae* and *E. coli* strains were performed as described (Ditta *et al.*, 1980; Dehio and Meyer, 1997). For electroporation, *B. henselae* was grown for 3–5 days on CBA, harvested and washed three times in ice-cold 10% glycerol (Sigma-Aldrich). Competent cells were mixed with 7.5 ng of plasmid DNA per μl and Type One Restriction Inhibitor (Epicentre, Madison, WI, USA) and shocked at 25 μF, 2.5 kV and 200 Ω using a Gene Pulser II (Bio-Rad, München, Germany). Cells were regenerated in RPMI 1640 medium (Biochrom, Berlin, Germany) supplemented with 1% glutamine, 1% Hepes, 1% sodium pyruvate (both Biochrom), 5% FCS (Sigma-Aldrich) and 5% rabbit blood lysate for 3.5 h. Supplementary Table S1 lists all bacterial strains used in this study.

Cell lines and cell culture

Human umbilical vein endothelial cells (HUVEC) were isolated and cultivated in EC growth medium (PromoCell, Mannheim, Germany) as described (Dehio *et al.*, 1997; Kempf *et al.*, 2000). The stable transfected endothelial cell line Ea.hy926/pRS56-c#B1 was cultured in DMEM (Life technologies) supplemented with 10% FCS as reported (Schülein *et al.*, 2005). HeLa-229 cells were cultivated in RPMI-1640 medium supplemented with 10% FCS as described in Kempf *et al.* (2005).

Plasmid construction

DNA manipulations were carried out following standard protocols. Plasmid pML007 was obtained from pRS51 (Schülein *et al.*, 2005) by replacing gentamicin (Gm) resistance to kanamycin (Km) resistance. Km resistance cassette was amplified by primer pairs, prML214/prML215. The purified PCR product was digested by BglI and BspHI (creating a compatible end for NcoI) and by ligation into pRS51 cut by BglI and NcoI to substitute for Gm resistance cassette. Furthermore, chloramphenicol resistance cassette in plasmid pTR15 (Riess *et al.*, 2004) was replaced by Gm resistance in order to produce plasmid pBF1. For this purpose, the Gm resistance gen of plasmid pBBR1-MCS5 was amplified by PCR using primer pair Gm-for/Gm-rev. Both primers were identical to the primers originally used for construction of plasmid pBBR1-MCS5 (Kovach *et al.*, 1995) with SphI and AatII restriction sites added to their respective 5′ ends. All constructs were confirmed by sequencing. Supplementary Table S3 lists all plasmids and primers constructed or used in this study respectively.

DNA sequencing and analysis of B. henselae *Marseille vir operon*

Sequencing of *B. henselae* Marseille *vir* operon was done by GATC Biotech AG (Konstanz, Germany) on an ABI 3730XL analyser (Applied Biosystems, Carlsbad, CA, USA) by two-sided analysis of 36 overlapping PCR fragments being 1.0–1.2 kb in length. Primers were deduced from *B. henselae* str. Houston-1 genomic sequence (Accession No. NC_005956) and are depicted in Supplementary Table S3. In case of unclear PCR and/or sequencing results, various primer pairs were used. Sequence data were assembled by using the SeqMan Pro-Module of Lasergene software (DNASTAR, Madison, WI, USA) and annotated by using the Open Reading Frame Finder (http://www.ncbi.nlm.nih.gov/gorf/gorf.html). CLUSTALW2 (http://www.ebi.ac.uk/Tools/msa/clustalw2/) was used for alignment of nucleotide sequences. Deduced amino acid sequences were analysed via BLASTP (http://www.ncbi.nlm.nih.gov/blast/Blast.cgi) using the non-redundant protein sequences (nr) database and CLUSTALW2. Sequence was deposited in GenBank with Accession No. JQ701698.

RNA extraction and quantitative PCR

RNA was isolated using modified hot-phenol extraction, including an RNA cleanup using the RNeasy Mini Kit (Qiagen, Hilden, Germany) combined with TURBO DNase digestion (Life technologies). RNA samples were prepared from *B. henselae* strains grown on CBA or cultured in M199/10% FCS. Bacterial pellets were suspended in 500 μl of TE buffer containing 0.5 mg ml^{-1} lysozyme, lysed by adding 50 μl of 10% SDS and naturalized by adding 55 μl of 3 M Sodium acetate (pH 5.2). RNA was extracted by adding 600 μl of water-saturated phenol (Roth, Karlsruhe, Germany) and incubation at 64°C for 6 min. The sample was chilled on ice for 5 min and centrifuged at 13 000 *g*

cells per image was determined by MetaXpress in-build analysis modules (CountNuclei). Invasomes on the same images were defined and counted by eye. In every experiment, at least 500 cells were analysed per condition.

Cre recombinase reporter assay for translocation (CRAfT)

Craft assays in a 96-well plate format have been performed according to previously published methods (Truttmann *et al.*, 2011c). In brief, 2000 Ea.hy926/pRS56-c#B1 cells were seeded in wells of a 96-well plate. The next day, cells were washed once with 50 μl of M199/10% FCS and infected with *B. henselae* strains harbouring plasmids containing NLS–Cre–BID fusions at moi = 400 (unless stated differently) per strain in 100 μl of medium M199/10% FCS supplemented with 500 μM isopropyl β-D-thiogalactoside (IPTG) (Promega) to induce GFP expression. After 96 h of infection, cells were fixed with 3.7% PFA, stained and subjected to automated microscopy as described above. At least 500 cells were analysed per condition.

Quantification of VEGF

HeLa-229 infections for analysis of bacterial induced VEGF secretion were performed as described in Kaiser *et al.* (2012). In brief, 1.0×10^5 cells per well were seeded in 24-well plates overnight and subsequently infected with *B. henselae* using a moi of 500. After 48 h, culture supernatants were centrifuged at 18 000 *g* for 10 min. Finally, centrifugation supernatants were stored at –20°C. Concentration of secreted VEGF was determined in culture supernatants of infected HeLa-229 cells using Quantikine® Immunoassay Human VEGF ELISA (R&D systems, Wiesbaden, Germany) according to the manufacturer's instructions.

Confocal laser scanning microscopy

For confocal laser microscopy, the stained samples were analysed using an IQ iXON spinning disc system from Andor in combination with an Olympus IX2-UCB microscope. Images were exported and finalized using ImageJ (National Institute of Mental Health, Rockville, Maryland, USA).

Fluorescence microscopy

Fluorescence of TRITC-labelled phalloidin and DAPI stained coverslips was detected using the Axio Imager.M2 (Zeiss, Oberkochen, Germany) equipped with a Spot RT3 Slider colour and monochrome camera (Visitron Systems, Puchheim, Germany) and images were visualized by VisiView Software (Visitron Systems). In total, nine coverslips were observed per *B. henselae* clinical isolate. Quantification of bacteria adhering to HUVEC was performed by counting cell-adherent bacteria on three images from three different coverslips.

Transmission electron microscopy (TEM)

HUVEC were seeded into gelatin-coated 10 cm dishes with 90% confluence and infected with 1.0×10^9 *B. henselae*. After 1 h post infection, cells were washed once with PBS and fixed with 3 ml of fixative [3% PFA and 0.5% glutaraldehyde (Sigma-Aldrich) in 10 mM PBS, pH 7.4] for 30 min at RT. After washing with PBS, secondary fixation was performed with 1% osmium tetroxide (Electron Microscopy Sciences, Hatfield, PA, USA) plus 1.5% potassium ferrocyanide (Sigma-Aldrich) for 40 min and third fixation was with 1% osmium tetroxide for 40 min. Afterwards the samples were washed once with ddH_2O and dehydrated with ethanol-gradient steps (50%, 70%, 90%, 100%; 10 min each). The samples were incubated with acetone for 10 min, then with ethanol:acetone = 1:1 for 1 h and with 100% ethanol for 2 h. Subsequently, samples were embedded at 60°C for 24 h. For staining, samples were incubated with 6% Uranyl acetate (Honeywell International, Morristown, NJ, USA) for 1 h and with lead citrate (Merck) for 2 min. In addition, for negative staining, a drop (~ 5 μl) of bacterial sample was placed on a glow-discharged specimen grid for 60 s. The girds were washed twice with ddH_2O. Samples were stained with 0.5% uranyl acetate first time for 1 s and second time for 10 s. Micrographs were taken on the Morgagni 268(D) transmission electron microscope (FEI, Hillsboro, OR, USA).

Determination of bacteria–cell surface distances

In micrographs, the shortest distances between bacterial body and HUVEC cellular membrane were measured by ImageJ (National Institute of Mental Health) and further referred to the scale. At least, 100 measurements were taken per sample.

Statistics analysis

The *t*-test was used to compare two groups, and *P*-values < 0.005 (alternatively < 0.05 when VEGF secretion induced by the three San Antonio 3 strains was analysed) were considered statistically significant and indicated by asterisks (*). The error bars represent the standard error of the mean.

Acknowledgements

We acknowledge excellent technical assistance by Claudia Mistl, Maxime Québatte and Wibke Ballhorn. We are grateful to Vesna Olivieri, Ursula Sauder and Markus Dürrenberger for transmission electron microscopy at the Basel Microscopy Center.

Work in Christoph Dehio's laboratory is supported by Grant 31003A_132979 from the Swiss National Science Foundation, Grant 51RT-0-126008 (InfectX) in the frame of SystemsX.ch, the Swiss Initiative for Systems Biology. Work in Volkhard Kempf's laboratory was partially supported by grants from the German Ministery of Education and Research (031A012A) and the Robert Koch-Institute, Berlin, Germany (1369-434).

References

Anderson, B.E., and Neuman, M.A. (1997) *Bartonella* spp. as emerging human pathogens. *Clin Microbiol Rev* **10:** 203–219.

Arvand, M., Wendt, C., Regnath, T., Ullrich, R., and Hahn, H. (1998) Characterization of *Bartonella henselae* isolated

for the barrier disruption induced by enteropathogenic *Escherichia coli*. *Biochem Biophys Res Commun* **337:** 922–927.

Mogensen, J.E., and Otzen, D.E. (2005) Interactions between folding factors and bacterial outer membrane proteins. *Mol Microbiol* **57:** 326–346.

Mota, L.J., Journet, L., Sorg, I., Agrain, C., and Cornelis, G.R. (2005) Bacterial injectisomes: needle length does matter. *Science* **307:** 1278.

Müller, N.F., Kaiser, P.O., Linke, D., Schwarz, H., Riess, T., Schäfer, A., *et al.* (2011) Trimeric autotransporter adhesin-dependent adherence of *Bartonella henselae*, *Bartonella quintana*, and *Yersinia enterocolitica* to matrix components and endothelial cells under static and dynamic flow conditions. *Infect Immun* **79:** 2544–2553.

O'Rourke, F., Schmidgen, T., Kaiser, P.O., Linke, D., and Kempf, V.A. (2011) Adhesins of *Bartonella* spp. *Adv Exp Med Biol* **715:** 51–70.

Quebatte, M., Dehio, M., Tropel, D., Basler, A., Toller, I., Raddatz, G., *et al.* (2010) The BatR/BatS two-component regulatory system controls the adaptive response of *Bartonella henselae* during human endothelial cell infection. *J Bacteriol* **192:** 3352–3367.

Regnery, R.L., Anderson, B.E., Clarridge, J.E., 3rd, Rodriguez-Barradas, M.C., Jones, D.C., and Carr, J.H. (1992) Characterization of a novel *Rochalimaea* species, *R. henselae* sp. nov., isolated from blood of a febrile, human immunodeficiency virus-positive patient. *J Clin Microbiol* **30:** 265–274.

Relman, D.A., Loutit, J.S., Schmidt, T.M., Falkow, S., and Tompkins, L.S. (1990) The agent of bacillary angiomatosis. An approach to the identification of uncultured pathogens. *N Engl J Med* **323:** 1573–1580.

Relman, D.A., Falkow, S., LeBoit, P.E., Perkocha, L.A., Min, K.W., Welch, D.F., and Slater, L.N. (1991) The organism causing bacillary angiomatosis, peliosis hepatis, and fever and bacteremia in immunocompromised patients. *N Engl J Med* **324:** 1514.

Resto-Ruiz, S.I., Schmiederer, M., Sweger, D., Newton, C., Klein, T.W., Friedman, H., and Anderson, B.E. (2002) Induction of a potential paracrine angiogenic loop between human THP-1 macrophages and human microvascular endothelial cells during *Bartonella henselae* infection. *Infect Immun* **70:** 4564–4570.

Rhomberg, T.A., Truttmann, M.C., Guye, P., Ellner, Y., and Dehio, C. (2009) A translocated protein of *Bartonella henselae* interferes with endocytic uptake of individual bacteria and triggers uptake of large bacterial aggregates via the invasome. *Cell Microbiol* **11:** 927–945.

Riess, T., Andersson, S.G., Lupas, A., Schaller, M., Schäfer, A., Kyme, P., *et al.* (2004) *Bartonella* adhesin A mediates a proangiogenic host cell response. *J Exp Med* **200:** 1267–1278.

Riess, T., Raddatz, G., Linke, D., Schäfer, A., and Kempf, V.A. (2007) Analysis of *Bartonella* adhesin A expression reveals differences between various *B. henselae* strains. *Infect Immun* **75:** 35–43.

Rolain, J.M., Scola, B.L., Liang, Z., Davoust, B., and Raoult, D. (2001) Immunofluorescent detection of intraerythrocytic *Bartonella henselae* in naturally infected cats. *J Clin Microbiol* **39:** 2978–2980.

Scheidegger, F., Ellner, Y., Guye, P., Rhomberg, T.A., Weber, H., Augustin, H.G., and Dehio, C. (2009) Distinct activities of *Bartonella henselae* type IV secretion effector proteins modulate capillary-like sprout formation. *Cell Microbiol* **11:** 1088–1101.

Scheidegger, F., Quebatte, M., Mistl, C., and Dehio, C. (2011) The *Bartonella henselae* VirB/Bep system interferes with vascular endothelial growth factor (VEGF) signalling in human vascular endothelial cells. *Cell Microbiol* **13:** 419–431.

Schmid, M.C., Schülein, R., Dehio, M., Denecker, G., Carena, I., and Dehio, C. (2004) The VirB type IV secretion system of *Bartonella henselae* mediates invasion, proinflammatory activation and antiapoptotic protection of endothelial cells. *Mol Microbiol* **52:** 81–92.

Schmid, M.C., Scheidegger, F., Dehio, M., Balmelle-Devaux, N., Schülein, R., Guye, P., *et al.* (2006) A translocated bacterial protein protects vascular endothelial cells from apoptosis. *PLoS Pathog* **2:** e115.

Schülein, R., Guye, P., Rhomberg, T.A., Schmid, M.C., Schroder, G., Vergunst, A.C., *et al.* (2005) A bipartite signal mediates the transfer of type IV secretion substrates of *Bartonella henselae* into human cells. *Proc Natl Acad Sci USA* **102:** 856–861.

Sundin, C., Wolfgang, M.C., Lory, S., Forsberg, A., and Frithz-Lindsten, E. (2002) Type IV pili are not specifically required for contact dependent translocation of exoenzymes by *Pseudomonas aeruginosa*. *Microb Pathog* **33:** 265–277.

Truttmann, M.C., Guye, P., and Dehio, C. (2011a) BID-F1 and BID-F2 domains of *Bartonella henselae* effector protein BepF trigger together with BepC the formation of invasome structures. *PLoS ONE* **6:** e25106.

Truttmann, M.C., Misselwitz, B., Huser, S., Hardt, W.D., Critchley, D.R., and Dehio, C. (2011b) *Bartonella henselae* engages inside-out and outside-in signaling by integrin beta1 and talin1 during invasome-mediated bacterial uptake. *J Cell Sci* **124:** 3591–3602.

Truttmann, M.C., Rhomberg, T.A., and Dehio, C. (2011c) Combined action of the type IV secretion effector proteins BepC and BepF promotes invasome formation of *Bartonella henselae* on endothelial and epithelial cells. *Cell Microbiol* **13:** 284–299.

Welch, D.F., Pickett, D.A., Slater, L.N., Steigerwalt, A.G., and Brenner, D.J. (1992) *Rochalimaea henselae* sp. nov., a cause of septicemia, bacillary angiomatosis, and parenchymal bacillary peliosis. *J Clin Microbiol* **30:** 275–280.

West, N.P., Sansonetti, P., Mounier, J., Exley, R.M., Parsot, C., Guadagnini, S., *et al.* (2005) Optimization of virulence functions through glucosylation of *Shigella* LPS. *Science* **307:** 1313–1317.

Zbinden, R., Hochli, M., and Nadal, D. (1995) Intracellular location of *Bartonella henselae* cocultivated with Vero cells and used for an indirect fluorescent-antibody test. *Clin Diagn Lab Immunol* **2:** 693–695.

Supporting information

Additional Supporting Information may be found in the online version of this article:

© 2012 Blackwell Publishing Ltd,

Fig. S1. Characterization of plasmid pML007 in CRAfT assay and VEGF secretion assay.
A. ATCC49882 var-1/pRS51 and ATCC49882 var-1/pML007 were derived from the same parental strain (ATCC49882 var-1). In CRAfT assays, Ea.hy926/pRS56-c#B1 cells were infected with ATCC49882 var-1/pRS51 or ATCC49882 var-1/pML007. Both strains provided similar percentages of GFP-positive cells increasing with bacterial moi.
B. Three different Marseille/pML007 mutants were unable to induce a significant ($P < 0.005$) VEGF secretion in HeLa-229 cells compared with the parental strain Marseille.
Fig. S2. Analysis of BadA, BepD, VirB5 and VirB7 expression in *B. henselae* mutants.
A. *B. henselae* strains ATCC49882 var-1/pML007, ATCC49882 var-1/pPK7+pML007, ATCC49882 var-1/pBF1+pML007, Marseille/pML007 and Marseille BadA$^-$/pRS51 were tested for BadA, BepD, VirB5 and VirB7 expression by immunoblotting.
B. Expression of NLS–Cre–BID fusion proteins of *B. henselae* mutant strains was verified by Cre immunoblotting.
C. Gene expression of *bepD*, *virB4* and *virB7* of *B. henselae* mutants analysed by quantitative PCR. Results were normalized to expression of the housekeeping gene *rpsL*. The genes *bepD*, *virB4* and *virB7* were twofold downregulated in strain ATCC49882 var-1/pBF1+pML007 compared with ATCC49882 var-1/pML007, *virB4* and *virB7* were upregulated twofold in Marseille BadA$^-$/pRS51 compared with its parental control.
Fig. S3. Comparative sequence analysis between VirB proteins and Beps of strains Houston-1 and Marseille. The amino acid sequence of VirB2-11, VirD4 and BepA-G was deduced by genomic sequencing of *B. henselae* Marseille using Open Reading Frame Finder (http://www.ncbi.nlm.nih.gov/gorf/gorf.html). Sequence was deposited in GenBank with Accession No. JQ701698 CLUSTALW2 (http://www.ebi.ac.uk/Tools/msa/clustalw2/) was used to align amino acid sequences of strain Marseille to strain Houston-1.
Table S1. Bacterial strains used in this study.
Table S2. Antibodies used in this study.
Table S3. Plasmids and primers used in this study.

3.2 Research article II

Bartonella translocated effectors, BepA and BepD, interfere with the maturation of dendritic cells

Yun-Yueh Lu, Christoph Schmutz, Rusudan Okujava, Claudia Mistl, Timo Glatter, Antonius G. Rolink and Christoph Dehio*

* Corresponding author

Manuscript in preparation

Statement of my contribution

My contributions in this study include the establishment of BMDCs as an *ex vivo* model system (Fig. S1), characterization of phenotypic changes of infected BMDCs by *Bartonella* strains and *E. coli* LPS treatment (Fig. 1-2) as well as various comparative analyses of impaired DC maturation patterns by a vast number of *Bhe* mutants (Fig. 3-8 and Fig. 10-13). I constructed the listed of plasmids and *Bhe* mutants which were first described in this study, including strains overexpressing $BepA_{Bhe}$ homologs, $BepD_{Bhe}$ homologs, all of the tyrosine substitution mutants of BepD-$BXBID_{Bhe}$, and lenti-constructs of BepD (table S1 and Fig. S2). Furthermore, I established an *in vitro* model of JAWSII cell line (Fig. S7 and 14) and an inducible lentiviral system to ectopically express interest proteins (Fig. S8). This model was further used for identifying the interaction partners of BepD by Dr. C. Schmutz. In the following, I analyzed the STAT3 activation of infected BMDCs using immunoblotting (Fig. 19-21). I also analyzed the gene regulation of DC maturation markers, cytokines, and crem in infected BMDCs using quantitative PCR (Fig. 9, S4, and S6). For *in vivo* experiments, I first sequenced the *B. taylorii*, its *virB2-11*, *virD4* and *beps* loci (Fig. S9 and S10), and established the *Bta* infection model in mice (Fig. 22). Following, I generated and examined the *Bta* deletion mutants for bacteremia development in mice (Fig. 23 and 24).

This study was done with the great support by Dr. C. Schmutz, Dr. R. Okujava, and C. Mistl. Particularly, Christoph identified the interaction partners of BepD by the quantitative interactomic screen (Fig. 16), phospho-proteomic screen (Fig. 17), and co-immunoprecipitation (Fig. 15 and 18).

3.2.1 Summary

In contrast to bacterial pathogens that cause acute diseases but rapidly cleared by host immune response, *Bartonella* infection in the natural reservoir host leads to long lasting bacteremia. A pre-requisite for this stealth-infection strategy is immune evasion. Dendritic cells (DCs), professional antigen-presenting cells, represent a cell type potentially relevant to the dermal stage of early *Bartonella* infection. To gain better understandings of immune evasion mediated by *Bartonella* immunomodulatory effectors, the murine bone marrow-derived DCs (BMDCs) were used as a model system. In response to *Bartonella* infection, BMDCs failed to fully mature. Impaired DC maturation was characterized by reduced surface expression of MHC class II complex and the co-stimulatory receptors CD40 and CD86, as well as strongly diminished secretion of the pro-inflammatory cytokines TNF-α and interleukin-6. These phenotypic changes were dependent on *Bartonella* effector proteins BepA and BepD, secreted via the type IV secretion system. The effect of BepA was narrowed down to its BID domain in association with elevations of intracellular cAMP level. BepD harbors an N-terminal array of tyrosine-phosphorylation motifs. Mutagenic analysis revealed the contribution of individual phospho-tyrosine residues to the impaired maturation phenotype. Several SH2 domain containing proteins were identified as interaction partners of BepD in dependence of its tyrosine-phosphorylation. Among them, STAT3 became significantly hyper-phosphorylated. STAT3 activation strongly correlated with the impaired DC maturation phenotype suggesting that it represents a key pathway hijacked by BepD to prevent DC maturation. These results showed that *Bartonella* was able to attenuate DC functions which may critically contribute to the modulation of T-cell mediated adaptive immunity. To further uncover the relevance of BepA and BepD in modulation of host immune response *in vivo*, a murine model with *B. taylorii* (*Bta*) infection was established. Through intradermal infection, *Bta* strains with deletion of *bepA* or/and *bepD* seemed to lose the fitness of bacteremia development. However, further optimizations and investigations are needed for a more sensitive *in vivo* system to study the function of Beps. Taken *in vitro* and *in vivo* data, we propose that *Bartonella* utilizes BepA and BepD as immnuomodulatory factors to mediate immune evasion and promote chronic bartonellosis.

3.2.2 Introduction

The host immune response eliminating bacterial infection is based on a combination of both innate and adaptive immune systems. The orchestration of the immune response strictly relies on the interaction of pathogens with professional antigen-presenting cells (APCs). Among APCs, dendritic cells (DCs) have the unique ability to induce a potent antigen-dependent stimulation and play a central role in the initiation of the primary immune response. DCs are strategically located in the peripheral tissues where they reside in an immature state to exert a sentinel function for detecting foreign agents. Microbial stimuli trigger DC "maturation" describing the changes from immature antigen-capturing cells to mature antigen-presenting cells. These significant phenotypes of DC maturation include increased surface expression of co-stimulatory molecules (e.g., CD40, CD80, and CD86) and major histocompatibility complex class II (MHCII), as well as pro-inflammatory cytokine secretion (e.g., IL-6 and TNF-α). Furthermore, modified expression of chemokine receptors and adhesion molecules leads matured DCs migrating from peripheral tissues to the T cell zone of secondary lymphoid organs. Subsequently, activated DCs display pathogen-encoded antigens to naïve T cells and initiate the adaptive immunity [1, 2]. Early recognition of the pathogen-associated molecular patterns (PAMPs), e.g., bacterial lipopolysaccharide (LPS), peptidoglycan (PG), and lipopeptides, plays an essential role in DC maturation through germline-encoded pattern recognition receptors (PRRs). Among PRRs, the family of Toll-like receptors (TLRs) is the most extensively studied. Different TLRs are coupled to distinct downstream signaling pathways by the selective use of different TIR-domain signaling adaptor molecules: MyD88, TRIF, TRAM, and TIRAP (Mal). In the following, three major signaling pathways are able to be activated by TLRs: mitogen-activated protein kinase (MAPK), nuclear factor - κB (NF - κB), and interferon regulatory factors (IRFs), thereby cooperatively mediating pro-inflammatory cytokine production [3, 4].

In recent times it has become clear that DCs are not only immune response initiators for T cell activation but also central inducers in the development of T cell tolerance. The particular immunological outcomes appear to be determined by the maturation state of DCs. Only the mature form promotes full blown T cell responses. In the steady state, immature DCs maintain T cell anergy to prevent self-destruction. More

than a simple “on/off” switch of DC activation, a semi-mature developmental stage of DCs is described in T cell tolerance mechanism. Inducible tolerance is believed to be generally attributed to semi-mature DCs, which are characterized by high levels of MHCII, but low or no expression of co-stimulatory molecules or pro-inflammatory cytokines. Such tolerogenic DCs can convert naïve T cells into regulatory T cells (Treg), which in turn suppress immune responses [5, 6].

Increasing evidence reveals that several bacterial pathogens develop unique mechanisms to subvert DC functions, thereby evading from host immune recognition. For example, *Francisella tularensis* exploits DCs not only as their replicative niches, but also for immune evasion. An attenuated type B strain of *F. tularensis* known as live vaccine strain (LVS) induces phenotypic activation with increased expression of MHCII and CD86 on the surface of DC. In the meanwhile, LVS inhibits the pro-inflammatory cytokines IL-12 and TNF-α secretion to facilitate pulmonary infection [7]. In addition, a virulent type A strain of *F. tularensis* Schu4 prevents the phenotypic activation of pulmonary DCs and macrophages as well as the secretion of pro-inflammatory cytokines [8, 9]. Similarly, other bacterial pathogens (e.g., *Bordetella pertussis* and *Salmonella* Typhimurium) also cause aberrant activation of DC but with limited bacterial growth in DCs. *Bordetella* infection causes phenotypic but not functional maturated DCs which secrete anti-inflammatory cytokine IL-10 and trigger activation of Treg cells [10, 11]. Although *S.* Typhimurium cannot prevent the induction co-stimulatory molecules and cytokine secretion, it is able to interfere with MHCII antigen presentation [12]. Additionally, other studies showed that *Mycobacterium tuberculosis* and *Brucella abortus* share similar profiles to comprehensively inhibit DC maturation. *M. tuberculosis* blocks NF-κB activation via the C-type lectin DC-SIGN, preventing DC maturation and reducing secretion of IL-12 [13-15]. As exemplified by *B. abortus*, its TIR-containing protein Btp1 interferes with TLR2 signaling pathway to inhibit DC maturation [16]. Overall, the manipulation of DC maturation by bacterial pathogens constitutes an effective and powerful strategy for immune evasion.

Bartonella transmission mainly replies on bloodsucking arthropods that initially inoculate bartonellae into the dermis. *Bartonella* infection results in a long-lasting bacteremia where erythrocytes serve as the immune-privileged niche. Little evidence

is available to understand precisely *Bartonella* infection stages from the intradermal inoculation to the bacteremic phase. A murine model of *B. henselae* infection revealed that bacterial DNA were detectable in liver and lymph nodes at 6 hours post intraperitoneal injection, proposing that lymphocytes or mononuclear phagocytes may be the vehicles of *Bartonella* transport [17]. A recent publication showed that *Bartonella* was capable of translocating bacterial effectors into DCs, thereby affecting cell migration [18]. Taken altogether, present evidences strongly suggest that DCs may constitute an important cellular niche to promote *Bartonella* dissemination from the dermis to the lymphatic system. Besides the migratory properties of DCs, we sought to understand consequences of *Bartonella* infection on the immune functions.

Several virulence factors allow bartonellae to adhere, invade, proliferate, and persist within various host-cell types. Particularly, the VirB/D4 type IV secretion system (T4SS) represents an essential virulence factor which is likely required for the initial colonization rather than for the subsequent blood-stage infection [19]. Seven distinct *Bartonella* effector proteins (BepA-G) of *B. henselae* have been identified as conjugative substrates through VirB/D4 T4SS. Evolutionally, Beps maintain their ancestral domain constitution with at least one *Bartonella* intracellular delivery (BID) domain and a positively-charged tail in the C-terminus together as the translocation signal [20]. To date, most studies of T4SS-dependent phenotypes mainly focus on the subversion of various endothelial cell (EC) functions, including massive rearrangements of the actin cytoskeleton (known as invasome structures), activation of the NF-κB-dependent pro-inflammatory response, anti-apoptotic protection, capillary-like sprout formation, and prevention of cell fragmentation [21-26].

Unlike bacterial pathogens which lead to acute infection and induce pro-inflammatory responses, *Bartonella* infection (e.g. *B. bacilliformis*, *B. quintana*, and *B. henselae*) elevates the levels of the anti-inflammatory cytokine IL-10 in human patients and various experimental models [27-30]. Though phenotypic descriptions on immunological attenuation by *Bartonella* infection, it is still unclear how *Bartonella* interferes with functions of the host immune system. Thus, we sought to explore whether *Bartonella* infection subverts DC functions for immune evasion, a strategy shared by other bacteria causing chronic diseases. In this study, we characterized the consequences of *Bartonella* infection on the inhibition of DC maturation, including

downregulation of MHCII, CD40, and CD86 surface expression as well as reduction of pro-inflammatory cytokine secretion, IL-6 and TNF-α. These specific immunosuppression phenotypes were assigned to BepA and BepD. The effect of BepA in DCs was associated with elevation of host cell cyclic adenosine monophosphate (cAMP) concentration. Furthermore, activated STAT3 strongly correlated with the impaired DC maturation phenotype caused by BepD. Thus, this article describes the remarkable features of these two Beps into a new perspective, highlighting the mechanisms they use to hijack host signaling pathways as stealth-attack strategies to evade the host immune responses.

3.2.3 Materials and Methods

Bacterial strains, growth conditions and conjugations

All bacterial strains used in this study were listed in the supplementary table S1. *Bartonella* strains were grown on Columbia base agar plates supplemented with 5% sheep blood (CBA) or cultured in medium M199 (Gibco) with 10% fetal calf serum (FCS) (Gibco) and appropriate antibiotics at 37℃ and 5% CO_2 for 2-4 days. *E. coli* strains were cultivated in Luria-Bertani liquid broth (LB) or on solid agar plates (LA) supplemented with appropriate antibiotics at 37℃ overnight. When indicated, antibiotics or supplements were used in the following concentrations: kanamycin 30 µg ml^{-1}, gentamycin 10 µg ml^{-1}, streptomycin 100 µg ml^{-1}, isopropyl-β-D-thiogalactoside (IPTG) 500 µM and diaminopimelic acid (DAP) 1 mM. Constructed plasmids were introduced into *Bartonella* strains by conjugation from *E. coli* strain β2150 using three-parental mating as described previously by Dehio et al., 1998 [31]

Cell lines and culture conditions

Mouse bone marrow-derived dendritic cells (BMDCs) were differentiated *in vitro* using standard protocol [32]. Briefly, bone marrow cells were flushed from the tibias and femurs of Balb/c mice with culture medium composed of GlutaMAX DMEM (Gibco) supplemented with 10% FCS, 10mM HEPES, 1mM sodium pyruvate, and 0.5 mM β-ME. After one centrifugation, BM cells were resuspended in RBC lysis buffer (Biolegend) for 2 min to lyse RBC. After one more centrifugation, BM cells were cultured at 1×10^6 cells/ml in culture medium supplemented with 200 ng/ml recombinant human Flt3L (produced by 40E1 hybridoma cells, kind gift from Prof. A. Rolink). Cultures were incubated at 37℃ in 5% CO_2 for 8-10 days.

JAWSII cell line (ATCC CRL-11904™, kindly provided from Prof. P. Broz) is a GM-CSF-dependent DC line established from bone marrow cells of a p53-knockout C57BL/6 mouse [33]. JAWSII cells were cultured at 37℃ in 5% CO_2 in complete culture medium consisting of MDM (Sigma-Aldrich) with 10% FCS, 4 mM l-glutamine, 1 mM sodium pyruvate, and 5 ng/ml GM-CSF (produced by X63 hybridoma cells, kind gift from Prof. A. Rolink).

Construction of strains and plasmids

DNA manipulations were performed according to standard techniques and all cloned inserts were DNA sequenced to confirm sequence integrity. Chromosomal deletions of *B. taylorii* were generated by a two-step gene replacement procedure as described previously by Schulein et al., 2002 [19]. For protein complementation/overexpression in *B. henselae* and *B. taylorii*, selected genes were cloned into the plasmid pPG100 or pPG180 under the control of the taclac promoter [20]. For protein overexpression in JAWSII cells, interest genes were cloned into the plasmid pCLX-pTF-R1-DEST-R2-EBR65, which is a lentivector, under the TET-inducible promoter pTF [34] through standard gateway cloning strategy (Gateway system, Invitrogen). TET-modified pTF promoter was induced by adding doxycycline (DOX) to a final concentration of 1 µg/ml. Detailed description for the construction of each plasmid is presented in supporting information. The sequence of all oligonucleotide primers used in this study is listed in table S2.

Infection of BMDCs

For *Bartonella* infection of BMDCs, bacterial strains were cultured in medium M199/10% FCS for 2 days. One day before infection, BMDCs were seeded at 2 × 10^6/well in 6-well plates. Next day, cells were washed once with M199 supplemented with 10% FCS and infected with a multiplicity of infection (MOI) of 25 bacteria per cell in M199/10% FCS/500 µM IPTG. Unless stated differently, infected BMDCs were harvested at 24 hours post-infection for following immunoblot analysis and flow cytometry. The supernatants were collected for cytokine detection.

Lentiviral transduction of JAWSII cells

To generate stable cell lines with integrated selected genes, lentiviral transduction was performed as previously described by Okujava et al., 2014 [18]. Subconfluent (3 × 10^6) HEK 293T cells in 10 cm cell-culture dishes were transfected with a total of 5 µg of plasmid DNA following the FuGENE transfection protocol (FuGENE 6 Transfection Reagent, Roche). After 6 h, the cell culture media was replaced. For viral production, the cells were kept in culture for additional 48 h. One day before the viral transduction, 5 × 10^4 JAWSII cells/well was seeded in the 6-well plate. The viral supernatant was filtered with the 0.45 µm filter and transferred onto the JAWSII cells,

3 ml of viral supernatant in presence of 0.5 µg/ml Polybrene (Sigma) was applied on each well. After 6 h, the cell culture media was replaced by the complete growth media for JWASII cells. Two days after transduction, blasticidin selection (5 µg/ml, Gibco) was performed for additional one week to enrich transduced JAWSII cells.

Determination of cell surface markers by flow cytometry

The following staining reagents from Biolegend were used: PE anti-mouse MHCII (M5/114.15.2), APC anti-mouse MHCII (M5/114.15.2), PE anti-mouse CD40 (3/23), PE anti-mouse CD80 (16-10A1), PE anti-mouse CD86 (GL-1), APC anti-mouse CD86 (GL-1), and APC anti-mouse CD11c (N418). Cell suspensions of BMDCs or JAWSII cells were stained at 4^{o}C with the appropriate antibodies in PBS containing 2% FCS. Surface markers MHCII, CD40, CD80, and CD86 were measured using a FACSCalibur flow cytometer (Becton Dickinson). Dead cells were excluded through the use of propidium iodide. Data were analyzed with FlowJo software (TreeStar). Expression levels of the maturation markers were given as the geometric mean of the fluorescence intensities (GMFI) normalized to samples of *Bhe* Δ*bepA-G* infection.

Determination of cytokine secretion

After 24 hours post-infection, cytokine production was measured in the medium of infected BMDCs with ELISA. All ELISA kits specific to mouse IL-6, IL-12p40, and TNF-α were from eBioscience. The assay was performed following the manufacturers' guidelines.

Immunoblot analysis

Sodium dodecyl sulphate-polyacrylamide gel electrophoresis (SDS-PAGE) and immunoblotting for the detection of the expressed proteins in *Bartonella* were performed as described by Schulein et al., 2005 [20]. *Bartonella* bacterial culture was harvested in PBS after 48 h of growth on CBA plates supplemented with appropriate antibiotics and IPTG. After centrifugation, bacterial cell pellets were directly resuspended in 1x Laemmli sample buffer to final OD_{600} of 4. To verify the interest protein expression levels, infected BMDCs or JAWSII cells were collected and washed twice with 2ml ice-cold PBS. Cell pellets were lyzed by adding 100 µl PhosphoSafe reagent (Novagen) containing 1x protease inhibitor (Roche). Protein concentrations of the cleared lysates were quantified using BCA kit (Thermo

Scientific) and diluted to final 1× Laemmli sample buffer. Immunoblots were examined by the specific primary antibody to the target protein and followed by a 1:5000 dilution of secondary horseradish peroxidase-conjugated antibody (GE Healthcare). In all experiments, immunoblots were developed using LumiGLO chemiluminescent substrate (KPL) and imaged using an ImageQuant LAS 4000 (GE Healthcare). Supplementary material Table S3 lists all primary antibodies used in this study.

Quantitative RT-PCR

RNA manipulation and real-time PCR was performed as previously described by Dehio et al., 2005 [35]. RNA extracts were purified with the RNeasy mini kit (Qiagen) and treated with DNase (RNase-Free DNase Set, Qiagen) to digest contaminating genomic DNA. Reverse transcription was performed using the SuperScript II Reverse Transcriptase (Invitrogen) according to the manufacturer's instructions. cDNA (5 µl of a 1:200 dilution) was subjected to real-time PCR on an ABI PRISM 7000 Sequence Detection System (Applied Biosystems) using a Power SYBR Green PCR Master Mix (Applied Biosystems). qPCRs were set up as follows: one cycle of 95°C for 10 min, followed by 45 cycles of 95°C for 15 sec and 60°C for 1 min. All samples were normalized to GAPDH signal and relative changes in gene expression were determined using the comparative C_T method [36]. Table S2 in the supplemental material lists all primers used for quantitative PCR in this study.

GFP-Trap® _A for Immunoprecipitation

24 hours after seeding JawsII cells, expression of GFP-fused BepD constructs was induced by the addition of 1µg/ml doxycycline for further 24 hours. Cells were put on ice and the supernatant containing cells in dispersion, as well as adherent cells were collected and washed twice with ice-cold PBS. Cells were resuspended in ice-cold lysis buffer (10 mM Tris/Cl pH 7.5; 150 mM NaCl; 0.5 mM EDTA; 0.5% NP-40, 1x PhosSTOP, 1x, 1x cOmplete, Mini, EDTA-free) and incubated for 30 minutes on ice. The cell lysate was centrifuged and the supernatant transferred to a new tube. The sample was subsequently diluted with 1.5x amount of dilution buffer (10 mM Tris/Cl pH 7.5; 150 mM NaCl; 0.5 mM EDTA). Meanwhile GFP-Trap® _A beads were taken and washed twice with ice-cold dilution buffer. The diluted cell lysate was then added to the GFP-Trap® _A beads and incubated for 1h at 4°C tumbled end-over end.

Afterwards, the mixture was washed 4 times with ice-cold dilution buffer and eluted 3 times with ice-cold 0.2M glycine pH 2.5. The eluate was neutralized with Ammoniumbicarbonate to a pH > 8.

Preparation of immunoprecipitated samples for mass spectrometry

Disulfide bonds were reduced with tris (2-carboxyethyl) phosphine at a final concentration of 10 mM at 37 ℃ for 1 h. Free thiols were alkylated with 20 mM iodoacetamide at room temperature for 30 min in the dark. The excess of iodoacetamide was quenched with N-acetyl cysteine at a final concentration of 25 mM for 10 min at room temperature. The proteins were digested overnight at 37 ℃ with sequencing-grade modified trypsin at a protein-to-enzyme ratio of 50:1. Peptides were desalted on a C18 Sep-Pak cartridge and dried under vacuum.

Sample preparation for phosphoproteomics

24 hours after seeding JawsII cells, expression of GFP-fused BepD constructs was induced by the addition of 1µg/ml doxycycline for further 24 hours. The plates were put on ice and washed twice with ice-cold PBS. Samples were then collected in urea solution [8 M Urea, 0.1 m Ammoniumbicarbonate, 1× PhosSTOP]. The samples were briefly vortexed, sonicated at 4 ℃, shaked for 5 min on a thermomixer and centrifuged for 20 min at 4 ℃ and 16 ´ 000g. Supernatants were collected and stored at −80 °C for further processing. BCA Protein Assay was used to measure protein concentration.

Phosphopeptide enrichment

Disulfide bonds were reduced with tris (2-carboxyethyl) phosphine at a final concentration of 10 mM at 37 ℃ for 1 h. Free thiols were alkylated with 20 mM iodoacetamide at room temperature for 30 min in the dark. The excess of iodoacetamide was quenched with N-acetyl cysteine at a final concentration of 25 mM for 10 min at room temperature. Lys-C endopeptidase was added to a final enzyme/protein ratio of 1:200 (w/w) and incubated for 4 h at 37 ℃. The solution was subsequently diluted with 0.1 M ammoniumbicarbonate to a final concentration below 2 M urea and digested overnight at 37 ℃ with sequencing-grade modified trypsin at a protein-to-enzyme ratio of 50:1. Peptides were desalted on a C18 Sep-Pak cartridge and dried under vacuum. Phosphopeptides were isolated from 2 mg of total peptide

mass with TiO2 as described previously [46]. Briefly, dried peptides were dissolved in an 80% acetonitrile (ACN)–2.5% trifluoroacetic acid (TFA) solution saturated with phthalic acid. Peptides were added to the same amount of equilibrated TiO2 (5-µm bead size, GL Sciences) in a blocked Mobicol spin column that was incubated for 30 min with end-over-end rotation. The column was washed twice with the saturated phthalic acid solution, twice with 80% ACN and 0.1% TFA, and finally twice with 0.1% TFA. The peptides were eluted with a 0.3 M NH4OH solution. The pH of the eluates was adjusted to be below 2.5 with 5% TFA solution and 2 M HCl. Phosphopeptides were again desalted with microspin C18 cartridges.

LC-MS/MS analysis

Chromatographic separation of peptides was carried out using an EASY nano-LC system (Thermo Fisher Scientific), equipped with a heated 30cm RP-HPLC column (75 µm x 45 cm) packed in-house with 1.9 µm C18 resin (Reprosil-AQ Pur, Dr. Maisch). Phosphopeptide samples were analyzed per LC-MS/MS run using a linear gradient ranging from 98% solvent A (0.15% formic acid) and 2% solvent B (98% acetonitrile, 2% water, 0.15% formic acid) to 30% solvent B over 120 minutes at a flow rate of 200 nl/min. Peptides derived from immunoprecipitation experiments were analyzed separated on a 60 min gradient. Mass spectrometry analysis was performed on a dual pressure LTQ-Orbitrap mass spectrometer equipped with a nanoelectrospray ion source (both Thermo Fisher Scientific). Each MS1 scan (acquired with the Orbitrap) was followed by collision-induced dissociation (CID, acquired in the LTQ) of the 10 most abundant precursor ions with dynamic exclusion for 30 seconds. For phosphopeptide analysis, the 10 most abundant precursor ions were subjected to CID with enabled multistage activation. Total cycle time was approximately 2 s. For MS1, 106 ions were accumulated in the Orbitrap cell over a maximum time of 300 ms and scanned at a resolution of 240,000 FWHM (at 400 m/z). MS2 scans were acquired using the rapid scan mode, a target setting of 104 ions, and accumulation time of 25 ms. Single charged ions and ions with unassigned charge state were excluded from triggering MS2 events. The normalized collision energy was set to 35%, and one microscan was acquired for each spectrum.

Label-free Quantification and Database Searching

The acquired raw-files were imported into the Progenesis software tool (Nonlinear

Dynamics) for label-free quantification using the default parameters. MS2 spectra were exported directly from Progenesis in mgf format and searched using the MASCOT algorithm (Matrix Science) against a decoy database containing normal and reverse sequences of the predicted SwissProt entries of Mus musculus (www.ebi.ac.uk) and commonly observed contaminants generated using the SequenceReverser tool from the MaxQuant software. The precursor ion tolerance was set to 10 ppm and fragment ion tolerance was set to 0.6 Da. The search criteria were set as follows: full tryptic specificity was required (cleavage after lysine or arginine residues unless followed by proline), 2 missed cleavages were allowed, carbamidomethylation (C) was set as fixed modification and phosphorylation (S,T,Y) or oxidation (M) as a variable modification for TiO2 enriched or not enriched samples, respectively. Finally, the database search results were exported as a xml-file and imported back to the Progenesis software for MS1 feature assignment. For phosphopeptide quantification, a csv-file containing the MS1 peak abundances of all detected features was exported and for not enriched samples, a csv-file containing all protein measurements based on the summed feature intensities of all identified peptides per protein was created. Importantly, the Progenesis software was set that proteins identified by similar sets of peptides are grouped together and that only non-conflicting peptides with specific sequences for single proteins in the database were employed for protein quantification. Both files were further processed using the in-house developed SafeQuant R script [74]. In brief, the software sets the identification level False Discovery Rate to 1% (based on the number of decoy protein sequence database hits) and normalizes the identified MS1 peak abundances (extracted ion chromatogram, XIC) across all samples, i.e. the summed XIC of all confidently identified peptide features is scaled to be equal for all LC-MS runs. In the case of the IP experiments, the summed XIC confidently identified peptide features, matching the bait proteins, were used for normalization. In the case of phosphoproteomoics, all quantified phosphopeptides/proteins are assigned an abundance ratio for each time point, based on the median XIC per time point. The statistical significance of each ratio is given by its q-value (false discovery rate adjusted p values), obtained by calculating modified t-statistic p values and adjusting for multiple testing. The location of the phosphorylated residues was automatically assigned by MASCOT (score >10).

Ethics statement

Animals were handled in strict accordance with good animal practice as defined by the relevant European (European standards of welfare for animals in research), national (Information and guidelines for animal experiments and alternative methods, Federal Veterinary Office of Switzerland) and/or local animal welfare bodies. Animal work was approved by the Veterinary Office of the Canton Basel City on June 2003 (licence no. 1741).

Infection of mice

Female BALB/cJRj mice were obtained at the age of 6-8 weeks from Janvier Labs. All animal studies were approved by the authors' institutional review boards. After one week of adaptation, the mice were infected with *B. taylorii* through the intradermal route. Bacterial strains were grown as described above, harvested in PBS, and diluted to OD_{600} = 0.01. Mice were infected with 10 µl of the bacterial suspension in the dermis of the right ear. Blood samples were taken from the tail vein and immediately mixed with PBS containing 3.8% sodium-citrate to avoid coagulation. After freezing at -70°C and subsequent thawing, undiluted and diluted blood samples were plated on CBA plates at 35°C and 5% CO_2. After 7-10 days of growth, colony forming units (CFU) were counted.

Statistical analysis

Statistical analyses were performed using Student's t test (two-tailed): $p<0.05$ was considered to be statistically significant.

Materials and Methods S1

DNA manipulations

Plasmids for expression of Flag-Beps.

The vector expressing the BepD-BXBID$_{Bhe}$ was constructed by PCR amplifying a fragment of 1104 bp from boiled colony of *B. henselae* RSE247 with the primers prLU174 and prLU175. After digesting the PCR product with *Nde*I, it was inserted in the respective site of the flag-tag expression vector pPG100, yielding pLU030.

The vector expressing the BepA$_{Bgr}$ was constructed by PCR amplifying a fragment of 1657 bp from boiled colony of *B. grahamii* CHDE142 with the primers prLU259 and prLU260. After digesting the PCR product with *Nde*I, it was inserted in the respective site of the flag-tag expression vector pPG100, yielding pLU054.

The vector expressing the BepA-BID$_{Bbi}$ was constructed by PCR amplifying a fragment of 748 bp from boiled colony of *B. birtlesii* PEE0249 with the primers prLU283 and prLU284. After digesting the PCR product with *Nde*I, it was inserted in the respective site of the flag-tag expression vector pPG100, yielding pLU065.

The vector expressing the BepA-BID$_{Bta}$ was constructed by PCR amplifying a fragment of 748 bp from boiled colony of *B. taylorii* LUB046 with the primers prLU285 and prLU286. After digesting the PCR product with *Nde*I, it was inserted in the respective site of the flag-tag expression vector pPG100, yielding pLU064.

The vector expressing the BepD$_{Btr}$ was constructed by PCR amplifying a fragment of 1597 bp from boiled colony of *B. tribocorum* RSE149 with the primers prLU265 and prLU266. After digesting the PCR product with *Nde*I, it was inserted in the respective site of the flag-tag expression vector pPG100, yielding pLU053.

The vector expressing the BepD$_{Bgr}$ was constructed by PCR amplifying a fragment of 1192 bp from boiled colony of *B. grahamii* CHDE142 with the primers prLU281 and prLU282. After digesting the PCR product with *Nde*I, it was inserted in the respective site of the flag-tag expression vector pPG100, yielding pLU061.

The vector expressing the BepD$_{Bbi}$ was constructed by PCR amplifying a fragment of

1078 bp from boiled colony of *B. birtlesii* PEE0249 with the primers prLU234 and prLU235. After digesting the PCR product with *Nde*I, it was inserted in the respective site of the flag-tag expression vector pPG100, yielding pLU060.

The vector expressing the $BepD_{Bta}$ was constructed by PCR amplifying a fragment of 1063 bp from boiled colony of *B. taylorii* LUB046 with the primers prLU074 and prLU075. After digesting the PCR product with *Nde*I, it was inserted in the respective site of the flag-tag expression vector pPG100, yielding pLU058.

Tyrosine to phenylalanine exchange mutant in $BepD_{Bhe}$.

To exchange the putatively phosphorylated tyrosines to phenylalanines in the N-terminus of BepD, we re-amplified the entire plasmid pLU030 containing the sequence coding for BepD-BXBID for site-directed mutagenesis. The template DNA was eliminated by DpnI digestion which specifically targets the methylated DNA. The mutated plasmid generated *in vitro* is unmethylated; thus it was left undigested. To avoid any unexpected mutation generated in the plasmid, the mutated *bepD-BXBID* fragment was cut and inserted into the parental pPG100 vector through the *Nde*I ligation. The Y32F; Y72F; Y92F; Y114F; Y134F (BepD-$BXBID_{Bhe}$ Y→F) mutant was generated after sequential mutation rounds.

Construction of in-frame deletions.

In-frame deletion mutants of *Bta* LUB046 were generated by a two-step gene replacement procedure as described [19, 37]. All mutagenesis plasmids derived from the mutagenesis vector pTR1000 harbor a cassette with the flanking regions of the in-frame deletion in the genes of interest. This cassette was generated from two PCR fragments amplified from chromosomal DNA of *Bta* LUB046 as template by conventional cloning.

pLU068 used for generating a *Bhe* Δ*bepA* mutant was constructed as follows. Oligonucleotide primers prLU299 and prLU318 amplified fragment 1 (1000 bp) and prLU319 and prLU302 amplified fragment 2 (1000 bp). Both fragments were combined by SOEing PCR with oligonucleotide primers prLU299 and prLU302, resulting in a fragment of 2 kb carrying an in-frame deletion in $bepA_{Bta}$. By using flanking *Xba*I sites, the fragment was inserted into the corresponding site of pTR1000,

yielding pLU068. The use of pLU068 for gene replacement in *Bta* LUB046 resulted in the *Bta* Δ*bepA* mutant LUB291.

pLU069 used for generating a *Bhe* Δ*bepD* mutant was constructed as follows. Oligonucleotide primers prLU063 and prLU320 amplified fragment 1 (750 bp*)* and prLU304 and prLU305 amplified fragment 2 (750 bp). Both fragments were combined by SOEing PCR with oligonucleotide primers prLU063 and prLU305, resulting in a fragment of 1.5 kb carrying an in-frame deletion in $bepD_{Bta}$. By using flanking *Xba*I sites, the fragment was inserted into the corresponding site of pTR1000, yielding pLU069. The use of pLU069 for gene replacement in *Bta* LUB046 resulted in the *Bta* Δ*bepD* mutant LUB293. Next, the use of pLU069 for gene replacement in *Bta* Δ*bepA* LUB291 resulted in the *Bta* Δ*bepAD* mutant LUB297.

pLU072 used for generating a *Bta* Δ*virD4* in-frame mutant was constructed as follows. Oligonucleotide primers prLU059 and prLU060 amplified fragment 1 (753 bp) and prLU061 and prLU062 amplified fragment 2 (790 bp). Both fragments were combined by SOEing PCR with oligonucleotide primers prLU059 and prLU062, resulting in a fragment of 1.54 kb carrying an in-frame deletion in $virD4_{Bta}$. By using flanking *XbaI* sites, the fragment was inserted into the corresponding site of pTR1000, yielding pLU072. The use of pLU072 for gene replacement in LUB046 resulted in the *Bta* Δ*virD4* mutant LUB163.

Plasmids for doxycycline-inducible lentiviral expression. The lentiviral doxycycline-inducible vector pCLX-pTF-R1-DEST-R2-EBR65 was constructed with the TET-inducible promoter pTF [34]. The GFP fragment of 796 bp was amplified by PCR from pRO300 using prLU276 and prLU277. The GFP fragment was recombined to pDONR by gateway BP clonase reaction (Life Technologies), yielding an entry clone pLU073. The GFP fragment in pLU073 was recombined into the destination vector pCLX-pTF-R1-DEST-R2-EBR65 by gateway LR clonase reaction (Life Technologies), yielding pLU077.

The vector expressing GFP-BepD-$BXBID_{Bhe}$, pLU078, was constructed by two steps of PCR. First, the GFP fragment of 778 bp was amplified from pRO300 using prLU276 and prRO90. The BepD-$BXBID_{Bhe}$ fragment of 1113 bp was amplified from pLU030 using prLU199 and prLU278. Second, SOEing PCR amplifying an extended

GFP-BepD-BXBID$_{Bhe}$ fragment of 1876 bp using the primers prLU276 and prLU278. Two steps of gateway cloning brought this GFP-BepD-BXBID$_{Bhe}$ fragment first into pDONR, yielding an entry clone pLU074. Subsequently, second reaction into the destination vector resulted in the pLU078.

The vector expressing GFP-BepD-BID$_{Bhe}$, pLU079, was constructed by two steps of PCR. First, the GFP fragment of 778 bp was amplified from pRO300 using prLU276 and prRO90. The BepD-BID$_{Bhe}$ fragment of 576 bp was amplified from pLU030 using prLU197 and prLU278. Second, SOEing PCR amplifying an extended GFP-BepD-BID$_{Bhe}$ fragment of 1339 bp using the primers prLU276 and prLU278. Two steps of gateway cloning brought this GFP-BepD-BID$_{Bhe}$ fragment first into pDONR, yielding an entry clone pLU075. Subsequently, second reaction into the destination vector resulted in the pLU079.

The vector expressing GFP-BepD-BXBID$_{Bhe}$ 5Ymuts (Y32/72/92/114/134F), pLU080, was constructed by two steps of PCR. First, the GFP fragment of 778 bp was amplified from pRO300 using prLU276 and prRO90. The BepD-BXBID$_{Bhe}$ 5Ymuts fragment of 1113 bp was amplified from pLU044 using prLU199 and prLU278. Second, SOEing PCR amplifying an extended GFP-BepD-BXBID$_{Bhe}$ fragment of 1876 bp using the primers prLU276 and prLU278. Two steps of gateway cloning brought this GFP-BepD-BXBID$_{Bhe}$ 5Ymuts fragment first into pDONR, yielding an entry clone pLU076. Subsequently, second reaction into the destination vector resulted in the pLU080.

3.2.4 Results

Bartonella inhibits a full maturation of infected BMDCs through T4SS dependent manner

Based on the current infection cycle of *Bartonella*, DCs represent one of the candidate cell types for the "dermal niche" and may serve as transporters of bacterial cargo to the lymph nodes [18]. However, it is still not fully understood how *Bartonella* is capable of exploiting these professional antigen presenting cells for pathogenicity. To better understand the consequences of *Bartonella* infection on the immune functions of DCs, we used murine bone marrow derived DCs (BMDCs) by Flt3-ligand (Flt3L) stimulation as a model *in vitro* system. Flt3L-dependent differentiation of DCs allows the generation of plasmacytoid (pDCs) and conventional (cDCs) dendritic cells from bone marrow precursors [32]. An anti-CD11c staining confirmed that a mixed culture of BMDCs contained 70% $CD11c^+$ differentiated DCs. Within the $CD11c^+$ DCs, 60% of cells were cDCs ($CD11b^+$) and 30% were pCDs ($B220^+$). Furthermore, 60% of $CD11c^+$ DCs were expressing MHCII, indicating that these BMDCs were partially activated during Flt3L differentiation (Fig. S1). Following experiments were performed using the described mixture of BMDCs. To further characterize the properties of Flt3L derived BMDCs, maturation patterns were monitored by the regulation of surface co-stimulatory (CD40, CD80, and CD86) and MHCII molecules using flow cytometry analysis (Fig. 1A). Expression levels of the maturation markers were presented as the geometric mean of the fluorescence intensities (GMFI). Flow cytometric analysis showed that BMDCs were able to fully maturate characterized by upregulation of MHCII, CD40, CD80, and CD86 on the cell surface upon *E. coli* LPS stimulation.

To study the role of *Bartonella* type IV secretion system (T4SS) in DC maturation, we used *B. birtlesii* (*Bbi*), a murine-specific strain, to infect murine BMDCs [38]. At 24 hours post-infection (hpi), infection of BMDCs with *Bbi* wild-type resulted in upregulation of all tested surface makers (MHCII, CD40, CD80, and CD86) compared to uninfected condition. Interestingly, *Bbi* wild-type caused significantly lower expression of MHCII, CD40, and CD86 than *Bbi Tn-virD4*, a T4SS secretion deficient strain. However, a converse effect was observed on the expression of CD80

(Fig. 1B). In addition, the culture medium of infected BMDCs was analyzed for detection of pro-inflammatory cytokines (TNF-α, IL-6, and IL-12p40) by ELISA. As compared to *Bbi Tn-virD4*, *Bbi* wild-type infection induced dramatically low TNF-α and slightly lowered IL-6 secretion by BMDCs. However, no difference in IL-12p40 secretion was observed (Fig. 2). Thus, analysis of maturation makers and cytokines revealed that *Bartonella* infection leads to semi-maturation of DCs in a T4SS dependent manner.

BepA$_{Bhe}$ and BepD$_{Bhe}$ display immunomodulatory effects on DCs

To further dissect which *Bartonella* effector protein (Bep) is involved in interfering with maturation of DCs, investigations with mutant strains of *Bartonella* are needed. However, due to the difficulty of genetic modification on *Bbi*, we had to switch to a well characterized strain - *B. henselae* (*Bhe*) [39]. First, experiments were performed to confirm that *Bhe* has a similar effect on DC maturation as *Bbi*. Indeed, compared to an effector-free mutant (*Bhe* Δ*bepA-G*), infection with *Bhe* wild-type induced lower MHCII, CD40, and CD86 but higher CD80 expression (Fig. 1A and 1B). The regulation of co-stimulatory molecules caused by *Bhe* infection was comparable to *Bbi* infection. Consistently, cytokine secretion (TNF-α and IL-6) was reduced upon *Bhe* wild-type infection. Even more, IL-12p40 suppression was observed with *Bhe* infection but not with *Bbi* infection (Fig. 2). All of the results from two different strains strongly indicate that Beps are capable of modulating the maturation state of infected BMDCs.

To identify which Bep contributes to the semi-maturation phenotype of BMDCs and potential modulation of the host immune system, infections with effector-complemented strains expressing individual Beps (BepA-G$_{Bhe}$) in the substrate-free background (*Bhe* Δ*bepA-G*) were analyzed (Fig. S2A). Strikingly, two Beps, BepA$_{Bhe}$ and BepD$_{Bhe}$, interfered with full maturation of infected BMDCs. BepA$_{Bhe}$ mainly affected MHCII and CD40 repression, while BepD$_{Bhe}$ inhibited MHCII and CD86 upregulation but induced CD80 expression (Fig. 3). Furthermore, both BepA$_{Bhe}$ and BepD$_{Bhe}$ reduced IL-6 and TNF-α secretion. However, BepD$_{Bhe}$ was more potent in TNF-α inhibition than BepA$_{Bhe}$ (Fig. 4). These differences of inhibition level imply that the two effectors might interfere differently with cellular signaling pathways.

The functions of BepA$_{Bhe}$ and BepD$_{Bhe}$ are related to its BID domain and the N-terminal fragment, respectively

As indicated earlier, both BepA$_{Bhe}$ and BepD$_{Bhe}$ contain one BID domain as the intracellular delivery signal at the C-terminus. In *Bartonella* infection models, the BID domain was indispensable for Bep translocation into host cells. At the N-terminal region, BepA$_{Bhe}$ carries a FIC domain and BepD$_{Bhe}$ several tandem-repeated tyrosine-containing peptide sequences [40, 41]. The tyrosine-phosphorylation sites of BepD$_{Bhe}$ were characterized by the presence of the Glu-Pro-Ile-Tyr-Ala (EPIYA) closely related sequences (referred to EPIYA-related motifs) [42]. To narrow down which domain is responsible for the effects of BepA$_{Bhe}$ and BepD$_{Bhe}$, strains expressing only BID domain of BepA$_{Bhe}$ or BepD$_{Bhe}$ were used to infect BMDCs (Fig. S2B). Interestingly, the results showed that the BID domain of BepA$_{Bhe}$ behaved comparably as the full length of BepA$_{Bhe}$ towards inhibition of the MHCII and CD40 expression as well as secretion of the cytokine TNF-α, IL-6, and IL-12p40 (Fig. 5 and 6). However, the BID domain of BepD$_{Bhe}$ lost its ability to trigger the DC phenotypes as observed by the full length protein (Fig. 5 and 6). It implies that the N-terminal region carrying the tandem EPIYA-related motifs is essential to interfere with DC maturation.

CD40 expression and inflammatory cytokine secretion are negatively regulated by BepA$_{Bhe}$ homologs

Based on the significant similarity of BepA homologs from the *Bartonella* lineage 4 species (Fig. S3), the functional conservation of BepA homologs from different *Bartonella* species (BepA$_{Btr}$ from *B. tribocorum*, BepA$_{Bgr}$ from *B. grahamii*, BepA-BID$_{Bbi}$ from *B. birtlesii*, and BepA-BID$_{Bta}$ from *B. taylorii*) on BMDCs was analyzed. However, due to the difficulty in cloning, only the BID domains of BepA from *B. birtlesii* and *B. taylorii* were constructed instead of the full length (Fig. S2C). Although the BID domains of BepA homologs share more than 50% amino acids (aa) identity, the activity among BepA homologs was discordant. Indeed, BepA$_{Btr}$ and BepA-BID$_{Bbi}$ interfered with the MHCII and CD40 expression as well as TNF-α and IL-6 secretion to a similar extend as BepA$_{Bhe}$. However, BepA-BID$_{Bta}$ led to weaker inhibition of DC maturation and no significant activity was observed by BepA$_{Bgr}$ (Fig. 7 and 8).

The effects of BepA$_{Bhe}$ homologs are in association with the acceleration of cellular cyclic AMP level

According to previous studies, the BID domain of BepA protects infected human ECs against apoptotic stimuli by elevation of cellular cAMP levels [43, 44]. Moreover, an artificial increase of cAMP by forskolin in DCs leads to reduced antigen uptake, lower surface expression of MHCII and CD40 [45]. Taken these results together, we suspected that the phenotypic changes of DC maturation caused by BepA might be due to stimulating intracellular cAMP level. To address this question, we tested whether BepA homologs activated the cAMP-dependent CREM/CREB pathway in BMDCs by quantitative real-time PCR of the cAMP-inducible gene, *crem*. At 24 hpi, RNA samples of infected BMDCs were extracted to monitor the transciptional regulation of *CD40* and *crem*. Strikingly, the repression of *CD40* by BepA homologs significantly correlated with upregulation of *crem* (Fig. 9). Similar to BepA$_{Bhe}$ and BepA-BID$_{Bhe}$, BepA$_{Btr}$ and BepA-BID$_{Bbi}$ showed strong activities on *CD40* inhibition in association with high level of *crem* gene activation. Consistently, BepA$_{Bgr}$ led to an increase of *CD40* mRNA expression but no induction of *crem* gene. Besides, quantitative PCR analysis revealed that BepA also transcriptionally inhibited the genes of inflammatory cytokines (*TNF-α*, *IL-6*, and *IL-12*) regulation (Fig. S4). In summary, these findings indicate that BepA acts as a potent negative regulator in DC maturation in association with an acceleration of intracellular cAMP level.

BepD$_{Bhe}$ homologs possess conserved activities on inhibition of MHCII and CD86 expression, as well as pro-inflammatory cytokine secretion

To study whether BepD homologs trigger similar phenotypes of interference with DC maturation, we first aligned the sequence of BepD homologs from the *Bartonella* lineage 4 species (e.g. *B. tribocorum*, *B. grahamii*, *B. birtlesii* and *B. taylorii*). Similarly as BepD$_{Bhe}$, BepD$_{Btr}$ contains duplicate fragments (refer to AX and BX) at its N-terminal region sharing 90% aa identity. Corresponding to BepD-BX$_{Bhe}$, the N-terminal fragments of BepD homologs showed pair-wise aa identity of 35-50% with conserved tyrosines in the putative phosphorylation motifs (Fig. S5). Various *Bhe* strains were constructed by heterologous complementation with BepD$_{Bhe}$ homologs (BepD$_{Btr}$, BepD$_{Bgr}$, BepD$_{Bbi}$, and BepD$_{Bta}$) in *Bhe* Δ*bepA-G* background

(Fig. S2C). At 24 hpi, FACS analysis showed that all tested BepD$_{Bhe}$ homologs resulted in inhibition of MHCII and CD86 but induction of CD80 expression (Fig. 10). Furthermore, BepD$_{Btr}$ and BepD$_{Bta}$ had a strong effect on TNF-α and IL-6 repression like BepD$_{Bhe}$. However, weak cytokine suppression was observed by BepD$_{Bgr}$ and BepD$_{Bbi}$ (Fig. 11).

The functional EPIYA-related motifs are delineated in BepD-BXBID$_{Bhe}$ by tyrosine to phenylalanine exchanges

Next, we sought to characterize which EPIYA-related motif in BepD$_{Bhe}$ contributes to the impaired DC maturation phenotype. A truncated mutant (refer to BepD-BXBID$_{Bhe}$) was generated to reduce the complexity of potential redundant effects by duplication of N-terminal fragments. The inhibition level of MHCII and CD86 in BMDCs was comparable between the full length of BepD$_{Bhe}$ and BepD-BXBID$_{Bhe}$ (Fig. 12). However, compared to BepD-BXBID$_{Bhe}$, the full length of BepD$_{Bhe}$ gave an additive effect on TNF-α and IL-6 repression (Fig. 13). Nine putative tyrosine-phosphorylation motifs are located in the BepD-BX$_{Bhe}$. To assess which tyrosine is critical for the immunomodulatory activity of BepD-BXBID$_{Bhe}$ in DCs, we performed a systematic mutagenesis to exchange the tyrosines to phenylalanines (Y32F, Y52F, Y62F, Y72F, Y92F, Y114F, Y134F, Y155F, and Y176F) (Fig. S2D). Strikingly, flow cytometric analysis of DC maturation markers revealed that three tyrosine-substitution mutants (Y92F, Y114F, and Y134F) significantly attenuated the phenotype caused by BepD-BXBID$_{Bhe}$ (Fig. 12). Consistent with flow cytometric results, these mutants (Y92F, Y114F, and Y134F) induced high level of TNF-α and IL-6 secretion. Two mutants (Y32F and Y72F) slightly lost the activity on cytokine suppression (Fig. 13). Additionally, two multi-tyrosine substitution mutants (Y32/114/134F and Y32/72/92/114/134F) were constructed by sequential mutation cloning rounds. Indeed, these two mutants did not interfere with DC maturation state infection with the effector-free strain *Bhe* Δ*bepA-G* (Fig. 12 and 13). In the following experiments, this multi-tyrosine substitution mutant (Y32/72/92/114/134F) was used as a loss-of-function mutant (refer to BepD-BXBID$_{Bhe}$ 5Ymuts).

Ectopic expression of BepD-BXBID$_{Bhe}$ actively suppresses JAWSII responses to *E. coli* LPS stimuli

Based on the solid phenotypes of impaired DC maturation, we became interested in

understanding the underlying mechanisms of BepD. Preliminary results of quantitative real-time PCR revealed that BepD transcriptionally interfered with cytokine regulation of *TNF-α*, *IL-6*, and *IL-12p40*, but not clearly influenced *MHCII*, *CD80* and *CD86* regulation (Fig. S6). To further uncover the molecular bases of BepD, we set up an *in vitro* model using the JAWSII cell line, a DC line established from bone marrow cells of a p53-knockout C57BL/6 mouse [33]. Anti-CD11c staining confirmed that more than 90% cells are $CD11c^+$. Moreover, JAWSII cells are identified as cDCs ($CD11b^+/B220^-$) (Fig. S7A). Upon *E. coli* LPS treatment, maturation patterns were monitored by the regulation of surface co-stimulatory (CD40, CD80, and CD86) and MHCII molecules to characterize DC properties of JAWSII cells. Compared to untreated JAWSII cells, *E. coli* LPS stimulated MHCII and CD86 upregulation, but not CD40 and CD80 (Fig. S7B). Since our results showed that $BepD_{Bhe}$ interfered with DC maturation, especially on MHCII and CD86 inhibition, JAWSII cells were suitable to be used for BepD study.

A lentiviral transduction system was used to ectopically express GFP or GFP-fusion proteins (GFP-BepD-$BXBID_{Bhe,}$ GFP-BepD-$BID_{Bhe,}$ and GFP-BepD-$BXBID_{Bhe}$ 5Ymuts) in JAWSII cells. Under the TET-inducible promoter pTF, these GFP and GFP-fusion proteins were easily induced by doxycycline treatment (Fig. S8). Upon challenging by *E. coli* LPS for 24 hours, only DOX-induced BepD-$BXBID_{Bhe}$ prevented the JAWSII cells from MHCII and CD86 upregulation. The BID domain alone and the tyrosine-substitution mutant (BepD-$BXBID_{Bhe}$ 5Ymuts) abolished the effect of BepD-$BXBID_{Bhe}$ (Fig 14).

BepD-$BXBID_{Bhe}$ co-immunoprecipitates with SHP2 and STAT3 in a phosphorylation-dependent manner

A previous study on the interactome of $BepD_{Bhe}$ revealed that several SH2 domain-containing signaling proteins (e.g. Csk and SHP-2) interact with $BepD_{Bhe}$ upon phosphorylation of specific tyrosines within the motifs [40]. To further investigate the potential intracellular targets of $BepD_{Bhe}$, GFP nanobodies coupled to agarose beads were used to pull down specific interaction partners of GFP-BepD-$BXBID_{Bhe}$ from lysates of JAWSII cells. Cells expressing the BID domain of $BepD_{Bhe}$ (GFP-BepD-BID_{Bhe}) or the tyrosine-substitution mutant (GFP-BepD-$BXBID_{Bhe}$ 5Ymuts) were employed as the negative controls to

distinguish between specific interaction partners and nonspecific contaminants. Upon immunoprecipitation with the GFP nanobodies, staining with anti-GFP and anti-phosphotyrosine antibodies confirmed that only BepD-BXBID$_{Bhe}$ as "wild-type" was tyrosine-phosphorylated by the endogenous levels of tyrosine kinases in the JAWSII cells. However, BepD-BID$_{Bhe}$ and BepD-BXBID$_{Bhe}$ 5Ymuts did not show any detectable tyrosine-phosphorylation (Fig. 15).

A quantitative interactomic screen showed that 12 candidates significantly interacted with BepD-BXBID$_{Bhe}$ (Fig. 16A). Significant changes of the BepD-BXBID$_{Bhe}$ versus BepD-BXBID$_{Bhe}$ 5Ymuts were defined by a q-value cutoff of < 0.01. The interactome was graphically illustrated based on the STRING database. Only proteins with at least one connection in STRING were represented. Data showed a complex network with several distinct functional modules (Fig. 16B). The top three potential interaction partners of BepD-BXBID$_{Bhe}$ were PTPN11 (SHP-2, a tyrosine phosphatase), STAT3 (a transcription factor), and Abl (a tyrosine kinase) (Fig. 16C). To obtain a systems-level overview of host signaling with BepD expression, we further analyzed the global dynamics of protein phosphorylation using a phosphoproteomics strategy combining with phosphopeptide enrichment [46] (Fig. 17A). For simplification, 27 proteins were identified undergoing a significant change of phosphorylation in dependence of BepD-BXBID$_{Bhe}$, 19 proteins with increase and 8 proteins with decrease in phosphorylation (Fig. 17B and 17C). Significant phosphorylation changes were defined by a q-value cutoff of < 0.01. Interestingly, the top candidate was STAT3 undergoing to be hyper-phosphorylated.

To examine the interaction between potential partners (e.g., SHP2 and STAT3) and BepD-BXBID$_{Bhe}$, upon immunoprecipitation with the GFP nanobodies, we probed the precipitate with anti-SHP2 and anti-STAT3 antibodies. In contrast to the tyrosine-substitution mutant (BepD-BXBID$_{Bhe}$ 5Ymuts), SHP-2 and STAT3 specifically co-immunoprecipitated with BepD-BXBID$_{Bhe}$, demonstrating that Y32/72/92/114/134 mediate the interaction of SHP2 and STAT3 to BepD-BXBID$_{Bhe}$ in dependence of its tyrosine-phosphorylation (Fig 18). Strikingly, staining with an anti-phosphoSTAT3 (Y705) antibody showed that the pulled down STAT3 by BepD-BXBID$_{Bhe}$ was in a activate form (Fig. 18). Together with the interactomic screen data, we suspected that BepD might provide a platform to recruit STAT3 and

tyrosine kinases (likely Abl), to subsequently activate STAT3 signaling.

Phosphorylation of STAT3 strongly correlates with semi-maturation phenotype of BMDCs

In order to determine whether inhibition of DC maturation by BepD relates with STAT3 activation, various *Bhe* strains expressing $BepD_{Bhe}$ homologs or $BepD\text{-}BXBID_{Bhe}$ tyrosine-substitution mutants were used for infection of BMDCs. At 24 hpi, the cell lysates of infected BMDCs were analyzed by western blotting using anti-STAT3 and anti-phosphoSTAT3 (Y705) antibodies. STAT3 activation was quantified by the ratio of phospho-STAT3 to total STAT3. Interestingly, only $BepD_{Bhe}$ led to hyper-phosphorylation of STAT3 but not $BepE_{Bhe}$ and $BepF_{Bhe}$ even though they also contain EPIYA-related motifs, indicating that STAT3 activation is specific in response to $BepD_{Bhe}$. Furthermore, $BepD_{Bhe}$ homologs ($BepD_{Btr}$, $BepD_{Bgr}$, $BepD_{Bbi}$, and $BepD_{Bta}$) shared similar properties like $BepD_{Bhe}$ to enhance cellular phospho-STAT3 level (Fig. 19). Consistently, analyses of $BepD\text{-}BXBID_{Bhe}$ tyrosine-substitution mutants showed that three individual-tyrosine substitution mutants (Y92F, Y114F, and Y134F) significantly diminished the upregulation of phospho-STAT3. A multi-tyrosine substitution mutant (Y32/72/92/114/134F) which was proved to no longer inhibit DC maturation failed in STAT3 activation (Fig. 20). Overall, quantification of STAT3 activation revealed that the level of phospho-STAT3 strongly correlated with phenotypes of impaired DC maturation caused by BepD.

The prolonged STAT3 activation is known to be essential for the anti-inflammatory signals mediated by IL-10 and subsequently inhibits LPS-triggered signaling [47]. To determine whether STAT3 phosphorylation caused by BepD is sustained, we performed a time course analysis. BMDCs were infected with strains expressing $BepD\text{-}BXBID_{Bhe}$ or $BepD\text{-}BXBID_{Bhe}$ 5Ymuts. Cell lysates were collected over a time course (1 h, 3 h, 6 h, 9 h, 12 h, and 24 h post-infection). Western blotting showed that compared to $BepD\text{-}BXBID_{Bhe}$ 5Ymuts, $BepD\text{-}BXBID_{Bhe}$ clearly enhanced STAT3 phosphorylation starting at 9 hpi. Furthermore, the accumulation of phsopho-STAT3 expression was sustained till 24 hpi (Fig. 21).

A murine model with *B. taylorii* intradermal infection is established for functional analysis of Beps *in vivo*

Next, we sought to explore the role of BepD in an *in vivo* establishment of *Bartonella* infection. However, *Bhe* causes intraerythrocytic bacteremia as a hallmark of infection in its feline natural reservoir host only, which for ethical reasons is not an accessible experimental model. To establish an optimal murine model for functional analysis of Beps *in vivo*, *B. taylorii* (*Bta*) a murine-specific strain was introduced. Based on its high conjugation efficiency, this strain was able to uptake the suicide mutagenesis plasmid for genetic manipulations. To gain more information about the VirB/D4 T4SS in *Bta*, we sequenced the respective genomic region including the *virB* operon, *virD4* and the *bep* genes. For sequencing purposes, primers for creating overlapping PCR fragments were deduced from the published *Bhe* strain Houston-1 genome (Accession No. NC_005956.1) [48] and fragments were subsequently sequenced. Annotation of the *Bta* genomic fragment revealed that open reading frames encoding for VirB2-11 and VirD4 show high similarities to *Bhe*. However, only five effector proteins were annotated in *Bta* instead of seven Beps (BepA-G) in *Bhe* (Fig. S9). Among them, two Beps of *Bta*, $BepD_{Bta}$ and $BepE_{Bta}$ contained putative tyrosine-phosphorylation motifs as homologs of $BepD_{Bhe}$ (identity of the N-terminal fragment: 53%) and $BepE_{Bhe}$ (identity of the N-terminal fragment: 24%), respectively. The *in vitro* data revealed that $BepD_{Bta}$ but not $BepE_{Bta}$ showed the immunomodulatory activity which was comparable to $BepD_{Bhe}$ in BMDCs. Thus, we reasoned that *Bta* could be used as an appropriate species to study BepD functions *in vivo*.

Mutations associated with streptomycin resistance have been identified in the genes encoding 16S rRNA (*rrs*) and ribosomal protein S12 (*rpsL*) [49]. For in-frame deletion mutagenesis, a spontaneous streptomycin-resistant (Sm^R) variant of *Bta* was selected serving as the "wild-type" in which *rpsL* changed with codon 43 mutation (AAG→AGG; K43R). Recently, an intradermal (i.d.) infection model of *B. birtlesii* (*Bbi*) has been introduced by Marignac *et al* [50], where the bacteria are inoculated in the derma on the ear pinnae of mice. This model likely reflects the natural route of infection, mimicking the infectious bacteria transmitted by the arthropod vector. Through i.d. infection, the Sm^R *Bta* wild-type was examined with different doses inoculum (1×10^7, 1×10^5, or 1×10^3 CFU/mouse) in Balb/c mice. Bacteremia was

monitored over time as CFU per ml of blood. Five out of five (100%) mice showed bacteremia with 1×10^7 CFU inoculum, four out of five (80%) with 1×10^5 CFU inoculum and four out of five (80%) with 1×10^3 CFU inoculum. The course of bacteremia revealed that *Bta* tended to develop higher bacteremia and delay of clearance with lower doses inoculum. However, the bacteremia establishment became lesser synchronized with lower doses inoculum (Fig. 22). It might reflect that high doses inoculum of bacteria may prime an efficient immune response for bacterial elimination. Thus, instead of 1×10^7 CFU/mouse which was used in most pervious *Bartonella* studies, bacterial inoculum of 1×10^5 CFU was used for i.d. infection in the following mice experiments.

Through intradermal infection, *Bta* Δ*bepAD* seems to lose the fitness of bacteremia development

To study the immnuomodulatory effect of *Bartonella* infection *in vivo*, several mutant strains derived from Sm^R *Bta* wild-type were made with in-frame deletion of *virD4*, *bepA*, or *bepD* (referred to *Bta* Δ*virD4*, *Bta* Δ*bepA*, and *Bta* Δ*bepD*, respectively). Both $BepA_{Bta}$ and $BepD_{Bta}$ showed inhibitory effects on DC maturation. To reduce their redundant functions, a mutant strain with deletions of both genes *bepA* and *bepD* was constructed (referred to *Bta* Δ*bepAD*). To analyze the relevance of VirD4, BepA, and BepD in bacteremia development, mice were infected with *Bta* wild-type, *Bta* Δ*virD4*, *Bta* Δ*bepA*, *Bta* Δ*bepD*, or *Bta* Δ*bepAD* (1x 10^5 CFU/mouse; five mice per group). Blood samples were collected from each mouse until up to 8 weeks (Fig. 23). Infection with *Bta* Δ*virD4* completely lost the ability to establish the bacteremia in mice, indicating that the VirB/D4 T4SS is an indispensable virulence factor for *Bta* pathogenicity. Except *Bta* Δ*virD4*, all of mice infected with *Bta* wild-type, *Bta* Δ*bepA*, *Bta* Δ*bepD*, or *Bta* Δ*bepAD* were bacteremic. The highest peak of each bacteremia from all the groups was reached at 14 dpi (Fig. 24). In the previous experiment, the infection with 1×10^5 CFU inoculum of *Bta* wild-type resulted in 100% bacteremic mice with similar kinetics of bacteremia (reaching to 1×10^6 CFU/ml blood) (Fig 22). However, in this experiment, four out of five mice infected with *Bta* wild-type developed expected course of bacteremia but one was only reaching to 5×10^3 CFU/ml blood. In the groups inoculated with mutants *Bta* Δ*bepA*, *Bta* Δ*bepD*, or *Bta* Δ*bepAD*, the bacteremia development showed a trend towards lower peak and shorter duration. More replicates are needed to gain statistically significance of the difference

between wild-type and mutant infections.

3.2.5 Discussion

Impaired DC maturation by *Bartonella* infection

In the arms race of host-microbe coevolution, successful microbial pathogens have evolved ingenious ways to evade, neutralize, or subvert host immunity. Interference with DC maturation is an example of a powerful mechanism used by various bacterial pathogens for host immune evasion. Since DCs are one of the potential vehicles for *Bartonella* transport in the host organism, we sought to examine the interaction between *Bartonella* and professional antigen-presenting DCs. Our data disclose immunosuppressive properties of *Bartonella* virulence factors, which are utilized to interfere with DC maturation. In response to *Bartonella* infection, murine BMDCs failed to fully mature and remained in a semi-developed stage. This impaired DC maturation was characterized by reduced surface expression of the MHCII complex and the co-stimulatory receptors CD40 and CD86, as well as strongly diminished secretion of the pro-inflammatory cytokines TNF-α and IL-6. Reminiscent of what is observed in *Bartonella*, also *H. pylori*-experienced DCs reach only a semi-mature state. These tolerogenic DCs secrete IL-18 and efficiently induce $Foxp3^+$ Treg response in favor of *H. pylori* persistence [51]. In accordance with this, our findings support the idea that by induction of semi-maturation and thus tolerogenic properties of DCs, *Bartonella* may subvert the host immune response to develop and sustain a chronic bartonellosis.

The impaired maturation of murine BMDCs was observed with both *Bbi* (a murine-specific strain) and *Bhe* (a feline-specific strain) infections in this study. This is contradictory to a previous publication, in which *Bhe* infection of human monocyte-derived DCs showed classical phenotypic changes of *Bhe*-driven DC activation including the increase of surface expression of co-stimulatory molecules (CD83 and CD86) and MHCII, as well as the release of cytokines (e.g., TNF-α, IL-6, IL-10, and CXCL13) [30]. These contradicting outcomes may be due to different host species, although *Bhe* infection in either murine or human DCs is heterogonous. Further, the experimental conditions diverge. Different from the RPMI medium used in [30], we took M199 medium for culturing bartonellae and for performing the bacterial infection in BMDCs. The latter may be a preferable condition to study the

function of T4SS because it was proven that regulation of VirB/D4 T4SS-related genes (e.g., *virB* and *bepD*), which is required for *Bartonella* virulence in DCs, is prominently induced in M199 medium [52].

cAMP in *Bartonella* pathogenicity

Interestingly, the induction of the phenotypic changes observed in DCs upon *Bartonella* infection could be attributed to two effector proteins, BepA and BepD. In particular, the BID domain of BepA strongly affected the downregulation of CD40 expression and TNF-α production. In fact, our findings in this study are not the first ones to describe a role for BepA in *Bartonella* pathogenicity. It was shown that the BepA-mediated elevation of cAMP levels is linked to reduced caspase-3 activation and prevents infected ECs from apoptosis [24]. A recent publication of our lab demonstrated that the enhanced cAMP production is due to a BepA interaction with the host cell adenylyl cyclase Gαs [53]. The cAMP signaling has been extensively studied in context of either inhibiting or stimulating apoptosis [54]. These adverse phenotypes are attributed to the antagonistic interaction of protein kinase A (PKA) and Exchange protein activated by cAMP (Epac-1), a guanine nucleotide exchange factor (GEF) for Ras-like small GTPases downstream of cAMP signaling [55, 56]. Remarkably, $BepA_{Bhe}$-mediated anti-apoptosis was cell type dependent. While BepA inhibited apoptosis in human umbilical vein ECs (HUVECs), it acted pro-apoptotically in the endothelial hybrid cell line (Ea.hy926) (Dr. A. Pulliainen, data unpublished). Both *in vitro* phenotypes of BepA described in different cell types were closely related to its BID domain and associated with cAMP elevation, likely through the same molecular mechanism. The cAMP signaling is known to influence a plethora of cellular functions based on its broad modulatory capabilities. We thus investigated the involvement of cAMP in the DC phenotype. The activation of cAMP-dependent CREM/CREB pathway in BMDCs was determined by quantitative real-time PCR of the cAMP-inducible gene, *crem*. It showed that this effect of BepA on BMDCs was associated with induction of intracellular cAMP levels.

The inhibitory effects of BepA on DC maturation are in line with the general concept of cellular cAMP as a negative regulator of immune stimulation in phagocytes (e.g., macrophages and DCs). *Bartonella* BepA provides an intriguing example of cAMP level control by one single bacterial effector leading to a multifaceted manipulation in

different host cell types. Besides *Bartonella*, several other pathogenic bacteria (e.g., *B. pertussis* and *Vibrio cholerae*) have evolved mechanisms to exploit host cell cAMP signaling by virulence factors, such as pertussis toxin (PT) and AC toxin (CyaA) of *B. pertussis*, and the cholera toxin (CT) of *V. cholerae.* Though by distinct mechanisms, these toxins ultimately lead to a sustained increase of intracellular cAMP in target cells. Moreover, they share similar negative effects on phagocyte activation, including phagocytosis, cytokine production, chemotaxis, and superoxide production [57].

In addition to $BepA_{Bhe}$, we analyzed the effect of several BepA homologs on DC maturation: $BepA_{Btr}$, $BepA_{Bgr}$, $BepA\text{-}BID_{Bbi}$, and $BepA\text{-}BID_{Bta}$. Although BepA homologs share high sequence identity, the functional readouts of them were not congruent. Particularly, $BepA_{Bgr}$ showed hardly any immunosuppressive activity in BMDCs. Additionally, it is interesting to note that $BepA_{Btr}$ displayed opposing actions in different cells. A previous publication of our lab revealed that $BepA_{Btr}$ failed to inhibit apoptosis of human ECs. However, $BepA_{Btr}$ in this study strongly repressed CD40 expression and TNF-α production in BMDCs. Further investigations are needed to elucidate a potential cell type or host species specificity of BepA.

Impact of BepD and STAT3 interaction of DC function

Tyrosine-phosphorylation of proteins plays a central role during signal transduction in eukaryotes. Recent progress in the description of several bacterial effectors has shown that tyrosine-phosphorylation is a common feature on these proteins, which capacitates them for recruiting and binding host cellular interaction partners, thereby manipulating signaling pathways. To date, nine effectors displaying phosphorylated EPIYA-motifs have been identified in various bacteria, including *Bartonella* BepD-F [58]. Although these bacterial effectors are capable of undergoing versatile interactions with mammalian SH2 domain-containing proteins, only a few of them (e.g., CagA of *H. pylori* and Tir of enteropathogenic *E. coli* (EPEC)) have been proved so far to display pathogenic functions upon delivery into mammalian host cells. Most previous evidence relates to actin-cytoskeletal rearrangements influenced by EPIYA effectors. CagA for instance was found to be involved in cell scattering and Tir in pedestal formation [59, 60]. Recently, a second function of Tir in association with SHP-1 and SHP-2 has been discovered in the anti-inflammatory response [61, 62]. Here we demonstrate that another bacterial EPIYA effector, *Bartonella* BepD,

displays immunomodulatory properties similarly to EPEC Tir, but likely through a distinct mechanism. The phenotypic changes of infected DCs triggered by *Bartonella* BepD were represented by a downregulation of surface MHCII and CD86 expression, as well as by the repression of TNF-α and IL-6 production. Strikingly, analyses of tyrosine-substitution mutants showed that the effects of BepD are strongly linked to its EPIYA-related motifs (in particular Y92, Y114, and Y134). A loss-of-function mutant of BepD (Y32/72/92/114/134F) did not show any detectable tyrosine-phosphorylation and consequently no effect on DC maturation. Taken together, these findings indicate that the phosphorylation of certain EPIYA-related motifs is critical for the immunosuppressive activity of BepD. In fact, BepD was highly tyrosine-phosphorylated by endogenous tyrosine kinases in JAWSII cells. However, phosphorylation of BepD in HeLa cells was only observed by pre-treatment with vanadate to inhibit protein tyrosine phosphatases (data not shown), indicating that phosphorylation-based interaction of BepD with host factors may be cell type-specific.

E. coli LPS is a well-known TLR4 agonist to induce massive inflammation [3]. Interestingly, ectopic expression of BepD in JAWSII cells prevented DC activation by *E. coli* LPS stimulation, strongly suggesting antagonistic effects of BepD on LPS-dependent TLR signaling. Based on a quantitative proteomic screen in JAWSII cells, several SH2 domain-containing eukaryotic interaction partners were identified for differentially tyrosine-phosphorylated forms of BepD. Among them were SHP-2 and STAT3 whose interaction with a GFP-fusion of BepD-BXBIDBhe could be verified by co-immunopercipitation. SHP-2, as described above, is exploited by EPEC Tir as one of the interaction partners for its anti-inflammatory activity. The phosphorylation of Tir promotes the formation of the Tir/SHP-2/TRAF6 complex to prevent the ubiquitination of TRAF6, and that subsequently inhibits the MAP kinase and NF-κB pathways [62]. This molecular basis of Tir provides a potential working model for BepD signaling. Further experiments are needed to seek for evidence of such a mechanism utilized by BepD.

Besides the potential mechanism associated with SHP-2, we found another intriguing pathway to be connected with the immunomodulatory activity of BepD. A pull down assay with a GFP-fusion of BepD-BXBID$_{Bhe}$ showed on an immunoblot a

hyper-phosphorylated form of STAT3. The STAT3 activation strongly correlated with the impaired DC maturation phenotypes caused by infection with various *Bartonella* strains. It suggests that STAT3 signaling represents a key pathway hijacked by BepD in DCs. Although BepE and BepF, themselves containing several EPIYA-related motifs, were also tyrosine-phosphorylated in host cells [40], STAT3 activation was specific for BepD. Based on the proteomic data, we propose that BepD may serve as a platform to recruit host kinases (such as Abl and c-Src) and STAT3, thereby preparing for a subsequent activation of STAT3 signaling.

Numerous studies illustrate the important role of STAT3 in DC differentiation and function in cancer [63]. STAT3 signaling has been well-studied in connection with tumor-related factors, such as the pro-inflammatory cytokine IL-6 and the anti-inflammatory cytokine IL-10. Although IL-6 and IL-10 generate nearly opposing cellular responses, both cytokines activate STAT3 signaling and subsequently induce SOCS3 expression. The divergent actions of these two cytokines are based on the kinetics of STAT3 activation. In contrast to transient STAT3 activation by IL-6, stimulated IL-10 signaling leads to sustained STAT3 activation and results in an anti-inflammatory response [64, 65]. Similar to the effect of IL-10, also *Bartonella* BepD leads to a prolonged STAT3 phosphorylation and activation, which may explain the anti-inflammatory properties of BepD. Although *H. pylori* was described to induce phosphorylation of STAT3 in gastric cancer cells [66], a recent publication revealed that the STAT3 signaling is indirectly activated by the *H. pylori* effector protein CagA. In other words, CagA-secreting *H. pylori* induces a predominant secretion of IL-10, what in turn leads to enhanced STAT3 phosphorylation as required for induction of tolerogenic DCs [67]. These immunosuppressive properties of IL-10 are markedly exploited by many bacterial pathogens (e.g., *B. pertussis* and *M. tuberculosis*) with a stealth-infection strategy to shut off the host inflammatory responses [68, 69]. In contrast to the manipulation of IL-10 production, our findings shed light on a previously unknown mechanism, in which *Bartonella* BepD acts as a signaling hub and recruits host kinases together with STAT3. Subsequently, prolonged STAT3 phosphorylation is triggered and eventually results in inhibition of DC maturation.

Relevance of Beps' function *in vivo*

The phenotypes of BepA and BepD were majorly described in the *in vitro* model. To

translate our findings and put them into an *in vivo* context, we analyzed the bacteremia as a hallmark of *Bartonella* infection in mice. A minor impairment of bacteremia development was observed after infection with *Bta* strains harboring deletions of *bepA* or/and *bepD*, indicating that BepA and BepD contribute to the fitness of bacteremia. It is important to take into account that the inoculum of 1 x10^5 CFU/mouse used for i.d. infection may be still much higher than the dose occurring in natural infections. With high doses inoculum of bacteria, we might saturate our *in vivo* system, likely by priming an efficient immune response. Based on the results of bacterial inoculum titrations, we concluded that 80% mice infected with *Bta* wild-type 1 × 10^3 CFU/mouse led to stable bacteremia, yet its development was less synchronized. To sensitize our murine model, lower doses of inoculum (<10^3 CFU/mouse) will be tested in the next experiment.

Although *Bartonella* harbors an atypical LPS with low endotoxic activities, which enables these bacteria to be less noticeable for host immune recognition, it is interesting that *Bartonella* develops two effector proteins, BepA and BepD, to interfere with DC maturation and particularly with the production of pro-inflammatory cytokines. Thus, we speculate that BepA and BepD may contribute to establishing chronic infection by evading from host immune surveillance within specific tissues. Further investigations are needed to uncover the local inflammation of *Bartonella* infection.

Perspective in immune-attenuation by *Bartonella* infection

In summary, our findings demonstrate that two immnunomodulatory *Bartonella* effectors, BepA and BepD, both have a role in generating a “semi-mature” state of DCs through independent mechanisms. BepA may take advantage of the regulation of host cAMP levels to repress upregulation of surface CD40 expression and TNF-α production. BepD instead may work as a signaling hub for triggering prolonged STAT3 activation to suppress certain consequences of an immune response, in particular the inhibition of MHCII and CD86 expression and the secretion of pro-inflammatory cytokines. Overall, these “semi-mature” DCs may display tolerogenic properties to convert the T cell response into Treg immunotolerance reflecting part of the *Bartonella* stealth-infection strategy.

3.2.6 Figure Legends

Figure 1. DC maturation is impaired by *Bartonella* infection in a VirB/D4 T4SS dependent manner. (A) *E. Coli* LPS treatment (1 μg/ml) triggered DC maturation as the positive control. The BMDCs were infected with *Bhe* wild-type or *Bhe* Δ*bepA-G* (MOI = 25). After 24 hpi, maturation patterns were monitored by the regulation of surface co-stimulatory (CD40, CD80, and CD86) and MHCII molecules using flow cytometry analysis. Expression levels of the maturation markers were presented as the geometric mean of the fluorescence intensities (GMFI). One representative histogram image is displayed from three independent experiments. **(B)** The BMDCs were infected with *Bbi* wild-type, *Bbi Tn-virD4*, *Bhe* wild-type or *Bhe* Δ*bepA-G* (MOI = 25) for 24 h. Expression levels of MHCII, CD40, CD80, and CD86 were presented as relative GMFI. All data were normalized to infection with *Bhe* Δ*bepA-G* as 1 and showed as the mean ± SEM from three independent experiments. Statistical significance was determined using Student's t-test. $P<0.05$ was considered statistically significant.

Figure 2. Pro-inflammatory cytokine secretion is diminished by *Bartonella* infection in a VirB/D4 T4SS dependent manner. The BMDCs were infected with *Bbi* wild-type, *Bbi Tn-virD4*, *Bhe* wild-type or *Bhe* Δ*bepA-G* (MOI = 25) for 24 h. Culture media were collected for cytokine detection (TNF-α, IL-6, and IL-12p40). The data showed as the mean ± SEM from three independent experiments. Statistical significance was determined using Student's t-test. $P<0.05$ was considered statistically significant. Data from one representative experiment (n = 3) are presented.

Figure 3. $BepA_{Bhe}$ and $BepD_{Bhe}$ inhibit upregulation of surface receptors of infected BMDCs. BMDCs were infected with *Bhe* Δ*bepA-G* mutant complemented with the indicated Bep-expression plasmids at MOI = 25 for 24 h. The maturation markers were monitored by the surface expression of MHCII, CD40, CD80, and CD86 using flow cytometry analysis. Expression levels of the maturation markers were presented as relative GMFI. All data were normalized to infection with *Bhe* Δ*bepA-G* as 1 and showed as the mean ± SEM from three independent experiments. Statistical significance was determined using Student's t-test. Data marked by an asterisk differ statistically significantly ($P<0.05$) from infection with *Bhe* Δ*bepA-G*.

Figure 4. Repression of pro-inflammatory cytokine secretion is assigned to BepA$_{Bhe}$ and BepD$_{Bhe}$. BMDCs were infected with *Bhe* Δ*bepA-G* mutant complemented with the indicated Bep-expression plasmids at MOI = 25. At 24 hpi, Culture media were collected for cytokine detection (TNF-α and IL-6) by ELISA. The data showed as the mean ± SEM from three independent experiments. Statistical significance was determined using Student's t-test. Data marked by an asterisk differ statistically significantly (P<0.05) from infection with *Bhe* Δ*bepA-G*. Data from one representative experiment (n = 3) are presented.

Figure 5. The functions of BepA$_{Bhe}$ and BepD$_{Bhe}$ on inhibition of DC mutation receptors are narrowed down to its BID domain and the N-terminal fragment, respectively. BMDCs were infected with *Bhe* Δ*bepA-G* mutant complemented with the indicated Bep-expression plasmids at MOI = 25 for 24 h. The surface expression of MHCII, CD40, CD80, and CD86 was monitored by flow cytometry analysis. Expression levels of the maturation markers were presented as relative GMFI. All data were normalized to infection with *Bhe* Δ*bepA-G* as 1 and showed as the mean ± SEM from three independent experiments. Statistical significance was determined using Student's t-test. Data marked by an asterisk differ statistically significantly (P<0.05) from infection with *Bhe* Δ*bepA-G*.

Figure 6. The effects of BepA$_{Bhe}$ and BepD$_{Bhe}$ on repression of pro-inflammatory cytokine secretion are related to its BID domain and the N-terminal fragment, respectively. BMDCs were infected with Bhe ΔbepA-G mutant complemented with the indicated Bep-expression plasmids at MOI = 25. After 24 hpi, Culture media were collected for cytokine detection (TNF-α and IL-6) by ELISA. The data showed as the mean ± SEM from three independent experiments. Statistical significance was determined using Student's t-test. Data marked by an asterisk differ statistically significantly (P<0.05) from infection with *Bhe* Δ*bepA-G*. Data from one representative experiment (n = 3) are presented.

Figure 7. Expression of BepA$_{Bhe}$ homologs in the *Bhe* Δ*bepA-G* inhibits DC maturation receptors. BMDCs were infected with *Bhe* Δ*bepA-G* mutant complemented with the indicated Bep-expression plasmids at MOI = 25 for 24 h. The surface expression of MHCII, CD40, CD80, and CD86 was monitored by flow cytometry analysis. Expression levels of the maturation markers were presented as

relative GMFI. All data were normalized to infection with *Bhe* Δ*bepA-G* as 1 and showed as the mean ± SEM from three independent experiments. Statistical significance was determined using Student's t-test. Data marked by an asterisk differ statistically significantly (P<0.05) from infection with *Bhe* Δ*bepA-G*.

Figure 8. Expression of BepA$_{Bhe}$ homologs in the *Bhe* Δ*bepA-G* represses pro-inflammatory cytokine secretion. BMDCs were infected with *Bhe* Δ*bepA-G* mutant complemented with the indicated Bep-expression plasmids at MOI = 25. After 24 hpi, Culture media were collected for cytokine detection (TNF-α and IL-6) by ELISA. The data showed as the mean ± SEM from three independent experiments. Statistical significance was determined using Student's t-test. Data marked by an asterisk differ statistically significantly (P<0.05) from infection with *Bhe* Δ*bepA-G*. Data from one representative experiment (n = 3) are presented.

Figure 9. BepA homologs mediate a downregulation of *CD40* gene and an upregulation of cAMP response gene. BMDCs were infected with *Bhe* Δ*bepA-G* mutant complemented with the indicated Bep-expression plasmids at MOI = 25. After 24 hpi, regulations of *CD40* and the cAMP-responsive gene *crem* were determined by quantitative real-time PCR. Results were normalized to expression of the housekeeping gene *GAPDH*. The bars represent the mean of triplicate samples ± SEM. Statistical significance was determined using Student's t-test. Data marked by an asterisk differ statistically significantly (P<0.05) from infection with *Bhe* Δ*bepA-G*. Data from one representative experiment (n = 3) are presented.

Figure 10. Expression of BepD$_{Bhe}$ homologs in the *Bhe* Δ*bepA-G* inhibits DC maturation receptors. BMDCs were infected with *Bhe* Δ*bepA-G* mutant complemented with the indicated Bep-expression plasmids at MOI = 25 for 24 h. The surface expression of MHCII, CD40, CD80, and CD86 was monitored by flow cytometry analysis. Expression levels of the maturation markers were presented as relative GMFI. All data were normalized to infection with *Bhe* Δ*bepA-G* as 1 and showed as the mean ± SEM from three independent experiments. Statistical significance was determined using Student's t-test. Data marked by an asterisk differ statistically significantly (P<0.05) from infection with *Bhe* Δ*bepA-G*.

Figure 11. Expression of BepD$_{Bhe}$ homologs in the *Bhe* Δ*bepA-G* represses

pro-inflammatory cytokine secretion. BMDCs were infected with *Bhe* Δ*bepA-G* mutant complemented with the indicated Bep-expression plasmids at MOI = 25. At 24 hpi, culture media were collected for cytokine detection (TNF-α and IL-6) by ELISA. The data showed as the mean ± SEM from three independent experiments. Statistical significance was determined using Student's t-test. Data marked by an asterisk differ statistically significantly ($P<0.05$) from infection with *Bhe* Δ*bepA-G*. Data from one representative experiment (n = 3) are presented.

Figure 12. The functional tyrosine residue in BepD-BXBID$_{Bhe}$ is delineated for the inhibition of DC maturation receptors. BMDCs were infected with *Bhe* Δ*bepA-G* mutant complemented with the indicated tyrosine substitution mutants derived from BepD-BXBID$_{Bhe}$ at MOI = 25 for 24 h. The DC surface expression of MHCII, CD40, CD80, and CD86 was monitored by flow cytometry analysis. Expression levels of the maturation markers were presented as relative GMFI. All data were normalized to infection with *Bhe* Δ*bepA-G* as 1 and showed as the mean ± SEM from three independent experiments. Statistical significance was determined using Student's t-test. Data marked by an asterisk differ statistically significantly ($P<0.05$) from infection with the strain expressing BepD-BXBID$_{Bhe}$.

Figure 13. The functional tyrosine residue in BepD-BXBID$_{Bhe}$ is delineated for the repression of pro-inflammatory cytokine secretion. BMDCs were infected with *Bhe* Δ*bepA-G* mutant complemented with the indicated tyrosine substitution mutants derived from BepD-BXBID$_{Bhe}$ at MOI = 25. At 24 hpi, culture media were collected for cytokine detection (TNF-α and IL-6) by ELISA. The data showed as the mean ± SEM from three independent experiments. Statistical significance was determined using Student's t-test. Data marked by an asterisk differ statistically significantly ($P<0.05$) from infection with the strain expressing BepD-BXBID$_{Bhe}$. Data from one representative experiment (n = 3) are presented.

Figure 14. Ectopic expression of BepD-BXBID$_{Bhe}$ actively suppresses JAWSII responses to *E. coli* LPS stimuli. The GFP or GFP-fusion protein (GFP-BepD-BXBID$_{Bhe}$, GFP-BepD-BID$_{Bhe}$, and GFP-BepD-BXBID$_{Bhe}$ 5Ymuts) was ectopically expressed in JAWSII cells using the lentiviral transduction system. Under the TET-inducible promoter pTF, the GFP or GFP-fusion proteins was induced by doxycycline treatment (1 μg/ml) for 24 h. Upon challenging with *E. Coli* LPS (0.1

µg/ml or 1 µg/ml) for 24 h, the DC surface expression of MHCII and CD86 was monitored by flow cytometry analysis. Expression levels of the maturation markers were presented as relative GMFI. All data were normalized to JAWSII cells without treatments as 1 and showed as the mean ± SEM from three independent experiments. Statistical significance was determined using Student's t-test. Data marked by an asterisk differ statistically significantly ($P<0.05$) from each constructed cell line without doxycycline and *E. coli* LPS treatments.

Figure 15. Ectopically expressed BepD-BXBID$_{Bhe}$ is phosphorylated in JAWSII cells. Upon immunoprecipitation with GFP nanobodies coupled to agarose beads, immunoblot of GFP and tyrosine-phosphorylation were determined from total cell lysates (input), the supernatant (flow-through), and the precipitate (IP) of JAWSII cells ectopically expressing corresponding BepD constructs depicted in figure.

Figure 16. Interactomics reveals several putative BepD binding partners. (A) Volcano plot representing significance (q-values) versus the BepD-BXBID$_{Bhe}$ /BepD-BXBID$_{Bhe}$ 5Ymuts interaction ratio of indicated partners on the y- and x-axes, respectively. Interactions showing a q-value <0.01 were considered significantly regulated among the two conditions and are represented in red. Underlined proteins harbor an SH2 domain. **(B)** Graphical representation of the interactome using STRING (high confidence 0.7). The color indicates the ratio for each interaction partner between BepD-BXBID$_{Bhe}$ and BepD-BXBID$_{Bhe}$ 5Ymuts. Only proteins with at least one connection in STRING are represented. **(C)** Table showing all 27 significantly regulated interaction partners (q-value <0.01) among BepD-BXBID$_{Bhe}$ /BepD-BXBID$_{Bhe}$ 5Ymuts.

Figure 17. Phosphoproteomics reveals STAT3 hyper-phosphorylation in dependency of Bep-BXBID$_{Bhe}$. (A) Diagram of the phosphoproteomics protocol applied to BepD-BXBID$_{Bhe}$ expression compared to BepD-BXBID$_{Bhe}$ 5Ymuts in JAWSII cells. **(B)** Volcano plot representing significance (q-values) versus the BepD-BXBID$_{Bhe}$/BepD-BXBID$_{Bhe}$ 5Ymuts phosphorylation ratio on the y- and x-axes, respectively. Phosphopeptides showing a q-value <0.01 were considered significantly regulated among the two conditions and are represented in red. **(C)** Table showing all 27 significantly regulated phosphopeptides (q-value <0.01) among BepD-BXBID$_{Bhe}$ /BepD-BXBID$_{Bhe}$ 5Ymuts.

Figure 18. SHP-2 and STAT3 specifically co-immunoprecipitates with GFP-BepD-BXBID$_{Bhe}$. (A) Upon immunoprecipitation with GFP nanobodies coupled to agarose beads, immunoblot of SHP-2 was determined from total cell lysates (input), the supernatant (flow-through), and the precipitate (IP) of JAWSII cells ectopically expressing corresponding BepD constructs depicted in figure. **(B)** Immunoblots of STAT3 and STAT3 phosphorylation at Tyr-705 were determined from total cell lysates (input), the supernatant (flow-through), and the precipitate (IP) of JAWSII cells ectopically expressing corresponding BepD constructs depicted in figure.

Figure 19. The enhanced phospho-STAT3 expression is BepD specific. Immunoblot of STAT3 phosphorylation at Tyr-705 was determined from total cell lysate of BMDCs infected with corresponding *Bartonella* strains depicted in figure. Actin was used as a loading control. Quantitative data showed as the mean ± SEM from two independent experiments. Data from one representative experiment (n = 2) are presented.

Figure 20. The function of EPIYA-related motifs in STAT3 phosphorylation is delineated in BepD-BXBID$_{Bhe}$ by tyrosine to phenylalanine exchanges. Immunoblot of STAT3 phosphorylation at Tyr-705 was determined from total cell lysate of BMDCs infected with corresponding *Bartonella* strains depicted in figure. Actin was used as a loading control. Quantitative data showed as the mean ± SEM from two independent experiments. Data from one representative experiment (n = 2) are presented.

Figure 21. STAT3 phosphorylation caused by BepD-BXBID$_{Bhe}$ is sustained until 24 hpi. Immunoblot of STAT3 phosphorylation at Tyr-705 was determined for the indicated time periods from total cell lysate of BMDCs infected with strains expressing BepD-BXBID$_{Bhe}$ or BepD-BXBID$_{Bhe}$ 5Ymuts. Actin was used as a loading control. Quantitative data showed as the mean ± SEM from two independent experiments. Data from one representative experiment (n = 2) are presented.

Figure 22. Lower doses of bacterial inoculation develop higher bacteremia by *B. taylorii* intradermal infection. Mice were inoculated in the ear dermis with Sm^R *Bta* wild-type: five mice per group with 1×10^7, 1×10^5, or 1×10^3 CFU/mouse. Blood

was drawn at the indicated dpi, diluted and plated on sheep blood supplemented CBA plates for counting bacterial CFU.

Figure 23. BepA$_{Bta}$ and BepD$_{Bta}$ seem to be potent for the fitness of bacteremia development. Mice were inoculated in the ear dermis with Sm^R *Bta* wild-type (blue), *Bta* Δ*virD4* (brown), *Bta* Δ*bepA* (red), *Bta* Δ*bepD* (green), or *Bta* Δ*bepAD* (purple): five mice per group with 1×10^5 CFU/mouse. Blood was drawn at the indicated dpi, diluted and plated on sheep blood supplemented CBA plates for counting bacterial CFU.

Figure 24. *Bta* mutants with deletion of *bepA* or/and *bepD* tend to lose the fitness to reach the highest peak of bacteremia. The infections were performed as described for Fig 22. The highest peak of each bacteremia was displayed at 14 dpi.

Figure S1. Up to 70% of BMDCs differentiated by Flt3L are CD11c$^+$. BMDCs were generated by culturing BM cells with Flt3 ligand for 7 – 10 days. Cell suspensions were stained with anti-CD11c antibody combined with anti-CD11b or anti-B220 antibodies to determine subtypes of DCs: conventional DCs or plasmacytoid DCs, respectively. Staining with anti-MHCII indicated the activation state of DCs

Figure S2. Immunoblots confirm the protein levels of the indicated Beps by overexpression in *Bhe* Δ*bepA-G*. All constructs for overexpression of individual Beps were derived from the flag-tag expression vector pPG100. *Bartonella* bacterial culture was harvested after 48 h of growth on CBA plates supplemented with appropriate antibiotics and IPTG (500 µM). The anti-Flag western blot **(A-D)** was obtained from total lysate of corresponding *Bartonella* strains depicted in figure.

Figure S3. BepA homologs show the significant similarity from the *Bartonella* lineage 4 species. (A) The BepA homologs from *Bartonella* species depicted in the figure (BepA$_{Btr}$, BepA$_{Bgr}$, BepA$_{Bbi}$, and BepA$_{Bta}$) were aligned to BepA$_{Bhe}$ using Geneious Pro 5.3.4. The amino acid sequence alignment with pairwise % identity is indicated. The FIC and BID domains were aligned independently. **(B)** The sequence alignment of BID domains of BepA homologs.

Figure S4. Except BepA$_{Bgr}$, BepA homologs mediate downregulations of cytokine

genes *TNF-α, IL-6,* and *IL-12*. BMDCs were infected with *Bhe* Δ*bepA-G* mutant complemented with overexpression of indicated BepA homologs at MOI = 25. After 24 hpi, regulations of *TNF-α*, *IL-6*, and *IL-12* were determined by quantitative real-time PCR. Results were normalized to expression of the housekeeping gene *GAPDH*.

Figure S5. BepD homologs show the conserved EPIYA-related motifs from the *Bartonella* lineage 4 species. (A) The BepD homologs from *Bartonella* species depicted in the figure ($BepD_{Btr}$, $BepD_{Bgr}$, $BepD_{Bbi}$, and $BepD_{Bta}$) were aligned to $BepD_{Bhe}$ using Geneious Pro 5.3.4. The amino acid sequence alignment with pairwise % identity is indicated. The tyrosine-containing N-termini and BID domains were aligned independently. **(B)** The sequence alignments of tyrosine-containing N-termini of BepD homologs.

Figure S6. BepD homologs mediate downregulations of genes of cytokines *TNF-α, IL-6,* and *IL-12* but not of surface receptors. BMDCs were infected with *Bhe* Δ*bepA-G* mutant complemented with overexpression of indicated BepD homologs at MOI = 25. After 24 hpi, gene regulations of surface receptors (*MHCII*, *CD80*, and *CD86*) and cytokines (*TNF-α*, *IL-6*, and *IL-12*) were determined by quantitative real-time PCR. Results were normalized to expression of the housekeeping gene *GAPDH*.

Figure S7. DC properties of JAWSII cells are confirmed by *E. coli* LPS treatment. (A) JAWSII cells were stained with anti-CD11c, anti-CD11b, or anti-B220 antibodies and analyzed by flow cytometry. **(B)** Upon *E. coli* LPS treatment with different concentrations (0.1 μg/ml, 1.0μg/ml, or 5.0 μg/ml) for 24 h, the surface expression of MHCII, CD40, CD80, and CD86 was monitored by flow cytometry analysis.

Figure S8. Ectopic expression of the GFP or GFP-fusion proteins is well induced by doxycycline treatment. (A) All constructs for overexpression of indicated proteins were derived from lentiviral doxycycline-inducible vector pCLX-pTF-R1-DEST-R2-EBR65 and transduced into JAWSII cells. Upon 24 h doxycycline treatment (1 μg/ml), total cell lysate was harvested for the anti-GFP western blot. **(B)** Upon 24 h doxycycline treatment (1 μg/ml), these stable cell lines carrying indicated constructs were analyzed by flow cytometry.

Figure S9. Genomic organization of the *virB/D4* T4SS and *beps* loci in *B. taylorii* and *B. henselae*. Alignment of the conserved T4SS VirB/VirD4 (*virB2-11* and *virD4* genes) and the highly variable translocated effectors (*beps* genes) in *Bta* and *Bhe* was analyzed using Geneious Pro 5.3.4. Sequence similarity is shown with the percent identity indicated according to the color scales.

3.2.7 Figures

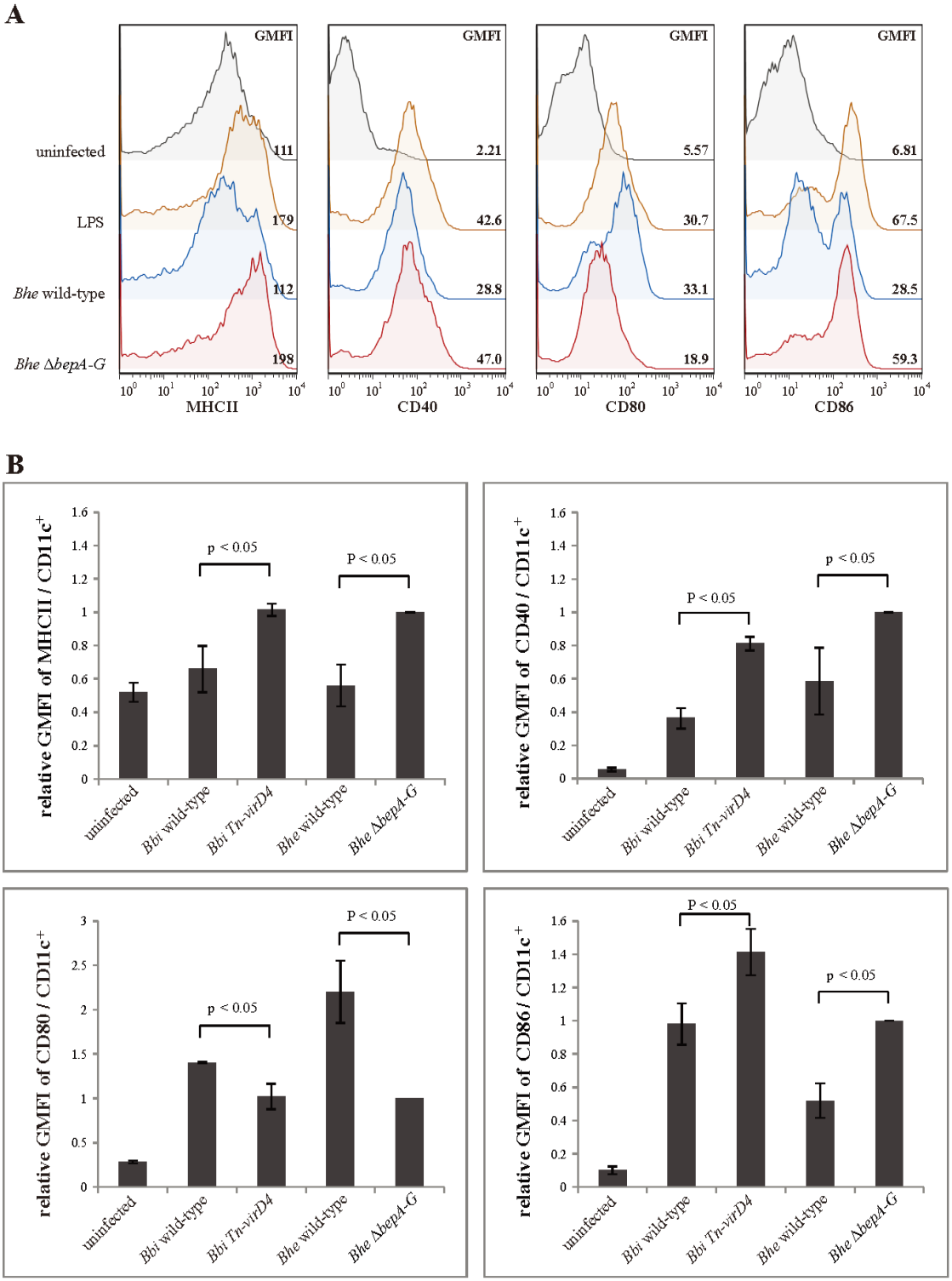

Figure 1.

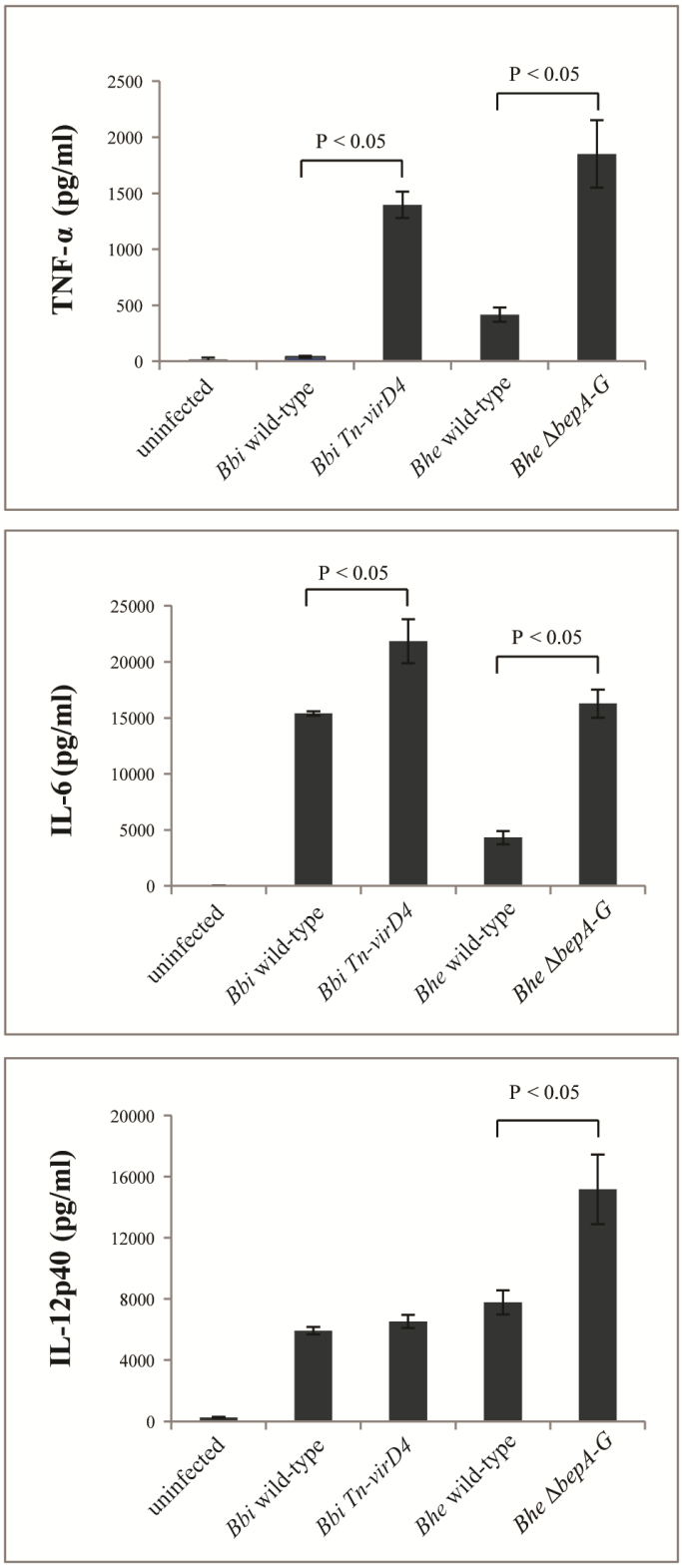
TNF-α (pg/ml)
2500
2000
1500
1000
500
0
P < 0.05
P < 0.05
uninfected
Bbi wild-type
Bbi Tn-virD4
Bhe wild-type
Bhe ΔbepA-G
IL-6 (pg/ml)
25000
20000
15000
10000
5000
0
P < 0.05
P < 0.05
uninfected
Bbi wild-type
Bbi Tn-virD4
Bhe wild-type
Bhe ΔbepA-G
IL-12p40 (pg/ml)
20000
16000
12000
8000
4000
0
P < 0.05
uninfected
Bbi wild-type
Bbi Tn-virD4
Bhe wild-type
Bhe ΔbepA-G

Figure 2.

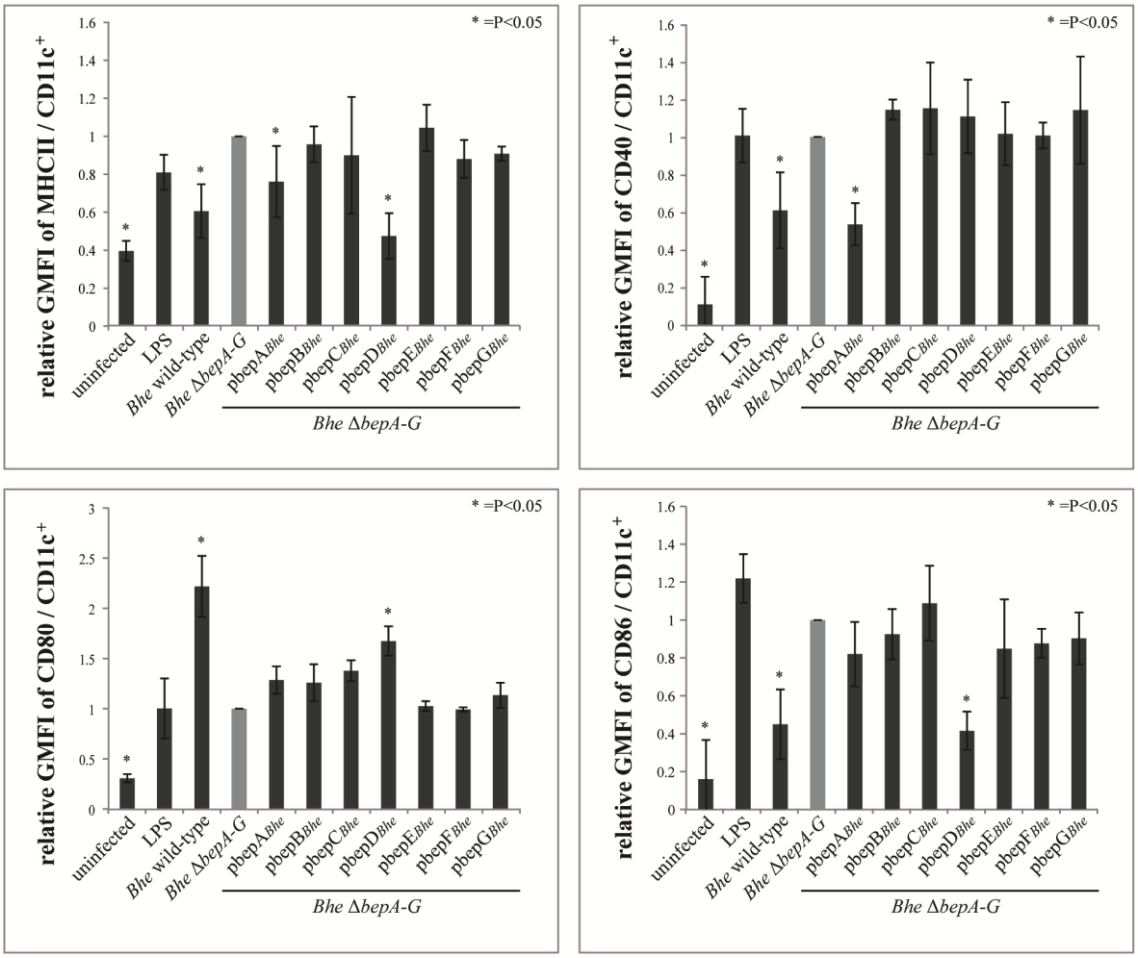
relative GMFI of MHCII / CD11c+
relative GMFI of CD40 / CD11c+
relative GMFI of CD80 / CD11c+
relative GMFI of CD86 / CD11c+
* =P<0.05
uninfected
LPS
Bhe wild-type
Bhe ΔbepA-G
pbepABhe
pbepBBhe
pbepCBhe
pbepDBhe
pbepEBhe
pbepFBhe
pbepGBhe
Bhe ΔbepA-G

Figure 3.

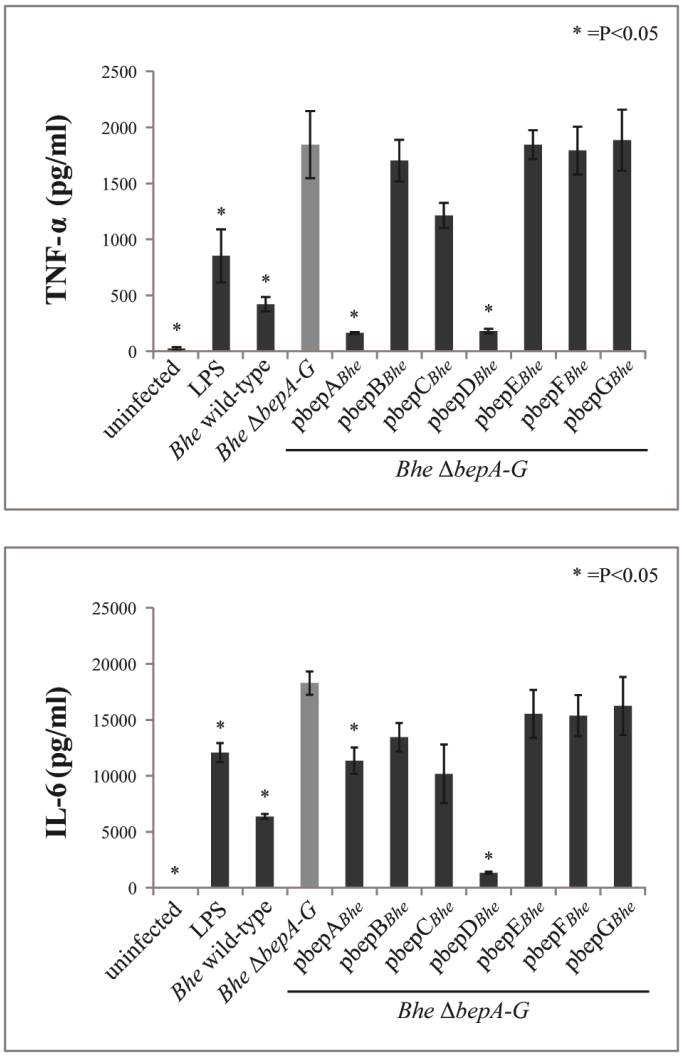
* =P<0.05
TNF-α (pg/ml)
2500
2000
1500
1000
500
0
uninfected
LPS
Bhe wild-type
Bhe ΔbepA-G
pbepABhe
pbepBBhe
pbepCBhe
pbepDBhe
pbepEBhe
pbepFBhe
pbepGBhe
Bhe ΔbepA-G
* =P<0.05
IL-6 (pg/ml)
25000
20000
15000
10000
5000
0
uninfected
LPS
Bhe wild-type
Bhe ΔbepA-G
pbepABhe
pbepBBhe
pbepCBhe
pbepDBhe
pbepEBhe
pbepFBhe
pbepGBhe
Bhe ΔbepA-G

Figure 4.

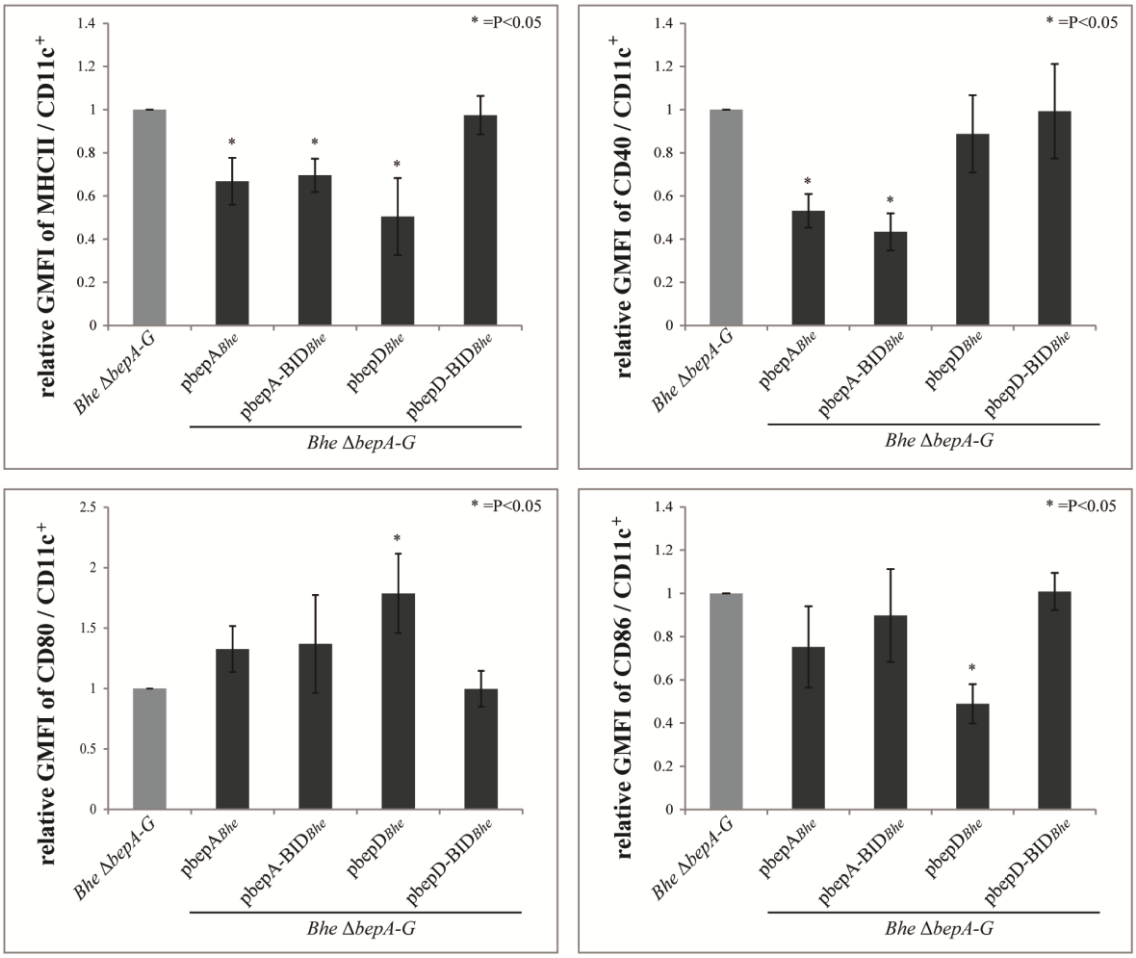
relative GMFI of MHCII / CD11c+
relative GMFI of CD40 / CD11c+
relative GMFI of CD80 / CD11c+
relative GMFI of CD86 / CD11c+
* =P<0.05
Bhe ΔbepA-G
pbepABhe
pbepA-BIDBhe
pbepDBhe
pbepD-BIDBhe
Bhe ΔbepA-G

Figure 5.

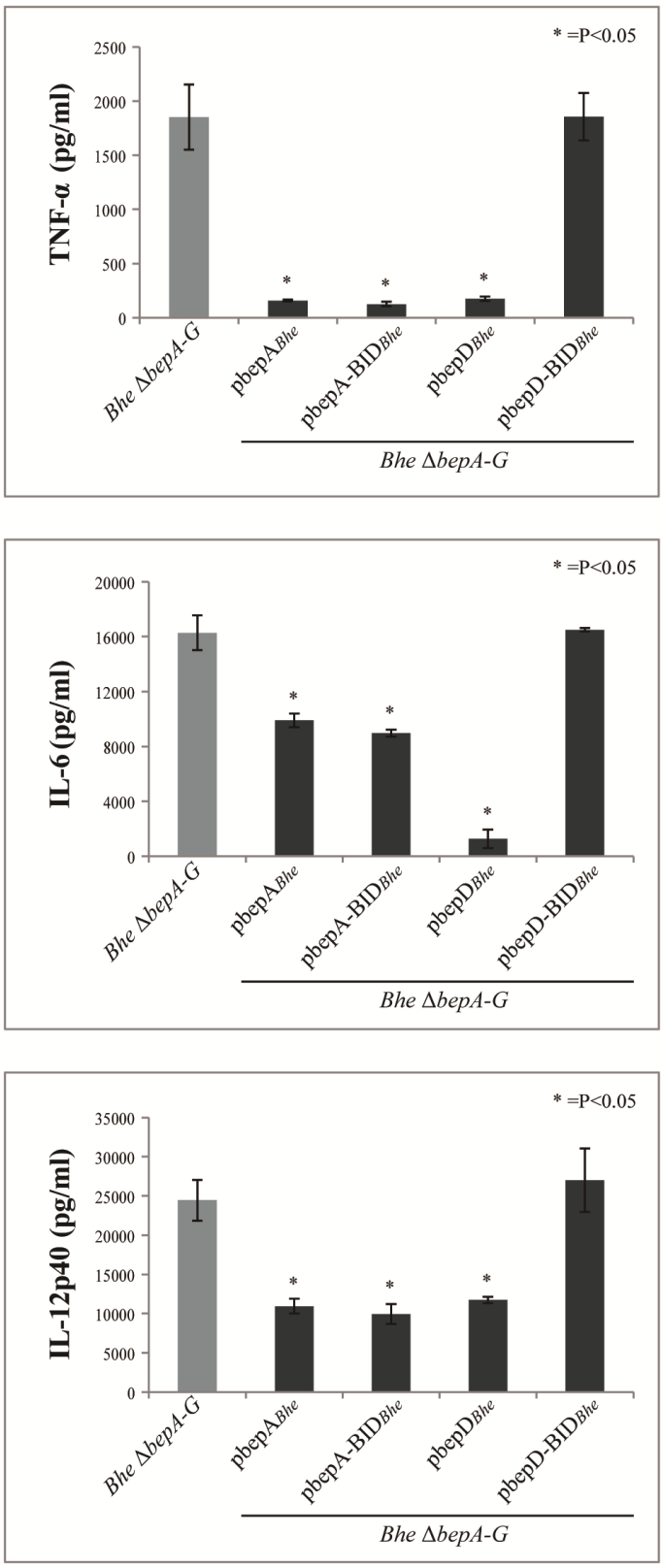
* =P<0.05
TNF-α (pg/ml)
2500
2000
1500
1000
500
0
IL-6 (pg/ml)
20000
16000
12000
8000
4000
0
IL-12p40 (pg/ml)
35000
30000
25000
20000
15000
10000
5000
0
Bhe ΔbepA-G
pbepABhe
pbepA-BIDBhe
pbepDBhe
pbepD-BIDBhe
Bhe ΔbepA-G

Figure 6.

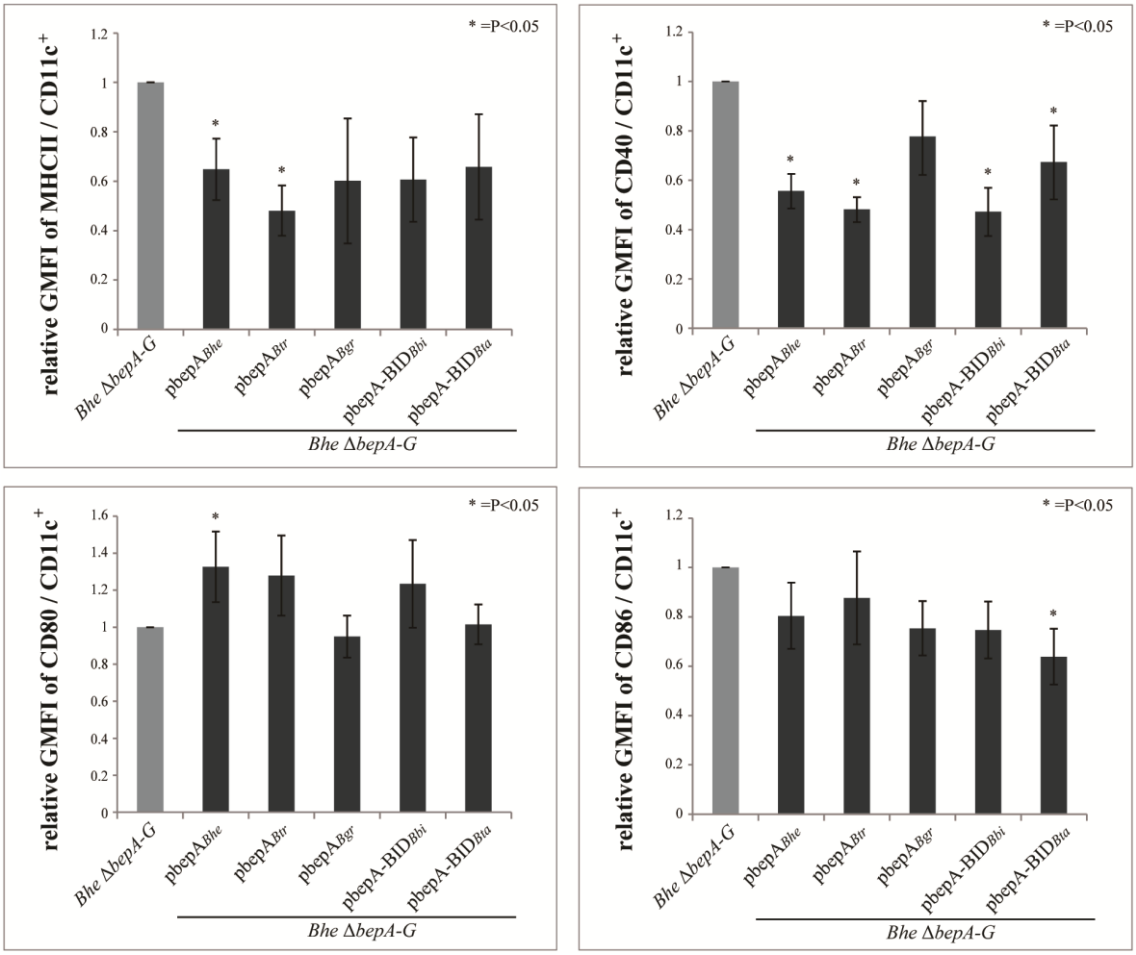
relative GMFI of MHCII / CD11c+
relative GMFI of CD40 / CD11c+
relative GMFI of CD80 / CD11c+
relative GMFI of CD86 / CD11c+
* =P<0.05
Bhe ΔbepA-G
pbepABhe
pbepABtr
pbepABgr
pbepA-BIDBbi
pbepA-BIDBta
Bhe ΔbepA-G

Figure 7.

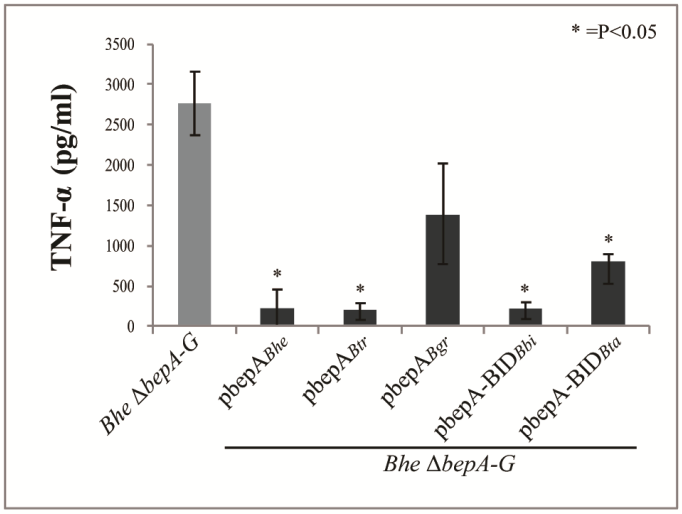
* =P<0.05
TNF-α (pg/ml)
3500
3000
2500
2000
1500
1000
500
0
*
*
*
*
Bhe ΔbepA-G
pbepABhe
pbepABtr
pbepABgr
pbepA-BIDBbi
pbepA-BIDBta
Bhe ΔbepA-G

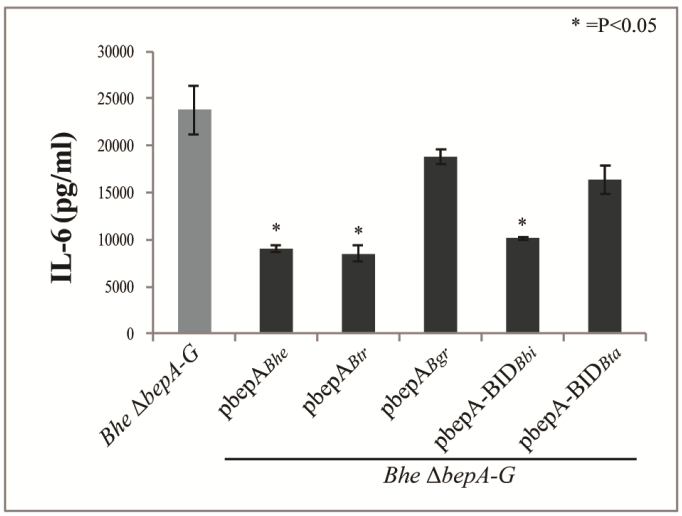
* =P<0.05
IL-6 (pg/ml)
30000
25000
20000
15000
10000
5000
0
*
*
*
Bhe ΔbepA-G
pbepABhe
pbepABtr
pbepABgr
pbepA-BIDBbi
pbepA-BIDBta
Bhe ΔbepA-G

Figure 8.

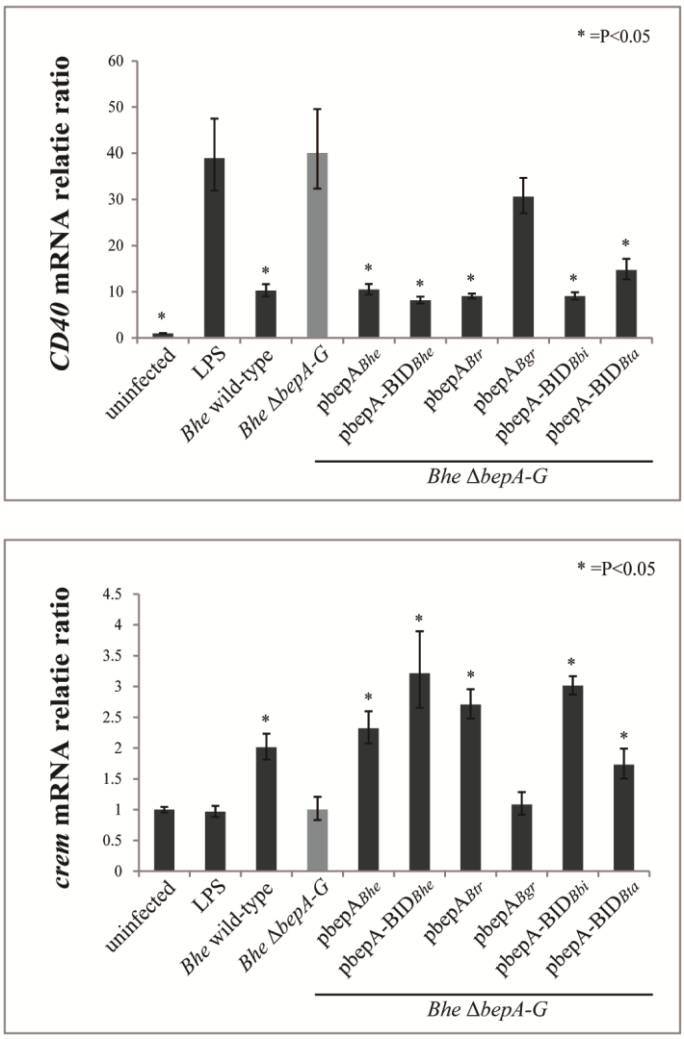
* =P<0.05
CD40 mRNA relatie ratio
60
50
40
30
20
10
0
uninfected
LPS
Bhe wild-type
Bhe ΔbepA-G
pbepABhe
pbepA-BIDBhe
pbepABtr
pbepABgr
pbepA-BIDBbi
pbepA-BIDBta
Bhe ΔbepA-G
* =P<0.05
crem mRNA relatie ratio
4.5
4
3.5
3
2.5
2
1.5
1
0.5
0
uninfected
LPS
Bhe wild-type
Bhe ΔbepA-G
pbepABhe
pbepA-BIDBhe
pbepABtr
pbepABgr
pbepA-BIDBbi
pbepA-BIDBta
Bhe ΔbepA-G

Figure 9.

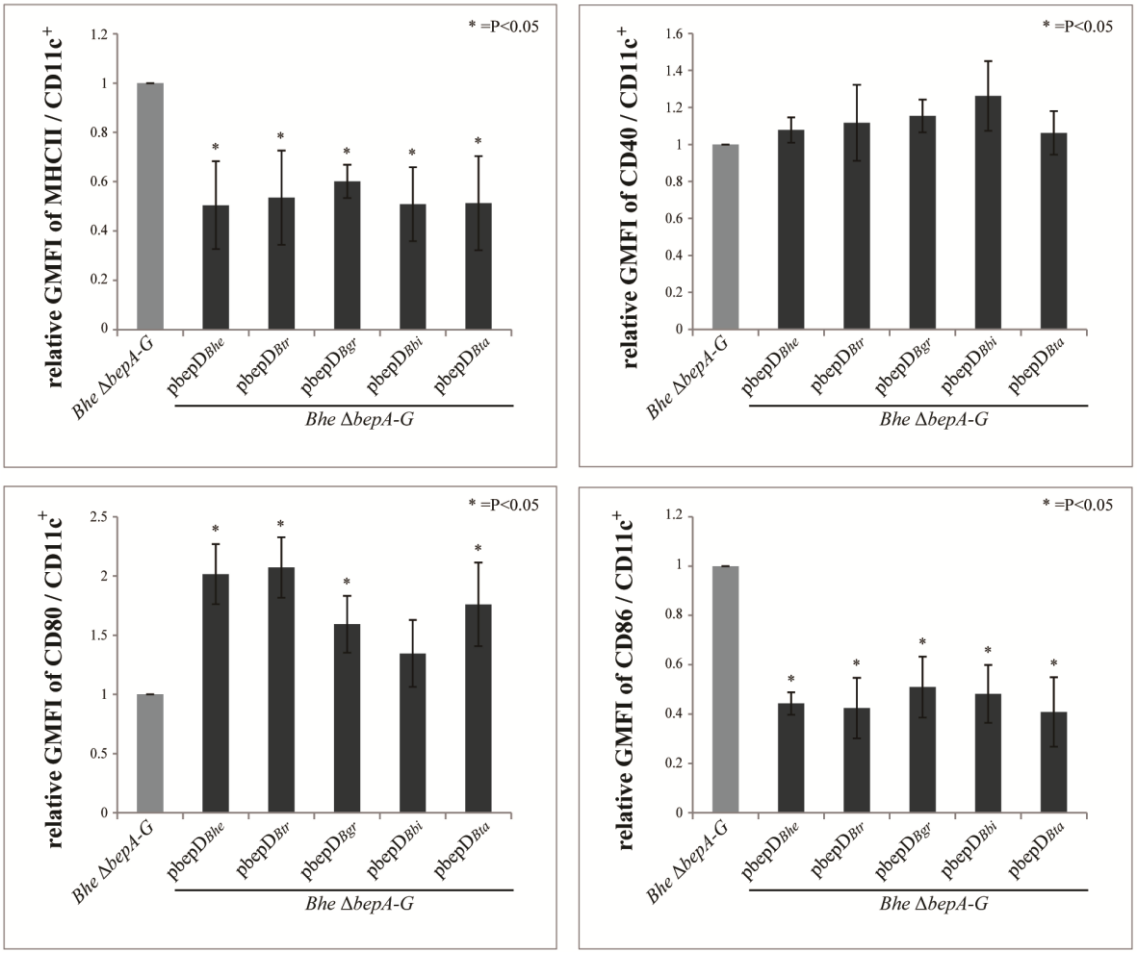
relative GMFI of MHCII / CD11c+
* =P<0.05
Bhe ΔbepA-G
pbepDBhe
pbepDBtr
pbepDBgr
pbepDBbi
pbepDBta
Bhe ΔbepA-G
relative GMFI of CD40 / CD11c+
* =P<0.05
Bhe ΔbepA-G
pbepDBhe
pbepDBtr
pbepDBgr
pbepDBbi
pbepDBta
Bhe ΔbepA-G
relative GMFI of CD80 / CD11c+
* =P<0.05
Bhe ΔbepA-G
pbepDBhe
pbepDBtr
pbepDBgr
pbepDBbi
pbepDBta
Bhe ΔbepA-G
relative GMFI of CD86 / CD11c+
* =P<0.05
Bhe ΔbepA-G
pbepDBhe
pbepDBtr
pbepDBgr
pbepDBbi
pbepDBta
Bhe ΔbepA-G

Figure 10.

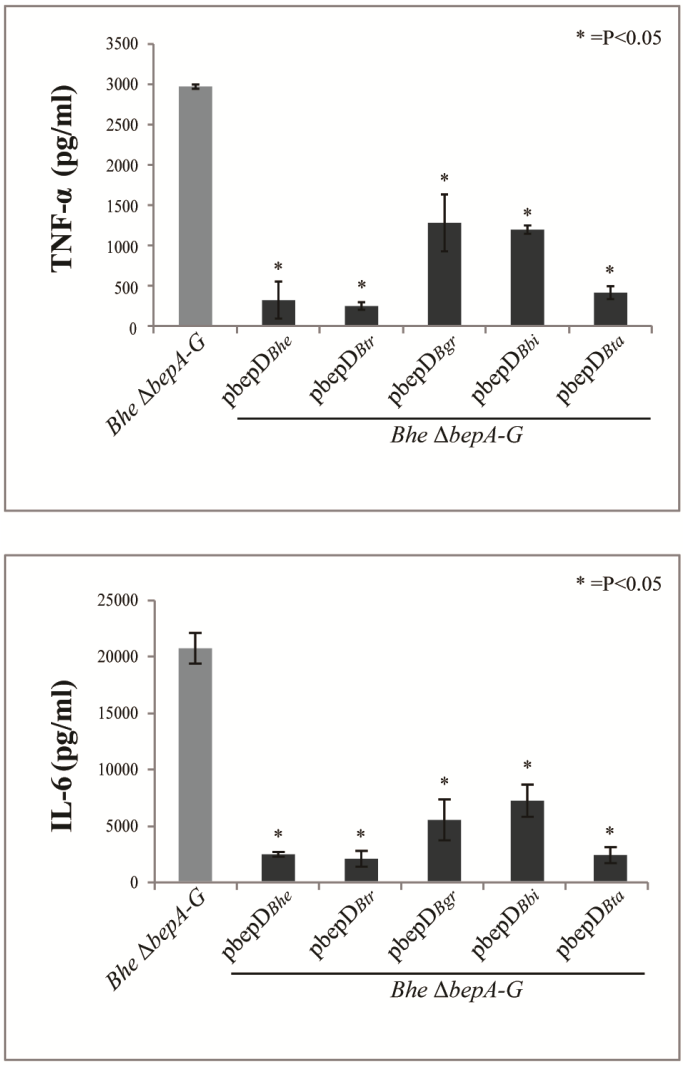
* =P<0.05
TNF-α (pg/ml)
3500
3000
2500
2000
1500
1000
500
0
Bhe ΔbepA-G
pbepDBhe
pbepDBtr
pbepDBgr
pbepDBbi
pbepDBta
Bhe ΔbepA-G
* =P<0.05
IL-6 (pg/ml)
25000
20000
15000
10000
5000
0
Bhe ΔbepA-G
pbepDBhe
pbepDBtr
pbepDBgr
pbepDBbi
pbepDBta
Bhe ΔbepA-G

Figure 11.

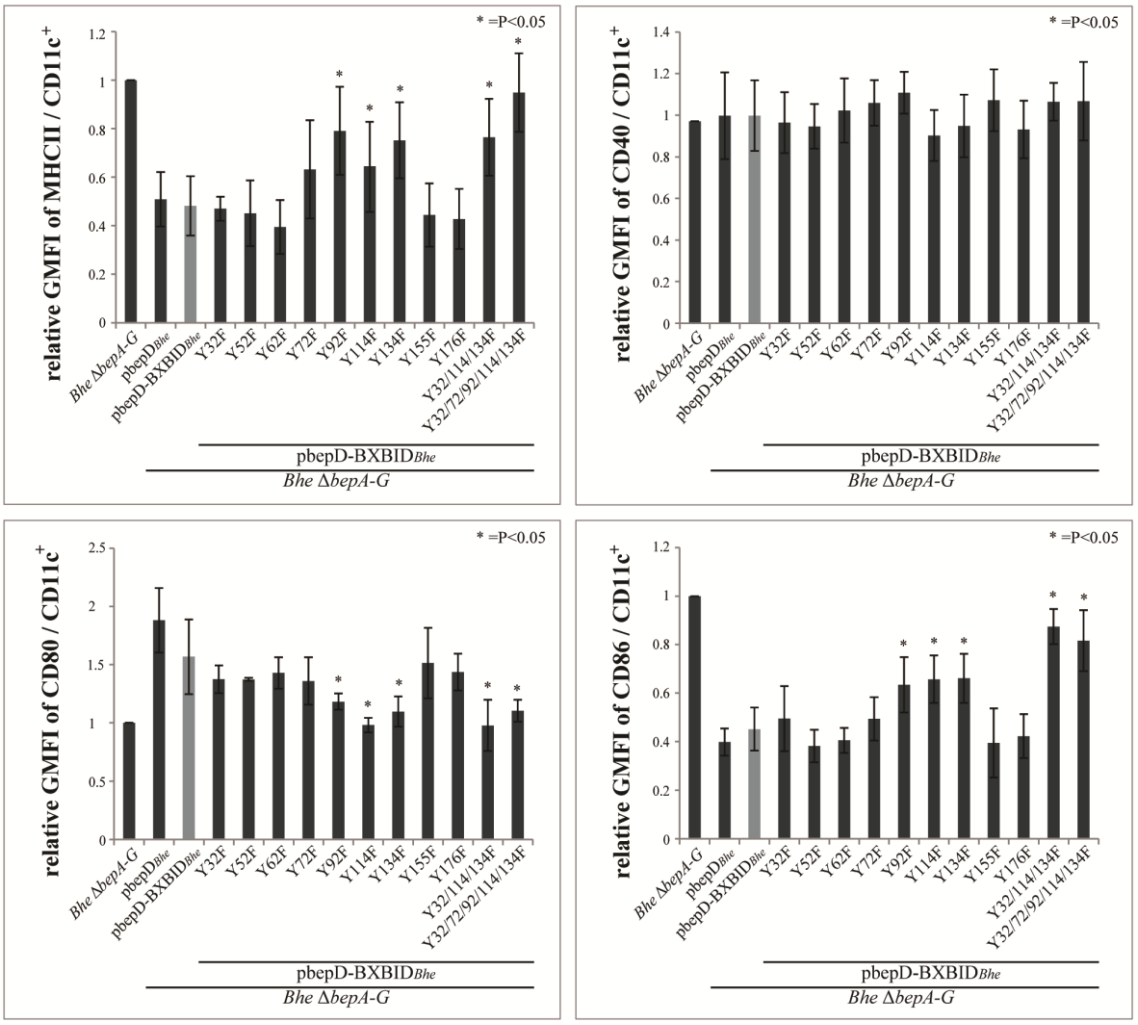
relative GMFI of MHCII / CD11c+
relative GMFI of CD40 / CD11c+
relative GMFI of CD80 / CD11c+
relative GMFI of CD86 / CD11c+
* =P<0.05
Bhe ΔbepA-G
pbepDBhe
pbepD-BXBIDBhe
Y32F
Y52F
Y62F
Y72F
Y92F
Y114F
Y134F
Y155F
Y176F
Y32/114/134F
Y32/72/92/114/134F
pbepD-BXBIDBhe
Bhe ΔbepA-G

Figure 12.

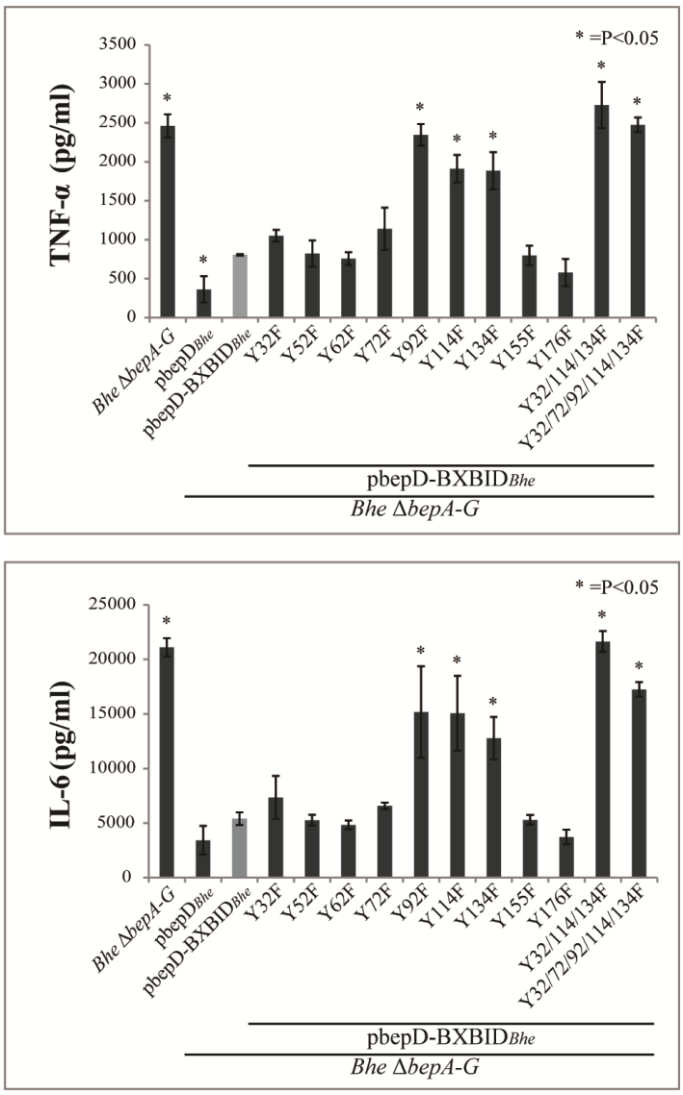
* =P<0.05
TNF-α (pg/ml)
3500
3000
2500
2000
1500
1000
500
0
Bhe ΔbepA-G
pbepDBhe
pbepD-BXBIDBhe
Y32F
Y52F
Y62F
Y72F
Y92F
Y114F
Y134F
Y155F
Y176F
Y32/114/134F
Y32/72/92/114/134F
pbepD-BXBIDBhe
Bhe ΔbepA-G
* =P<0.05
IL-6 (pg/ml)
25000
20000
15000
10000
5000
0
Bhe ΔbepA-G
pbepDBhe
pbepD-BXBIDBhe
Y32F
Y52F
Y62F
Y72F
Y92F
Y114F
Y134F
Y155F
Y176F
Y32/114/134F
Y32/72/92/114/134F
pbepD-BXBIDBhe
Bhe ΔbepA-G

Figure 13.

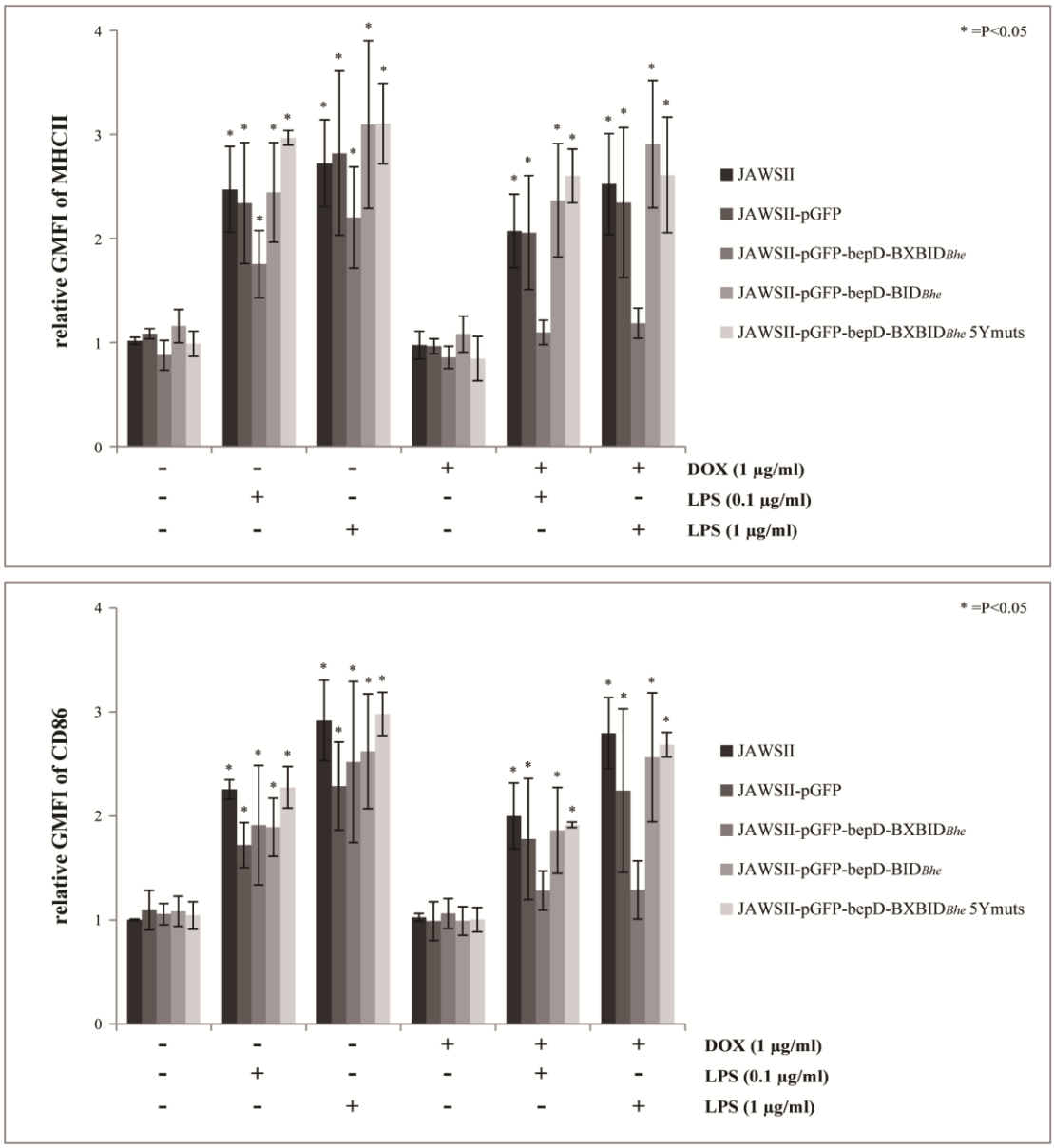
* =P<0.05
relative GMFI of MHCII
JAWSII
JAWSII-pGFP
JAWSII-pGFP-bepD-BXBIDBhe
JAWSII-pGFP-bepD-BIDBhe
JAWSII-pGFP-bepD-BXBIDBhe 5Ymuts
DOX (1 µg/ml)
LPS (0.1 µg/ml)
LPS (1 µg/ml)
* =P<0.05
relative GMFI of CD86
JAWSII
JAWSII-pGFP
JAWSII-pGFP-bepD-BXBIDBhe
JAWSII-pGFP-bepD-BIDBhe
JAWSII-pGFP-bepD-BXBIDBhe 5Ymuts
DOX (1 µg/ml)
LPS (0.1 µg/ml)
LPS (1 µg/ml)

Figure 14.

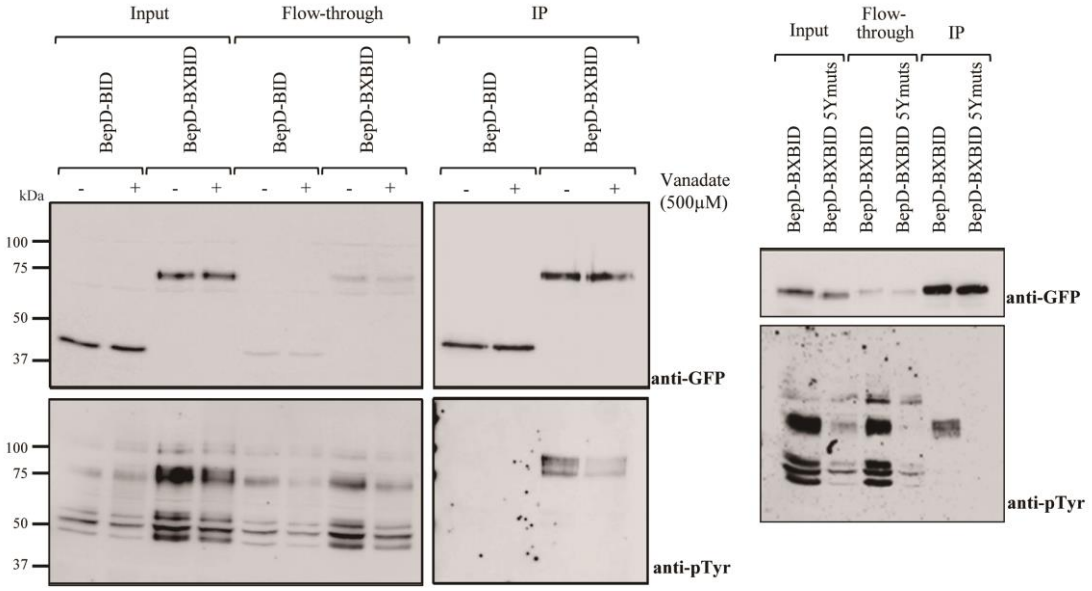
Input
Flow-through
IP
BepD-BID
BepD-BXBID
BepD-BID
BepD-BXBID
BepD-BID
BepD-BXBID
Vanadate (500µM)
kDa
100
75
50
37
anti-GFP
anti-pTyr
Input
Flow-through
IP
BepD-BXBID
BepD-BXBID 5Ymuts
BepD-BXBID
BepD-BXBID 5Ymuts
BepD-BXBID
BepD-BXBID 5Ymuts
anti-GFP
anti-pTyr

Figure 15.

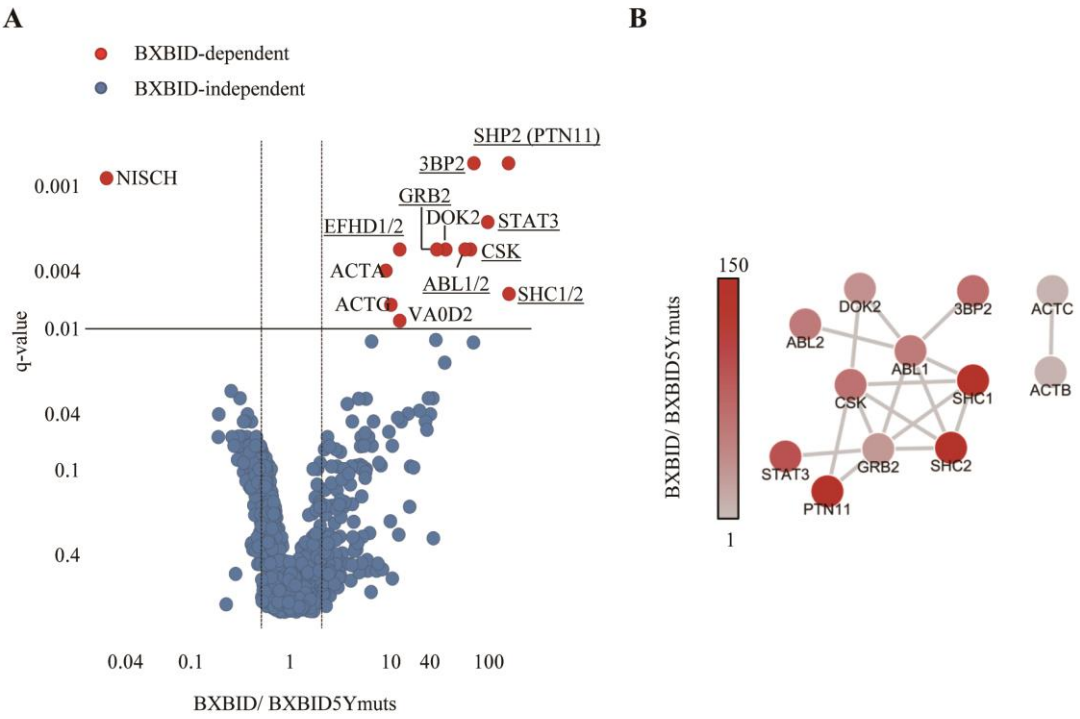

C

Accession	Description	# peptides	BXBID/BXBID5Ymut	q-value
SHC1|SHC2	SHC-transforming protein 1	3	153.5	0.0057
PTN11	Tyrosine-protein phosphatase non-receptor type 11	58	151.7	0.0007
STAT3	Signal transducer and activator of transcription 3	53	94.3	0.0018
3BP2	SH3 domain-binding protein 2	2	68.3	0.0007
CSK	Tyrosine-protein kinase CSK	8	63.2	0.0028
ABL2|ABL1	Abelson tyrosine-protein kinase 2	22	55.7	0.0028
DOK2	Docking protein 2	14	35.7	0.0028
GRB2	Growth factor receptor-bound protein 2	11	29.1	0.0028
EFHD2|EFHD1	EF-hand domain-containing protein D2	6	12.4	0.0028
VA0D2	V-type proton ATPase subunit d 2	3	12.3	0.0088
ACTB|ACTG	Actin, cytoplasmic 1	13	10.1	0.0068
ACTC|ACTA	Actin, alpha cardiac muscle 1	3	9.0	0.0039
NISCH	Nischarin	26	0.0	0.0009

Figure 16.

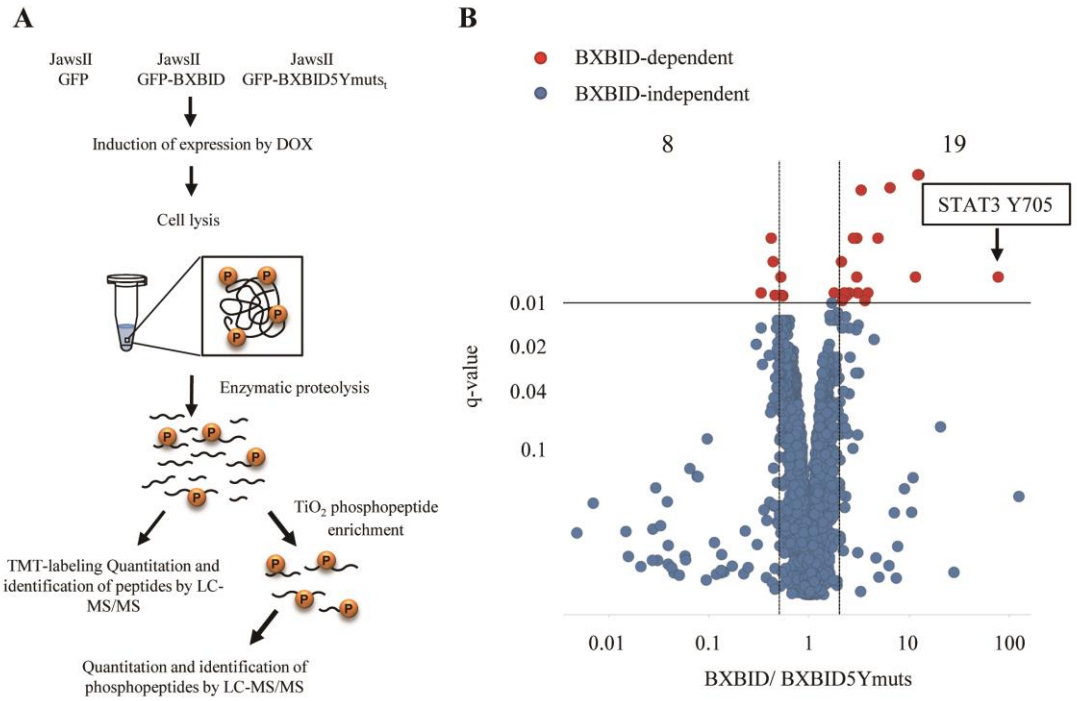

C

Accession	Description	BXBID/BXBID5Ymut	q-value
STAT3	Signal transducer and activator of transcription 3	77.8	0.007
OSTP	Osteopontin	12.5	0.001
OSTP	Osteopontin	12.3	0.001
CRK	Adapter molecule crk	11.6	0.007
OSTP	Osteopontin	6.5	0.002
CBL	E3 ubiquitin-protein ligase CBL	4.9	0.004
OSTP	Osteopontin	3.9	0.009
TBC14	TBC1 domain family member 14	3.6	0.010
IRS2	Insulin receptor substrate 2	3.3	0.002
BCAP	Phosphoinositide 3-kinase adapter protein 1	3.1	0.009
STAT3	Signal transducer and activator of transcription 3	3.0	0.004
IRS2	Insulin receptor substrate 2	3.0	0.007
IRS2	Insulin receptor substrate 2	2.8	0.004
ZN703	Zinc finger protein 703	2.5	0.009
IRS2	Insulin receptor substrate 2	2.4	0.009
FYB	FYN-binding protein	2.3	0.009
RHG17	Rho GTPase-activating protein 17	2.2	0.010
I2BPL	Interferon regulatory factor 2-binding protein-like	2.1	0.005
OSBP1	Oxysterol-binding protein 1	1.8	0.009
THOC4	THO complex subunit 4	0.5	0.009
KI20A	Kinesin-like protein KIF20A	0.5	0.009
UHRF1	E3 ubiquitin-protein ligase UHRF1	0.5	0.009
LCP2	Lymphocyte cytosolic protein 2	0.5	0.007
SIR2	NAD-dependent protein deacetylase sirtuin-2	0.5	0.009
CAP1	Adenylyl cyclase-associated protein 1	0.4	0.005
NADK	NAD kinase	0.4	0.004
NECP2	Adaptin ear-binding coat-associated protein 2	0.3	0.009

Figure 17.

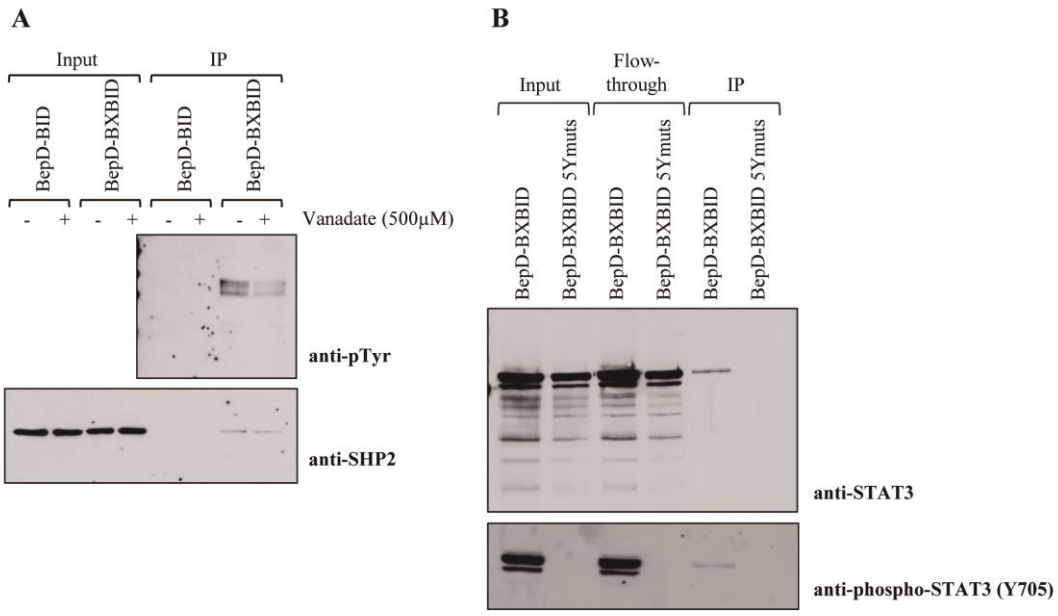
A
Input
IP
BepD-BID
BepD-BXBID
BepD-BID
BepD-BXBID
- + - + - + - +
Vanadate (500µM)
anti-pTyr
anti-SHP2
B
Input
Flow-through
IP
BepD-BXBID
BepD-BXBID 5Ymuts
BepD-BXBID
BepD-BXBID 5Ymuts
BepD-BXBID
BepD-BXBID 5Ymuts
anti-STAT3
anti-phospho-STAT3 (Y705)

Figure 18.

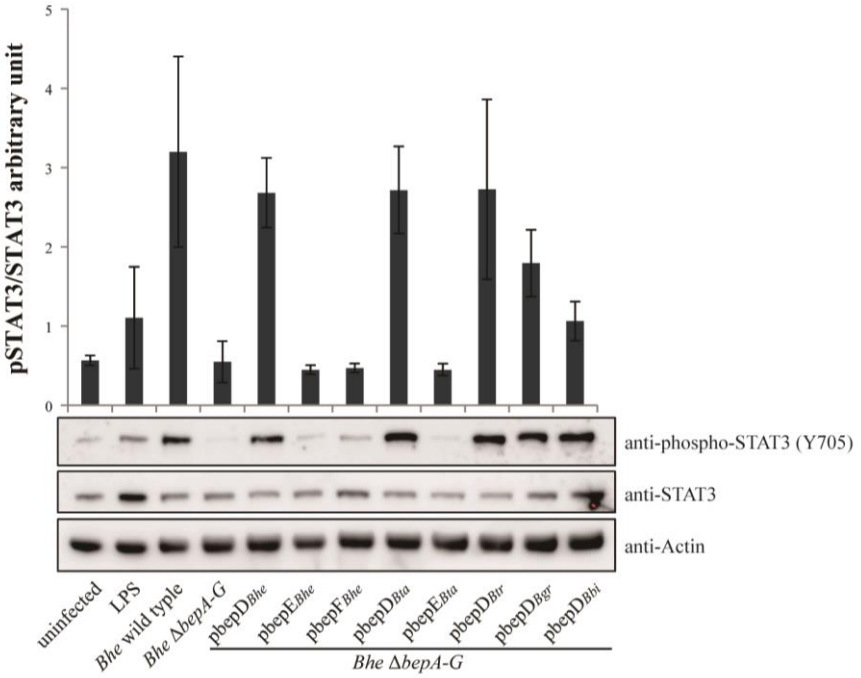
pSTAT3/STAT3 arbitrary unit
0
1
2
3
4
5
anti-phospho-STAT3 (Y705)
anti-STAT3
anti-Actin
uninfected
LPS
Bhe wild typle
Bhe ΔbepA-G
pbepDBhe
pbepEBhe
pbepFBhe
pbepDBta
pbepEBta
pbepDBtr
pbepDBgr
pbepDBhi
Bhe ΔbepA-G

Figure 19.

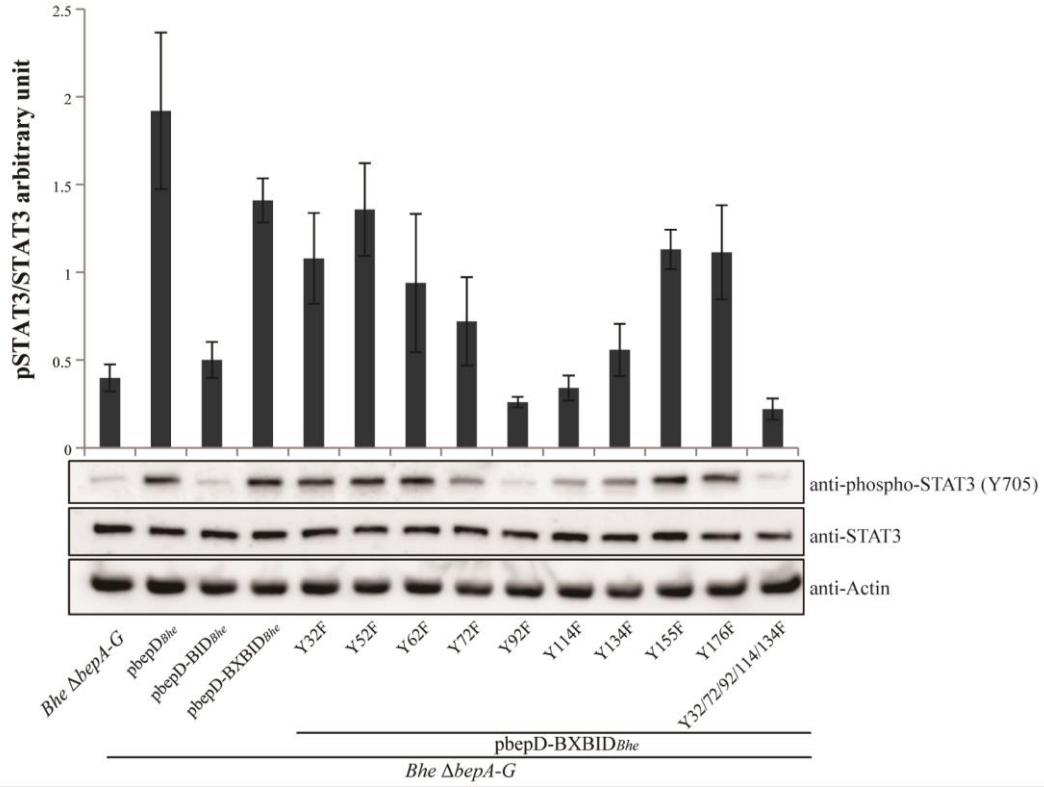
pSTAT3/STAT3 arbitrary unit
2.5
2
1.5
1
0.5
0
anti-phospho-STAT3 (Y705)
anti-STAT3
anti-Actin
Bhe ΔbepA-G
pbepDBhe
pbepD-BIDBhe
pbepD-BXBIDBhe
Y32F
Y52F
Y62F
Y72F
Y92F
Y114F
Y134F
Y155F
Y176F
Y32/72/92/114/134F
pbepD-BXBIDBhe
Bhe ΔbepA-G

Figure 20.

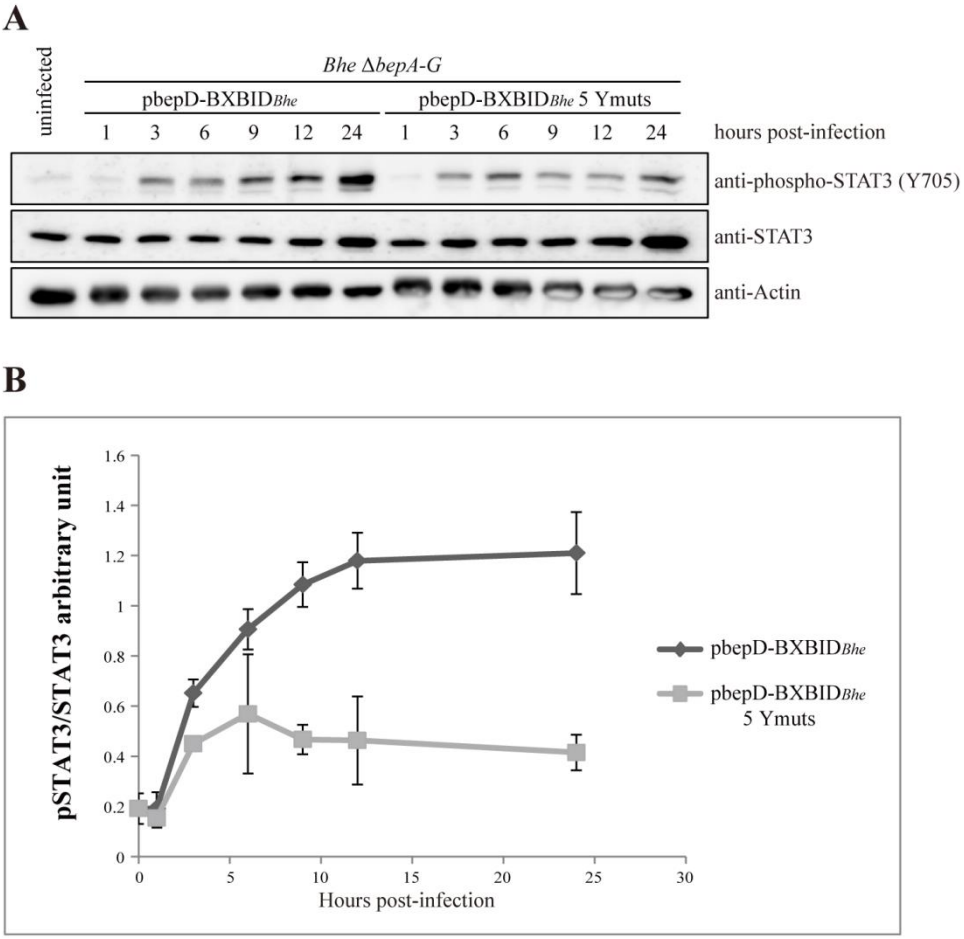
A
uninfected
Bhe ΔbepA-G
pbepD-BXBIDBhe
pbepD-BXBIDBhe 5 Ymuts
1 3 6 9 12 24 1 3 6 9 12 24
hours post-infection
anti-phospho-STAT3 (Y705)
anti-STAT3
anti-Actin
B
pSTAT3/STAT3 arbitrary unit
1.6
1.4
1.2
1
0.8
0.6
0.4
0.2
0
0 5 10 15 20 25 30
Hours post-infection
pbepD-BXBIDBhe
pbepD-BXBIDBhe 5 Ymuts

Figure 21.

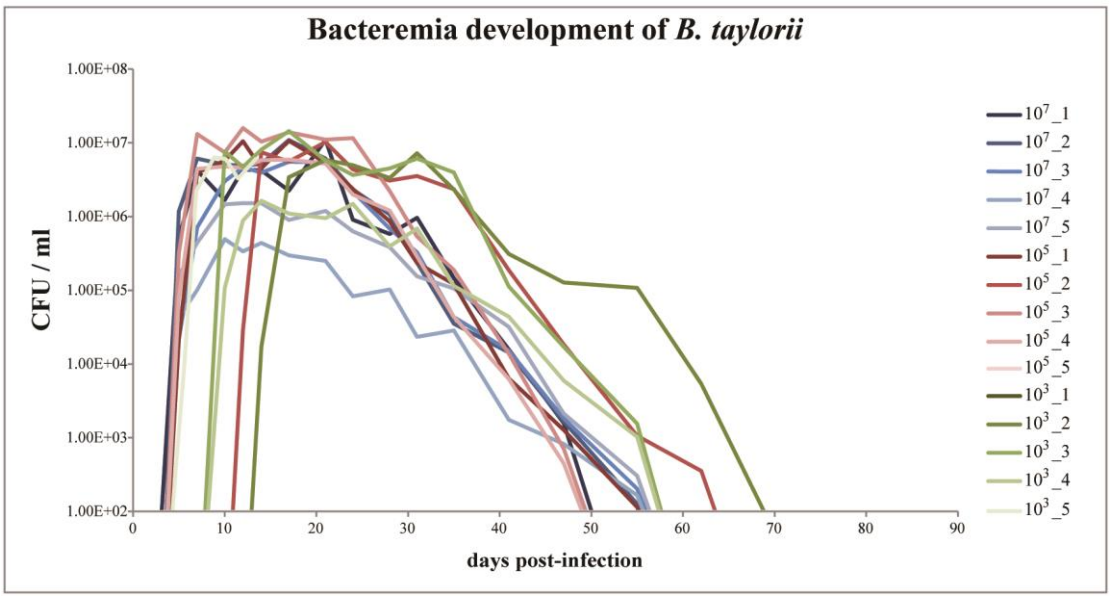
Bacteremia development of B. taylorii
CFU / ml
1.00E+08
1.00E+07
1.00E+06
1.00E+05
1.00E+04
1.00E+03
1.00E+02
0
10
20
30
40
50
60
70
80
90
days post-infection
10^7_1
10^7_2
10^7_3
10^7_4
10^7_5
10^5_1
10^5_2
10^5_3
10^5_4
10^5_5
10^3_1
10^3_2
10^3_3
10^3_4
10^3_5

Figure 22.

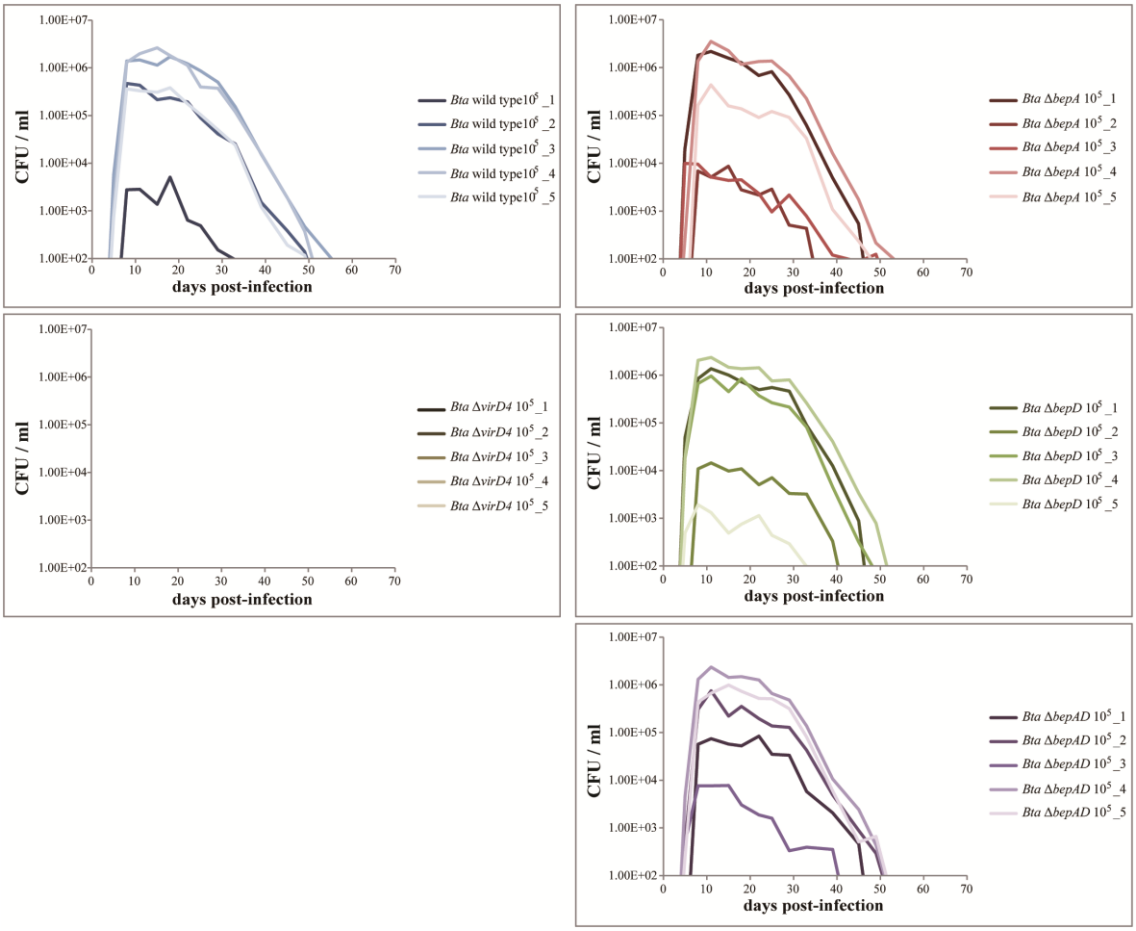
CFU / ml
days post-infection
Bta wild type10^5 _1
Bta wild type10^5 _2
Bta wild type10^5 _3
Bta wild type10^5 _4
Bta wild type10^5 _5
Bta ΔbepA 10^5_1
Bta ΔbepA 10^5_2
Bta ΔbepA 10^5_3
Bta ΔbepA 10^5_4
Bta ΔbepA 10^5_5
Bta ΔvirD4 10^5_1
Bta ΔvirD4 10^5_2
Bta ΔvirD4 10^5_3
Bta ΔvirD4 10^5_4
Bta ΔvirD4 10^5_5
Bta ΔbepD 10^5_1
Bta ΔbepD 10^5_2
Bta ΔbepD 10^5_3
Bta ΔbepD 10^5_4
Bta ΔbepD 10^5_5
Bta ΔbepAD 10^5_1
Bta ΔbepAD 10^5_2
Bta ΔbepAD 10^5_3
Bta ΔbepAD 10^5_4
Bta ΔbepAD 10^5_5

Figure 23.

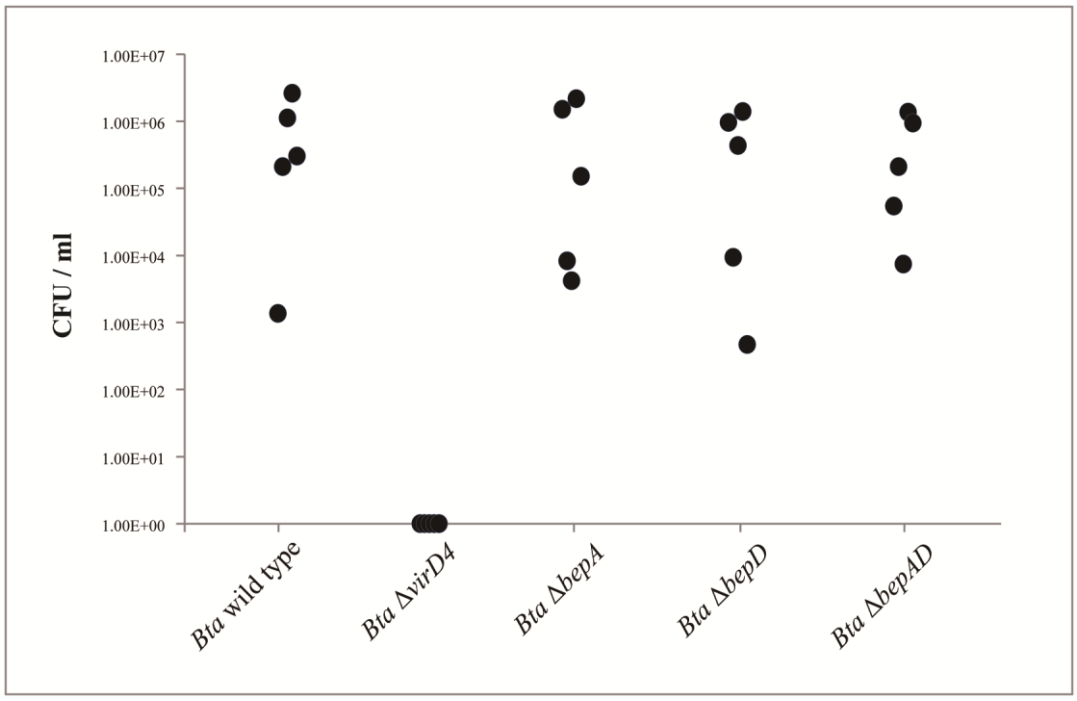
CFU / ml
1.00E+07
1.00E+06
1.00E+05
1.00E+04
1.00E+03
1.00E+02
1.00E+01
1.00E+00
Bta wild type
Bta ΔvirD4
Bta ΔbepA
Bta ΔbepD
Bta ΔbepAD

Figure 24.

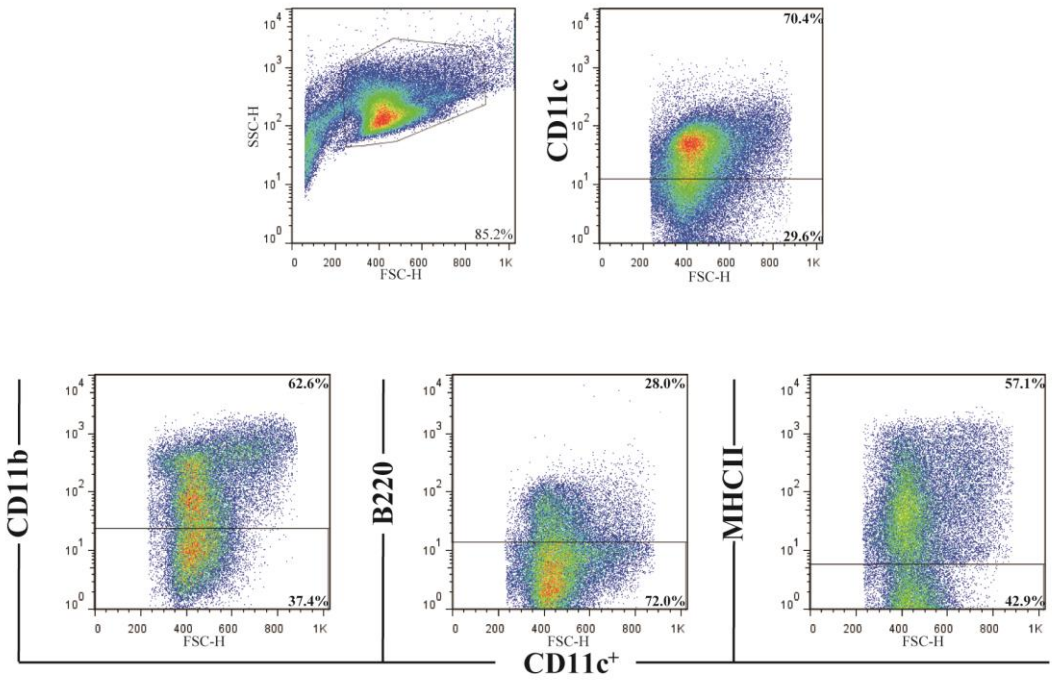
SSC-H
FSC-H
85.2%
CD11c
70.4%
29.6%
CD11b
62.6%
37.4%
B220
28.0%
72.0%
MHCII
57.1%
42.9%
CD11c+

Figure S1.

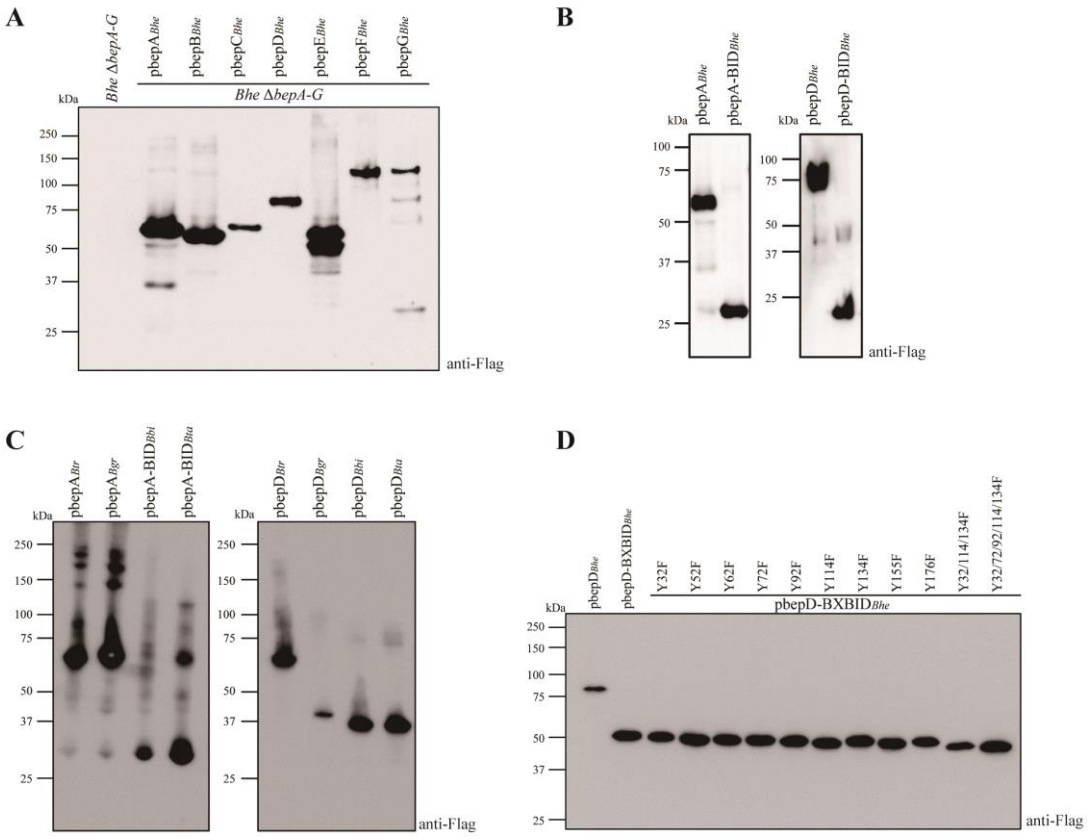
A
Bhe ΔbepA-G
pbepABhe
pbepBBhe
pbepCBhe
pbepDBhe
pbepEBhe
pbepFBhe
pbepGBhe
Bhe ΔbepA-G
kDa
250
150
100
75
50
37
25
anti-Flag
B
pbepABhe
pbepA-BIDBhe
pbepDBhe
pbepD-BIDBhe
kDa
100
75
50
37
25
anti-Flag
C
pbepABtr
pbepABgr
pbepA-BIDBbi
pbepA-BIDBta
pbepDBtr
pbepDBgr
pbepDBbi
pbepDBta
kDa
250
150
100
75
50
37
25
anti-Flag
D
pbepDBhe
pbepD-BXBIDBhe
Y32F
Y52F
Y62F
Y72F
Y92F
Y114F
Y134F
Y155F
Y176F
Y32/114/134F
Y32/72/92/114/134F
pbepD-BXBIDBhe
kDa
250
150
100
75
50
37
25
anti-Flag

Figure S2.

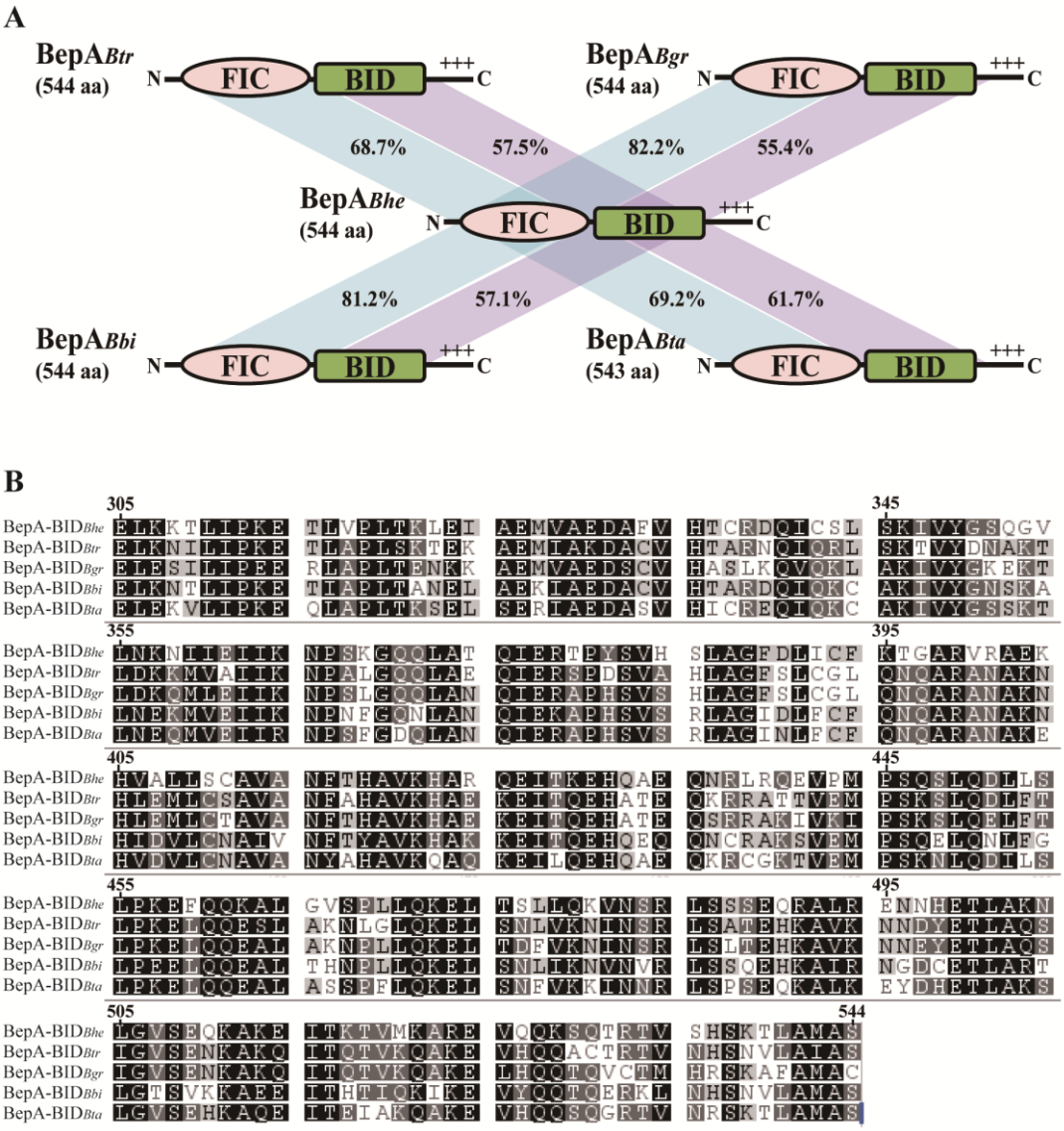
A
BepABtr
(544 aa)
N
FIC
BID
+++
C
BepABgr
(544 aa)
68.7%
57.5%
82.2%
55.4%
BepABhe
(544 aa)
81.2%
57.1%
69.2%
61.7%
BepABbi
(544 aa)
BepABta
(543 aa)
B
305
345
355
395
405
445
455
495
505
544
BepA-BIDBhe
BepA-BIDBtr
BepA-BIDBgr
BepA-BIDBbi
BepA-BIDBta

Figure S3.

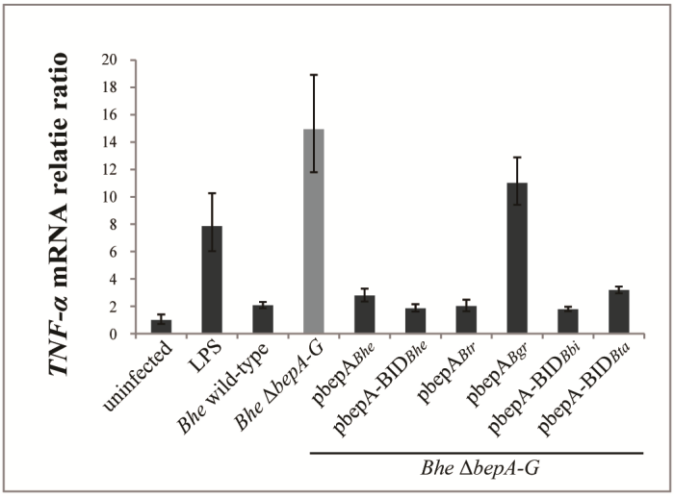
TNF-α mRNA relatie ratio
20
18
16
14
12
10
8
6
4
2
0
uninfected
LPS
Bhe wild-type
Bhe ΔbepA-G
pbepABhe
pbepA-BIDBhe
pbepABtr
pbepABgr
pbepA-BIDBbi
pbepA-BIDBta
Bhe ΔbepA-G

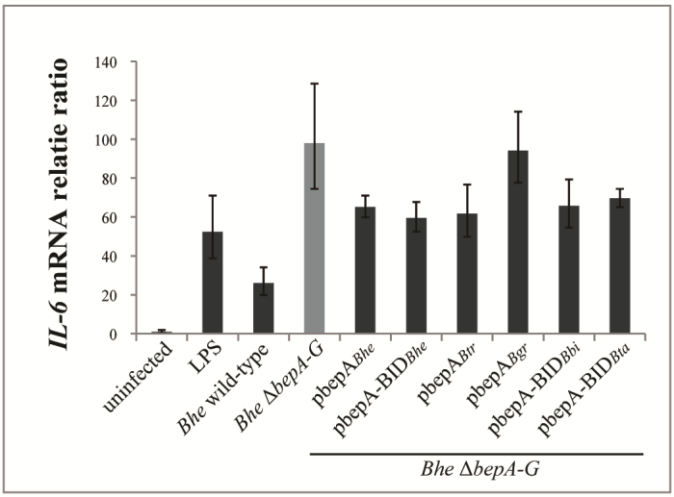
IL-6 mRNA relatie ratio
140
120
100
80
60
40
20
0
uninfected
LPS
Bhe wild-type
Bhe ΔbepA-G
pbepABhe
pbepA-BIDBhe
pbepABtr
pbepABgr
pbepA-BIDBbi
pbepA-BIDBta
Bhe ΔbepA-G

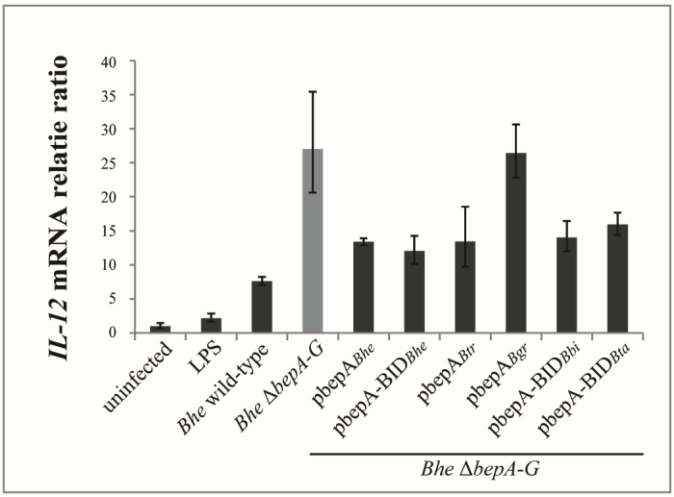
IL-12 mRNA relatie ratio
40
35
30
25
20
15
10
5
0
uninfected
LPS
Bhe wild-type
Bhe ΔbepA-G
pbepABhe
pbepA-BIDBhe
pbepABtr
pbepABgr
pbepA-BIDBbi
pbepA-BIDBta
Bhe ΔbepA-G

Figure S4.

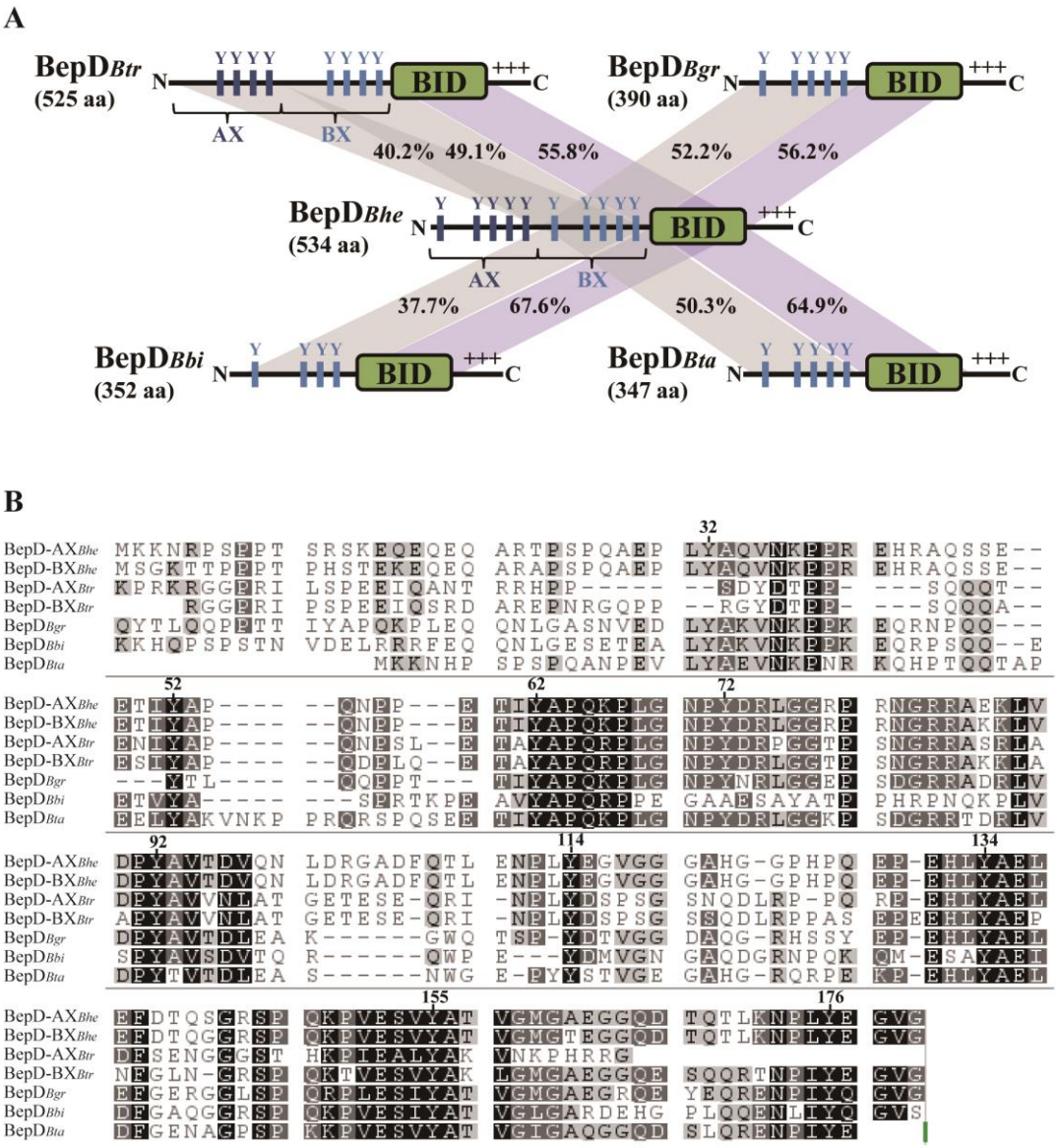
A
BepDBtr
(525 aa)
BepDBgr
(390 aa)
BepDBhe
(534 aa)
BepDBbi
(352 aa)
BepDBta
(347 aa)
BID
AX
BX
40.2%
49.1%
55.8%
52.2%
56.2%
37.7%
67.6%
50.3%
64.9%
B
BepD-AXBhe
BepD-BXBhe
BepD-AXBtr
BepD-BXBtr
BepDBgr
BepDBbi
BepDBta

Figure S5.

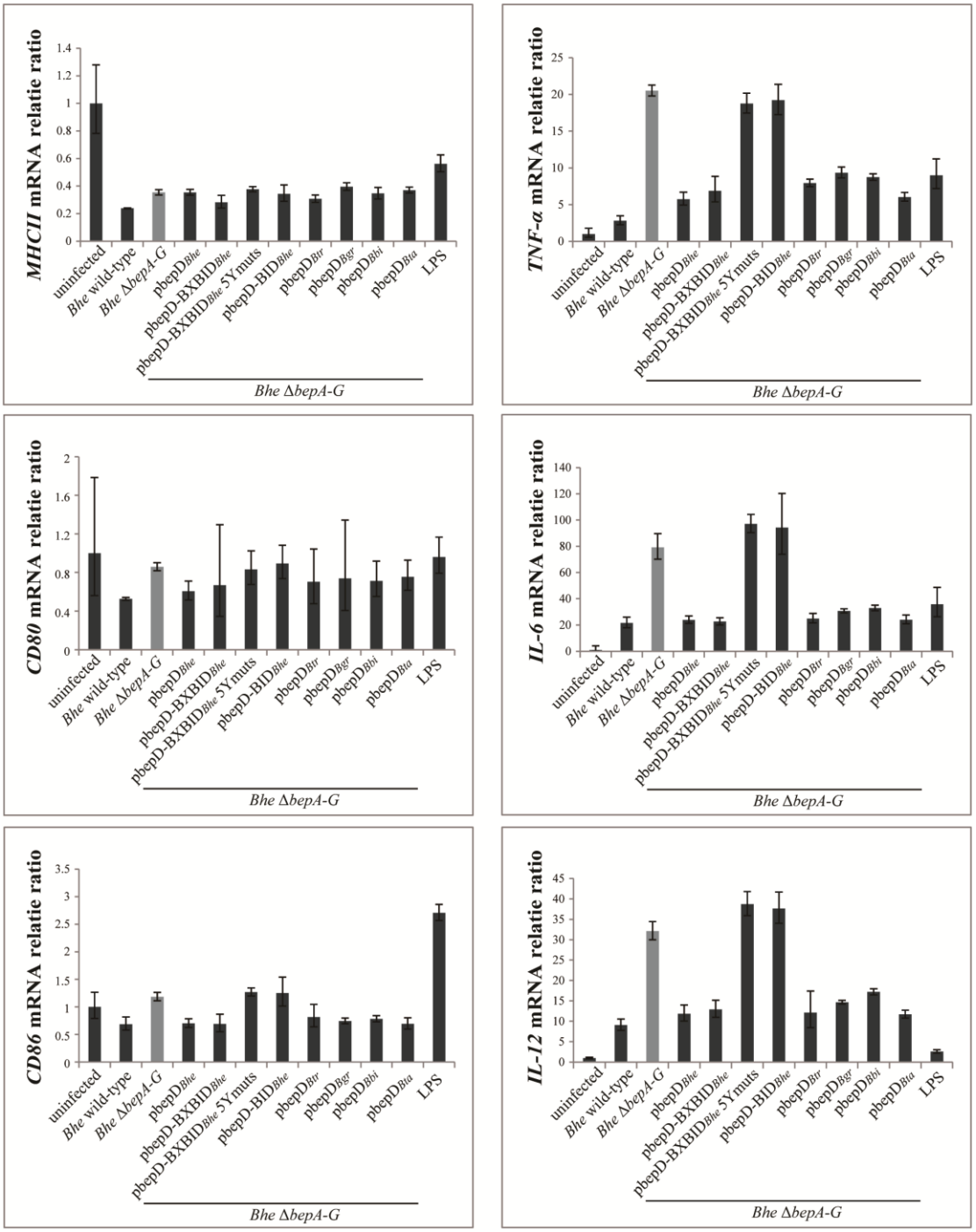
MHCII mRNA relatie ratio
TNF-α mRNA relatie ratio
CD80 mRNA relatie ratio
IL-6 mRNA relatie ratio
CD86 mRNA relatie ratio
IL-12 mRNA relatie ratio
uninfected
Bhe wild-type
Bhe ΔbepA-G
pbepDBhe
pbepD-BXBIDBhe
pbepD-BXBIDBhe 5Ymuts
pbepD-BIDBhe
pbepDBtr
pbepDBgr
pbepDBbi
pbepDBta
LPS
Bhe ΔbepA-G

Figure S6.

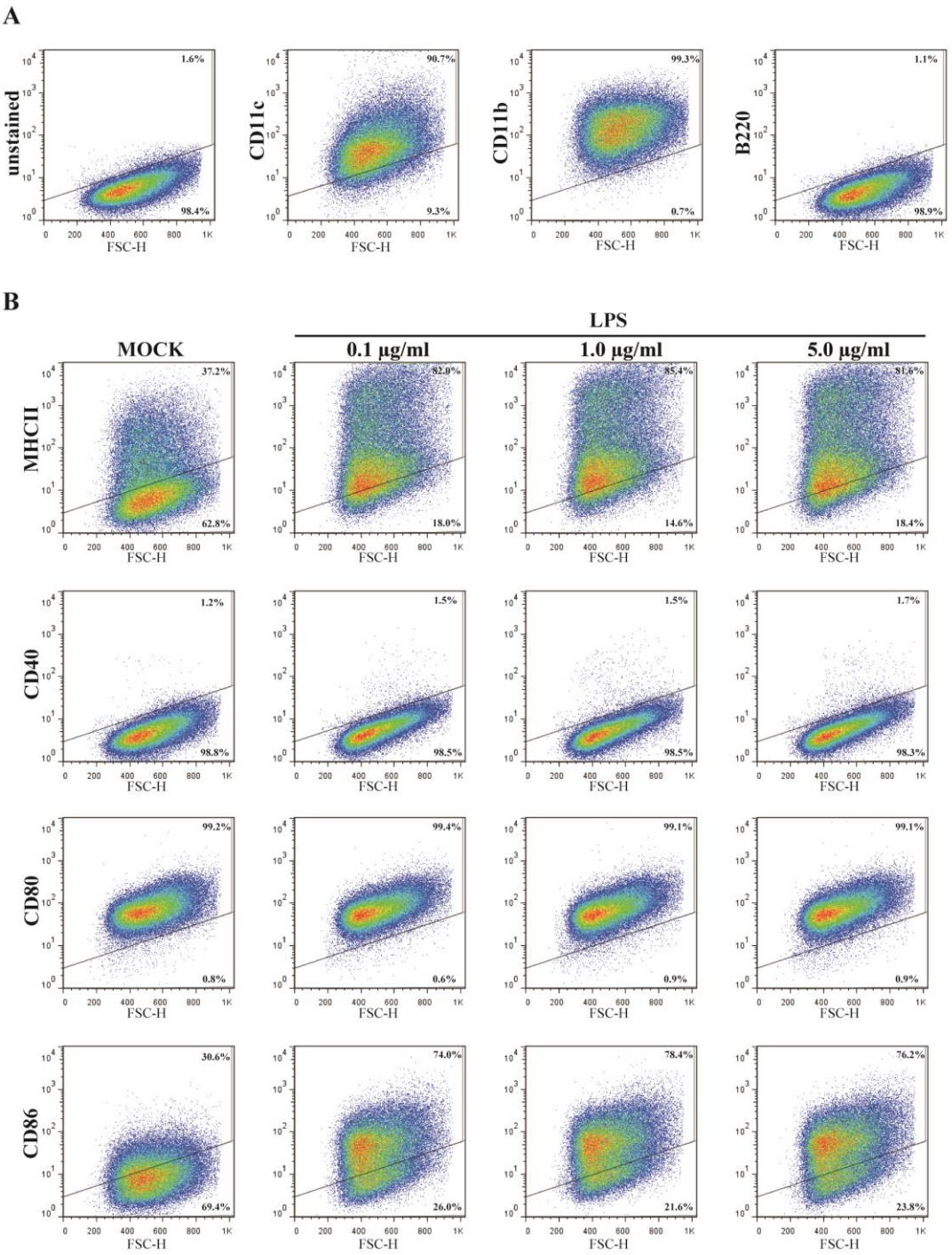
A
unstained
1.6%
98.4%
CD11c
90.7%
9.3%
CD11b
99.3%
0.7%
B220
1.1%
98.9%
FSC-H
B
MOCK
LPS
0.1 µg/ml
1.0 µg/ml
5.0 µg/ml
MHCII
37.2%
62.8%
82.0%
18.0%
85.4%
14.6%
81.6%
18.4%
CD40
1.2%
98.8%
1.5%
98.5%
1.5%
98.5%
1.7%
98.3%
CD80
99.2%
0.8%
99.4%
0.6%
99.1%
0.9%
99.1%
0.9%
CD86
30.6%
69.4%
74.0%
26.0%
78.4%
21.6%
76.2%
23.8%

Figure S7.

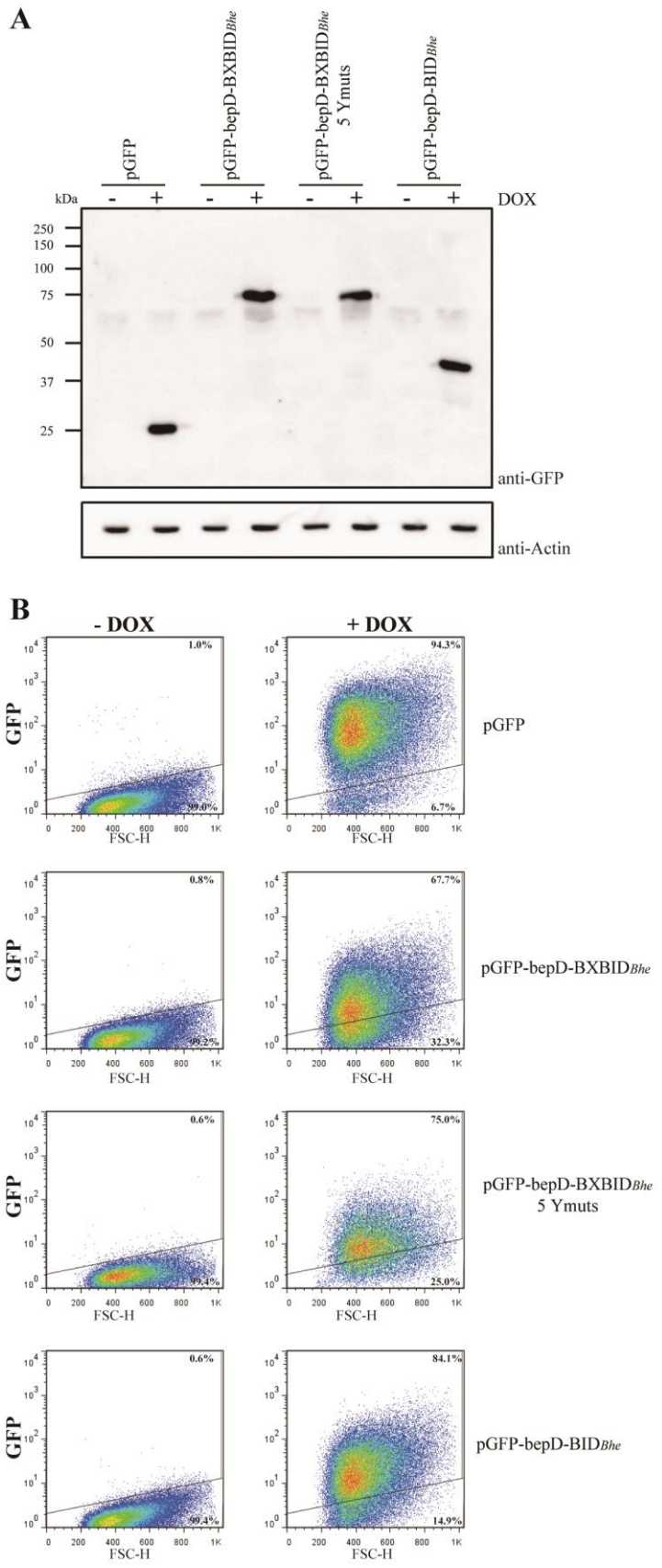
A
pGFP
pGFP-bepD-BXBID*Bhe*
pGFP-bepD-BXBID*Bhe* 5 Ymuts
pGFP-bepD-BID*Bhe*
kDa
- + - + - + - +
DOX
250
150
100
75
50
37
25
anti-GFP
anti-Actin
B
- DOX
+ DOX
GFP
FSC-H
1.0%
99.0%
94.3%
6.7%
pGFP
0.8%
99.2%
67.7%
32.3%
pGFP-bepD-BXBID*Bhe*
0.6%
99.4%
75.0%
25.0%
pGFP-bepD-BXBID*Bhe* 5 Ymuts
0.6%
99.4%
84.1%
14.9%
pGFP-bepD-BID*Bhe*

Figure S8.

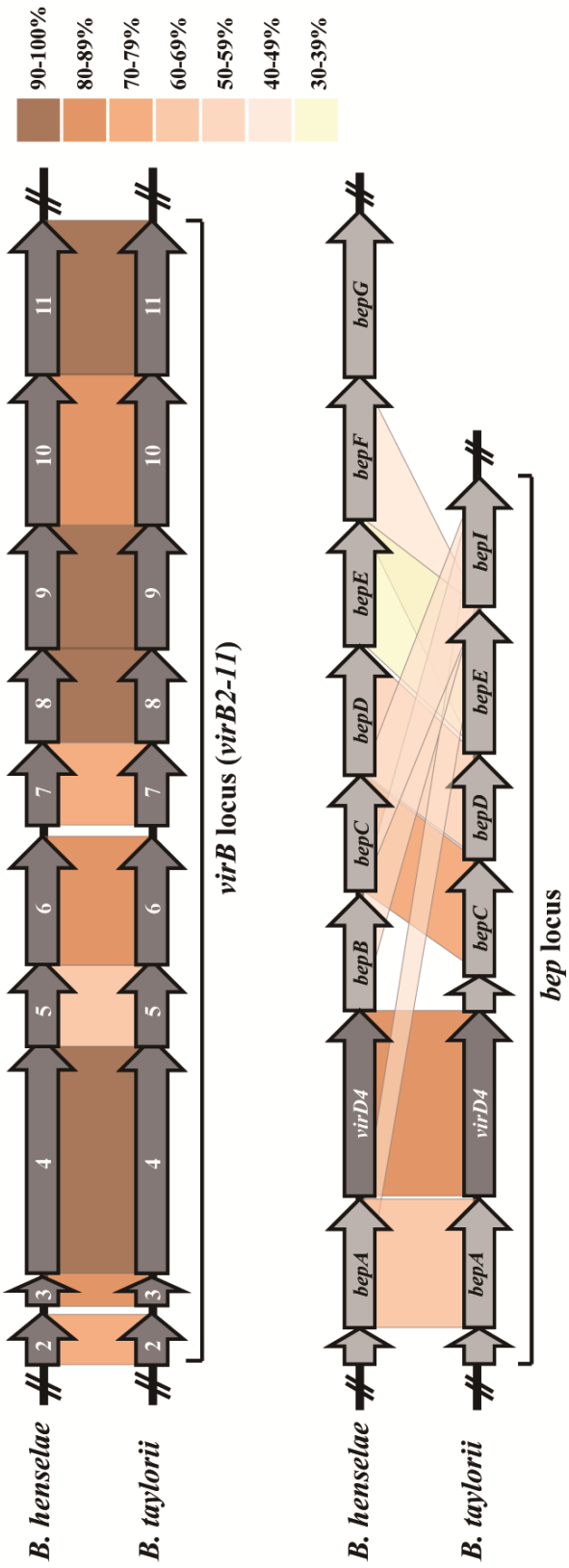
90-100%
80-89%
70-79%
60-69%
50-59%
40-49%
30-39%
virB locus (virB2-11)
2
3
4
5
6
7
8
9
10
11
B. henselae
B. taylorii
bep locus
bepA
virD4
bepB
bepC
bepD
bepE
bepF
bepG
bepI

Figure S9.

3.2.8 Supplementary Tables

Table 1: Bacterial strains and plasmids used in this study

***Bartonella* strains**		
Strain	**Relevant Genotype /Description**	**Reference**
RSE247	Spontaneous Sm^R strain of *B. henselae* ATCC49882^T, serving as wild-type	[70]
MSE150	*bepA-bepG* deletion mutant, derivative of RSE247	[20]
MSE156	MSE150 containing pPG101 (Δ*bepA-G*/p*bepABhe*)	[24]
MSE167	MSE150 containing pMS006 (Δ*bepA-G*/p*bepBBhe*)	[24]
MSE159	MSE150 containing pMS007 (Δ*bepA-G*/p*bepCBhe*)	[24]
PG4D03	MSE150 containing pPG104 (Δ*bepA-G*/p*bepDBhe*)	[20]
PG4D10	MSE150 containing pPG105 (Δ*bepA-G*/p*bepEBhe*)	[71]
TRB171	MSE150 containing pPG106 (Δ*bepA-G*/p*bepFBhe*)	[71]
TRB169	MSE150 containing pPG107 (Δ*bepA-G*/p*bepGBhe*)	[71]
MSE218	MSE150 containing pMS100-A (Δ*bepA-G*/p*bepA-BIDBhe*)	[24]
MSE220	MSE150 containing pMS100-D (Δ*bepA-G*/p*bepD-BIDBhe*)	[24]
LUB169	MSE150 containing pLU030 (Δ*bepA-G*/p*bepD-BXBIDBhe*)	This study
LUB186	MSE150 containing pLU032 (Δ*bepA-G*/p*bepD-BXBIDBhe* Y32F)	This study
LUB220	MSE150 containing pLU033 (Δ*bepA-G*/p*bepD-BXBIDBhe* Y52F)	This study
LUB222	MSE150 containing pLU034 (Δ*bepA-G*/p*bepD-BXBIDBhe* Y62F)	This study
LUB224	MSE150 containing pLU035 (Δ*bepA-G*/p*bepD-BXBIDBhe* Y72F)	This study
LUB226	MSE150 containing pLU036 (Δ*bepA-G*/p*bepD-BXBIDBhe* Y92F)	This study
LUB195	MSE150 containing pLU037 (Δ*bepA-G*/p*bepD-BXBIDBhe* Y114F)	This study
LUB197	MSE150 containing pLU038 (Δ*bepA-G*/p*bepD-BXBIDBhe* Y134F)	This study

Table 1-continued

LUB188	MSE150 containing pLU039 (Δ*bepA-G*/p*bepD-BXBIDBhe* Y155F)	This study
LUB206	MSE150 containing pLU040 (Δ*bepA-G*/p*bepD-BXBIDBhe* Y176F)	This study
LUB268	MSE150 containing pLU044 (Δ*bepA-G*/p*bepD-BXBIDBhe* Y32/72/92/114/134F)	This study
MSE175	MSE150 containing pMS011 (Δ*bepA-G*/p*bepABtr*)	[24]
LUB234	MSE150 containing pLU054 (Δ*bepA-G*/p*bepABgr*)	This study
LUB270	MSE150 containing pLU065 (Δ*bepA-G*/p*bepA-BIDBbi*)	This study
LUB266	MSE150 containing pLU064 (Δ*bepA-G*/p*bepA-BIDBta*)	This study
LUB232	MSE150 containing pLU053 (Δ*bepA-G*/p*bepDBtr*)	This study
LUB258	MSE150 containing pLU061 (Δ*bepA-G*/p*bepDBgr*)	This study
LUB247	MSE150 containing pLU060 (Δ*bepA-G*/p*bepDBbi*)	This study
LUB242	MSE150 containing pLU058 (Δ*bepA-G*/p*bepDBta*)	This study
LUB046	Spontaneous Sm^R strain of *B. taylorii*, serving as wild-type	This study
LUB163	*virD4* deletion mutant, derivative of LUB046	This study
LUB291	*bepA* deletion mutant, derivative of LUB046	This study
LUB293	*bepD* deletion mutant, derivative of LUB046	This study
LUB297	*bepA* and *bepD* deletion mutant, derivative of LUB291	This study
RSE149	Spontaneous Sm^R strain of *B. tribocorum* IBS 506T, serving as wild-type	[19]
CHDE142	*B. grahamii*, No 376, isolated from *Microtus sp.*	[13]
PEE0249	*B. birtlesii* IBS 325T, isolated from *Apodemus spp.*	[72]

***E. Coli* strains**		
Name	**Relevant characteristics**	**Reference**
DH5α	F- (Φ80dlacZDM15) D (lacZY AargF)U169 deoR recA1 endA1hsdR17 (rk-, mK+), sup E44 l -thi-1 gyrA96 relA1 l -CH616	[73]
β2150	F' lacZΔM15 lacIq traD36 proA+B+ thrB1004 pro thi strA hsdS ΔdapA::erm (Ermr) pir	[31]
Helper strain	β2150 containing pRK2013	[31]

Table 1-continued

Plasmids		
Name	**Relevant characteristics**	**Reference**
pPG100	*Bartonella* shuttle vector, encoding a short FLAG epitope	[20]
pPG101	Derivative of pPG100, encoding FLAG::Bhe BepA	[24]
pMS006	Derivative of pPG100, encoding FLAG::Bhe BepB	[24]
pMS007	Derivative of pPG100, encoding FLAG::Bhe BepC	[24]
pPG104	Derivative of pPG100, encoding FLAG::Bhe BepD	[20]
pPG105	Derivative of pPG100, encoding FLAG::Bhe BepE	[71]
pPG106	Derivative of pPG100, encoding FLAG::Bhe BepF	[71]
pPG107	Derivative of pPG100, encoding FLAG::Bhe BepG	[71]
pMS100-A	Derivative of pPG100, encoding FLAG::Bhe BepA-BID	[24]
pMS100-D	Derivative of pPG100, encoding FLAG::Bhe BepD-BID	[24]
pLU030	Derivative of pPG100, encoding FLAG::Bhe BepD-BXBID	This study
pLU032	Derivative of pPG100, encoding FLAG::Bhe BepD-BXBID Y32F	This study
pLU033	Derivative of pPG100, encoding FLAG::Bhe BepD-BXBID Y52F	This study
pLU034	Derivative of pPG100, encoding FLAG::Bhe BepD-BXBID Y62F	This study
pLU035	Derivative of pPG100, encoding FLAG::Bhe BepD-BXBID Y72F	This study
pLU036	Derivative of pPG100, encoding FLAG::Bhe BepD-BXBID Y92F	This study
pLU037	Derivative of pPG100, encoding FLAG::Bhe BepD-BXBID Y114F	This study
pLU038	Derivative of pPG100, encoding FLAG::Bhe BepD-BXBID Y134F	This study
pLU039	Derivative of pPG100, encoding FLAG::Bhe BepD-BXBID Y155F	This study
pLU040	Derivative of pPG100, encoding FLAG::Bhe BepD-BXBID Y176F	This study
pLU044	Derivative of pPG100, encoding FLAG::Bhe BepD-BXBID Y32/72/92/114/134F	This study

Table 1-continued

pMS011	Derivative of pPG100, encoding FLAG::Btr BepA	[24]
pLU054	Derivative of pPG100, encoding FLAG::Bgr BepA	This study
pLU065	Derivative of pPG100, encoding FLAG::Bbi BepA-BID	This study
pLU064	Derivative of pPG100, encoding FLAG::Bta BepA-BID	This study
pLU053	Derivative of pPG100, encoding FLAG::Btr BepD	This study
pLU061	Derivative of pPG100, encoding FLAG::Bgr BepD	This study
pLU060	Derivative of pPG100, encoding FLAG::Bbi BepD	This study
pLU058	Derivative of pPG100, encoding FLAG::Bta BepD	This study
pTR1000	Mutagenesis vector for in-frame deletion in *Bartonella* spp.	[20]
pLU068	Derivative of pTR1000, used for $bepA_{Bta}$ deletion	This study
pLU069	Derivative of pTR1000, used for $bepD_{Bta}$ deletion	This study
pLU072	Derivative of pTR1000, used for $virD4_{Bta}$ deletion	This study
pLU073	pDONR-GFP, for gateway cloning	This study
pLU074	pDONR-*Bhe* BepD-BXBID, for gateway cloning	This study
pLU075	pDONR-*Bhe* BepD-BID, for gateway cloning	This study
pLU076	pDONR-*Bhe* BepD-BXBID 5Ymuts, for gateway cloning	This study
pLU077	pCLX, encoding GFP	This study
pLU078	pCLX, encoding GFP::*Bhe* BepD-BXBID	This study
pLU079	pCLX, encoding GFP::*Bhe* BepD-BID	This study
pLU080	pCLX, encoding GFP::*Bhe* BepD-BXBID 5Ymuts	This study
pMDL	packaging vector for plenty	[18]
pREV	packaging vector for plenty	[18]
pVSVG	packaging vector for plenty	[18]

Table 2: Oligonucleotides used in this study

Cloning primers		
Name	**Sequence (5'-3')** **(restriction endonuclease cleavage sites are underlined)**	**Restriction site**
prLU174	CGGCATATGTCAGGAAAGACAACACCCCCTCCGACA	*NdeI*
prLU175	CGGCATATGTTACATACCAAAGGCCATTCC	*NdeI*
prLU259	GGGAATTCCATATGCCAAAAGCAAAAGAA	*NdeI*
prLU260	GGGAATTCCATATGTTAGCAAGCCATAGCAAA	*NdeI*
prLU283	GGGAATTCCATATGGAGTTAAAAAACACGCTCATTCCA	*NdeI*
prLU284	GGGAATTCCATATGTTAGCTAGCCATAGCAAGCACATT	*NdeI*
prLU285	GGGAATTCCATATGGAACTTGAAAAAGTGCTCATCCC	*NdeI*
prLU286	GGGAATTCCATATGTTAGCTGGCCATAGCGAGCG	*NdeI*
prLU265	GGGAATTCCATATGCCAAAAGCCAAAGAA	*NdeI*
prLU266	GGGAATTCCATATGTTAGCTGGCTATAGCGAG	*NdeI*
prLU281	GGGAATTCCATATGAAAAAAAGTCACCCAACCGCT	*NdeI*
prLU282	GGGAATTCCATATGTTACATGGCAAAAGCCATTCC	*NdeI*
prLU234	GGGCATATGAAAAAACACCAGCCATCCCC	*NdeI*
prLU235	GGGCATATGTTACATCGCAAACGCCATTCC	*NdeI*
prLU74	CTTCATATGAAAAAGAATCATCCATCCCCTTCTC	*NdeI*
prLU75	AATCATATGTTACATCGCAAAAGCCATTCCTTTTCC	*NdeI*
prLU299	GCTCTAGAGCAGAGTTTTTCTCTCGAAGATCTTGC	*XbaI*
prLU318	CTGAAACACCAAGACTTTTCGCAAGTGTTTTGTTACCTCCTTATA ATATAGCGTTGT	
prLU319	AAACACTTGCGAAAAGTCTTGGTGTTTCAG	
prLU302	GCTCTAGACCAGGCGCAAAGGGAATATTGCACACA	*XbaI*
prLU63	GCCTCTAGAGTGCGGAAGAGGCTGTTCCACAGCTAGTTG	*XbaI*
prLU320	GCTTGGGGATTTCACACCAAGTACTTTGTATGTTTCCTTTCAAGA ATTATTTTAGAA	
prLU304	AAAGTACTTGGTGTGAAATCCCCAAGC	
prLU305	GCTCTAGACGGTATAGTCTTTTCTGGGCGTTTTGG	*XbaI*
prLU59	CCGTCTAGATGTTTATGGCAGCTCAAAAACATTAAACGAAC	

Table 2-continued

prLU60	CAGCAGCCGCTAACATTTCTTTTCTTCTCATTGTCTCTTACTTTC GATTTTTTCTGACTATGCCAC	
prLU61	AGAAGAAAAGAAATGTTAGCGGCTGCTG	
prLU62	GGCTCTAGAAGCACAACGTTCATACAGTTTGTGTGGG	*XbaI*
prLU197	GGTGGCGGGCCCGGGATGCCAGGAAGGGCA	
prLU199	GGTGGCGGGCCCGGGATGTCAGGAAAGACA	
prLU276	GGGGACAAGTTTGTACAAAAAAGCAGGCTTCGAAGGAGATAGA ACCATGGTGAGCAAGGGCGAGGAGCTG	
prLU277	GGGGACCACTTTGTACAAGAAAGCTGGGTCCTACTTGTACAGCT CGTCCATGC	
prLU278	GGGGACCACTTTGTACAAGAAAGCTGGGTCCTACATACCAAAG GCCATTCCTT	

Primers for tyrosine to phenylalanine exchange mutant		
Name	**Sequence (5'-3')**	**Y→F**
prLU172	GCAGAACCCCTCTTTGCACAGGTAAAT	Y32F
prLU173	ATTTACCTGTGCAAAGAGGGGTTCTGC	Y32F
prLU183	AGAAGAAACTATCTTTGCACCTCAAAACC	Y52F
prLU184	GGTTTTGAGGTGCAAAGATAGTTTCTTCT	Y52F
prLU185	ACCAGAAACTATCTTTGCACCCCAAAAAC	Y62F
prLU186	GTTTTTGGGGTGCAAAGATAGTTTCTGGT	Y62F
prLU252	CCTCTAGGAAATCCCTTTGACAGACTTGGTGGG	Y72F
prLU253	CCCACCAAGTCTGTCAAAGGGATTTCCTAGAGG	Y72F
prLU187	ACTAGTAGACCCCTTTGCAGTAACTGATG	Y92F
prLU188	CATCAGTTACTGCAAAGGGGTCTACTAGT	Y92F
prLU189	AGAAAATCCCCTCTTTGAGGGAGTTGGCG	Y114F
prLU190	CGCCAACTCCCTCAAAGAGGGGATTTTCT	Y114F
prLU191	ACCAGAACATCTCTTTGCAGAGCTTGAAT	Y134F
prLU192	ATTCAAGCTCTGCAAAGAGATGTTCTGGT	Y134F
prLU160	TAGAATCTGTCTTTGCAACAGTTGGCA	Y155F
prLU161	TGCCAACTGTTGCAAAGACAGATTCTA	Y155F

Table 2-continued

prLU193	TAAAAAATCCCCTCTTCGAAGGAGTTGGCC	Y176F
prLU194	GGCCAACTCCTTCGAAGAGGGGATTTTTTA	Y176F

qPCR Primers		
Name	**Sequence (5'-3')**	**Gene**
prLU214	AACGACCCCTTCATTGAC	*GAPDH*
prLU215	TCCACGACATACTCAGCAC	*GAPDH*
prLU236	TTGTTGACAGCGGTCCATCTA	*CD40*
prLU237	GCCATCGTGGAGGTACTGTTT	*CD40*
prLU290	CTCACCAGGAAGCCTGC	*crem*
prLU291	CAGCTCCCGCTTGCGAGTTG	*crem*
prLU238	TGCTGCTGATTCGTCTTTCAC	*CD80*
prLU239	GAGGAGAGTTGTAACGGCAAG	*CD80*
prLU240	CTGGACTCTACGACTTCACAATG	*CD86*
prLU241	AGTTGGCGATCACTGACAGTT	*CD86*
prLU330	GAGGATACCACTCCCAACAGACC	*IL-6*
prLU331	AAGTGCATCATCGTTGTTCATACA	*IL-6*
prLU334	CATCTTCTCAAAATTCGAGTGACAA	*TNF-α*
prLU335	TGGGAGTAGACAAGGTACAACCC	*TNF-α*
prLU336	GGAAGCACGGCAGCAGAATA	*IL-12*
prLU337	AACTTGAGGGAGAAGTAGGAATGG	*IL-12*

Sequencing primers for *B. taylorii*	
Name	**Sequence (5'-3')**
prLU006	GTTTAAGGTCACAGAAATTTATTATGATCCCTTC
prLU007	GAATATCGTTAAAGCACCTAAAGCGATTGG
prLU008	CCTTGCATAAGAATAATTTGTTCATCTTGACGCAT
prLU009	CATCATCGTCGTCATCACGCA
prLU010	GGAACCCTCATGAGCCGTATTTTTGGCTTCGT

Table 2-continued

prLU011	TGCAAAACAGAGTCAATATAACCACTTTCTTGAT
prLU012	TCTTGCCAAAGCAGCAGGCCATCAGCTT
prLU013	CTTCACGTTGTGTACGTGGTACACTATCAT
prLU014	GCTATATGAACATTCTAGAAGAAGCGCGTG
prLU015	CAAATTCAAGCTCTGCATAGAGATGTTCTGG
prLU016	ATAAGATGTTTGCAGTTCAACCCAATGCTT
prLU017	CCTCTCTCAAATCAGGAAATTGCCCGCAGAGTTC
prLU018	ATGCCAAGGATTTGCTTACCAGCAAGCGGAGCAAA
prLU021	ATCCCTTCAAGTGCATGGCTGCTGATGG
prLU022	GCTTGTTTAATGCAAGTGTTGAAACGTT
prLU023	CATGAACTTGAGAGCATAGTTCCAAGTTAT
prLU024	GTGCATGACCATAATCCCAAAGGAACATTC
prLU025	CGGTAAGAGCTAGCGATGAAGAGCGACT
prLU026	TAACAACAGAGTTAATTCAATAGAGCGA
prLU027	CACAATCAGAAGAAACTATCTATGCACC
prLU028	AAACCACCACGCTGTAATGGCAAA
prLU029	AGGGAGTTTAACGATATTCCTTGTTCC
prLU030	GAACGCCTGACACAGGCTAGTATTGAAGCA
prLU031	CATTAAGTCCAGCACGTCTCATTTGAGA
prLU032	TGCGCTATTCGTAGCTCTCATAATCGACAT
prLU033	TAGAAGAGCCCCTCTATGCGACGCCT
prLU034	CTGCGTGACAATATTGGACCACCGTATTAC
prLU035	ACCGGCTTGGTGCTCGACCACGCACAGT
prLU036	GCATGCGGTTTCTTGACCATCTTCGGTA
prLU037	TGCGTGCCAGCACCTTGGCAGGGATAAT
prLU038	ATCGTCACGCAAGAGAAGAACGCCAGACTT
prLU039	CAGCACATAGGGAAGGAACAGCGCCTTC
prLU040	CTATGAAGTAAAGGAGAGAAGCATCGC
prLU041	CAAACCATGAGCGCGCTCCCGCTTCTCC

Table 2-continued

prLU042	GGTATTGGCTGGATGTACGGCTTTATTGAT
prLU043	TATCACCTCTGGATCAGATCTATATTCCGA
prLU044	TCGGAATATAGATCTGATCCAGAGGTGATA
prLU045	CCTTGAACAAAACATTGCGCATAATAAA
prLU046	ACCACCAGAACAACAAAGAGAAGCTTTG
prLU047	TGCTTCATGAGCACAACGTTCATACAGT
prLU048	CACAGTGTGCTCACGATTCAGCAAGAGCAA
prLU049	GCGCCGCAACAAAGTATTCAACGGCATA
prLU050	TATGCCGTTGAATACTTTGTTGCGGCGC
prLU051	TTGCTCTTGCTGAATCGTGAGCACACTGTG
prLU052	GAACGCATGAATCTTGCTAGCATTGCGTCA
prLU053	CCACTGCCGGAGGAATGACAATTTGAATAC
prLU054	GGCAACTTGCCAAGCAACGGAATTGCCA
prLU055	GGCAACAAGGTCATTGTACATGCTACAG
prLU056	AGGTGGATCTACATCTCCATTATGCCTT
prLU057	TCGCATGCATGGCATGCGCGTGCGGATG
prLU058	GTTATCGCTTCATCATAGTTGTTGGGAG
prLU071	CACGCCCAGGTATGACCGATGGTTTA
prLU072	CAGCACCAGAGAGTTTTGAAGCTGCAC
prLU073	GCACCAGTTGAACGACGAAACCGTCGC
prLU080	CATTATGGTGACCTTGGAAACACC
prLU081	ATTCGTTGCCATTGTCGTTACAAC
prLU082	GTCATTCTCTTCCGTGCGCTTCCTG
prLU083	AATTCAGGCCATCCAGGTTCGA
prLU084	TCTGAAGCCGGATTCCAGAGCAGTG
prLU087	CTCAACAATTGCACACACGATTATTGAG
prLU088	TGGTTAGGGTTTGTCCCATATTCG
prLU095	ATAACATAGAACCCACAATGTAGAGAATAACAAT
prLU098	CCTTGAACAAAACATTGCGCATAATAAA

Table 2-continued

prLU106	CATCCCTATGTTTTGCCATTGAAAATTATGCCG
prLU109	GCGATAAAGGCTGTAAGCTGTAAAGCAA
prLU110	AATAAAGCCGTACATCCAGCCAATGCCCAC

Table 3: Primary antibodies used in this study

Primary antibodies	
Specificity	**Source / Reference**
Flag	Sigma
GFP	Molecular Probes
Actin	Millipore
STAT3	Cell Signaling
SHP-2	BD Transduction Laboratories
phospho-STAT3	Cell Signaling
phospho-tyrosine	Millipore
Secondary anti-mouse IgG-HRP antibodies	GE healthcare
Secondary anti-rabbit IgG-HRP antibodies	GE healthcare

3.2.9 References

1. Banchereau, J., et al., Immunobiology of dendritic cells. Annu Rev Immunol, 2000. 18: p. 767-811.
2. Guermonprez, P., et al., Antigen presentation and T cell stimulation by dendritic cells. Annu Rev Immunol, 2002. 20: p. 621-67.
3. Lu, Y.C., W.C. Yeh, and P.S. Ohashi, LPS/TLR4 signal transduction pathway. Cytokine, 2008. 42(2): p. 145-51.
4. Dalod, M., et al., Dendritic cell maturation: functional specialization through signaling specificity and transcriptional programming. EMBO J, 2014. 33(10): p. 1104-16.
5. Lutz, M.B. and G. Schuler, Immature, semi-mature and fully mature dendritic cells: which signals induce tolerance or immunity? Trends Immunol, 2002. 23(9): p. 445-9.
6. Tan, J.K. and H.C. O'Neill, Maturation requirements for dendritic cells in T cell stimulation leading to tolerance versus immunity. J Leukoc Biol, 2005. 78(2): p. 319-24.
7. Bosio, C.M. and S.W. Dow, Francisella tularensis induces aberrant activation of pulmonary dendritic cells. J Immunol, 2005. 175(10): p. 6792-801.
8. Bosio, C.M., H. Bielefeldt-Ohmann, and J.T. Belisle, Active suppression of the pulmonary immune response by Francisella tularensis Schu4. J Immunol, 2007. 178(7): p. 4538-47.
9. Chase, J.C., J. Celli, and C.M. Bosio, Direct and indirect impairment of human dendritic cell function by virulent Francisella tularensis Schu S4. Infect Immun, 2009. 77(1): p. 180-95.
10. Skinner, J.A., et al., Bordetella type III secretion and adenylate cyclase toxin synergize to drive dendritic cells into a semimature state. J Immunol, 2004. 173(3): p. 1934-40.
11. Skinner, J.A., et al., Bordetella type III secretion modulates dendritic cell migration resulting in immunosuppression and bacterial persistence. J Immunol, 2005. 175(7): p. 4647-52.
12. Mihret, A., The role of dendritic cells in Mycobacterium tuberculosis infection. Virulence, 2012. 3(7): p. 654-9.
13. Geijtenbeek, T.B., et al., Mycobacteria target DC-SIGN to suppress dendritic cell function. J Exp Med, 2003. 197(1): p. 7-17.
14. Hanekom, W.A., et al., Mycobacterium tuberculosis inhibits maturation of human monocyte-derived dendritic cells in vitro. J Infect Dis, 2003. 188(2): p. 257-66.
15. Dulphy, N., et al., Intermediate maturation of Mycobacterium tuberculosis

LAM-activated human dendritic cells. Cell Microbiol, 2007. 9(6): p. 1412-25.
16. Salcedo, S.P., et al., Brucella control of dendritic cell maturation is dependent on the TIR-containing protein Btp1. PLoS pathogens, 2008. 4(2): p. e21.
17. Karem, K.L., et al., Characterization of Bartonella henselae-specific immunity in BALB/c mice. Immunology, 1999. 97(2): p. 352-8.
18. Okujava, R., et al., A translocated effector required for bartonella dissemination from derma to blood safeguards migratory host cells from damage by co-translocated effectors. PLoS pathogens, 2014. 10(6): p. e1004187.
19. Schulein, R. and C. Dehio, The VirB/VirD4 type IV secretion system of Bartonella is essential for establishing intraerythrocytic infection. Molecular microbiology, 2002. 46(4): p. 1053-67.
20. Schulein, R., et al., A bipartite signal mediates the transfer of type IV secretion substrates of Bartonella henselae into human cells. Proceedings of the National Academy of Sciences of the United States of America, 2005. 102(3): p. 856-61.
21. Dehio, C., et al., Interaction of Bartonella henselae with endothelial cells results in bacterial aggregation on the cell surface and the subsequent engulfment and internalisation of the bacterial aggregate by a unique structure, the invasome. J Cell Sci, 1997. 110 (Pt 18): p. 2141-54.
22. Truttmann, M.C., T.A. Rhomberg, and C. Dehio, Combined action of the type IV secretion effector proteins BepC and BepF promotes invasome formation of Bartonella henselae on endothelial and epithelial cells. Cell Microbiol, 2011. 13(2): p. 284-99.
23. Schmid, M.C., et al., The VirB type IV secretion system of Bartonella henselae mediates invasion, proinflammatory activation and antiapoptotic protection of endothelial cells. Mol Microbiol, 2004. 52(1): p. 81-92.
24. Schmid, M.C., et al., A translocated bacterial protein protects vascular endothelial cells from apoptosis. PLoS Pathog, 2006. 2(11): p. e115.
25. Scheidegger, F., et al., Distinct activities of Bartonella henselae type IV secretion effector proteins modulate capillary-like sprout formation. Cell Microbiol, 2009. 11(7): p. 1088-101.
26. Okujava, R., et al., A translocated effector required for bartonella dissemination from derma to blood safeguards migratory host cells from damage by co-translocated effectors. PLoS Pathog, 2014. 10(6): p. e1004187.
27. Capo, C., et al., Bartonella quintana bacteremia and overproduction of interleukin-10: model of bacterial persistence in homeless people. J Infect Dis, 2003. 187(5): p. 837-44.
28. Kabeya, H., et al., Characterization of Th1 activation by Bartonella henselae stimulation in BALB/c mice: Inhibitory activities of interleukin-10 for the

production of interferon-gamma in spleen cells. Vet Microbiol, 2007. 119(2-4): p. 290-6.
29. Papadopoulos, N.G., et al., Circulating cytokines in patients with cat scratch disease. Clin Infect Dis, 2001. 33(6): p. e54-6.
30. Vermi, W., et al., Role of dendritic cell-derived CXCL13 in the pathogenesis of Bartonella henselae B-rich granuloma. Blood, 2006. 107(2): p. 454-62.
31. Dehio, C. and M. Meyer, Maintenance of broad-host-range incompatibility group P and group Q plasmids and transposition of Tn5 in Bartonella henselae following conjugal plasmid transfer from Escherichia coli. Journal of bacteriology, 1997. 179(2): p. 538-40.
32. Brasel, K., et al., Generation of murine dendritic cells from flt3-ligand-supplemented bone marrow cultures. Blood, 2000. 96(9): p. 3029-39.
33. Nunez, R., M. Ackermann, and M. Suter, Immortalized cell lines with dendritic morphology derived from mice lacking both type I and type II interferon receptors present MHC II restricted antigen to T cells and induce mixed leukocyte reactions. Advances in experimental medicine and biology, 1997. 417: p. 425-32.
34. Giry-Laterriere, M., et al., Polyswitch lentivectors: "all-in-one" lentiviral vectors for drug-inducible gene expression, live selection, and recombination cloning. Human gene therapy, 2011. 22(10): p. 1255-67.
35. Dehio, M., et al., The transcriptional response of human endothelial cells to infection with Bartonella henselae is dominated by genes controlling innate immune responses, cell cycle, and vascular remodelling. Thrombosis and haemostasis, 2005. 94(2): p. 347-61.
36. Eisen, M.B., et al., Cluster analysis and display of genome-wide expression patterns. Proceedings of the National Academy of Sciences of the United States of America, 1998. 95(25): p. 14863-8.
37. Schmid, M.C., et al., The VirB type IV secretion system of Bartonella henselae mediates invasion, proinflammatory activation and antiapoptotic protection of endothelial cells. Molecular microbiology, 2004. 52(1): p. 81-92.
38. Engel, P., et al., Parallel evolution of a type IV secretion system in radiating lineages of the host-restricted bacterial pathogen Bartonella. PLoS Genet, 2011. 7(2): p. e1001296.
39. Schroder, G. and C. Dehio, Virulence-associated type IV secretion systems of Bartonella. Trends Microbiol, 2005. 13(7): p. 336-42.
40. Selbach, M., et al., Host cell interactome of tyrosine-phosphorylated bacterial proteins. Cell Host Microbe, 2009. 5(4): p. 397-403.
41. Palanivelu, D.V., et al., Fic domain-catalyzed adenylylation: insight provided by the structural analysis of the type IV secretion system effector BepA. Protein Sci,

2011. 20(3): p. 492-9.
42. Backert, S. and M. Selbach, Tyrosine-phosphorylated bacterial effector proteins: the enemies within. Trends Microbiol, 2005. 13(10): p. 476-84.
43. Schmid, M.C., et al., A translocated bacterial protein protects vascular endothelial cells from apoptosis. PLoS pathogens, 2006. 2(11): p. e115.
44. Pulliainen, A.T., et al., Bacterial effector binds host cell adenylyl cyclase to potentiate Galphas-dependent cAMP production. Proceedings of the National Academy of Sciences of the United States of America, 2012. 109(24): p. 9581-6.
45. Li, K., et al., Cyclic AMP plays a critical role in C3a-receptor-mediated regulation of dendritic cells in antigen uptake and T-cell stimulation. Blood, 2008. 112(13): p. 5084-94.
46. Schmutz, C., et al., Systems-level overview of host protein phosphorylation during Shigella flexneri infection revealed by phosphoproteomics. Mol Cell Proteomics, 2013. 12(10): p. 2952-68.
47. Yasukawa, H., et al., IL-6 induces an anti-inflammatory response in the absence of SOCS3 in macrophages. Nat Immunol, 2003. 4(6): p. 551-6.
48. Regnery, R.L., et al., Characterization of a novel Rochalimaea species, R. henselae sp. nov., isolated from blood of a febrile, human immunodeficiency virus-positive patient. J Clin Microbiol, 1992. 30(2): p. 265-74.
49. Sreevatsan, S., et al., Characterization of rpsL and rrs mutations in streptomycin-resistant Mycobacterium tuberculosis isolates from diverse geographic localities. Antimicrob Agents Chemother, 1996. 40(4): p. 1024-6.
50. Marignac, G., et al., Murine model for Bartonella birtlesii infection: New aspects. Comp Immunol Microbiol Infect Dis, 2010. 33(2): p. 95-107.
51. Oertli, M. and A. Muller, Helicobacter pylori targets dendritic cells to induce immune tolerance, promote persistence and confer protection against allergic asthma. Gut Microbes, 2012. 3(6): p. 566-71.
52. Quebatte, M., et al., The BatR/BatS two-component regulatory system controls the adaptive response of Bartonella henselae during human endothelial cell infection. J Bacteriol, 2010. 192(13): p. 3352-67.
53. Pulliainen, A.T., et al., Bacterial effector binds host cell adenylyl cyclase to potentiate Galphas-dependent cAMP production. Proc Natl Acad Sci U S A, 2012. 109(24): p. 9581-6.
54. Insel, P.A., et al., Cyclic AMP is both a pro-apoptotic and anti-apoptotic second messenger. Acta Physiol (Oxf), 2012. 204(2): p. 277-87.
55. Zhang, L., et al., Gene expression signatures of cAMP/protein kinase A (PKA)-promoted, mitochondrial-dependent apoptosis. Comparative analysis of wild-type and cAMP-deathless S49 lymphoma cells. J Biol Chem, 2008. 283(7):

p. 4304-13.
56. Gloerich, M. and J.L. Bos, Epac: defining a new mechanism for cAMP action. Annu Rev Pharmacol Toxicol, 2010. 50: p. 355-75.
57. Serezani, C.H., et al., Cyclic AMP: master regulator of innate immune cell function. Am J Respir Cell Mol Biol, 2008. 39(2): p. 127-32.
58. Hayashi, T., H. Morohashi, and M. Hatakeyama, Bacterial EPIYA effectors--where do they come from? What are they? Where are they going? Cell Microbiol, 2013. 15(3): p. 377-85.
59. Backert, S., N. Tegtmeyer, and M. Selbach, The versatility of Helicobacter pylori CagA effector protein functions: The master key hypothesis. Helicobacter, 2010. 15(3): p. 163-76.
60. Gruenheid, S., et al., Enteropathogenic E. coli Tir binds Nck to initiate actin pedestal formation in host cells. Nat Cell Biol, 2001. 3(9): p. 856-9.
61. Yan, D., et al., Inhibition of TLR signaling by a bacterial protein containing immunoreceptor tyrosine-based inhibitory motifs. Nat Immunol, 2012. 13(11): p. 1063-71.
62. Yan, D., et al., Enteropathogenic Escherichia coli Tir recruits cellular SHP-2 through ITIM motifs to suppress host immune response. Cell Signal, 2013. 25(9): p. 1887-94.
63. Yu, H., et al., Revisiting STAT3 signalling in cancer: new and unexpected biological functions. Nat Rev Cancer, 2014. 14(11): p. 736-46.
64. Yoshimura, A., et al., Negative regulation of cytokine signaling and immune responses by SOCS proteins. Arthritis Res Ther, 2005. 7(3): p. 100-10.
65. Braun, D.A., M. Fribourg, and S.C. Sealfon, Cytokine response is determined by duration of receptor and signal transducers and activators of transcription 3 (STAT3) activation. J Biol Chem, 2013. 288(5): p. 2986-93.
66. Bronte-Tinkew, D.M., et al., Helicobacter pylori cytotoxin-associated gene A activates the signal transducer and activator of transcription 3 pathway in vitro and in vivo. Cancer Res, 2009. 69(2): p. 632-9.
67. Kaebisch, R., et al., Helicobacter pylori cytotoxin-associated gene A impairs human dendritic cell maturation and function through IL-10-mediated activation of STAT3. J Immunol, 2014. 192(1): p. 316-23.
68. Nagamatsu, K., et al., Bordetella evades the host immune system by inducing IL-10 through a type III effector, BopN. J Exp Med, 2009. 206(13): p. 3073-88.
69. Motta, A., et al., Mycobacterium tuberculosis heat-shock protein 70 impairs maturation of dendritic cells from bone marrow precursors, induces interleukin-10 production and inhibits T-cell proliferation in vitro. Immunology, 2007. 121(4): p. 462-72.

70. Regnery, R., et al., Characterization of a novel Rochalimaea species, R. henselae sp. nov., isolated from blood of a febrile, human immunodeficiency virus-positive patient. Microbiol, 1992. 30: 265–274.
71. Rhomberg, T., et al., A translocated protein of Bartonella henselae interferes with endocytic uptake of individual bacteria and triggers uptake of large bacterial aggregates via the invasome. Cellular Microbiol, 2009. 11(6), 927-945.
72. Bermond, D., et al., Bartonella birtlesii sp. nov., isolated from small mammals (Apodemus spp.). Int J Syst Evol Microbiol, 2000. 50 (6): 1973–9.
73. Odenbreit, S., et al., Translocation of Helicobacter pylori CagA into gastric epithelial cells by type IV secretion. Science, 2000. 287(5457):1497-500.
74. Glatter, T., et al., Large-Scale Quantitative Assessment of Different In-Solution Protein Digestion Protocols Reveals Superior Cleavage Efficiency of Tandem Lys-C/Trypsin Proteolysis over Trypsin Digestion. J. Proteome Res. 2012, 11 (11):5145–5156

3.3 Additional data (preliminary)

This chapter mainly describes *in vivo* preliminary data. To study the relevance of Beps in the modulation of host immune response, we aimed to establish various *in vivo* assays. All of work has been done in mice with two murine-specific strains: *B. birtlesii* (*Bbi*) and *B. taylorii* (*Bta*). Unless indicated, Balb/c mice (6 to 8 weeks old) were used. Although both strains are considered to lead to homogenous infections in mice, *Bta* developed more reliable and higher bacteremia than *Bbi*. *Bbi* wild-type (IBS 325^{T}) was used in the chapter 3.3.2. In addition, spontaneous streptomycin-resistant (Sm^{R}) variants of *Bta* (LUB046) and *Bbi* (JKB016) were selected and used as "wild-type" in the following experiments. However, we realized later that Sm^{R} *Bbi* (JKB016) was attenuated and failed to develop the bacteremia. Thus, the studies of *Bbi* infection in mice (chapter 3.3.3 and 3.3.4) need to be carefully interpreted and re-performed.

In vivo work has been done with the great support from Dr. R. Okujava and C. Mistl. Particulartly, the adoptive transfer of BMDCs was set up together with Rusudan. Furthermore, Claudia assisted me to establish the neonatal mice model.

3.3.1 Upregulation of co-stimulatory molecules by *Bhe* Δ *bepA-G* infection is MyD88-independent

Introduction

DCs with highly professional antigen presenting function as critical sentinels in antimicrobial immune responses. Exposure to microbial components (PAMPs) such as LPS can provoke DC maturation characterized by upregulation of co-stimulatory molecules expression and of pro-inflammatory cytokine secretion. The DC maturation plays a central role in initiating and modulating the immune adaptive response [1]. TLR4, one of the pattern recognition receptors presented on DCs, is a potent receptor and signal transducer in response to bacterial LPS. Upon engagement with ligands, TLR4 recruits the adaptor proteins via the cytoplasmic TIR domain, such as MyD88, and subsequently triggers the activation of NF-κB pathway and MAKP signaling cascades. MyD88-depedent pathway is commonly shared within all the TLR signaling, with the exception of TLR3 [2]. The LPS of enteric bacteria, such as *E. coli*, is recognized by TLR4 with regard to their highly endotoxic activities. Unlike to other bacterial pathogens, LPS of *Bartonella* was shown to be modified with significantly lower endotoxic effect [3, 4]. However, previous work done in this thesis showed that infection by *Bartonella* effector-free strain (*Bhe* Δ*bepA-G*) triggered BMDC full maturation with enhanced expression of MHCII, CD40, and CD86, as well as increased production of pro-inflammatory cytokines (e.g., TNF-α and IL-6) (chapter 3.2, Fig. 1 and 2). We became interested in understanding which TLR signaling of DCs is activated by *Bartonella* infection. To address this question, we investigated the maturation patterns of wild-type, MyD88/Ripk2-, and TLR4-deficient BMDCs in response to *Bhe* infection. These knock-out strains (MyD88$^{-/-}$/Ripk2$^{-/-}$ and TLR4$^{-/-}$) of C57BL6 mice were kindly provided from Prof. W. Hardt. MyD88 is a potent adaptor protein in most TLR singling pathways. Ripk2 plays a central role in NOD-like receptor (NLR) activation.

Results

To assess the effects of *Bartonella* infection on DCs, BMDCs were generated by culturing bone marrow cells with Flt3 ligand (the experimental procedure is described

in chapter 3.2). BMDCs derived from C57BL6 wild-type, MyD88$^{-/-}$/Ripk2$^{-/-}$, and TLR4$^{-/-}$ mice were infected with *Bhe* wild-type or *Bhe* Δ*bepA-G*. *E. coli* LPS, a TLR4 ligand, served as the positive control to monitor the state of DC maturation. After 24 hpi, we measured the surface expression of co-stimulatory (CD40, CD80, and CD86) and MHCII molecules using flow cytometry analysis (Fig. 1). As expected, *E. coli* LPS enhanced the expression of MHCII, CD40, CD80, and CD86 on wild-type BMDCs. These phenotypic changes of DC maturation patterns caused by *E. coli* LPS were diminished in TLR4- but not MyD88/Ripk2-deficient BMDCs. Consistent with pervious results (chapter 3.2), infection with *Bhe* Δ*bepA-G* compared to *Bhe* wild-type led to significantly higher expression of MHCII and CD86 on wild-type BMDCs. Similar to *E. coli* LPS stimulation, this enhanced expression of MHCII and CD86 in response to *Bartonella* infection seemed to be reduced in TLR4- but not MyD88/Ripk2-deficient BMDCs. However, since this was one experiment and results were quite variable, more replicates are needed before we draw a strong conclusion.

Furthermore, the secretion of pro-inflammatory cytokines was measured (Fig. 2). Upon stimulation of *E. coli* LPS, wild-type BMDCs produced TNF-α and dramatically high IL-6. This cytokine induction by *E. coli* LPS was abolished in both TLR4- and MyD88/Ripk2-deficient BMDCs. Confirming with previous results (chapter 3.2), infection with *Bhe* Δ*bepA-G* compared to *Bhe* wild-type resulted in high levels of cytokine secretion (TNF-α and IL-6) in wild-type BMDCs. This induction of cytokines by *Bartonella* infection was abolished in MyD88/Ripk2-deficient BMDCs. However, in response to *Bartonella* infection, only TNF-α but not IL-6 production was reduced in TLR4-deficient BMDCs.

Discussion

LPS, a major component of the cell wall of gram-negative bacteria, is recognized by TLR4 and induces a variety of biological responses (e.g., cytokine secretion from macrophages and B cell proliferative response). MyD88-deficient mice show complete resistance to LPS responses, indicating that MyD88 is an essential component in LPS signaling [5]. However, it is known that while TLR4 moves from cytoplasm membrane to the endosomes, its downstream signaling is switched from MyD88-dependent to MyD88-independent pathway with another required adaptor TRIF [6]. Kaisho et al published that upon *E. coli* LPS stimulation, BMDCs and

splenic DCs from both wild-type and MyD88-deficient, but not TLR4-deficient mice are able to enhance the expression of co-stimulatory molecules. Furthermore, they demonstrated that both NF-κB and JNK are still activated with delayed kinetics in MyD88-deficient BMDCs, although IRAK activation is abolished [7]. Another study emphasizes that various bacterial endotoxins selectively induce MyD88-dependent and -independent signaling pathways of TLR4 [8]. Moreover, the MyD88-independent (TRIF/TICAM-1) pathway of TLR4 signaling activated by endotoxins was proved to be critical for DC maturation, in particular the upregulation of co-stimulatory molecules [9]. Consistent with these findings, our preliminary results showed that *E. coli* LPS-induced co-stimulatory molecules of BMDCs were dependent on TLR4 but can proceed in the absence of MyD88/Ripk2. The cytokine production triggered by *E. coli* LPS through TLR4 relied on a MyD88/Ripk2-dependent manner. Similarly, in response to *Bartonella* infection, MyD88 and Ripk2 were not required for the upregulation of co-stimulatory molecules on BMDCs but essential for cytokine production. Single gene knock-out mice are needed to specify the relevance of MyD88 and Ripk2 in response to *Bartonella* infection. Though low endotoxic activities of *Bartonella* LPS, TLR4 seemed to play a role in triggering the TNF-α but not IL-6 secretion, implying that another receptor may be activated to mediate IL-6 induction. Further examination of different receptors involving in *Bartonella* recognition will be performed. Moreover,

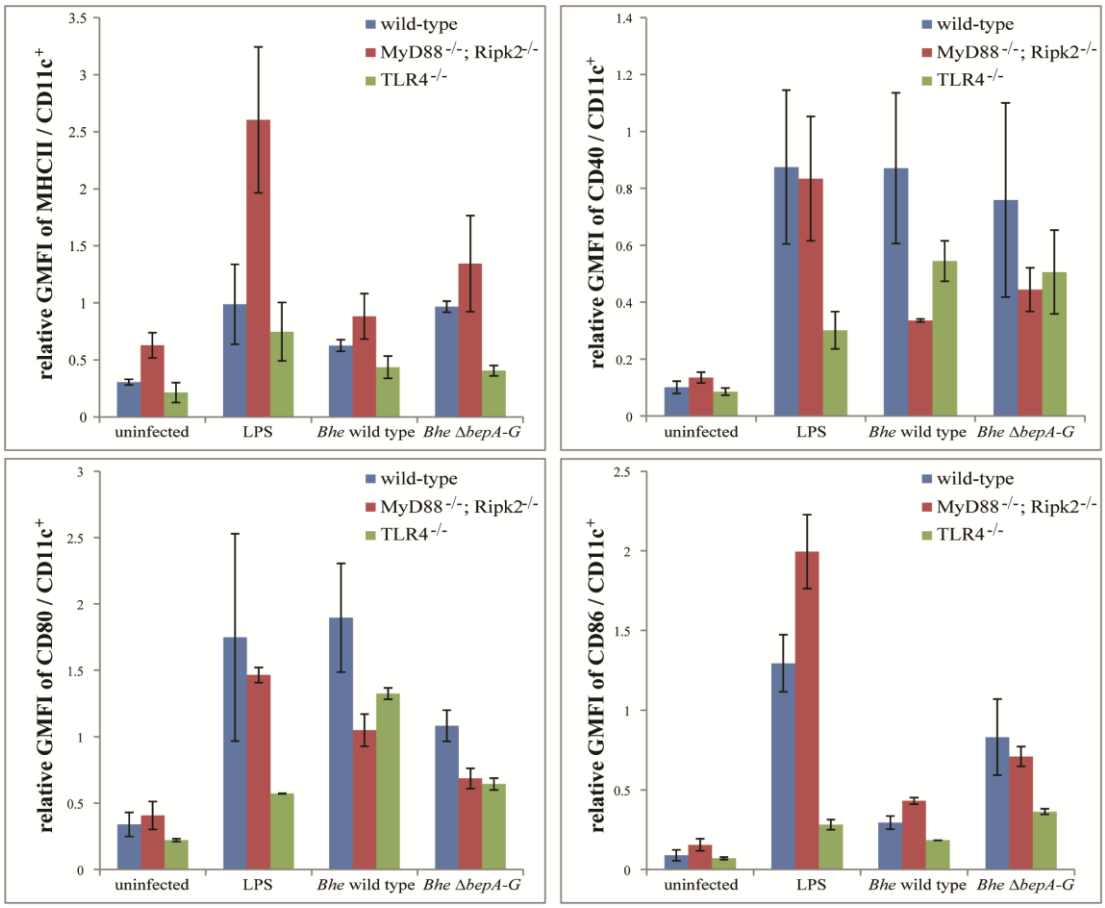

Figure 1. Upregulation of co-stimulatory receptors in BMDCs is through MyD88/Ripk2-independent manner. BMDCs were derived from wild-type (blue), MyD88/Ripk2- (red), or TLR4-deficient (green) mice. In the following, BMDCs were incubated with *E. coli* LPS (1 µg/ml), or infected with *Bhe* wild-type or *Bhe* Δ*bepA-G* (MOI = 25). After 24 hpi, cells were stained with fluorescently labeled antibodies and analyzed by flow cytometry. Expression levels of the maturation markers were presented as relative GMFI. All data were normalized to infection with *Bhe* Δ*bepA-G*. Data were analyzed from one experiment.

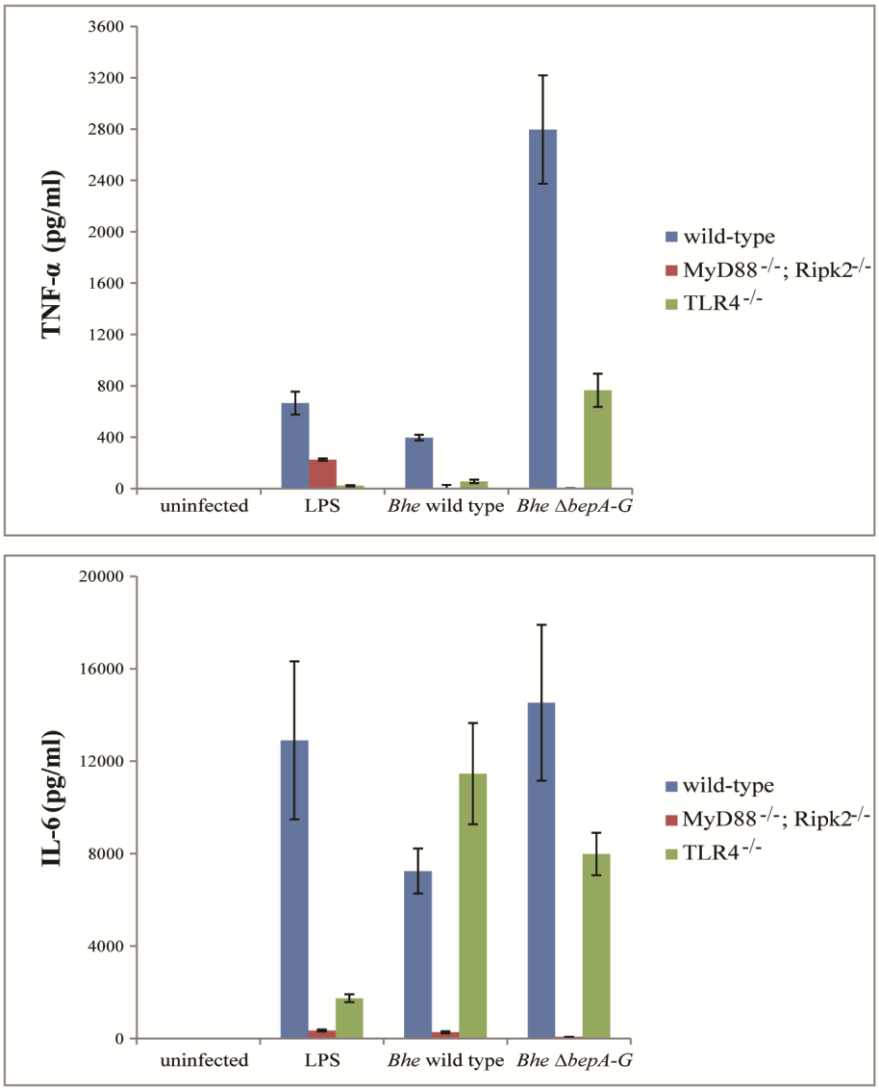

Figure 2. Cytokine production of BMDCs is MyD88- or Ripk2-dependent. BMDCs were derived from wild-type (blue), MyD88/Ripk2- (red), or TLR4-deficient (green) mice. In the following, BMDCs were incubated with *E. coli* LPS (1 µg/ml), or infected with *Bhe* wild-type or *Bhe* Δ*bepA-G* (MOI = 25) for 24 h. Amounts of TNF-α and IL-6 in the cell culture supernatants were measured by ELISA. Data were analyzed from one experiment.

3.3.2 *B. birtlesii* infection with a lower-dose inoculum induces higher bacteremia.

Introduction

Natural infection in animals, such as cats with *Bhe*, is mainly considered to be asymptomatic, despite developing long-lasting bacteremia. However, some evidence showed that experimental *Bhe* infection through intradermal (i.d.) route in cats induces various symptoms (e.g., fever, lymphadenopathy, and reproductive failure) [10, 11]. To investigate the pathogenicity of *Bartonella* on the laboratory mice, two types of murine models have been described: a homologous infection using several species of *Bartonella* isolated from wild rodents [12-14] and a heterologous infection with *Bhe* [15-17]. The very high inoculum doses (> 1×10^7 CFU/mouse) used in most previous publications may be much higher than those occurring in natural infections. This may be the reason why experimental setup of homologous infection results in various clinical symptoms.

How various inoculum doses impact the *Bbi* infection in mice was studied by Marignac et al. Three groups of eight C57BL/6 mice inoculated through the subcutaneous (s.c.) route with 5×10^3, 5×10^5 or 1.4×10^7 CFU/mouse of *Bbi* showed similar bacteremia kinetics. Interestingly, the bacteremia was significantly higher and lasted one week longer with the lower inoculum doses compared to the higher inoculum doses [18]. It suggests that high inoculum doses may prime an efficient immune response to eliminate bacteria faster. Taken this into consideration, i.d. infection of a murine-specific strain *Bbi* with different inoculum doses was performed to determine minimal infection dose in our murine model.

Results

In two independent experiments, Balb/c mice were intradermally infected with 1×10^2, 1×10^5, or 1×10^7 CFU/mouse of *Bbi* wild-type (IBS 325T). Blood samples were collected from each mouse until up to 8 weeks (Fig. 1). Combining these two experiments, four out of four (100%) mice with 1×10^7 CFU inoculum were all bacteremic at day 7. For the other two groups with lower-doses inoculum, the bacteremia became less synchronized. Four out of six (67%) mice with 1×10^5 CFU

inoculum and three out of six (50%) mice with 1×10^2 CFU inoculum were bacteremic. The highest peak of bacteremia reached to 10^6 CFU/ml blood in the group inoculated with 1×10^2 CFU inoculum.

Discussion

Consistent with the pervious study by Marignac et al. [18], our results confirmed that bacterial doses of inoculation affected the development of bacteremia in the host. Although reduced numbers of mice became bacteremic with low inoculum doses of *Bbi* infection, as soon as bacteria colonized in the blood, they tended to develop higher bacteremia and to delay the clearance. This phenomenon was also observed with *Bta* infection (chapter 3.2, Fig. 22). There as well higher levels and longer duration of bacteremia were observed with lower inoculum doses. Taken bacteremia results from two strains together, it suggests that *Bartonella* infection with low inoculum doses may be more capable of evading immune response, thereby resulting in high bacteremia. In nature, *Bartonella* transmission occurs passively when a vector leaves infective bacteria on the host skin (e.g., infected vector feces), indicating only a few bacteria are likely to be transferred to the host. Therefore, low inoculum doses may be closer to the natural situation and are more preferable to be used for *Bartonella* study *in vivo*.

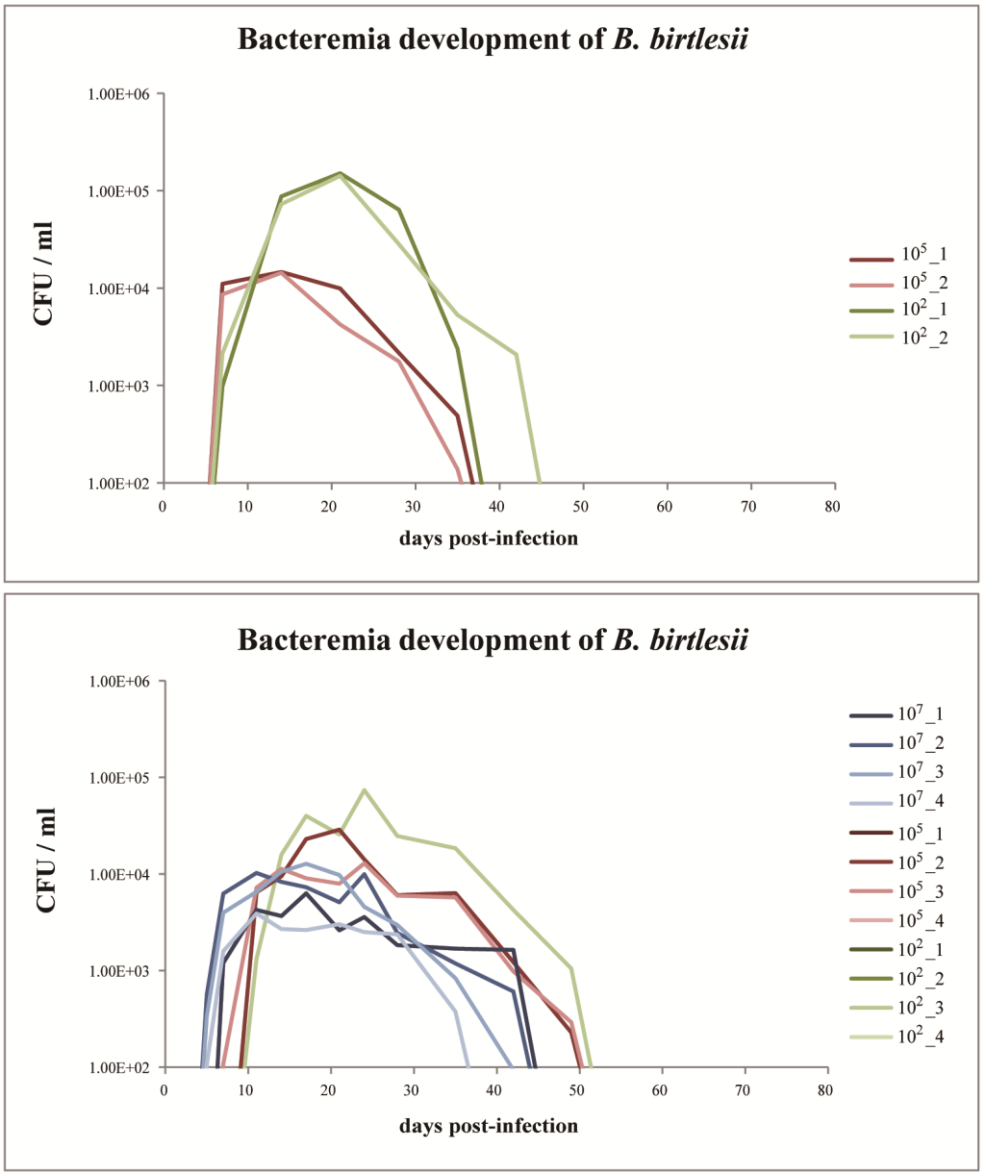

Figure 1. *B. birtlesii* bacteremia kinetics in Balb/c mice through the intradermal infection. In the first experiment (upper), mice (n = 4) were inoculated with *Bbi* wild-type in the ear dermis: two with 1×10^5 CFU (red) and two with 1×10^2 CFU (green). In the second experiment (lower), mice (n = 12) were inoculated with *Bbi* wild-type in the ear dermis: four with 1×10^7 CFU (blue), four with 1×10^5 CFU (red), and four with 1×10^5 CFU (green). Blood was drawn at the indicated days post-infection, diluted and plated on sheep blood supplemented CBA plates for counting the bacterial CFU.

3.3.3 *B. birtlesii* infection leads to lymphadenopathy in mice

Introduction

The clinical syndrome of cat scratch disease (CSD) was first reported in 1950 by Debré et al. The most typical form of CSD manifests subacute regional lymphadenopathy with an associated inoculation site due to a cat scratch or bite [19]. CSD granulomas resulting from *Bhe* infection are markedly characterized by the high content of B lymphocytes and neutrophils [20]. Similarly, a heterologous infection with *Bhe* in the murine model leads to lymphadenopathy as observed for CSD in humans but fails to establish bacteremia [16]. This lymph node swelling caused by heterologous *Bartonella* infections may indicate that bartonellae transport via the lymphatic system and trigger the granulomatous inflammation. However, *Bartonella* infection develops subclinical symptoms in the reservoir hosts. Thus, we speculate that homologous strains have evolved specific strategies to evade from host immune responses, thereby resulting in the prolonged bacteremia. In this study, we investigated the local inflammation by *Bbi* infection in mice, in particular focusing on ears and draining lymph nodes (LNs).

Results

To access the local inflammation in response to homologous infection, *Bbi* was used in the i.d. infection model where the bacteria were inoculated in the derma on the ear pinnae of mice. Mice were injected with 1×10^7 CFU/mouse of *Bbi* wild-type (Sm^R *Bbi*) or *Bbi Tn-virD4*, a translocation-deficient strain. Additionally, a group of mice were injected with phosphate-buffered saline (PBS) for comparison of the host response to the injection itself. At 2 dpi, cell suspensions from ears and draining lymph nodes were harvested. Cell samples of ear dermis were stained with a panel of fluorescently labeled antibodies specific for surface receptors of mouse DCs, macrophages, and neutrophils and analyzed by flow cytometry (Fig. 1). Moreover, the activation state of the dermal DCs ($CD11c^+$) and macrophages ($F4/80^+$) was determined by measuring MHCII expression levels. The activated neutrophils ($LyG6^+$) were detected by anti-CD11b antibody staining. Analysis of the total population of DCs showed no difference among all three tested conditions. Compared to injection with PBS, infections with *Bbi* wild-type and *Bbi Tn-virD4* recruited comparable

populations of macrophages (~ 20%) and neutrophils (~ 10-15%) to the ear dermis. These recruited neutrophils were $CD11b^+$, indicating that they were activated.

Previously, Dr. R. Okujava reported that *Bbi* i.d. infection (1×10^7 CFU/mouse) led to the swelling LNs after 2 dpi even till 7 dpi. Indeed, the similar phenotype was observed in this study. Compared to PBS injection, infections with *Bbi* wild-type and *Bbi Tn-virD4* caused the enlarged draining LNs (superficial cervical LNs) at 2 dpi. To determine the cell composition of swelling LNs, cell suspensions were stained with fluorescently labeled anti-CD3 and anti-CD19 antibodies specific for mouse T cells and B cells, respectively. Subtypes of T cells were distinguished by staining with anti-CD4 and anti-CD8 antibodies. Distant LNs (axillary and brachial LNs) were collected as a negative control. The diagram showing the locations of the principal LNs is displayed in Figure 2 [21]. Flow cytometric analysis revealed that comparable results were observed between infections with *Bbi* wild-type and *Bbi Tn-virD4* (Fig. 3). Compared to PBS injection, *Bbi* infection increased total population of $CD19^+$ B cells ~ 10% in the draining LNs. Interestingly, a subgroup of cells expressing $CD3^+/CD19^+$ was increased ~ 5%. Staining with anti-CD4 and anti-CD8 antibodies showed a slight increased population of $CD4^+/CD8^+$ double positive cells. However, the population of single positive $CD8^+$ maintained the same, but $CD4^+$ cells decreased. In distant LNs, the cell composition remained similar in all three conditions.

Discussion

The results from two different locations (ears and draining LNs) showed no significant difference between infections with *Bbi* wild-type and *Bbi Tn-virD4*. Both *Bbi* strains induced the recruitment of macrophages and neutrophils to the inoculation site of the ear dermis and led to B cell-rich swelling draining LNs. It implies that T4SS of *Bartonella* does not involve in these phenotypes. However, the enlarged LNs caused by *Bbi* infection were not observed with low inoculum doses (1×10^5 CFU/mouse) (data not shown). This result along with previous data (chapter 3.3.2) may suggest that high inoculum doses of *Bartonella* non-selectively induce strong host innate immune responses, thus resulting in local immune cell recruitment, LN enlargement, and eventually low bacteremia.

It was shown that *B. grahamii* (*Bgr*), a rodent-specific *Bartonella* species, compared

to *Bhe* develops only a mild and short-lived lymphadenopathy in mice. The distinct course of LN swelling resulted from *Bhe* is due to the lymphocyte proliferation rather than migration. However, the relative increase of B cells compared to T cells is equivalent, but the rise of the absolute B cell and T cell numbers is larger in the case of *Bhe* infection because of the much pronounced lymphadenopathy [17]. Thus, using the relative percentage of cell population in this experiment may be not a proper way to study the lymphadenopathy caused by *Bbi* infection. The absolute cell numbers will be analyzed for the next investigation.

Based on our results, a subgroup of $CD3^+/CD19^+$ double-positive cells was increased in the swelling LNs. However, we cannot exclude that these $CD3^+/CD19^+$ cells were doublets involving T cells. B cells appear as large cells that require a wide lymphocyte gate to be detected. By doing so, the risk of inclusion of cell doublets in the analysis is high. The expression of CD4 or CD8 molecules is associated with T helper or cytotoxic T cells, respectively. During thymic T cell development, a $CD4^+/CD8^+$ immature T cell stage exists. In the following, the expression of CD4 and CD8 cell surface molecules on mature T cells is thought to be mutually exclusive. Increasing evidence revealed that extrathymic $CD4^+/CD8^+$ double positive T cells are enhanced in the peripheral blood in patients with viral infections where these cells may harbor antiviral functions [22]. Besides, $CD4^+/CD8^+$ T cell population is commonly found in reactive LNs of nodular lymphocyte predominant Hodgkin lymphoma as a clue for the diagnosis [23]. These phenotypically distinct T cells appear to be comprised of memory cells based on their responses of antigen recall, expression of memory T cell markers, production of IFN-γ, and localization to inflammatory sites [24]. Interestingly, our results showed the $CD4^+/CD8^+$ population of T cells were slightly increased by *Bbi* infection. However, the function and significance of this induced small group of T cells remains to be elucidated.

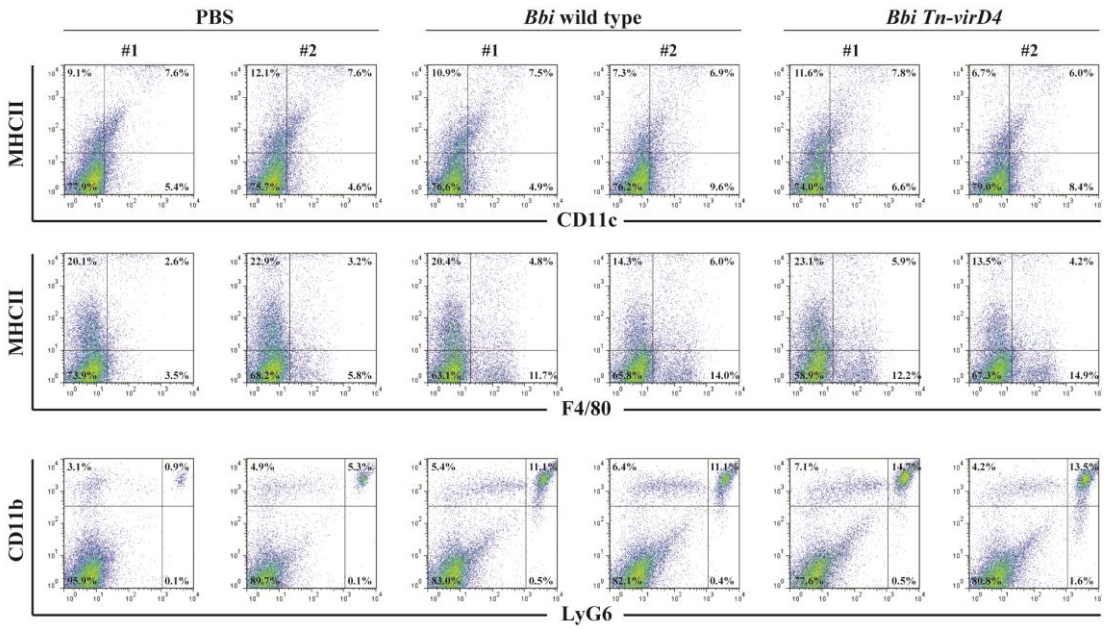

Figure 1. *Bbi* infection induces the recruitment of macrophages and neutrophils to the ear dermis. Mice (n = 4) were intradermally infected with *Bbi* (1×10^7 CFU/mouse). Two inoculated with *Bbi* wild-type and two with *Bbi Tn-virD4*. Besides, two mice were injected with PBS. At 2 dpi, cell suspensions from the ear dermis were stained with anti-CD11c, anti-F4/80, or anti-LyG6 antibodies to determine DCs, macrophages, or neutrophils, respectively. The activation state of DCs and macrophages was determined by measuring MHCII expression levels. The activated neutrophils were detected by anti-CD11b staining. Results are presented as percentages of the total acquired events.

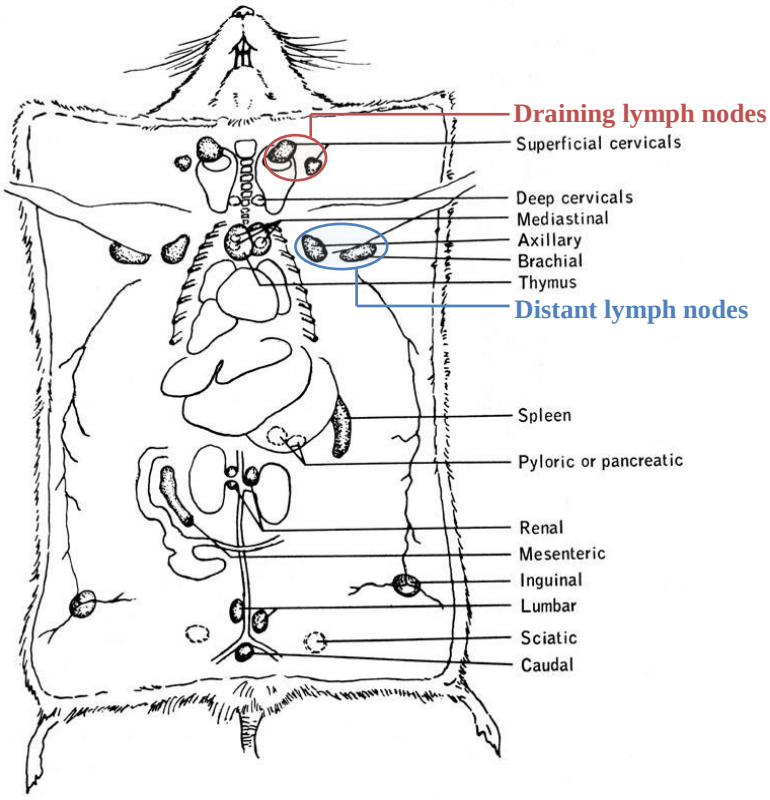

Figure 2. A scheme of the murine lymphatic system. All superficial LNs are bilateral and can be classified as: cervical superficial LNs (referred as draining LNs in red), situated immediately above the submandibular salivary glands; axillary LNs, present in the axillary fossa; brachial LNs, in proximity to the angle of the scapula; inguinal lymph nodes situated closed to the bifurcation of the superficial epigastric vein. Both axillary and brachial LNs are referred as distanced LNs in blue [21].

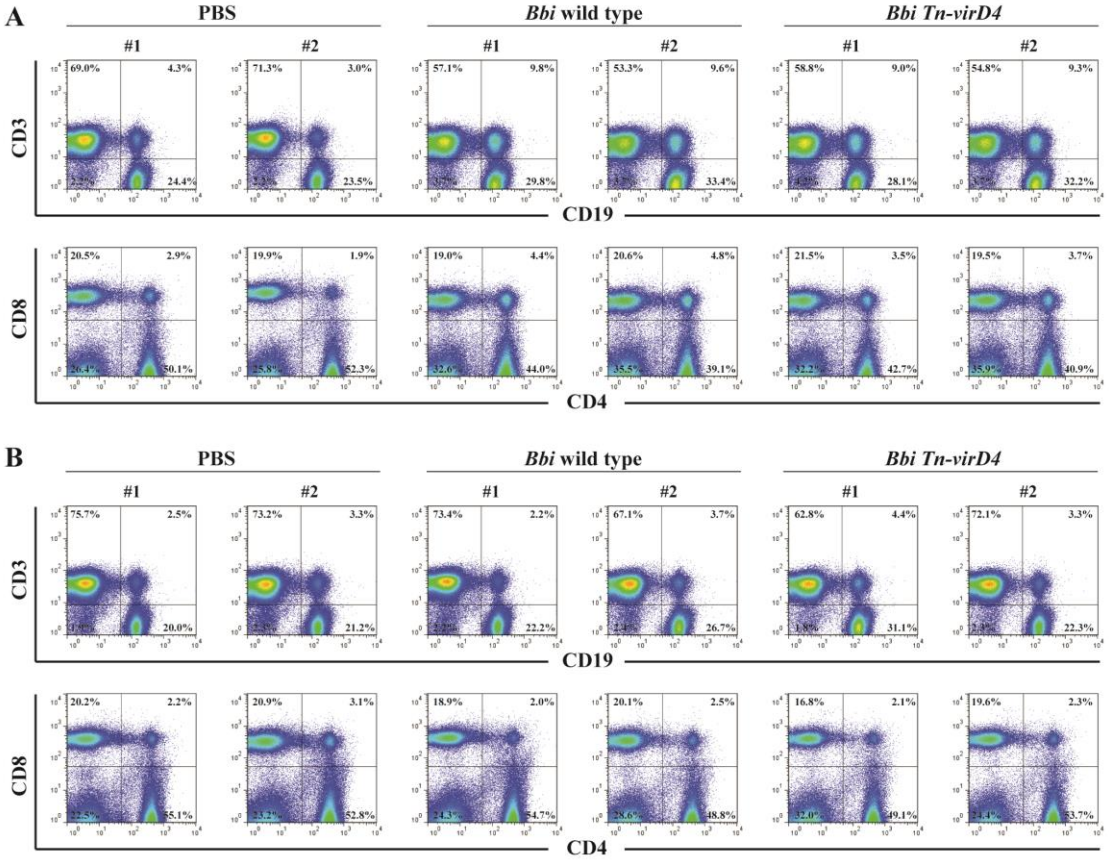

Figure 3. *Bbi* infection induces recruitment of B cells to the draining LNs. Mice (n = 4) were intradermally infected with *Bbi* (1×10^7 CFU/mouse). Two inoculated with *Bbi* wild-type and two with *Bbi Tn-virD4*. Besides, two mice were injected with PBS. At 2 dpi, cell suspensions of draining LNs **(A)** and distant LNs **(B)** were stained with a panel of fluorescently labeled anti-CD19 and anti-CD3 antibodies specific for B cells and T cells, respectively. Subtypes of T cells were distinguished by staining with anti-CD4 and anti-CD8 antibodies. Results are presented as percentages of the total acquired events.

3.3.4 *Bartonella*-infected BMDCs migrate from the site of injection to draining LNs

Introduction

It was shown that *Bhe* infection leads to subacute regional lymphadenopathy in mice (also observed in chapter 3.3.3) and bacterial DNA is detected in LNs after 6 hpi, indicating that *Bartonella* is transported via the lymphatic system in the host [16]. Furthermore, a recent publication by Okujava et al revealed that *Bhe* affects BMDC cell migration through a T4SS-dependent manner [25]. Taken these two independent lines of evidence together, we speculate that *Bartonella* initially enters migratory cells, likely DCs, in the intradermal inoculation. In the following, DCs may serve as vehicles for *Bartonella* transport via the lymphatic system towards the blood stream. To assess this hypothesis, we established the hind-foot adoptive transfer of *Bartonella*-infected BMDCs in mice. Followed with the lymphatic drainage, migration of injected BMDCs was traced. Additionally, bacteremia development was analyzed to study whether *Bartonella* potentially exploits DCs as the carriers, eventually leading to successful colonization in erythrocytes.

Results

Adoptive transfer of *Bartonella*-infected BMDCs was established in Balb/c mice. BMDCs were infected ex vivo with *Bbi* wild-type (SmR *Bbi*) at MOI = 50. After 15 hpi, infected BMDCs were treated with gentamycin (200 μg/ml) for 2 hours to remove extracellular bacteria. In the following, 5 × 105 uninfected or *Bbi*-infected BMDCs labeled with Vibrant DiO were injected subcutaneously (s.c.) in the right hind foot of mouse. The lymph drainage from the hind-foot primarily goes through the popliteal (PO) LN and inguinal (IN) LN. The PO LN drains centrally to the iliac (IL) LNs and following to the renal (RE) LN. (Fig. 1) [26]. At 1, 2, and 3 dpi, cell suspensions of the PO and IN LNs (referred as draining LNs) were collected and analyzed by flow cytometry. Our results clearly showed both uninfected and *Bbi*-infected BMDCs were able to migrate from the hind-foot to the draining LNs. Compared to the uninjected side as the negative control, the labeled cells were recovered from the draining LNs (0.2 - 0.3%) even until 3 dpi (Fig. 2). The absolute

cell numbers were showed in the figure 3. The highest amounts of fluorescent cells were detected at 1 dpi and decreased gradually.

Discussion

Our results showed that *Bbi*-infected BMDCs similar as uninfected BMDCs were detected within the draining LNs at 1 dpi, indicating that *Bbi* infection did not impair the DC migratory capability. However, only few bacterial colonies were recovered form cell suspensions of draining LNs (data not shown). It is difficult to interpret how well *Bbi* wild-type survived in BMDCs and passaged to lymphatic system in the established adoptive transfer model. Bacteria may be already released from BMDCs before cell suspensions were harvested. To address this question, bacteremia analysis could be a better way. The development of bacteremia from mice adoptively transferred with *Bbi*-infected BMDCs was analyzed from 3 to 28 dpi. However, five out of five mice were abacteremic. Later, we realized that different from *Bbi* wild-type (IBS 325T) leading to stable bacteremia (chapter 3.3.2), the Sm^R *Bbi* wild-type used in this experiment was attenuated and failed to develop the bacteremia in the i.d. infection model. Thus, experiments of adoptive transfer were re-performed using Sm^R *Bta* wild-type which was confirmed to be capable of establishing stable bacteremia in mice (chapter 3.2, Fig 22). Five out of Five mice became bacteremic with inoculation of *Bta*-infected BMDCs through the hind-foot of mouse (data not shown). It suggests that BMDCs may potentially serve as vehicles for *Bartonella* transport, thereby resulting in colonization in erythrocytes. However, more investigations are needed to exclude that BMDCs are lysed during injection and bacteria are exposed directly under the skin.

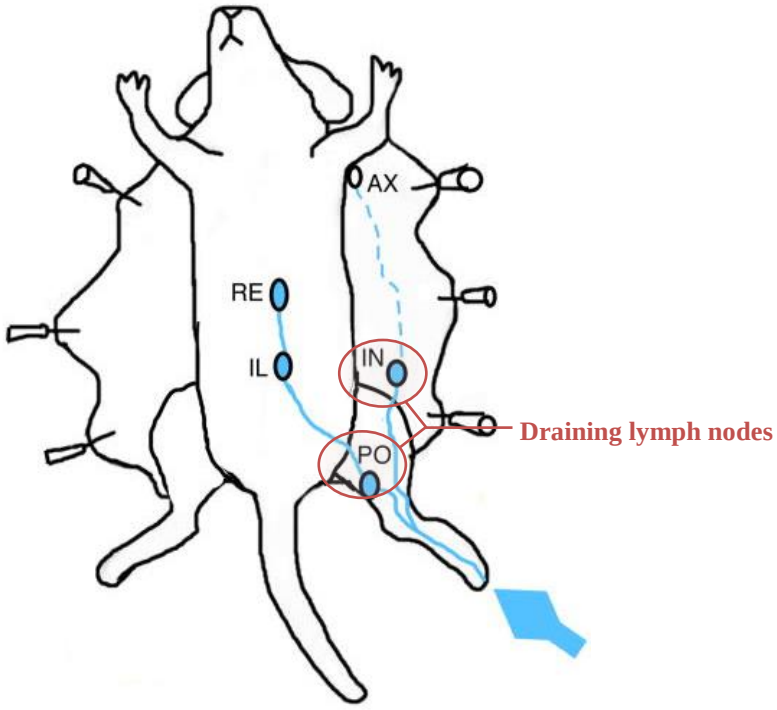

Figure 1. A diagram shows lymphatic drainage in the mouse. The adoptive transfer was performed through hind-foot (arrow in blue). The lymph drainage from the hind-foot primarily goes through the popliteal (PO) LN and inguinal (IN) LN. The popliteal LN drains centrally to the iliac (IL) LNs and following to the renal (RE) LN. Both PO and IN LNs are referred as draining LNs labeled in red. [26]

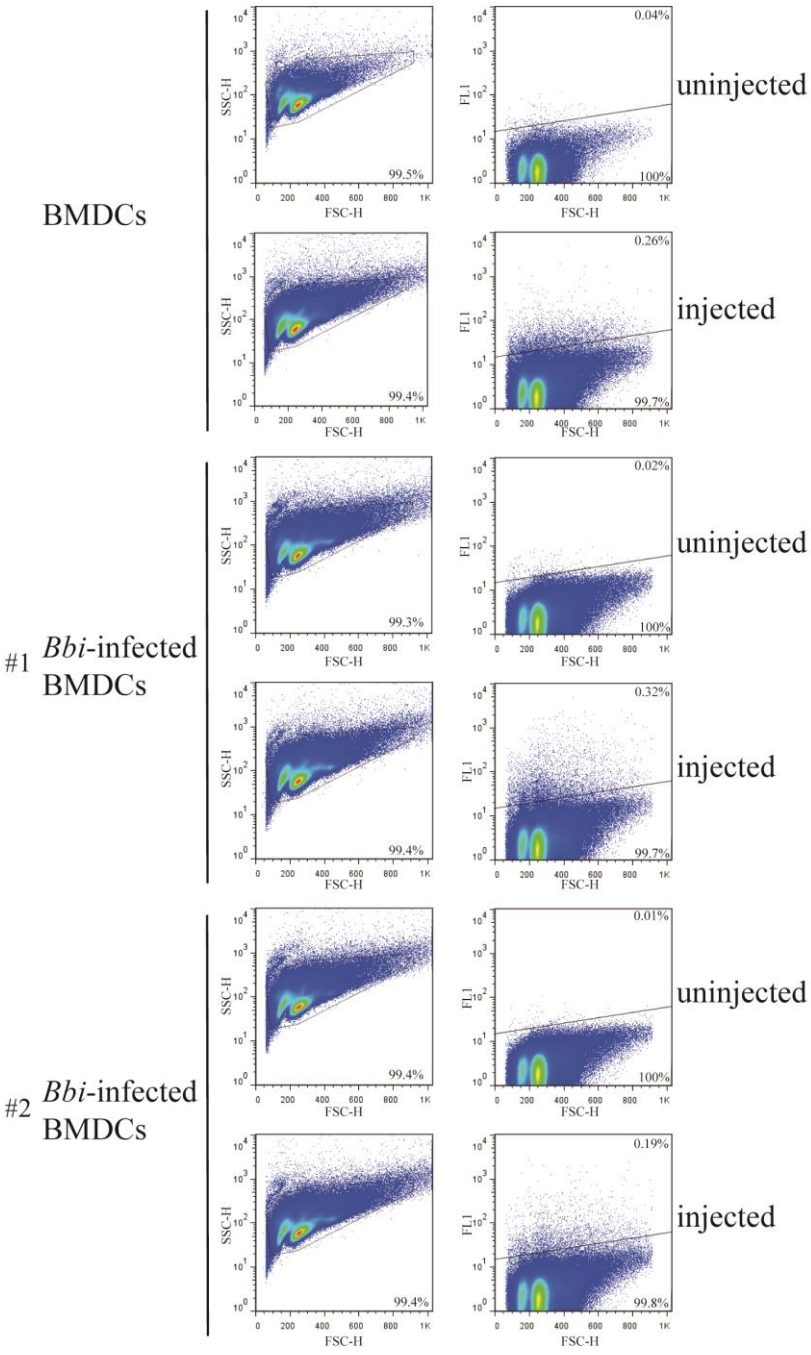

Figure 2. Both uninfected and *Bartonella*-infected BMDCs migrate from the hind-foot to draining LNs. BMDCs were infected *ex vivo* with *Bbi* wild-type (Sm^R *Bbi*) at MOI = 50. Gentamycin (200 µg/ml) treatment was used to remove extracellular bacteria. In the following, 5×10^5 uninfected (n = 1) or *Bbi*-infected (n = 2) BMDCs labeled with Vibrant DiO (FL1 channel) were injected subcutaneously (s.c.) in the right hind foot of mouse. At 1 dpi, cell suspensions of PO and IN LNs were collected from both sides and analyzed by flow cytometry.

Injection	DAY 1	DAY 2	DAY 3
BMDCs	**3687**	**1136**	**1883**
#1 *Bbi*-infected BMDCs	**4441**	**1513**	**1309**
#2 *Bbi*-infected BMDCs	**2492**	**226**	**475**

Figure 3. The absolute numbers of fluorescent cells are detected in draining LNs. BMDCs were infected *ex vivo* with *Bbi* wild-type (Sm^R *Bbi*) at MOI = 50. Gentamycin (200 μg/ml) treatment was used to remove extracellular bacteria. In the following, 5×10^5 uninfected (n = 1) or *Bbi*-infected (n = 2) BMDCs labeled with Vibrant DiO (FL1 channel) were injected subcutaneously (s.c.) in the right hind foot of mouse. At 1, 2, and 3 dpi, cell suspensions of PO and IN LNs were collected from both sides and analyzed by flow cytometry. This figure presents the absolute number of FL1 positive cells after subtraction of the background of autoflourescent events from control LNs.

3.3.5 *B. taylorii* infection in the neonatal murine model leads to extremely high bacteremia but not to bacterial persistence

Introduction

As reported, the domestic cats naturally infected with a feline-specific strain *Bhe* developed prolonged bacteremia for several weeks to more than one year [27]. With current experimental setup, Balb/c mice (6 to 8 weeks old) infected with homologous strains *Bbi* and *Bta* led to transient two-month bacteremia, which may be much shorter from those occurring in nature. As exemplified by *H. pylori*, experimental infection in mice during the neonatal period leads to bacterial persistence based on a mechanism of tolerogenic DCs reprogramming via a T4SS independent manner [28]. To get closer with the situation that *Bartonella* homogenous infection may persist for life, a neonatal murine model for *Bta* infection was established. Neonatal life is characterized by heightened sensitivity to infectious agents with severely reduced specific cellular and humoral immune responses. The sensitivity of newborns to infectious diseases is partly due to the lack of pre-existing immunological memory and the small number of immune cells presenting in peripheral lymphoid tissues. Aside from these quantitative differences, newborn immune cells are qualitatively distinct from adult cells. However, neonates are considered as immunodeviant instead of immunodeficient. Depending on the conditions of antigen exposure, neonates are able to mount various responses, ranging from deficient or deviant to fully mature [29]. Newborn mice are defined experimentally as those ages from 1 to 10 days. There are major changes in lymphoid-organ development during the first week. However, some adaptive immune responses are similar in 7-day-old and 1-day-old mice. In this study, *Bta* infections in mice at different ages: 7 days or 1 day, as well as in two species: C57BL6 or Balb/c were compared.

Results

Mice were infected with *Bta* wild-type during the neonatal period (i.e., at the age of 7 days or 1 day) through an intraperitoneal route. After injection, neonates were placed back to the same cage with the mother mouse. Until they reached 21 days old, infected mice were separated by gender. Blood samples were collected from 21 dpi

until no detectable bacteremia. When C57BL6 mice were infected at the age of 7 days, four out of four (100%) mice with 1×10^7 CFU inoculum, five out of five (100%) mice with 1×10^5 CFU inoculum, and one out of four (25%) mice with 1×10^3 CFU inoculum were bacteremic. The highest peak of bacteremia was almost 10^8 CFU/ml blood in the group inoculated with 1×10^5 CFU/mouse (Fig. 1). When C57BL6 mice were infected at 1 day old, six out of six (100%) mice with 1×10^7 CFU inoculum, six out of six (100%) mice with 1×10^5 CFU inoculum, and one out of two (50%) mice with 1×10^3 CFU inoculum were bacteremic. The highest peak of bacteremia reached to 7×10^8 CFU/ml blood in the groups inoculated with 1×10^5 CFU/mouse and $1x10^3$ CFU/mouse (Fig. 2A). Furthermore, when Balb/c mice were infected with *Bta* wild-type at the age of day 1, all of the mice with different inoculum doses (1×10^7, 1×10^5, and 1×10^3 CFU/mouse) were bacteremic. The highest peak of bacteremia reached 3×10^9 CFU/ml blood in the groups inoculated with 1×10^5 CFU/mouse and 1×10^3 CFU/mouse (Fig. 2B). The bacteremia kinetics was similar in all of tested groups (range, 8 to 9 weeks).

Discussion

In this study, *Bta* infection in neonatal mice (both at the age of 7 days and 1 day) did not lead to bacterial persistence. Similar to infection in 8 weeks old mice (considered as adults), the bacteremia kinetics in neonatal mice was in a range until 8 to 9 weeks. Based on pervious results in adult mice (chapter 3.2, Fig. 22), the highest peak of bacteremia reached at 14 dpi. In neonatal murine model, we started to collect blood sample at 21 dpi due to handling issues. Thus, we might have missed the highest peak of bacteremia in the neonates. Even so, *Bta* infection in 1-day-old C57BL6 mice showed that the highest detectable peak of bacteremia was around 1 log higher than infection in adult mice. Infection in 1-day-old Balb/c mice led to almost 2 log higher bacteremia than infection in adult mice. Interestingly, the age of infected mice has a significant effect on bacteremia development. Comparing bacteremia of different mice strains showed that Balb/c mice were more susceptible to *Bartonella* infection. Based on extremely high bacteremia in the neonatal mice model, it indicates that immunodeviant neonates poorly control the *Bartonella* replication in the early phase. While mice grow up and develop an intact immune system, the bacteremia is gradually cleared out. So far, it was never supported by *in vivo* data where *Bartonella* survives and replicates in the primary niche before the bacteremic stage. Based on the

extremely high bacteremia in newborn mice, this neonatal murine model may provide a better platform to study the primary niche of *Bartonella* infection.

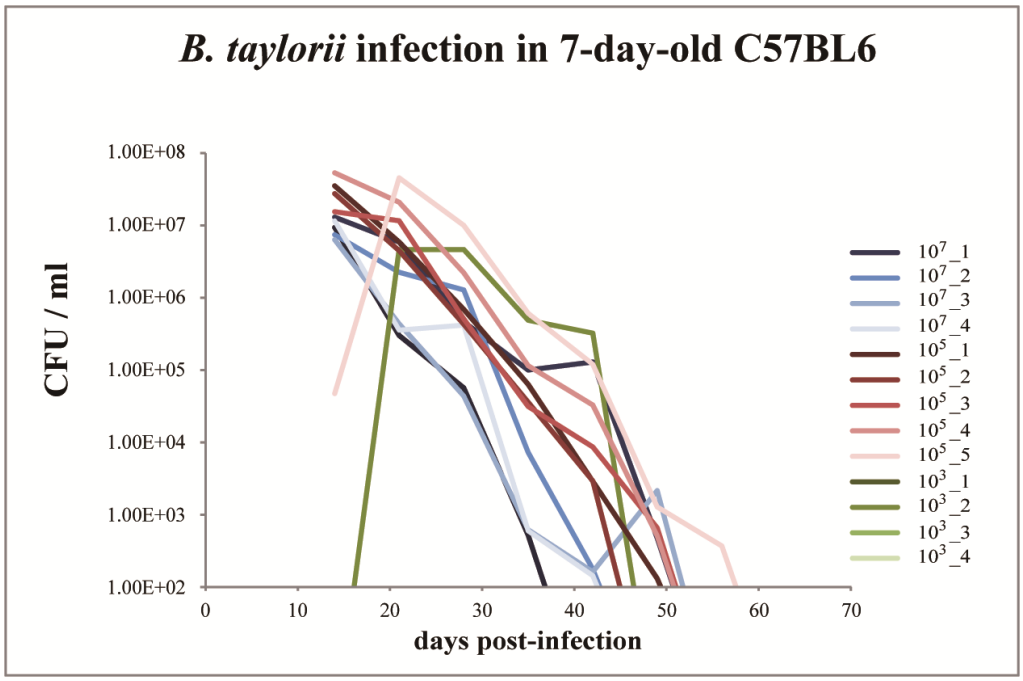

Figure 1. Bacteremia kinetics of *B. taylorii* infection in 7-day-old mice. 7-day-old C57BL6 mice (n = 14) were inoculated with *Bta* wild-type via i.p. route: five with 1×10^7 CFU (blue), five with 1×10^5 CFU (red), and four with 1×10^3 CFU (green). Blood was drawn at the indicated days post-infection, diluted and plated on sheep blood supplemented CBA plates for counting bacterial CFU.

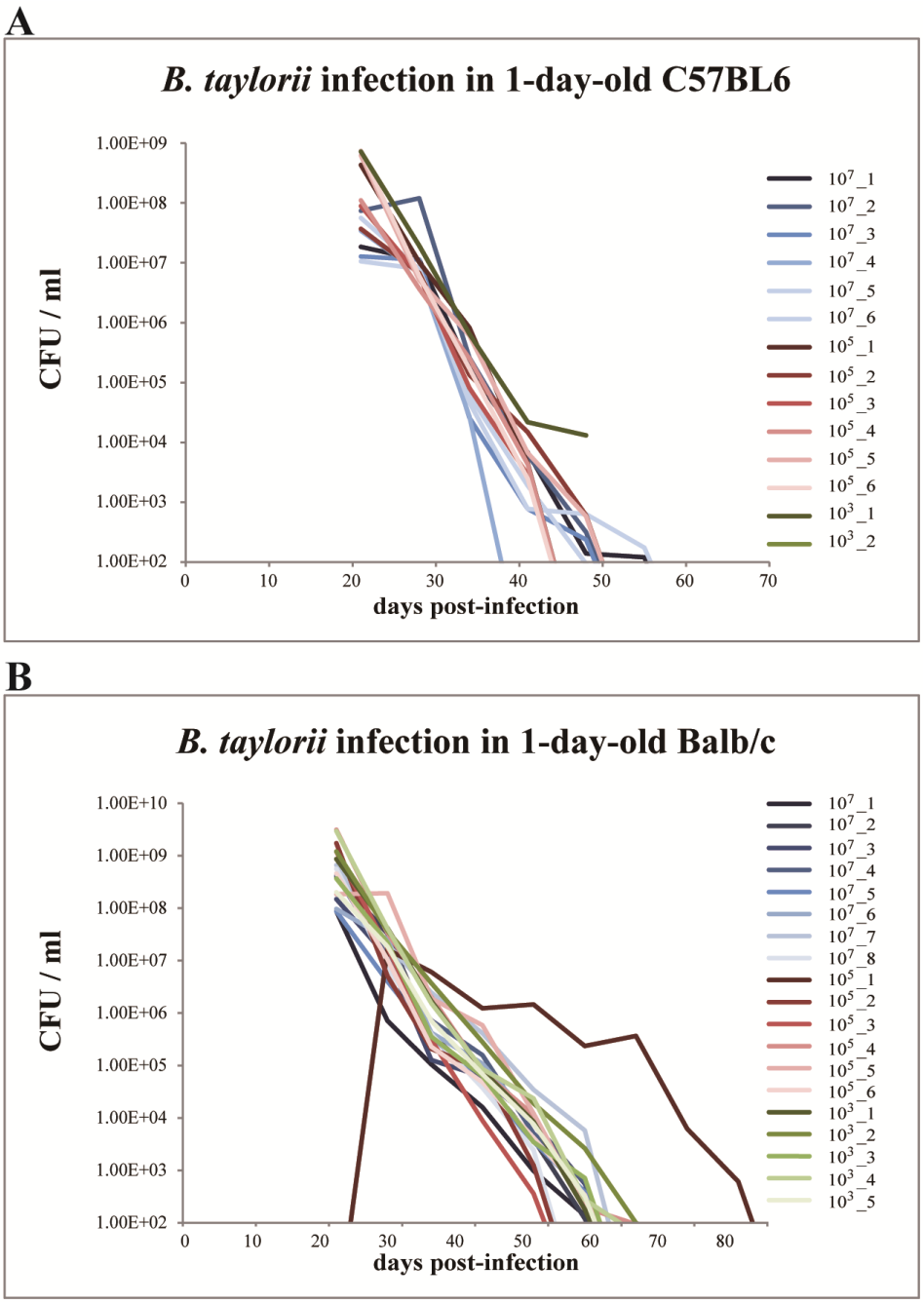

Figure 2. Bacteremia kinetics of *B. taylorii* infection in 1-day-old mice. (A) 1-day-old C57BL6 mice (n = 14) were inoculated intraperitoneally with *Bta* wild-type: six with 1×10^7 CFU (blue), six with 1×10^5 CFU (red), and two with 1×10^3 CFU (green). **(B)** 1-day-old Balb/c mice (n = 19) were inoculated intraperitoneally with *Bta* wild-type: eight with 1×10^7 CFU (blue), six with 1×10^5 CFU (red), and five with 1×10^3 CFU (green). For both experiments, blood was drawn at the indicated days post-infection, diluted and plated on sheep blood supplemented CBA plates for counting bacterial CFU.

3.3.6 *Bta* ∆ *bepDE* loses the fitness of bacteremia development

Introduction

The immunomodulatory activities of $BepD_{Bhe}$ were majorly studied *in vitro* analyses (chapter 3.2). In the following, we became interested in the role of BepD in an *in vivo* establishment of *Bartonella* infection. However, *Bhe* causes bacteremia as a hallmark of infection in its feline natural reservoir host only, which for ethical reasons is not an accessible experimental model. To establish an optimal murine model for the functional analysis of Beps, *Bta*, a murine-specific strain, was introduced with its feasibility of genetic manipulations. Annotation of the genomic fragment revealed that only five effector proteins can be annotated in *Bta* instead of seven Beps (BepA-G) in *Bhe*. Among them, two Beps, $BepD_{Bta}$ and $BepE_{Bta}$ contain putative tyrosine-phosphorylation motifs as homologs of $BepD_{Bhe}$ (identity of the N-terminal fragment: 53%) and $BepE_{Bhe}$ (identity of the N-terminal fragment: 24%), respectively. To avoid their potentially redundant functions, a mutant strain of *Bta* with deletions of both genes *bepD* and *bepE* was constructed (referred to *Bta* Δ*bepDE*). Mice were infected intradermally with *Bta* Δ*bepDE* and bacteremia was monitored up to 8 weeks.

Results

In this experiment, ten mice were intradermally infected: five with *Bta* wild-type (1×10^5 CFU/mouse) and five with *Bta* Δ*bepDE* (1×10^5 CFU/mouse). Different from *Bta* wild-type infection which led to five out of five (100%) bacteremic mice at 7 dpi, *Bta* ∆ *bepDE* infection resulted in three out of five (60%) mice developing less synchronized bacteremia. The highest peak of bacteremia caused by *Bta* wild-type reached to 10^6 CFU/ml blood. Although 60% mice were bacteremic, *Bta* Δ*bepDE* developed lower titer (range from 10^3 to 10^5 CFU/ml) and shorter duration (range from 3 to 5 weeks) of bacteremia (Fig. 1).

Discussion

Infection with *Bta* Δ*bepDE* led to lower and shorter bacteremia, indicating that less fitness of bacteremia development resulted from combined consequences of loss of

BepD$_{Bta}$ and BepE$_{Bta}$. However, when the effect of BepD$_{Bta}$ and BepE$_{Bta}$ on DC maturation was analyzed *in vitro*, we realized that impaired DC maturation only resulted from BepD$_{Bta}$ but not BepE$_{Bta}$. Most likely, these two effectors containing EPIYA-related motifs process different functions. To study the specific relevance of BepD$_{Bta}$ *in vivo*, *Bta* Δ*bepD* was generated and analyzed in the Research article II (chapter 3.2).

A recent publication by Dr. R. Okujava demonstrated a potent role of BepE in bacterial dissemination from derma to blood. *In vitro* analysis revealed that BepE$_{Bhe}$ rescued the cell fragmentation which was triggered by BepC$_{Bhe}$. In the rat model, when the *B. tribocorum* mutant *Btr* Δ*bepDE* was abacteremic through the i.d. infection, complementation with BepE$_{Btr}$, BepE$_{Bhe}$ or BID domains of BepE$_{Bhe}$ restored bacteremia. [25]. However, though leading to impaired bacteremia, *Bta* Δ*bepDE* was not abacteremic. One of the possibilities is that BID domain of other *Bta* effectors aside from BepD$_{Bta}$ and BepE$_{Bta}$ may possess similar function as BID domains of BepE$_{Bhe}$. Also, it remains unclear whether any of *Bta* effectors containing a FIC domain triggers the deleterious phenotypes as BepC$_{Bhe}$.

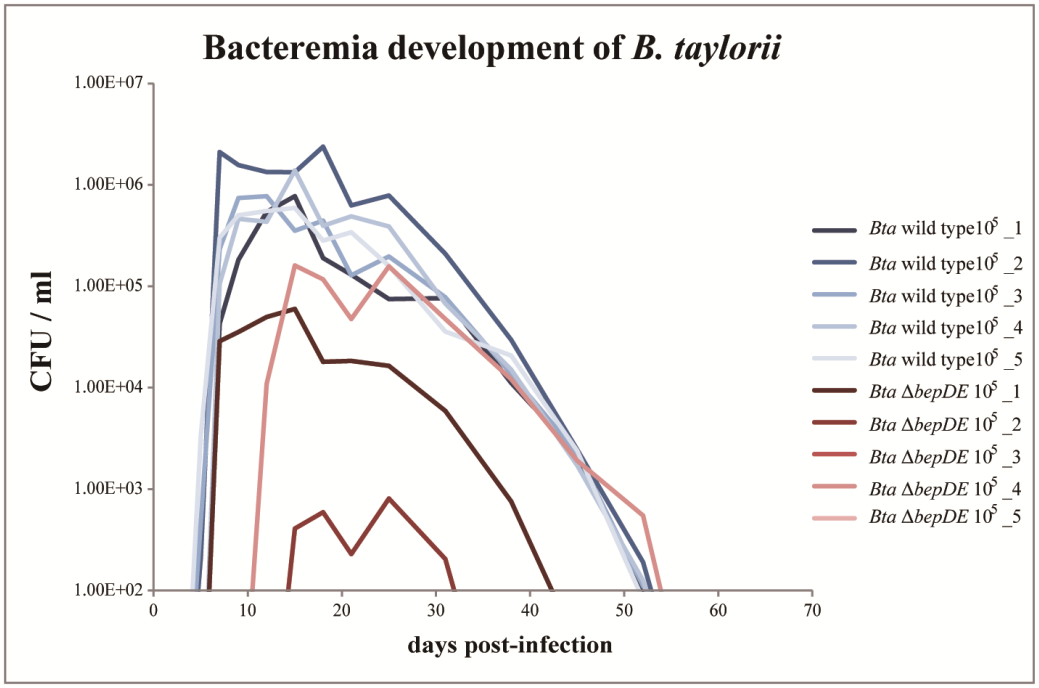

Figure 1. *Bta* Δ*bepDE* loses the fitness of bacteremia development. Mice (n = 10) were inoculated intradermally: five with 1 x 10^5 CFU of *Bta* wild-type (blue), and five with 1 x 10^5 CFU of *Bta ΔbepDE* (red). Blood was drawn at the indicated days post-infection, diluted and plated on sheep blood supplemented CBA plates for counting bacterial CFU.

3.3.7 References

1. Banchereau, J. and R.M. Steinman, Dendritic cells and the control of immunity. Nature, 1998. 392(6673): p. 245-52.
2. Akira, S. and K. Takeda, Toll-like receptor signalling. Nat Rev Immunol, 2004. 4(7): p. 499-511.
3. Zahringer, U., et al., Structure and biological activity of the short-chain lipopolysaccharide from Bartonella henselae ATCC 49882T. J Biol Chem, 2004. 279(20): p. 21046-54.
4. Popa, C., et al., Bartonella quintana lipopolysaccharide is a natural antagonist of Toll-like receptor 4. Infect Immun, 2007. 75(10): p. 4831-7.
5. Kawai, T., et al., Unresponsiveness of MyD88-deficient mice to endotoxin. Immunity, 1999. 11(1): p. 115-22.
6. Yamamoto, M., et al., Role of adaptor TRIF in the MyD88-independent toll-like receptor signaling pathway. Science, 2003. 301(5633): p. 640-3.
7. Kaisho, T., et al., Endotoxin-induced maturation of MyD88-deficient dendritic cells. J Immunol, 2001. 166(9): p. 5688-94.
8. Zughaier, S.M., et al., Differential induction of the toll-like receptor 4-MyD88-dependent and -independent signaling pathways by endotoxins. Infect Immun, 2005. 73(5): p. 2940-50.
9. Hoebe, K., et al., Upregulation of costimulatory molecules induced by lipopolysaccharide and double-stranded RNA occurs by Trif-dependent and Trif-independent pathways. Nat Immunol, 2003. 4(12): p. 1223-9.
10. O'Reilly, K.L., et al., Acute clinical disease in cats following infection with a pathogenic strain of Bartonella henselae (LSU16). Infect Immun, 1999. 67(6): p. 3066-72.
11. Guptill, L., et al., Evidence of reproductive failure and lack of perinatal transmission of Bartonella henselae in experimentally infected cats. Vet Immunol Immunopathol, 1998. 65(2-4): p. 177-89.
12. Kosoy, M.Y., et al., Experimental evidence of host specificity of Bartonella infection in rodents. Comp Immunol Microbiol Infect Dis, 2000. 23(4): p. 221-38.
13. Koesling, J., et al., Cutting edge: antibody-mediated cessation of hemotropic infection by the intraerythrocytic mouse pathogen Bartonella grahamii. J Immunol, 2001. 167(1): p. 11-4.
14. Boulouis, H.J., et al., Kinetics of Bartonella birtlesii infection in experimentally infected mice and pathogenic effect on reproductive functions. Infect Immun, 2001. 69(9): p. 5313-7.
15. Arvand, M., et al., Bartonella henselae-specific cell-mediated immune responses

display a predominantly Th1 phenotype in experimentally infected C57BL/6 mice. Infect Immun, 2001. 69(10): p. 6427-33.
16. Karem, K.L., et al., Characterization of Bartonella henselae-specific immunity in BALB/c mice. Immunology, 1999. 97(2): p. 352-8.
17. Kunz, S., et al., Lymphadenopathy in a novel mouse model of Bartonella-induced cat scratch disease results from lymphocyte immigration and proliferation and is regulated by interferon-alpha/beta. Am J Pathol, 2008. 172(4): p. 1005-18.
18. Marignac, G., et al., Murine model for Bartonella birtlesii infection: New aspects. Comp Immunol Microbiol Infect Dis, 2010. 33(2): p. 95-107.
19. Klein, J.D., Cat scratch disease. Pediatr Rev, 1994. 15(9): p. 348-53; quiz 353.
20. Vermi, W., et al., Role of dendritic cell-derived CXCL13 in the pathogenesis of Bartonella henselae B-rich granuloma. Blood, 2006. 107(2): p. 454-62.
21. Dunn, T.B., Normal and pathologic anatomy of the reticular tissue in laboratory mice, with a classification and discussion of neoplasms. J Natl Cancer Inst, 1954. 14(6): p. 1281-433.
22. Nascimbeni, M., et al., Peripheral CD4(+)CD8(+) T cells are differentiated effector memory cells with antiviral functions. Blood, 2004. 104(2): p. 478-86.
23. Rahemtullah, A., et al., A double-positive CD4+CD8+ T-cell population is commonly found in nodular lymphocyte predominant Hodgkin lymphoma. Am J Clin Pathol, 2006. 126(5): p. 805-14.
24. Zuckermann, F.A., Extrathymic CD4/CD8 double positive T cells. Vet Immunol Immunopathol, 1999. 72(1-2): p. 55-66.
25. Okujava, R., et al., A translocated effector required for bartonella dissemination from derma to blood safeguards migratory host cells from damage by co-translocated effectors. PLoS Pathog, 2014. 10(6): p. e1004187.
26. Harrell, M.I., B.M. Iritani, and A. Ruddell, Lymph node mapping in the mouse. J Immunol Methods, 2008. 332(1-2): p. 170-4.
27. Kordick, D.L., et al., Prolonged Bartonella bacteremia in cats associated with cat-scratch disease patients. J Clin Microbiol, 1995. 33(12): p. 3245-51.
28. Oertli, M., et al., DC-derived IL-18 drives Treg differentiation, murine Helicobacter pylori-specific immune tolerance, and asthma protection. J Clin Invest, 2012. 122(3): p. 1082-96.
29. Adkins, B., C. Leclerc, and S. Marshall-Clarke, Neonatal adaptive immunity comes of age. Nat Rev Immunol, 2004. 4(7): p. 553-64.

4. CONCLUSIONS AND OUTLOOK

Functional interaction between BadA and VirB/D4 T4SS

The first published report "*Bartonella henselae* trimeric autotransporter adhesin BadA expression interferes with effector translocation by the VirB/D4 type IV secretion system" (chapter 3.1) in my Ph.D. thesis was accomplished by collaboration with the group of Prof. V. Kempf. Our findings revealed that most *Bartonella* clinical isolates had lost expression of either BadA or VirB/D4 during *in vitro* passages. Only one exception of clinical isolate (strain San Antonio 3 variant-2) from our screen stably coexpressed BadA and VirB/D4. Furthermore, the phenotypic effects of coexpression of both virulence factors demonstrated that BadA interfered with the function of VirB/D4 T4SS, but kept its intact capabilities. Based on our data obtained from this study, we propose that BadA negatively affects VirB/D4-dependent Bep translocation and invasome formation by likely forming a physical barrier between the bacterial cell envelope and the host cell membrane. In contrast, BadA-dependent phenotypes are not affected by a functional VirB/D4 T4SS. Both virulence factors, each displaying multiple functions in host cell interaction, were described to be essential for *Bartonella* pathogenicity. Potentially, BadA and VirB/D4 are differentially regulated during the different stages of the infection cycle of *Bartonella*. Further experiments to elucidate the regulatory patterns of these two systems are needed.

Immunomodulatory properties of BepA and BepD

Through the intradermal infection, *Bartonella* VirB/D4 T4SS is known to be an indispensable virulence factor for the successful development of bacteremia. Particularly, it is required at an early stage of infection before the onset of intraerythrocytic bacteremia. Since DCs are one of the potential vehicles for *Bartonella* transport in the host organism, we sought to examine the functional consequences of professional antigen-presenting DCs in response to *Bartonella* infection. This resulted in the second manuscript "*Bartonella* translocated effectors, BepA and BepD, interfere with the maturation of dendritic cells" (chapter 3.2). Our data revealed that *Bartonella* infected DCs remained a "semi-mature" developmental stage, which was characterized by reduced surface expression of MHCII complex and co-stimulatory receptors CD40 and CD86, as well as strongly diminished secretion of the pro-inflammatory cytokines TNF-α and IL-6. These phenotypic changes of

impaired DC maturation observed upon *Bartonella* infection were attributed to two effector proteins, BepA and BepD.

The BID domain of BepA strongly affected the downregulation of CD40 expression and TNF-α production, likely through cAMP elevation in BMDCs. In the following, how PKA and Epac-1, known as key players in the downstream of cAMP signaling, antagonistically interact with each other for the anti-inflammatory response of BepA will be further analyzed. Also, although BepA homologs share high sequence identity, the functional readouts of them were not congruent. Further investigations are needed to elucidate a potential cell type or host species specificity of BepA.

The phenotypic changes of infected BMDCs triggered by *Bartonella* BepD were represented by the downregulation of surface MHCII and CD86 expression, as well as by the repression of TNF-α and IL-6 production. Besides in primary BMDCs, ectopic expression of BepD in JAWSII cells showed antagonistic effects on LPS-triggering TLR signaling. In this study, we demonstrated that BepD led to a prolonged STAT3 phosphorylation and activation similar to IL-10 signaling, which may explain the immunosuppressive properties of BepD. Moreover, constitutive tyrosine-phosphorylation of BepD in JAWSII cells suggests that BepD acts as a signaling hub to actively trigger the STAT3 activation, in contrast to IL-10 receptor, which is thought to only become active upon engagement of its extracellular signals. To further verify this hypothesis, we will examine the effects of STAT3 protein knockdown by RNA interference on the immunomodulatory activity of BepD.

DCs reaching a stage of semi-maturation are believed to be capable of driving naïve T cell into a regulatory cell fate characteristic for immunotolerance. To support this idea, functional analyses of these semi-mature DCs are needed. One was performed by using *ex vivo* T cell response assay. BMDCs from naïve mice were infected with *Bartonella* and subsequently co-cultured with OTII-transgenic T cells under conditions of ovalbumin-specific priming. Subsequently, the state of T cell activation was monitored by cell proliferation. However, in this experiment, BMDCs without *Bartonella* infection already primed a strong T cell activation, and thus this result was not conclusive (data not shown). In addition, to translate our findings into an *in vivo* context, we analyzed the bacteremia as a hallmark of *Bartonella* infection in mice. Although a trend of losing the bacterial fitness was observed after infection with *B.*

taylorii strains harboring deletions of *bepA* or/and *bepD*, the effects of BepA and BepD on bacteremia development were not strong. To sensitize our murine model, lower doses of inoculum will be tested in the next experiment. Also, further investigations uncovering the local inflammation (particularly at the site of injection and draining lymph nodes (LNs)) of *Bartonella* infection will be performed.

Immunological signaling triggered by *Bartonella* infection

Even though LPS of *Bartonella* shows unusual structural features connected to a significantly lower endotoxic activity, a strong inflammation in BMDCs was observed after infection with an effector-free strain of *Bartonella* (see chapter 3.2). We became interested in studying which immunological signaling in DCs was triggered by *Bartonella* infection (chapter 3.3.1). Examination of BMDCs from TLR4- and MyD88/Ripk2- deficient mice revealed that upregulation of surface MHCII complex and co-stimulatory receptors by *E. coli* LPS treatment or by *Bartonella* infection was through a MyD88/Ripk2-indepednent pathway. Contrarily, MyD88 or Ripk2 plays an essential role in cytokine production (TNF-α and IL-6). Results obtained from this experiment indicate that *Bartonella* infection of BMDCs provokes both MyD88/Ripk2-dependent and -independent immunological signaling pathways. To specify the relevance of MyD88 and Ripk2 to DC inflammation, single gene knock-out BMDCs will be used. Furthermore, upon *Bartonella* infection, TNF-α production was diminished in TLR4-deficient BMDCs, whereas IL-6 induction remained the same. It implies that besides TLR4, another receptor engaged with *Bartonella* to mediate IL-6 production. To assess this question, other TLR-deficient BMDCs will be analyzed.

Bartonella transport at an early stage of infection

To explore how *Bartonella* transport in the host organism, different *in vivo* analyses were established. We found that intradermal infection of *B. birtlesii* led to the enlargement of draining LNs in mice (chapter 3.3.3). Moreover, bacterial colonies could be recovered from the draining LNs at 24 hours post-infection (Dr. R. Okujava, data not shown). Taken together, these results indicate that *Bartonella* is transported through the lymphatic system and triggers the granulomatous inflammation in the

LNs. Furthermore, the adoptive transfer of *Bartonella*-infected BMDCs revealed that infected BMDCs were capable of migrating from the site of inoculation to draining LNs and eventually led to the bacteremia (chapter 3.3.4). Although there were some technical concerns, this result supports the idea that DCs are potential vehicles for bacterial spreading in the host. Upon migration, it is tempting to speculate that *Bartonella* colonizes the primary niche for preparing its competency to subsequently interact with erythrocytes. However, so far this assumption is not yet supported by *in vivo* experimental data. A neonatal murine model established in this thesis may provide a better platform to study the primary niche of *Bartonella* infection. Compared to adult mice, *Bartonella* infection in newborn mice developed extremely high bacteremia (chapter 3.3.5), indicating that immunodeviant neonates poorly control the *Bartonella* replication in the early phase of infection.

A potential model of *Bartonella* stealth-infection strategy

To summarize, a potential model of *Bartonella* stealth-infection strategy can be built based on results obtained from my Ph.D. thesis (Figure in next page). Upon inoculation into the host, *Bartonella* initially enters migratory cells, such as DCs, which assist the passage of bacteria from the intradermal environment via lymphatic system to the primary niche, eventually culminating in their release to the bloodstream. On one hand, DCs may be exploited by *Bartonella* for bacterial transport passing through the draining LNs. On the other hand, in the LNs, “semi-mature” DCs triggered by *Bartonella* infection may possess potential tolerogenic activities to subvert T cell response. The induction of semi-maturation observed in DCs is attributed to two effector proteins, BepA and BepD. Moreover, the underlying mechanisms of BepA and BepD involve in distinct host signaling pathways, cAMP and STAT3, respectively. In my Ph.D. thesis, this is the first time to reveal the immunomodulatory properties of the VirB/D4 T4SS reflecting part of the *Bartonella* stealth-infection strategy for a chronic bartonellosis.

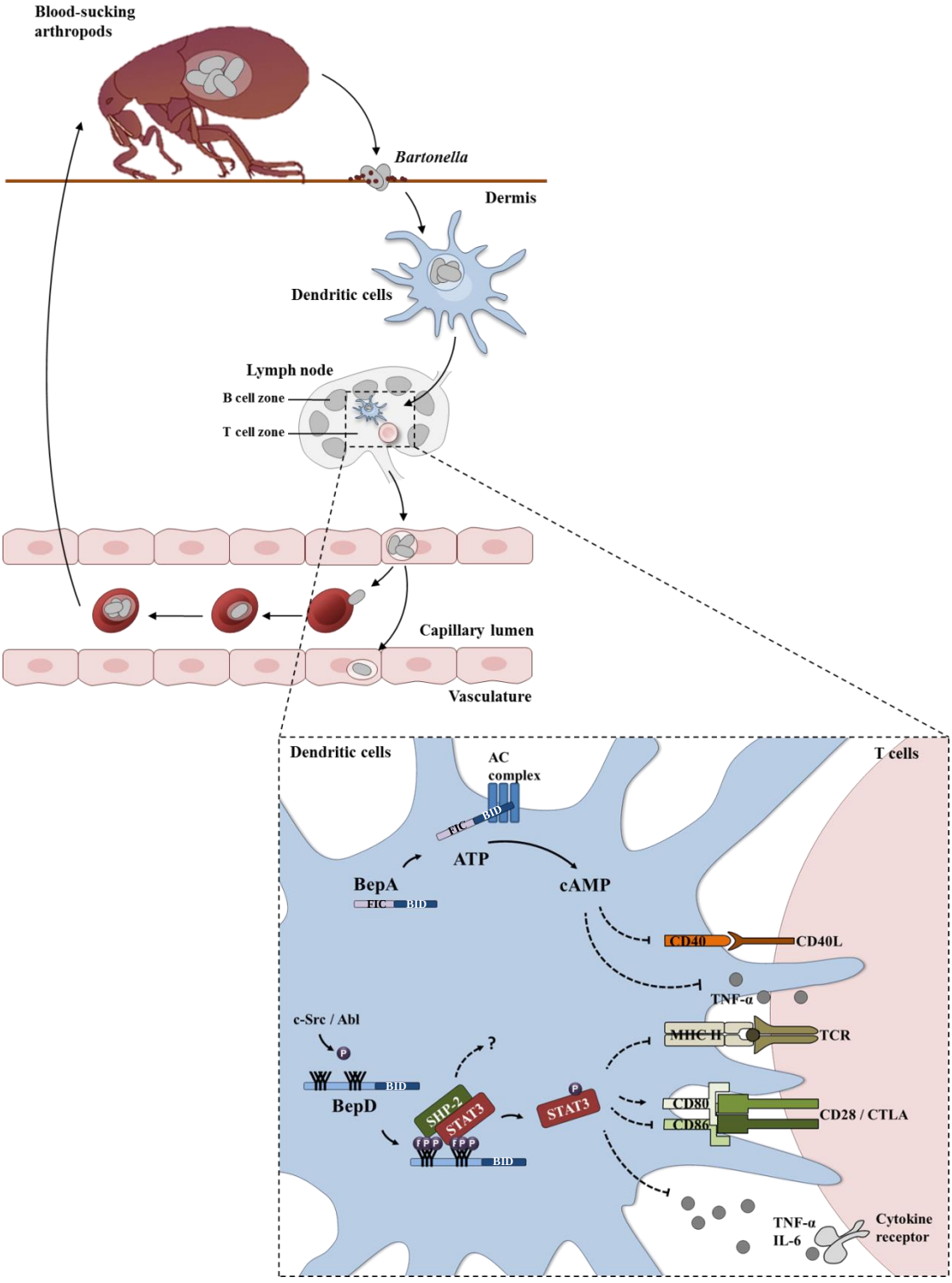

Figure. A potential model of *Bartonella* infection cycle. Upon inoculation into the host, *Bartonella* initially enters migratory cells, such as DCs, for bacterial transport from the intradermal environment via lymphatic system to the primary niche, eventually culminating in their release to the bloodstream. Upon *Bartonella* infection, "semi-mature" DCs possess potential tolerogenic activities to subvert T cell response in the LNs. This induction of the semi-maturation observed in DCs is attributed to two effector proteins, BepA and BepD. The underlying mechanisms of BepA and BepD involve in distinct host signaling pathways, cAMP and STAT3, respectively.

5. ACKNOWLEDGMENTS

This work was performed in the group of Prof. Christoph Dehio in the Focal area Infection Biology at the Biozentrum belonging to the University of Basel, Switzland.

First and foremost, I would like to thank my supervisor Prof. Christoph Dehio for giving me the opportunity to conduct my PhD in his lab. I appreciate his always support and open discussion we had all the time.

I would like to acknowledge the other members of my thesis committee, Prof. Dirk Bumann and Prof. Antonius Rolink, for their valuable suggestions and analytical criticism to my research projects.

I want to thank Mattias Trutmman and Rusudan Okujava for introducing me as a PhD student to the *Bartonella* field, for their valuable advice, and for developing methods which laid the foundations for my work with *Bartonella*.

I am very grateful to Rusudan Okujava and Claudia Mistl for their great assistance with animal experiments.

I would like to thank Christoph Schmutz for supporting me in the BepD project, in particular the underlying mechanism of BepD. I am also grateful to Timo Glatter for the mass spectrometry assay.

For the critical and careful reading of my thesis, I am very grateful to Simone Eicher, Rusudan Okujava, and Christoph Schmutz.

Besides those mentioned above, I wish to express my thanks to all present and past members of the Dehio lab for all the help, discussions, ideas, and extra-lab activities: Maxime Quebatte, Kathrin Pieles, Shyan Huey Low, Alain Casanova, Houchaima Ben Tekaya, Alexander Harms, Isabel Sorg, Sabrina Siamer, Frédéric Stanger, Jonas Körner, Caroline Grey Hackett, Tjaart De Beer, Clement Barbier, Simon Marlaire, Kevin Charles Smith, Sarah Stiegeler, Nikolaus Schmitz, Simone Muntwiler, Pauli Rämö, and Mario Emmenlauer.

Also, I would like to acknowledge the constant support from the people working on the technical and administrative staff of the 4th floor. Thank you all very much for all the things running in the back of the everyday business of science.

Special thanks go to Ruso, Claudia, Kathrin, Simone, Sarah, and Shyan who helped me in keeping the balance of work and leisure. I enjoyed what we have done together. I don`t know how I could pass through these four years without you.

I was funded by the Werner Siemens Foundation “Fellowship for Excellence”.

Last but not least, a very big thank goes to my family, especailly my husband Eddy Wu, for being patient, for always understanding, and for supporting me in any way they could. This Ph.D. thesis would have never been possible without them.

6. CURRICULUM VITAE

Yun-Yueh Lu

Date of Birth: 20.02.1984
Nationality : Taiwan
Address : Kannenfeldstrasse 18,
4056 Basel, Switzerland
Email : luna.lu025@gmail.com

EDUCATION

2011 - 2015 **Ph.D. in Microbiology | Specialization of Infection Biology**
Biozentrum, Basel University, Switzerland

2007 - 2009 **M.Sc. in Plant Science | Specialization of Virology**
Wageningen University, The Netherlands

2002 - 2006 **B.Sc. in Plant Pathology**
National Chung-Hsing University, Taiwan

RESEARCH EXPERIENCE

2011 - 2015 **Ph.D. candidate | Biozentrum, Basel University, Switzerland**
Research topic: Functional characterization of *Bartonella* effector proteins as the immunomodulatory molecules to interfere with dendritic cell maturation.

2009 - 2010 **Research assistant | Academia Sinica, Taiwan**
Research topic I: Functional characterization of a novel protein TET1, a dioxygenase, involving in cytosine demethylation in cancer research.
Research topic II: Investigation of the relationship between autophagy and HIV infection.

2007 - 2009 **Master student | Wageningen University, The Netherlands**
Research topic: A role of *Tomato spotted wilt virus* hairpin structure in the concerted action with a poly(A)-tail-binding protein in translation.

2006 - 2007 **Research assistant | National Chung-Hsing University, Taiwan**
Research topic: Identification and Reclassification of *Melon yellow spot virus* as a Member of WSMoV Serogroup. Production the MYSV NP MAb and the WSMoV NP MAb for identification of MYSV and WSMoV from single or mixed infection in field surveys.

CERTIFICATE SKILL

Education and Training of Animal Experiments: EFLASA Category B ID: LTK1329

LANGUAGES

Native: Mandarin; **Fluent:** English

HONORS AND AWARDS

2011 - 2014 Fellowships for Excellence by Werner Siemens-Foundation

2007 - 2009 The Y.C. Lo Scholarship

EXTRACURRICULAR ACTIVITIES

2014 Antelope program at Novartis to thoroughly investigate career opportunities and gain insights into the pharmaceutical industry

2010 Summer school in the Interdisciplinary Center of Infection Biology and Immunity of the Humboldt-University (ZIBI): Pathogen-Host Interplay

PUBLICATIONS

Okujava R, Guye P, Lu YY, Mistl C, Polus F, Vayssier-Taussat M, Winter CH, Rolink AG, Dehio C. A translocated effector required for Bartonella dissemination from derma to blood safeguards migratory host cells from damage by co-translocated effectors. PLos Pathogen. 2014; 10(6): e1004187.

*Lu YY, *Franz B, *Truttmann MC, Riess T, Gay-Fraret J, Faustmann M, Kempf VA, Dehio C. Bartonella henselae trimeric autotransporter adhesin BadA expression interferes with effector translocation by the VirB/D4 type IV secretion system. Cell Microbiol. 2013; 15(5):759-78. *Equal contribution

Geerts-Dimitriadou C, Lu YY, Geertsema C, Goldbach R, Kormelink R. Analysis of the Tomato spotted wilt virus ambisense S RNA-encoded hairpin structure in translation. PLoS One. 2012; 7(2):e31013.

Hsu CH, Peng KL, Kang ML, Chen YR, Yang YC, Tsai CH, Chu CS, Jeng YM, Chen YT, Lin FM, Huang HD, Lu YY, Teng YC, Lin ST, Lin RK, Tang FM, Lee SB, Hsu HM, Yu JC, Hsiao PW, Juan LJ. TET1 suppresses cancer invasion by activating the tissue inhibitors of metalloproteinases. Cell Rep. 2012; 27;2(3):568-79.

Lin RK, Wu CY, Chang JW, Juan LJ, Hsu HS, Chen CY, Lu YY, Tang YA, Yang YC, Yang PC, Wang YC. Dysregulation of p53/Sp1 control leads to DNA methyltransferase-1 overexpression in lung cancer. Cancer Res. 2010; 70(14):5807-17.

Chen TC, Lu YY, Cheng YH, Li JT, Yeh YC, Kang YC, Chang CP, Huang LH, Peng JC, Yeh SD. Serological relationship between Melon yellow spot virus and Watermelon silver mottle virus and differential detection of the two viruses in cucurbits. Arch Virol. 2010; 155(7):1085-95

Chen TC, Lu YY, Cheng YH, Chang CA, Yeh SD. Melon yellow spot virus in watermelon: a first record from Taiwan. Plant Pathology. 2008; 57(4):765 - 765.